October 2010

High-Powered Microwaves for Boost Phase Intercept

Christopher James Horgan
Worcester Polytechnic Institute

Justin Edward Fraize
Worcester Polytechnic Institute

Matthew Stephen Sirocki
Worcester Polytechnic Institute

HIGH-POWERED MICROWAVES FOR BOOST PHASE INTERCEPT

MAJOR QUALIFYING PROJECT REPORT:

SUBMITTED TO THE FACULTY

OF THE

WORCESTER POLYTECHNIC INSTITUTE

IN PARTIAL FULFILLMENT OF THE REQUIREMENTS FOR THE

DEGREE OF BACHELOR OF SCIENCE

BY

JUSTIN FRAIZE	CHRISTOPHER HORGAN	MATTHEW SIROCKI
ECE	PHYSICS	ECE

DATE: OCTOBER 21, 2010

APPROVED:

ASSOCIATE PROFESSOR EDWARD A. CLANCY

ELECTRICAL & COMPUTER ENGINEERING

ASSOCIATE PROFESSOR GERMANO S. IANNACCHIONE

PHYSICS

Abstract

The United States military currently lacks a defense system capable of intercepting an intercontinental ballistic missile during boost phase. Missiles typically spend less than five minutes in boost, rendering traditional approaches, which utilize nuclear and kinetic tipped interceptors, infeasible due to their required flight times. Directed energy weapons, however, promise to overcome the tight timing constraints of boost phase by propagating at the speed of light. Specifically, the use of directed high-powered microwaves for boost phase interception is an interesting proposition. Microwaves may be used to achieve a "mission kill" by inducing failure of a missile's navigational electronics via electromagnetic pulses. The energy required for a high-powered microwave to be effective is three orders of magnitude lower than the energy required by the Boeing Airborne Laser, another directed energy weapon. This paper details a coverage-based analysis of high-powered microwave systems, drawing conclusions of system feasibility and future interest.

Analysis software was developed to calculate the effectiveness of directed high-powered microwaves in a ballistic missile defense context. Analysis showed space basing to be infeasible with current technology, requiring hundreds to thousands of orbital platforms. On the other hand, ground basing analysis showed promising results, requiring only one to five ground-based regional platforms to cover small countries, and would require no radical advances in technology. However, these conclusions are highly dependent on key assumptions about a target's vulnerability to an applied high-powered microwave. To address these assumptions, further research is necessary to quantify an ICBM's actual vulnerability.

Statement of Authorship

The contributions of the authors Justin Fraize, Christopher Horgan, and Matthew Sirocki are as follows:

Justin Fraize designed and implemented a first generation version of the MECSTAR coverage analysis tool with the capability to plot correlations between core system parameters of space-based systems. Additionally, he was the primary author of background sections detailing the flight stages, propulsion systems, and guidance of systems of intercontinental ballistic missiles as well as ground and space deployments. Furthermore, he was responsible for the majority of the space-based system methods and analysis, deriving equations necessary to calculate global coverage and implementing MATLAB routines to dynamically examine permutations of system parameters. Also, Justin developed the concept of ballistic missiles having characteristic critical altitudes. Finally, Justin authored the space-based results and discussion sections.

Christopher Horgan conducted research into the modus operandi of high-powered microwaves, authoring background sections involving atmospheric propagation, antenna considerations, target penetration, target response, target interactions, the definition of a "soft" mission kill as well as the state of the art of high-powered microwaves. Furthermore, he derived the majority of ground-based methods and analysis, producing an extensive code base capable of calculating the critical altitude of various ballistic threat profiles, calculating the maximum vacuum, atmospheric, and effective ranges of systems, their downranges, and the resultant coverage maps of system footprints for select countries of interest. He fused a continuous atmospheric attenuation model for altitudes ranging from zero to eighteen kilometers from a variety of sources which considered the effects of dry air, temperature, pressure, water vapor.

Matthew Sirocki investigated and authored the background sections concerning the explored nuclear, kinetic, and directed energy technologies as well as the history of ballistic missile defense from the mid-1940's to present day. Furthermore, he was the primary software architect for the second version of the MECSTAR software, which was based on

Justin's earlier work and added support for defense, sensor, and threat profiles. He authored the methods chapters on the maximum vacuum range, ground-based system analysis, and MECSTAR. He contributed to the ground-based system results by envisioning the "Earth" plot and adapting Chris' earlier "Downrange/Altitude" plot routines to create this primary output. Finally, he authored the section on ground-based plot types while being responsible for the Introduction and Executive Summary.

Acknowledgements

The authors would like to gratefully acknowledge the astute assistance, incisive input, and perennial patience of their advisors, Professors Ted Clancy and Germano Iannacchione of Worcester Polytechnic Institute. Special thanks go to the Massachusetts Institute of Technology Lincoln Laboratory for providing the facilities to perform our research and to our on-site mentor Dr. Stephen Weiner for being an indispensible reference for all topics related to missile defense. Finally, to the warm and welcoming staff members of Group 31, please accept our heartfelt thanks for remembering us in times of cake, field trips, and kickball.

Executive Summary

Since the advent of the intercontinental ballistic missile, the idea of using directed energy weapons has long captured the imaginations of ballistic missile defense designers. The United States military currently lacks a deployed defense system capable of intercepting an intercontinental ballistic missile during boost phase. Missiles typically spend less than five minutes in boost phase, rendering traditional approaches which utilize kinetic kill missiles infeasible due to the required close-in flight times. Directed energy weapons, however, overcome the tight timing constraints of boost phase interception by propagating to a target at the speed of light. While directed energy weapons remove some of the issues faced by traditional interceptors, the technical challenge of focusing and delivering sufficient power on a target missile has contributed to a lack of progress in directed energy weapons. Recent technological advances in areas such as power generation and energy storage, however, give cause to re-evaluate the feasibility of directed energy weapon systems in a missile defense context.

E.1. Problem Statement

There were two main goals for this project. The first objective was the development of a MATLAB analysis tool called MECSTAR (Modeling Effective Coverage for a Stellar/Terrestrial Advanced Response) for the purpose of modeling the effectiveness of both ground and space-based high-powered microwave (HPM) systems in a ballistic missile defense context. The second objective was to perform a coverage-based analysis of using MECSTAR for both ground and space-based HPM systems. For ground-basing, the analysis deliverable being the number of ground stations required for regional ballistic missile defense coverage, and for the case of space-basing, the number of orbital platforms required for worldwide coverage.

E.2. High-Powered Microwave Systems

It is postulated that a high-powered microwave, when fired at a boosting ICBM, would disable or disrupt a missile's navigational electronics. Ideally, this disruption of

navigational or other mission critical components would be enough to induce a "mission kill," rendering the ballistic missile unable to meet its operational objectives. Research into the baseline capabilities of high-powered microwaves revealed that their effectiveness is highly dependent upon the assumed vulnerability of a target, i.e. the level of intensity (power per unit area) required for disruption a target's navigational systems. This intensity can be as low as $10^{-4}\ W/m^2$ and as high as $10^{7}\ W/m^2$. To account for this range, three distinct Vulnerability Models are used which correspond to specific intensity levels from this spectrum.

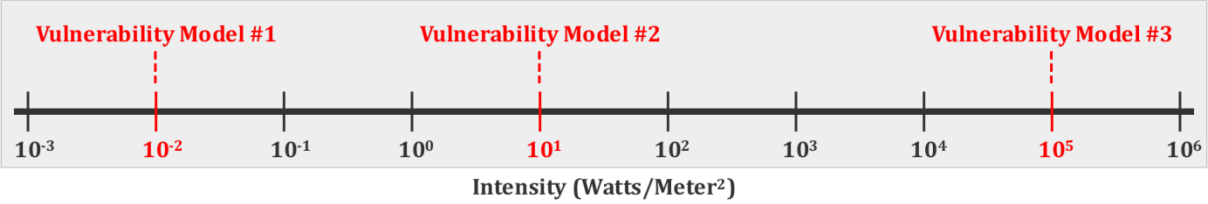

Figure E.2.a: Vulnerability Model Intensities

Three Vulnerability Models, which correspond to intensities of $10^{-2}\ W/m^2$, $10^{1}\ W/m^2$, and $10^{5}\ W/m^2$, are used to address the range of intensities found to disrupt electronics systems.

These Vulnerability Models, which correspond to intensities of $0.01\ W/m^2$, $10\ W/m^2$, and $100{,}000\ W/m^2$, represent estimates for the minimum required intensity which a high-powered microwave system must deliver onto a target in order to achieve a mission kill.

E.3. Calculating Effective System Ranges

The maximum vacuum range (R_{vac}) represents the farthest a microwave beam can propagate while delivering a level of intensity no less than the minimum required intensity (I_{req}) for a mission kill. To calculate R_{vac}, the range of a microwave beam was modeled as a function of the system parameters antenna diameter ($D\ in\ m$), operating frequency ($f\ in\ Hz$), source power ($P\ in\ W$), electromagnetic shielding of the target ($\gamma_s\ in\ dB\ loss$), and the minimum required intensity (I_{req}). This model for the vacuum range of a system is shown by Eq. (E.3.a) below.

$$R_{vac} = \frac{2 \cdot D \cdot f}{1.22 \cdot c \cdot \sqrt{\pi}} \sqrt{\frac{P \cdot \left(10^{-\left(\frac{\gamma_s}{10}\right)}\right)}{I_{req}}} \quad \text{(E.3.a)}$$

As can be seen, increasing the system parameters of antenna diameter (D), operating frequency (f), and source power (P) have a positive effect on the maximum vacuum range (R_{vac}). Furthermore, increasing the system parameters of electromagnetic shielding (γ_s) and minimum required intensity (I_{req}) have a negative effect on R_{Vac}.

For space-based systems, the maximum vacuum range defines the maximum system range because attenuation due to the atmosphere is negligible. For ground-based systems, however, atmospheric attenuation must also be accounted for because the path to the target contains levels of dense atmosphere. An atmospheric attenuation model sourced from NASA was used which provides the total attenuation ($\gamma_{total}(h)$) caused by dry air, water vapor, rain, and cloud cover at a given altitude (h) above the surface. For all altitudes passed through by a beam, the total attenuation is summed to determine the maximum system range of a ground-based system.

The maximum system ranges of both ground and space-based systems, however, are not equal to their respective effective ranges. The effective range of an HPM system is a subset of the maximum range, and is defined by a missile's critical altitude (h_c). An ICBM flying a downrange distance of 5,500 kilometers (the minimum distance to qualify as an ICBM) has a characteristic altitude (h_b) and time (t_b) for when it leaves boost phase (the first phase of a missile's flight). Additionally, there exists a time margin (t_m) in which an HPM system must engage an ICBM prior to the completion of boost phase in order to induce enough navigational error to qualify for a mission kill. The altitude corresponding to the end of boost time (t_b) minus the margin time (t_m) is called the critical altitude. The critical altitude describes the greatest height that an ICBM travelling 5,500 kilometers can be hit during the boost phase while still providing a great enough margin to induce a mission killing error. The effective system range of both ground and space-based platforms

is defined by the intersection of their respective maximum system ranges with a ballistic missile's critical altitude.

E.4. System Coverage Results

Shown below in Figure E.4.a for Vulnerability Model 2, the maximum (dotted lines) and effective (shaded areas) ranges of a high-powered microwave system are plotted for a given set of system parameters for a critical altitude of 100 km.

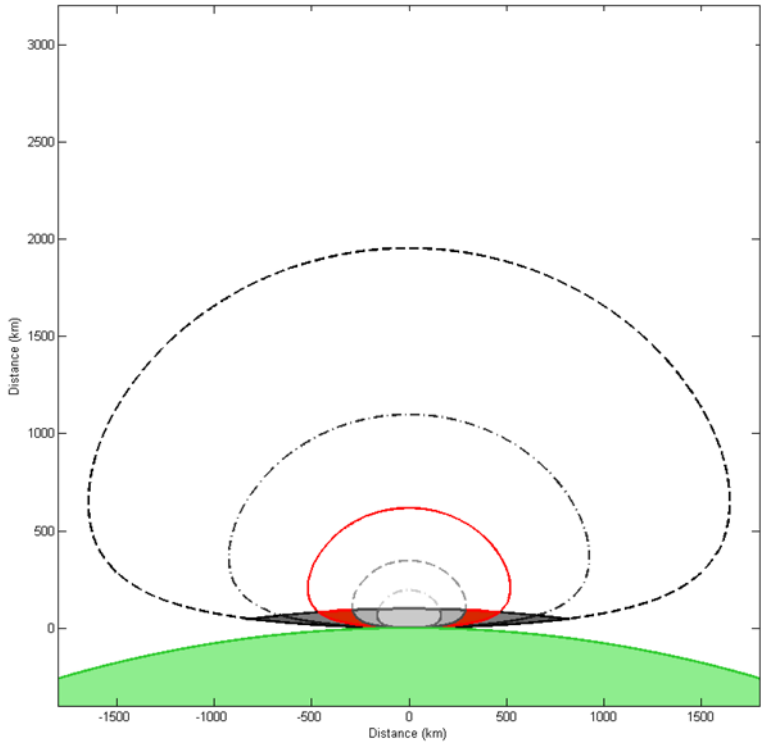

Figure E.4.a: Ground-Based Results - Vulnerability Model 2 - Sweeping Electromagnetic Shielding Cross-sections of the maximum system range (dotted lines) and of the effective system range (shaded in) are plotted for a system deployed on a spherical model of the Earth. Each dotted line represents the maximum range using 30, 35, 40, 45, and 50 dB of shielding attenuation.

Shown above, the electromagnetic shielding is swept across a 20 dB range to produce five different range "bubbles." The maximum downrange, i.e. the farthest distance from the system that can be covered as measured along the surface of the Earth, corresponds to a shielding level of 30 dB and is calculated to be 808 km. For Vulnerability Models 1 and 3, the maximum downranges were 1,117 km and 38.79 km respectively.

For space-based results coverage was calculated on a global scale. Figure E.4.b below shows the total number of satellites required for a given HPM system range.

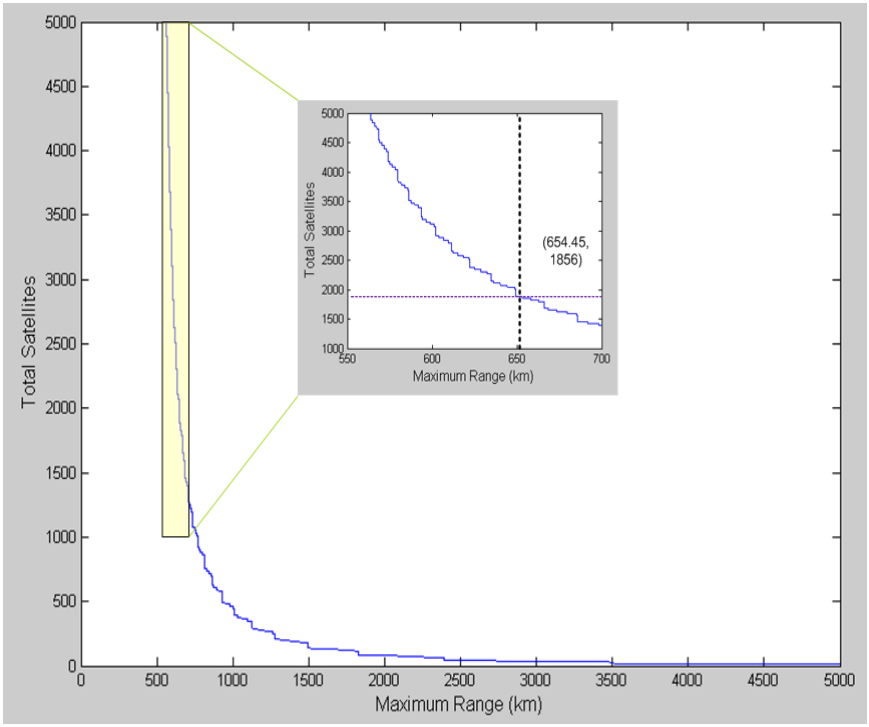

Figure E.4.b: Total Satellites for Global Coverage vs. Effective Range

The number of satellites required for continuous global coverage is a strong inverse function of the effective range. The range of Vulnerability Model 2 is highlighted, with a maximum range of $654.45\ km$ corresponding to $1,856\ satellites$.

Shown above, 1,856 satellites are needed to achieve continuous global coverage for Vulnerability Model 2. Not visible on the scale, Vulnerability Model 1 necessitates two satellites, each covering an entire hemisphere. Finally, for Vulnerability Model 3, the number of satellites is undefined, as the range of the HPM system is only 146.3 km, and is incapable of reaching the critical altitude of 100 km from the system's orbital altitude of 600 km.

E.5. Conclusions

The ambiguity of required intensity levels highlights the need for further research. Therefore, only general conclusions are made; space-basing is currently infeasible, requiring hundreds to thousands of orbital platforms when considering any required

intensity levels aside from the lowest estimates. Ground-basing, however, has more promise being as stationary systems can be larger in size while requiring fewer installments to counter regional threats. When using moderate intensity estimates, small countries like Iran and North Korea need four or fewer high-powered microwave stations in the vicinity to ensure coverage. When using the upper bound of intensity estimates, both ground and space systems would require significant advances in technology to realize practical ranges. However, as mentioned previously, before any consideration is made to pursue high-powered microwave solutions for ballistic missile threats, empirical testing must be done to determine the actual intensity required for a mission kill on an in-flight boosting ICBM.

Table of Contents

Table of Figures

Table of Tables

1 Introduction

Since the advent of the intercontinental ballistic missile (ICBM), the idea of using directed energy weapons (DEWs) has long captured the imaginations of ballistic missile defense (BMD) policy makers. The United States military currently lacks a defense system capable of intercepting an intercontinental ballistic missile during boost phase. Missiles typically spend less than five minutes in boost, rendering traditional approaches, which utilize nuclear interceptors and kinetic kill vehicles, infeasible due to their required flight times. Directed energy weapons, however, promise to overcome the tight timing constraints of boost phase by propagating at the speed of light.

While, DEWs remove some of the issues faced by traditional interceptors, the technical challenge of focusing and delivering sufficient power to a target missile has contributed to a lack of progress in DEWs. Ultimately, it is due to these difficulties that public, political, and private interests in such systems have waned. Thus, while DEWs have continually fallen short of their original deployment goals, kinetic kill vehicles have become the current mechanism used in United States BMD (Parrington, 1997). Today, despite the previous shortcomings of DEWs, there exists continued research interest with respect to DEW platforms and their place within a BMD context (Defense Science Board, 2007). Specifically, as technological advances occur in areas such as power generation and energy storage, it is appropriate to re-evaluate the feasibility of previously considered DEW systems.

1.1 Project Area

Of the DEW programs currently undergoing research and development by the Department of Defense, most can be separated into two distinct groups: high-energy lasers (HELs), and high-powered microwaves (HPMs). The effects of these technologies range from the disruption to the complete destruction of a target. HEL systems, like the Airborne Laser for example, attempt to induce enough structural damage during the boost phase of an ICBM to physically destroy it (Barton, et al., 2004). While an HEL system causes damage

via the transfer of thermal energy, HPM systems are effective via electromagnetic radiation. It is postulated that an HPM, when fired at a boosting ICBM, would disable or disrupt electronic equipment. Ideally, this disruption of navigational or other mission critical components would be enough to induce a mission kill, rendering the ballistic missile unable to meet its operational objectives.

As noted by a 2007 Defense Science Board report, HPM programs remain "the preferred solution for many nonlethal applications to include active denial, vehicle denial, and electronic defeat systems." Several factors contribute to the effectiveness of an HPM system. Investigations into an HPM's value must incorporate all of the distinct phases through which the propagating wave travels and make note of how each event drives the output and is constrained by the input. An image illustrating a simplified process for wave propagation can be seen in Figure1.1.a below.

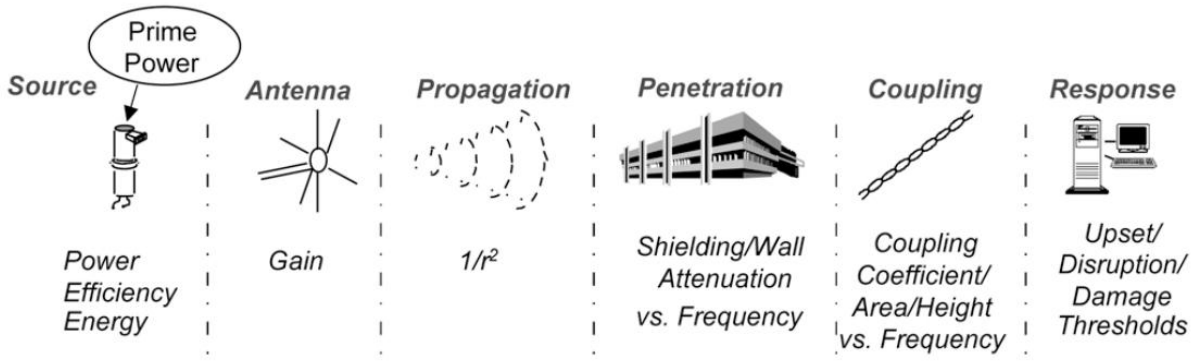

Figure1.1.a: Source-to-Target Response

The propagation of an electromagnetic wave can be broken down into several distinct phases such as source, antenna, propagation, penetration, coupling, and response. (Defense Science Board, 2007)

For modeling the effectiveness of an HPM against a given target, each stage's qualities (e.g. shielding attenuation and signal divergence) must be quantified. Depending on the granularity required, creating these models can be a tremendous undertaking. As the purpose of this project was an assessment of viability, a first order approximation is considered to be sufficient.

1.2 Specific Problem and Justification

As mentioned previously, the United States has no deployed system to intercept ICBMs in boost phase. Instead, the United States relies on forms of mid-course interception which have inherent drawbacks. These drawbacks include having to discern between real and dummy warheads, a reduced target profile due to stage shedding, and additional countermeasures such as chaff. The ballistic nature of mid-course leaves the warheads free to engage in unpredictable evasive maneuvers and, additionally, a failure to intercept during mid-course would leave little to no time to re-engage the warheads. Boost phase interception, however, deals with only a single target, because the ICBM has yet to separate. Furthermore, evasive maneuvers are rarely seen in boost phase as the flight path of an ICBM before entering a ballistic trajectory must be tightly controlled in order to achieve the required terminal accuracy. Finally, a significant light and heat signature enhances threat detection and tracking.

The primary hindrance of using kinetic interceptors for boost phase defense is the short amount of time an ICBM spends thrusting, which is on the order of minutes. Given the flight time of an interceptor missile, as well as the time it takes to detect the threat, the combined total often exceeds the total time spent in boost, making interception impossible. DEWs such as HPMs propagate at the speed of light, however, and it is this strength which makes them well suited for boost phase ICBM defense.

1.3 Detailed Project Goals

There were two main goals for this project. The first objective was the development of a MATLAB analysis tool called MECSTAR (Modeling Effective Coverage for a Stellar/Terrestrial Advanced Response) for the purpose of modeling the effectiveness of both ground and space-based HPM systems in a BMD context. The second objective was to demonstrate the use of this tool in an analysis of design feasibility.

The MATLAB analysis tool MECSTAR was to be capable of addressing both ground and space-based platforms. To accomplish this goal, it was to account for the following parameters:

- Transmission power
- Power per unit area requirements on target
- Signal attenuation due to atmosphere for ground-based systems
- Signal attenuation due to shielding
- Signal divergence due to frequency
- Orbital altitude for space-based systems
- Microwave antenna diameter
- Boost margin time
- Curvature of the Earth

Furthermore, the tool was to output the following information after performing its analysis:

- Effective range profile
- Minimum number of satellites required to provide continuous worldwide coverage
- Coverage map for ground-based systems
- Dynamic relational graphs for system parameters

The mechanism of action of our proposed HPM system is to achieve a "mission kill" by inducing failure of a missile's navigational electronics via electromagnetic pulses. Using MECSTAR, which was developed in the first phase of the project, the aforementioned analysis of design feasibility was to be approached in a coverage-based context. By determining the number of installments required to achieve various levels of coverage, conclusions of a system's potential feasibility may be drawn. In performing this analysis, the values of the HPM system parameters considered were constrained to the range of values found in unclassified literature.

2 Background

In order to provide a baseline of comparative effectiveness of both ground and space-based high-powered microwave (HPM) systems in a ballistic missile defense (BMD) context, background research on ballistic missiles and the physics of their operation, with a specific focus on intercontinental ballistic missiles. Additionally, BMD history and explored defense technologies were investigated. Finally, high-powered microwaves and the corresponding nature of ground and space-based realms of platform deployment were examined.

2.1 Ballistic Missiles

Missiles, of which ballistic missiles are a subset, can be classified by their respective mechanisms of travel. While some missiles travel to their target by continuously thrusting, a ballistic missile travels to its target via a short initial thrust which is followed by a long ballistic phase. Ballistic, in this context, means that the trajectory of the missile is gravity driven rather than thrust driven. Ballistic missiles have existed in their modern definition since World War II. Germany's V-2, the first ballistic missile used in combat, set the stage for future advancements in missile technology when it was initially deployed in 1944. (Calow & Zaloga, 2003)

Ballistic missiles are classified by their maximum range, which is defined as the "maximum distance measured along the surface of the earth's ellipsoid from the point of launch … to the point of impact of the last element of its payload" (Federation of American Scientists, 2000). Today, countries capable of deploying ballistic missiles use a number of classification schemes. For example, the classification schemes of the United States and the Russian Federation are shown in Table 2.1.a below.

United States of America		
Intercontinental Ballistic Missile	(ICBM)	5,500 $km \leq range$
Intermediate-Range Ballistic Missile	(IRBM)	3,000 $km \leq$ range $<$ 5,500 km
Medium-Range Ballistic Missile	(MRBM)	1,000 $km \leq range <$ 3,000 km
Short-Range Ballistic Missile	(SRBM)	0 $km \leq range <$ 1,000 km

Soviet Union/Russian Federation	
Strategic	1,000 $km \leq range$
Operational-Strategic	500 $km \leq range <$ 1,000 km
Operational	300 $km \leq range <$ 500 km
Operational-Tactical	50 $km \leq range <$ 300 km

Table 2.1.a: Ballistic missile classification schemes of the United States and the Russian Federation
The United States' system broadly classifies all ballistic missiles into four categories while the Russian scheme uses five categories over a smaller range of distances (Federation of American Scientists, 2000).

For a missile to be classified as ballistic, it must follow a ballistic trajectory once completing a relatively short period of thrust. The maximum speed reached at burn-out, the point at which thrust ends, varies with the type of ballistic missile. Short-range ballistic missiles (SRBMs), such as the Iraqi Scuds used in the Gulf War, may exceed four times the speed of sound (1.50 km/s) at burn-out. ICBMs, however, can reach speeds over seven kilometers per second (American Physical Society, 1987). Although short-range ballistic missiles have been used to great effect in a number of conflicts, this project focused on ICBMs.

2.1.1 Intercontinental Ballistic Missiles

As shown in Table 2.1.a above, the United States classifies a missile as an ICBM if it has a range exceeding 5,500 kilometers. In addition to a greatly extended range, ICBMs differ from other ballistic missiles in their flight stages, propulsion, and guidance systems.

2.1.1.1 Flight Stages

The flight of an ICBM has three distinct phases: boost, mid-course, and terminal. These phases are depicted below in Figure 2.1.a.

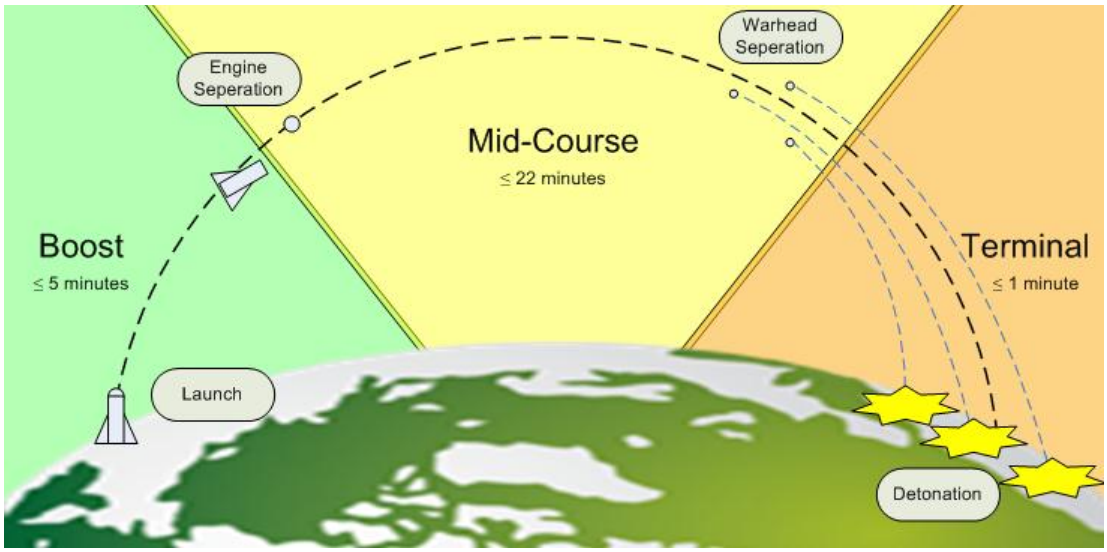

Figure 2.1.a: ICBM Flight Phases

This figure shows the three distinct phases of an ICBM's flight. Time and distance traveled increases from left to right. Phase order is boost, mid-course, and then terminal.

Boost phase may last up to five minutes, primarily dependent on fuel type and target distance. During the boost phase, the missile sheds spent fuel stages and makes course corrections based on guidance system data. Boost phase ends when the missile has finished propelling and all fuel stages have detached from the payload. The mid-course phase follows the boost phase and may last up to twenty-two minutes, defining the longest phase of an ICBM's flight. During mid-course, the ICBM may deploy decoys or multiple warheads, and may apex at an altitude up to 1,200 kilometers. The terminal phase is the last phase of an ICBM's flight, starting when the ICBM reenters Earth's atmosphere and finishing when the warheads have hit their targets. Terminal is the shortest phase, lasting less than one minute. (American Physical Society, 1987)

2.1.1.2 Propulsion Systems

ICBMs are fueled with either liquid or solid propellant. Most countries that possess ICBMs use liquid-fueled designs due to their simplicity. However, this simplicity comes at the cost of longer burn times (around four to five minutes) as compared to their solid-fuel counterparts. This elongated time window allows for better tracking measurements and fewer restrictions on response times. Solid-fueled ICBMs have a boost phase that lasts approximately three minutes, making time constraints much more difficult to overcome

(Barton, et al., 2004). According to an American Physical Society report on boost phase intercept, it is expected that most small nuclear powers will possess solid fuel capabilities within the next 15-20 years (Barton, et al., 2004). This report also suggests that ICBMs with burn times of only two minutes are possible in the near future, rendering almost all kinetic kill vehicles ineffective for boost phase intercept.

2.1.1.3 Guidance Systems

ICBMs are guided using either inertial or celestial guidance systems. Inertial guidance systems work by calculating an ICBM's position by use of accelerometers. The accelerations measured are integrated with respect to time once to get velocity, and twice to get position. Celestial guidance systems calculate an ICBM's position by referencing stationary celestial objects like stars; this system may be used in conjunction with an inertial guidance system (Federation of American Scientists, 2000). Both types of guidance systems are well suited for missile guidance because they do not need to make contact with command and control centers, a communication of which could be scrambled or jammed by an enemy.

2.1.2 Missile Physics

The physics of a ballistic missile while thrusting in boost phase can be described by Tsiolkovsky's rocket equation, which provides the change in the missile's velocity (Δv) as a function of the exhaust velocity (v_e) of the fuel and the initial and final masses (m_0 and m_1, respectively) of the rocket for the period in question, as shown in Eq. (2.1.a).

$$\Delta v = v_e \ln\left(\frac{m_0}{m_1}\right) \tag{2.1.a}$$

Eq. (2.1.a) can be iterated multiple times to handle missiles with multiple stages. The exhaust velocity is directly related to the specific impulse (I_{sp}) and acceleration due to Earth's gravity at the surface (g_0), and can be used alongside the mass flow rate ($\frac{\Delta m}{\Delta t}$) to solve for the thrust (T) of the rocket, as shown in Eq. (2.1.b).

$$T = I_{sp} g_0 \left(\frac{\Delta m}{\Delta t}\right) = v_e \left(\frac{\Delta m}{\Delta t}\right) \tag{2.1.b}$$

Thrust force, when combined with the flight path angle (γ) which, measured from the horizontal, defines the direction of thrust, is used to find the velocities along the path of the rocket ($\frac{dv_x}{dt}$ and $\frac{dv_y}{dt}$, where x is the ground range and y is perpendicular to the earth's surface) as shown in Eq. (2.1.c) and Eq. (2.1.d).

$$\frac{dv_x}{dt} = \frac{T}{m(t)} \cos(\gamma) \tag{2.1.c}$$

$$\frac{dv_y}{dt} = \frac{T}{m(t)} \sin(\gamma) - g_0 \tag{2.1.d}$$

These velocities are then integrated to give the position of the rocket as a function of time, assuming no outside forces. Here, $m(t)$ is the mass of the rocket, which decreases over time due to the exhaustion of fuel.

2.2 Ballistic Missile Defense History

Progressions in the science of offensive ballistic missiles have not brought about comparable advances in its counter technology. Despite sixty years of effort since the advent of ballistic missiles, a full-scale BMD system has yet to be deployed by any nation. Technological, as well as political, forces have worked against the proponents of such systems and have placed the relevance of BMD itself under a high level of scrutiny. Yet today, in spite of the critics, research into effective and reasonably feasible BMD systems continues at a rapid pace.

2.2.1 The Beginnings: 1940's - 1970's

The first and largest ballistic missile campaign yet witnessed began in September of 1944 with Nazi Germany's V-2 ballistic missiles. Unlike the earlier V-1 flying bombs, the German V-2s, like all modern ballistic missiles, were capable of achieving supersonic speeds and thus were extremely difficult to defend against. In an attempt to counter the V-

2s, Britain, whom Germany had launched over one-thousand V-2 missiles against, attempted to exercise their air superiority in August of 1943 through a variety of preemptive air strikes against German missile facilities.

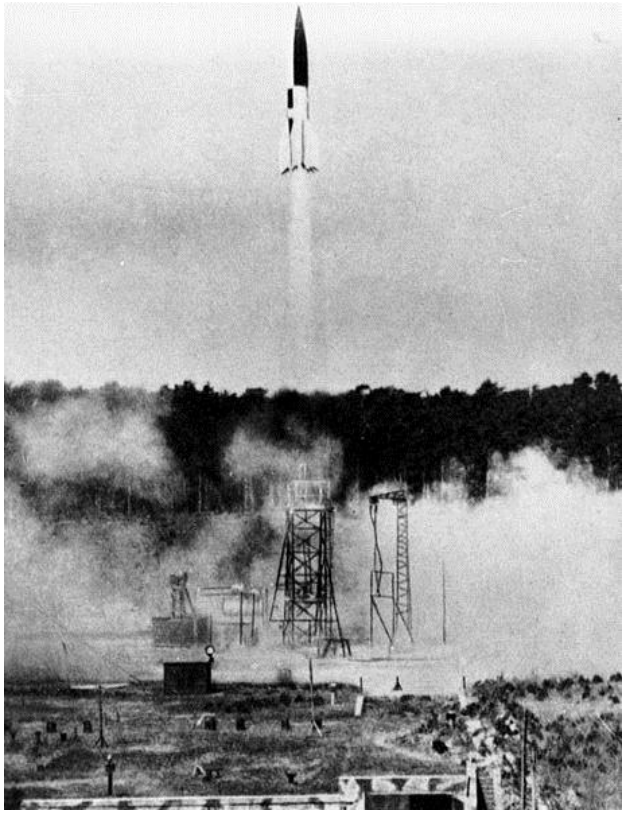

Figure 2.2.a: German V-2 Missile Launching at Peenemünde in 1943

Nazi Germany's experimental missile facility at Peenemünde was the site of testing for the V-2 ballistic missile. (Deutsches Bundesarchiv)

The strikes by the Royal Air Force, however, were ineffective against the Nazi missile efforts. The so-called "V-Weapons Campaign," despite consuming nine percent of Allied bomb tonnage over thirteen months between the fall of 1943 and the summer of 1944, was only able to delay the V-1 missiles by a handful of months while the V-2s were undeterred. Allied bombings of facilities, such as the experimental missile facility at Peenemünde (seen above in Figure 2.2.a), alerted Germany that a dispersion of their efforts was needed. Furthermore, despite their clear air dominance, the Allied forces never found a single German V-2 launch unit. The launch units, which were mobile, proved to be elusive despite being forty-six feet in length and weighing approximately 27,000 pounds. (Werrell, 2000)

During the months following the V-Weapons Campaign, analysis was performed by a team of British investigators regarding the use of a conventional artillery barrage against incoming German V-1 missiles. It had been determined that if given sufficient warning via a radar installation, it would be possible to shoot down a single V-1 missile by firing 320,000 shells into the air. This solution, apart from being prohibitively expensive, was also potentially counterproductive given estimations that two percent of the shells would not detonate as planned and the incoming rain of metal would cause more casualties than the incoming missile itself. Furthermore, when this analysis was applied to V-2s, it was found to be effective only three to ten percent of the time. Thus, given the technology available at the time, downing a ballistic missile after launch was essentially impossible. (Werrell, 2000)

Following WWII, the effectiveness of Germany's V-2 ballistic missile campaign caused both the United States Army and United States Army Air Forces (AAF) to develop an interest in both offensive and defensive ballistic missiles. As a result of this interest, a number of anti-ballistic missile (ABM) systems such as THUMPER, WIZARD, and PLATO were investigated. Ultimately, the United States Army developed a number of surface-to-air missiles (SAMs) for terminal defense, while the AAF, then United States Air Force (USAF), was to develop a long-range sensing system capable of alerting the terminal defenses.

In 1957, the Army had a plan for a full-scale defense system using the USAF's Ballistic Missile Early Warning system (BMEWS) and NIKE technology. This plan, however, was met with early criticisms which have to this day remained relevant in the BMD debate. Opponents doubted that an ABM system could sort out various warheads from decoys as well as whether defense against a "saturation" attack would be possible. Furthermore, the testing of such systems could only be carried out in separate components thus leaving doubt as to whether the system could be relied upon. On ABM, President Kennedy's Secretary of Defense, Robert McNamara, said it to be "neither technically feasible nor cost effective." Two technological advancements sought to change the impracticality of ABM systems, however, by increasing the ability of radar to detect ICBMs as well as furthering the abilities of long range interceptor missiles. Phased-array radar in addition to the NIKE X

program, which built upon the previous NIKE project, helped to propel the development of America's first ABM system which would be built in Grand Forks North Dakota. (Werrell, 2000)

Concurrent to the developments in ABM technology, the ideology of mutually assured destruction (MAD) formed the concept of deterrence. The principle of MAD was based on the assumption that if given two nations, each nation would have the ability not only to destroy the other via a nuclear attack but to retaliate with equal or greater force in the event of such destruction. The idea of possessing the ability of massive retaliation was known as "second strike" capability. MAD, a form of psychological deterrence was favored to costly ABM systems when dealing with countries such as Russia. As noted by Secretary McNamara in a 1967 speech, defense against a Soviet ICBM attack would be not only expensive but futile as well (Werrell, 2000). Yet, while defense against Russia was futile, defense against China was not. China had only recently developed its own nuclear capabilities in the 1960's and thus had not yet achieved second strike capability. Hence China was not bound by the principles of MAD. Today, a similar situation is faced when dealing with emerging small nuclear powers such as Iran and North Korea.

The conclusion of the 1960's saw the conflict between the interests of the MAD ideology and ABM supporters. MAD called for no ABM installments, lest they incite an offensive and defensive arms race, or trigger a pre-emptive strike before an opponent's ABM system goes online. The result was a record 29 day Senate debate concerning the future of the Army's proposed ABM system which concluded on August 6, 1969 in an evenly split vote. Vice President Spiro Agnew cast the deciding vote in favor of preserving support for ABM systems. However in May of 1972, the US and Soviets signed the SALT (Strategic Arms Limitation Talks) and ABM treaties, agreements over not only the number of permissible strategic weapons, but also, and more importantly, the maximum number of ABM sites. (Werrell, 2000)

The ABM treaty, following an additional protocol signed in 1974, permitted one ABM site within 150 kilometer of either an ICBM field or the national capital. Each site was limited to a strict maximum number of missiles, launchers, and radars. Additionally, the

treaty prohibited a variety of activities such as developing, testing, and deploying systems based in the air, sea, or space. (Werrell, 2000)

While the ABM and SALT talks were proceeding, the United States was debating the continuation of its first ABM system. The system, called Safeguard, was a compromise of the Army's earlier Sentinel program and employed NIKE X technology. The first phase of construction was approved in 1969 by one vote in the Senate and construction work commenced (Federation of American Scientists, 1998). While opinions varied wildly on the utility of the system against ballistic threats, the system gained support under the guise of arms control. By the early 1970's "the strongest and most pressing rationale for Safeguard had become its role as a bargaining chip with the Soviets" (Papp, 1987-88). The heated debates over the Safeguard continued beyond the signing of the ABM treaty into 1975.

In compliance with the ABM treaty, the Safeguard system was installed to protect the ICBM field near Grand Forks Air Force Base, North Dakota (Papp, 1987-88). Deemed operational in October 1, 1975, the system worked by detonating nuclear warheads in the atmosphere at incoming ICBMs (Federation of American Scientists, 1998). Operational status was short-lived, however, lasting less than a year as it proved too expensive. The high expense of ABM was reflected in financial policy as ABM expenses fell from an average of $1 billion per year in 1960 to $100 million per year by 1980. Following the deactivation of the Grand Forks installation in early 1976, ABM systems would receive little attention until 1983. (Werrell, 2000)

2.2.2 The Strategic Defense Initiative: 1980 - 1990

When President Reagan was elected, the state of BMD technology was primarily focused on the defense of United States ICBM launch sites. However, in a landmark speech in March of 1983, President Ronald Reagan unveiled the Strategic Defense Initiative (SDI) program. SDI represented a departure from the accepted line of MAD defense policy as it attempted to leverage America's industrial strengths against the technical obstacles of missile defense. (Werrell, 2000)

Ridiculed as “Star Wars”, the SDI was opposed by the Air Force, and Navy as well as the arms control community, mainstream media, and academia. Over 7,000 scientists opposed the program while the American Physics Society (APS) famously concluded in a 1987 study that not only were the goals of the SDI impossible using current technology, it would take a decade of research to ascertain if it would ever be possible (American Physical Society, 1987).

In spite of harrowing predictions, SDI did not unravel the ABM treaty, or result in a global nuclear conflict or even an operational BMD system. The SDI did, however, renew strategic arms negotiations between the Soviet Union and the United States. During a 1985 meeting in Geneva between the U.S. and U.S.S.R., the two superpowers agreed to reduce their strategic arms by fifty percent. (Werrell, 2000)

2.2.3 National Missile Defense: 1990 - Present

During President George H. W. Bush's administration, the comprehensive approach of SDI was scaled down after the collapse of the U.S.S.R. SDI's original goal of defending against a massive nuclear strike was considered out of scope and SDI was refocused to deal with engaging a limited ballistic attack. The Clinton administration supported BMD, but renamed SDI’s parent organization, known as the Strategic Defense Initiative Organization, to the Ballistic Missile Defense Organization (BMDO) and funding was reduced. President George W. Bush's administration further renamed the program two more times, from BMDO to National Missile Defense, and then again to Ground-Based Midcourse Defense. Additionally, President George W. Bush formally withdrew the U.S. from the ABM treaty signed with Russia in 1972. (U.S. Department of Defense)

2.3 Explored Technologies

Under the various past BMD programs a number of different technologies were explored. In general, these technologies can be separated into categories of nuclear, kinetic, and directed energy. The following sections provide an overview of several projects that

were built on each of these technologies, outline their benefits, and identify their respective shortcomings.

2.3.1 Nuclear Technologies

Nuclear warheads were the initial technology of missile defense. The Army's NIKE project, which began as an advanced antiaircraft system, evolved throughout the 1950's with the development of the NIKE-AJAX, NIKE-HERCULES, and finally the NIKE-ZEUS. This final iteration was authorized by the Army in 1958 as a full-scale BMD development program (Papp, 1987-88). NIKE-ZEUS interceptor missiles were equipped with atomic-tipped warheads and were provided long-range sensing capabilities by the Ballistic Missile Early Warning System (BMEWS), a project of the Air Force (Werrell, 2000). The system's method of action was to bring the incoming threat during mid-course flight within the lethal range of the interceptor missile and detonate its payload.

Although the replacement of the conventional warhead on the original AJAX missile with the atomic technology of the ZEUS missile increased its lethality from tens to hundreds of feet, several drawbacks inherent to the use of nuclear warheads on interceptors persisted. The detonation of a nuclear warhead in the atmosphere would blind the BMEWS, thus preventing the detection of additional threats. Furthermore, due to limitations on the effective range of the BMEWS systems and additional overhead introduced in command commit times, nuclear fallout over friendly territories was a real possibility.

Nevertheless, nuclear technologies were the first BMD methods to see deployment. The efforts of the NIKE-ZEUS project would eventually become NIKE-X, which, after a decade of debate, would see deployment as the Safeguard system. In its final form, the Safeguard employed two kinds of missiles, the Spartan and the Sprint, which were responsible for mid-course and terminal defense respectively (Papp, 1987-88). While the Spartan was capable of intercepts at ranges of about 556 kilometers and altitudes of 185 kilometers, the Sprint was a high-acceleration missile capable of intercepts between 1.5 kilometers and 30 kilometers within a range of 185 kilometers.

2.3.2 Kinetic Technologies

Atomic-tipped interceptors gradually were phased out in favor of kinetic solutions. Beginning the in 1980's, the Army studied the feasibility of destroying an incoming ballistic threat by merely colliding with it. A result of this study was the Homing Overlay Experiment (HOE). The HOE featured a new, non-explosive payload (see below in Figure 2.3.a). Kinetic based interceptor technology was affirmed in June of 1984 when a missile outfitted with the HOE successfully intercepted a Minuteman ICBM. The intercept took place with the ICBM traveling at more than 15,000 mph at an altitude of over 100 miles (Werrell, 2000).

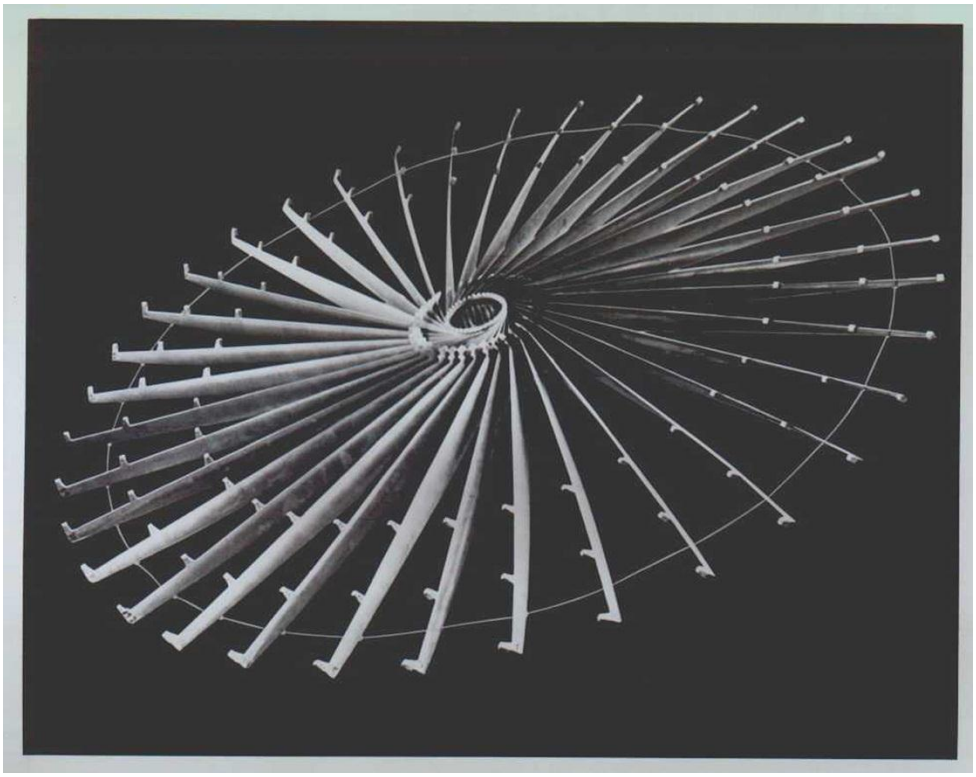

Figure 2.3.a: Homing Overlay Experiment Expanding Warhead

The Homing Overlay Experiment was an early form of kinetic BMD which used a unique expanding warhead. Once exospheric, the interceptor missile would expand its warhead, thus increasing its physical footprint, and reducing the proximity required to hit a target. (SMDC)

2.3.3 Directed Energy Technologies

A third type of missile defense technology whose effectiveness has only recently been shown is directed energy. Once a primary focus of the SDI, directed energy required

technology beyond the state of the art in the 1980's. Today, however, directed energy has been shown to be effective against ballistic threats, such as in the proof of concept Airborne Laser project.

The Airborne Laser (ABL), developed by Boeing, is a directed energy weapon (DEW) that hoped to fill the role of boost phase interception (Defense Science Board, 2007). This defense system involved a modified Boeing 747 aircraft which housed a chemical oxygen iodine laser (COIL). This laser's method of action involved focusing on a target long enough to reduce the structural integrity of a missile's skin thus impairing the ability of the target to withstand the stress of high-speed flight through the atmosphere (Barton, et al., 2004). On February 11, 2010, the ABL successfully engaged and destroyed a test ballistic threat while in boost (Selinger, 2010). Despite having a relatively low cost per intercept (the cost of firing the COIL), the system's range of several hundred kilometers dictated having multiple aircraft continuously in flight in order to achieve coverage of more than a localized theater (Alexander & Wolf, 2010). Given that the Airborne Laser was conceived in the early 1980's and was originally scheduled to demonstrate a lethal intercept in 2003, the technological, engineering, and testing phases of development of even a fully supported DEW system can clearly be quite long. Furthermore, despite the successful firing of the ABL system, Air Force Chief of Staff General Norton Schwartz was quoted on February 23, 2010 as stating that while the ABL is "a magnificent technical achievement … [it]does not reflect something that is operationally viable" (Hoffman, 2010).

Although the successful firing of the ABL represents the first time a ballistic missile has ever been destroyed (on purpose) while in its boost phase, lasers have their own drawbacks (Selinger, 2010). A simple ablative coating for example, such as cork, can provide several seconds of protection. Additionally, if the missile were to rotate, the laser may not be able to focus on one spot long enough to burn a hole through it quickly, thus providing additional protection to the missile. With a potentially long focus time, the laser might not be able to sustain its power long enough to cause meaningful structural damage to the ICBM.

Additional directed energy weapons such as charged and neutral particle beams have also been considered at length as demonstrated by the findings of the 1987 APS report entitled *The Science and Technology of Directed Energy Weapons* (American Physical Society, 1987). These technologies continue to prove elusive due to their highly technical nature, high cost, and large power requirements.

2.3.4 State of the Art

Despite many studies on BMD systems, kinetic kill vehicles have today remained the top choice for defense. The current national missile defense (NMD) system used by the United States consists of several components. Ground-based interceptor missiles are stationed strategically to protect the United States from so-called rogue-states such as North Korea, and advanced radar systems are used to track the incoming threats. This system, known as the Ground-Based Midcourse Defense (GMD), currently has installments in both Alaska and California (Northrop Grumman Aerospace Systems, 2009). Between October 2, 1999 and May 25, 2007, twelve hit-to-kill tests of the GMD were executed. Of these, only six (50%) have been successes (Samson & Black, 2007).

Additionally, the Aegis Ballistic Missile Defense System complements the GMD by providing sea-based mid-course defense and target tracking capabilities. Although the system is capable of engaging only short to medium range ballistic threats, it has the capability of passing target information to the GMD (O'Rourke, 2010). Furthermore, the system will, as indicated by current progress, eventually be capable of intercepting all ballistic threats in midcourse. The current and future versions of the Aegis BMD system, labeled according to their PAA (Phased Adaptive Approach) phase, can be seen below in Table 2.3.a. The current version of the Aegis BMD system (PAA Phase I - 3.6.1) is capable of handling only short to medium range ballistic threats with a limited capability for inter-mediate range. Looking forward, however, reveals plans to add limited capability for ICBM's as well. (O'Rourke, 2010)

Aegis System Information	PAA Phase I	PAA Phase II		PAA Phase III	
Version of Aegis BMD System	*3.6.1*	*4.0.1*	*5.0*	*5.1*	*5.2*
Certified for initial use	*2006*	*2012*	*2014*	*2016*	*2018*
OTE assessment	*2008*	*2014*	*2016*	*2018*	*2020*
Mid-course interceptor(s) used					
SM-3 Blk IA	■	■	■	■	■
SM-3 Blk IB		■	■	■	■
SM-3 Blk IIA				■	■
Terminal phase interceptor(s) used					
SM-2 Blk IV	■				
Eventual new missile					■
LRS&T capability	Yes	Yes	Yes	Yes	Yes
Types of ballistic missiles that can be engaged					
SRBM	Yes	Yes	Yes	Yes	Yes
MRBM	Yes	Yes	Yes	Yes	Yes
IRBM	Limited	Limited	Limited	Enhanced	Enhanced
ICBM	No	No	No	Limited	Limited
Launch on remote capability	Initial	Enhanced	Yes	Yes	Yes
Engage on remote capability	No	No	No	Yes	Yes

Notes: OTE is operational test and evaluation. **LRS&T** is long-range search and track - the ability to detect and track ballistic missiles. **SRBM** is short-range ballistic missile; **MRBM** is medium-range ballistic missile; **IRBM** is intermediate-range ballistic missile; **ICBM** is intercontinental ballistic missile. **Launch on remote** is the ability to launch the interceptor using data from off-board sensors. **Engage on remote** is the ability to engage targets using data from off-board sensors.

Table 2.3.a: Current and Future Aegis BMD System Version

Future plans for the naval-based Aegis BMD system reveal intent to expand from handling only short to medium range ballistic missiles to intermediate and intercontinental ranges as well. (O'Rourke, 2010)

Shown here, the Aegis BMD system is slated to support ICBMs in a limited capacity beginning in 2018 with version 5.1 of PAA Phase III.

2.4 High-Powered Microwaves

Electromagnetic waves with frequencies between 0.3 GHz and 300 GHz are broadly classified as microwaves. This frequency band corresponds to wavelengths of one meter and one millimeter respectively (Pozar, 1993). As stated in Section 1.1, investigations into HPM systems must incorporate all of the distinct phases through which the propagating

wave travels and make note of how each event drives the output and is constrained by the input. The following sections detail the power sources, antenna considerations, propagation effects, penetrability, coupling, and responses of high-powered microwaves.

2.4.1 Microwave Power Levels

The propagation of a high-power microwave begins with its source power ($P\ in\ W$). Current HPM technology has enabled systems to direct up to ten gigawatts of power without the need for stationary electrical generators (Fulghum, 2007). Furthermore, several innovative concepts are being investigated which promise to boost the power of HPM systems further. As stated in a 2007 report on military grade HPM systems:

> *Researchers predict leaps of 10-100 times in power output within two years. That advance could push the beam-weapon technology far beyond the 1-10-gigawatt limit of current tactical-size HPM devices. Long-standing industry estimates are that it would require a 100-gigawatt pulse for a few nanoseconds to disable a cruise missile at a useful range. (Fulghum, 2007)*

Although verifying the accuracy of this prediction is impossible due to the classified nature of the work, it is possible to use the range suggested as a basis for the analysis detailed in this report. Increasing the current limit of ten gigawatts by a factor of 10-100 would result in power levels of 100 GW to 1,000 GW. Taking the lower end of this range (100 GW) as the maximum power level which can be achieved today ($P_{max} = 100\ GW$), a power level which may be said to be reasonable (P_r) can then be defined as half of the maximum ($P_r = P_{max}/2 = 50\ GW$). This defines a somewhat conservative range of 50 GW to 100 GW as the power levels which can be achieved today. This range is shown below on a logarithmic scale along with other notable values for the purpose of placing this range in context.

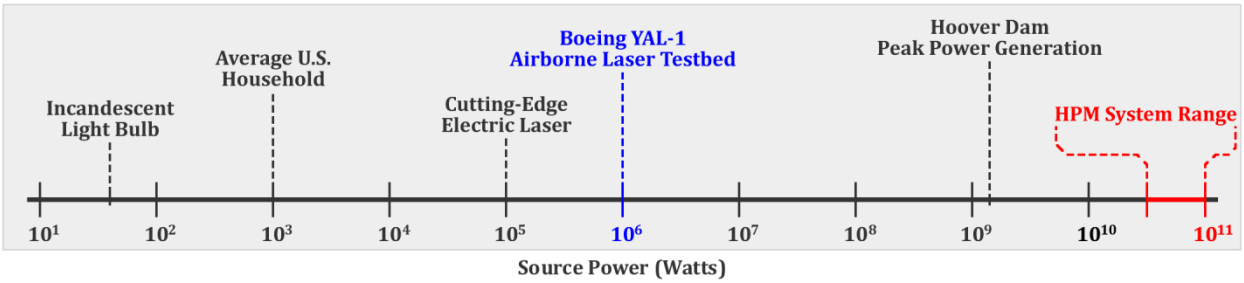

Figure 2.4.a: HPM Power Range on Logarithmic Scale

The range of reasonable power levels considered for an HPM system, 50 GW to 100 GW, are shown here on a logarithmic scale.

Note, that the aforementioned 2007 report claimed HPM systems to pulse "for a few nanoseconds" in order to be effective. Given that energy, for constant power, may be defined as seen in Eq. (2.4.a), it is possible to quantify the energy required by an HPM system.

$$E = PT \tag{2.4.a}$$

Assuming constant power levels and a conservative pulse duration of 50 ns, the operation of an HPM at 50 GW and 100 GW corresponds to energies of 2,500 J and 5,000 J respectively. Again, this range can be shown on a logarithmic scale as is done below in Figure 2.4.b.

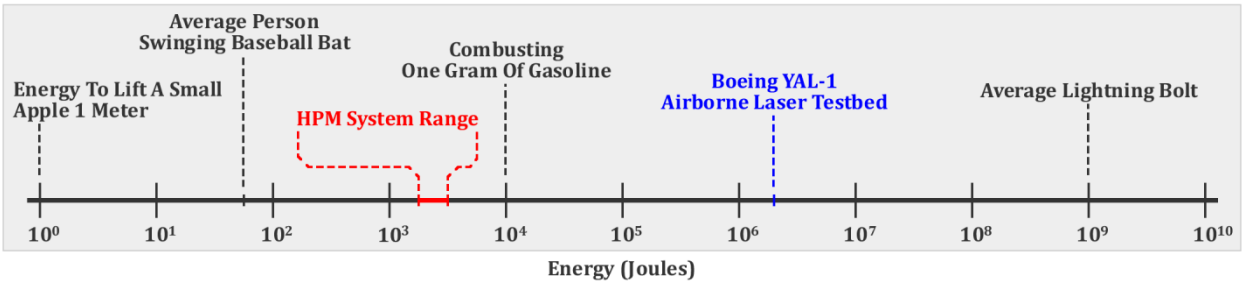

Figure 2.4.b: HPM Energy Range on Logarithmic Scale

If constant power and a pulse duration of 50 ns are assumed, then power levels of 50 GW and 100 GW correspond to $2,500$ J and $5,000$ J respectively.

Given source power and energy, the considerations made when a microwave is emitted from an antenna must next be discussed.

2.4.2 Antenna Considerations

In order to focus the microwave beam, a metallic parabolic antenna is a strong option. The level to which the beam can be focused by such an antenna is defined by the Rayleigh Criterion. This criterion gives the angular spread of the generated beam (θ_R) as a function of the radiation's wavelength ($\lambda\ in\ m$) and the antenna's diameter ($D\ in\ m$), as shown in Eq.(2.4.b) (Nave).

$$\sin(\theta_R) = \frac{1.22 \cdot \lambda}{D} \tag{2.4.b}$$

Eq. (2.4.b) shows that a wider antenna corresponds to a smaller dispersion rate. Wide antennae are difficult to build, however, and can become quite expensive at larger widths.

The Rayleigh Criterion allows for the width of a beam ($\omega\ in\ m$) at a distance ($R\ in\ m$) away from the beam source to be calculated, as shown in Eq. (2.4.c).

$$\omega = R\sin(\theta_R) = \frac{1.22 \cdot R}{D} \cdot \lambda \tag{2.4.c}$$

As defined, the width of the beam (ω) is related positively to the distance it travels and inversely to the diameter of the antenna used. Thus, as a beam propagates, it naturally diverges, causing the intensity delivered at distances much greater than the antenna diameter ($R \gg D$) to be significantly diminished. This observation has far-reaching implications for HPM systems as will be shown in later sections.

Because we are considering the propagation of electromagnetic waves, which are typically defined by their frequency rather than their wavelength, a substitution can be made.

$$\omega = \frac{1.22 \cdot R}{D} \cdot \frac{c}{f} \tag{2.4.d}$$

Replacing the wavelength (λ) from Eq. (2.4.c) with the speed of light ($c\ in\ m/s$) over the frequency ($f\ in\ Hz$) is shown in Eq. (2.4.d).This convention will be used throughout the report for consistency of variables.

Once emitted from an antenna, the electromagnetic wave will begin to propagate. If the system is based within the Earth's atmosphere, the wave will be attenuated by the atmosphere.

2.4.3 Atmospheric Propagation Effects

The atmosphere, in general, attenuates frequencies in the microwave range less than those in other frequency bands. Because of this phenomenon, they are of particular interest for applications requiring long range electromagnetic propagation. For frequencies above 300 GHz, the atmosphere is effectively opaque, meaning that the atmosphere absorbs a considerable amount of electromagnetic radiation (Crawford, Jordan, Kendall, Powers, & Varni, 1996). Although there are generally small levels of atmospheric attenuation in the microwave region of the electromagnetic spectrum, certain frequencies are attenuated more heavily due to dry air, water vapor, clouds, and rain. Atmospheric "windows" describe the frequencies in which the effects of atmospheric attenuation are minimal. Figure 2.4.c below shows these windows in graphic form.

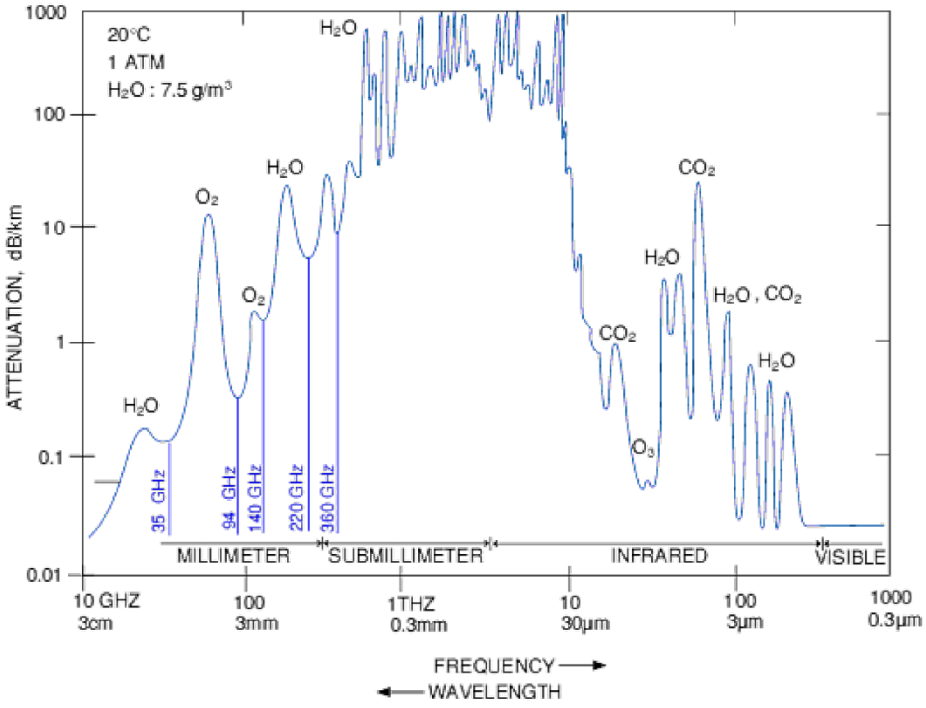

Figure 2.4.c: Atmospheric Attenuation as a Function of Frequency

Due to the makeup of the Earth's atmosphere, the attenuation of electromagnetic waves at different frequencies varies nonlinearly. (Lesurf)

The attenuations levels in dB/km as shown in Figure 2.4.c, for a temperature of 20° C and one atmosphere of pressure at sea level, clearly demonstrate the windows created between peaks of attenuation attributed to the water and oxygen content of the atmosphere. Additionally, the opacity of the atmosphere is shown for frequencies greater than 300 GHz where attenuations in excess of 10 dB/km are reached. Note that at 10 dB/km, the power of an electromagnetic beam is reduced by an order of magnitude for each kilometer traveled.

Additionally, the attenuation is a function of the altitude. As the altitude is increased, the observed attenuation decreases. This relationship is demonstrated by Figure 2.4.d below which depicts atmospheric attenuation rates for nominal altitudes.

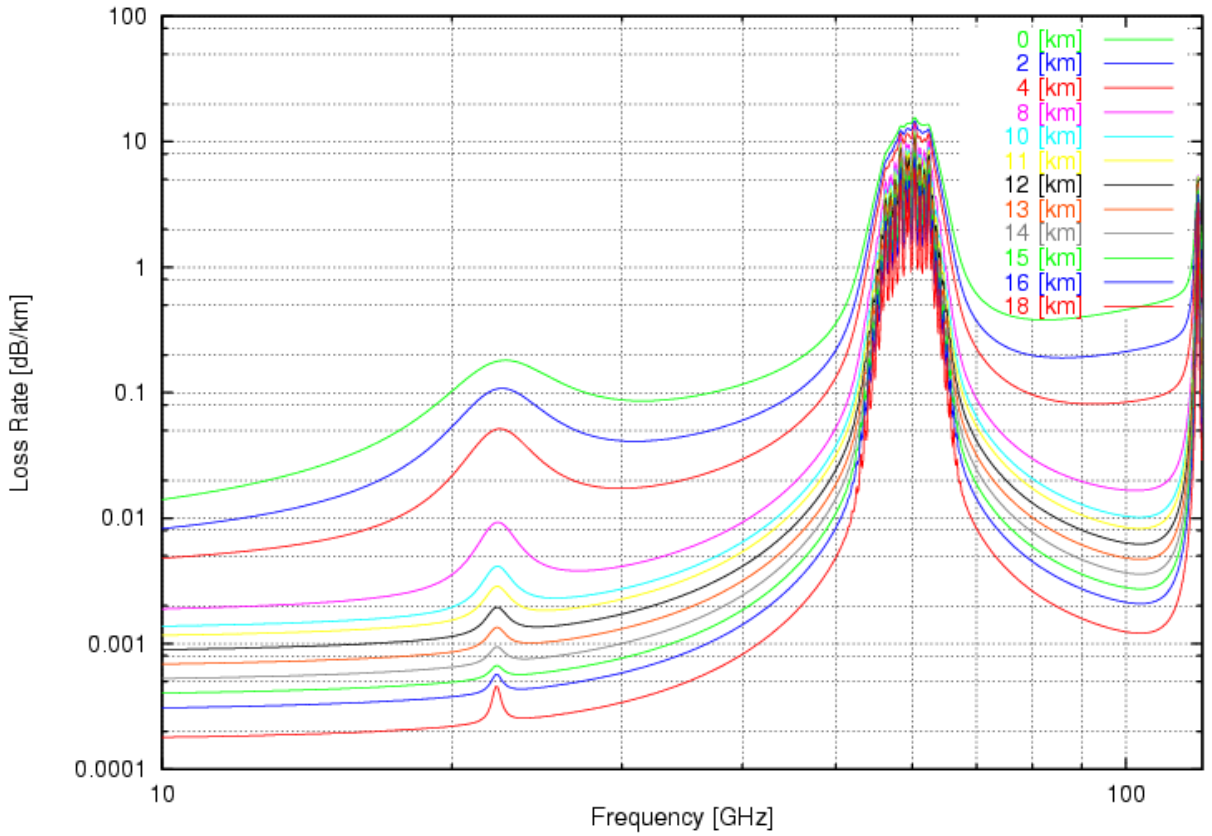

Figure 2.4.d: Atmospheric Attenuation Rates for Nominal Altitudes

As altitude is increased, the rate of signal loss decreases. At 18 km, the atmospheric attenuation at a frequency of 10 GHz is two orders of magnitude less than it is at sea level. (Kopp, 2000)

As seen in Figure 2.4.d above, attenuation rates for frequencies between 50 GHz and 70 GHz, and again at 118 GHz are significant. The former attenuation range coincides with the resonant frequencies of oxygen molecules and is called the 60 GHz complex (Shambayati, 2008). Frequencies outside these ranges are qualified as windows. In these windows, atmospheric attenuation rates drop off as a function of altitude.

To determine the range of an HPM system, attenuation due to the atmosphere must be considered. Given an initial location, pressure, temperature, and firing angle of a ground-based beam, an atmospheric attenuation model can be used to estimate the decibels of power loss encountered. To form an atmospheric model, attenuation due to the atmosphere can be broken into four independent components: attenuation due to dry air ($\gamma_{dry\ air}$), water vapor (γ_{vapor}), rain (γ_{rain}), and clouds (γ_{cloud}). Since the effects of these

components are independent of each other, their individual attenuations may be summed (Shambayati, 2008) to find the total attenuation due to the atmosphere ($\gamma_{total}\ in\ dB/km$). To reiterate, as seen above Figure 2.4.d, atmospheric attenuation is a function of altitude. To account for this relationship in an atmospheric model, each of the aforementioned components, and thus the sum as a whole, can be modeled as a function of the altitude ($h\ in\ km$) above sea level. The total attenuation of the atmosphere (γ_{total}) is thus described by Eq. (2.4.e).

$$\gamma_{total}(h) = \gamma_{dry\ air}(h) + \gamma_{vapor}(h) + \gamma_{rain}(h) + \gamma_{cloud}(h) \tag{2.4.e}$$

As the creation of a complete atmospheric model was beyond the scope of this project, a combination of existing models was used. Seen in Eqs. (2.4.f) and (2.4.j) from (Zhang, 1997), both $\gamma_{dry\ air}(h)$ and $\gamma_{vapor}(h)$ can be modeled as functions of altitude ($h\ in\ km$) for a given frequency ($f\ in\ GHz$). Furthermore, they both incorporate models for pressure ($P(h)\ in\ mbar$) and the temperature ($T_p(h)\ in\ K$) as functions of altitude. Additionally, γ_{vapor} incorporates water vapor density ($\rho(h)\ in\ \ g/m^3$) as a function of altitude as well.

It is important to note that these models, along with the other models presented in this section, are curve-fits that closely approximate measured values for atmospheric attenuation levels. Furthermore, note that while Eq. (2.4.f) ignores attenuation values between frequencies of 57 GHz and 63 GHz, this range is within the 60 GHz complex and therefore would not be considered for a ground-based HPM system. Thus, such an omission is acceptable within the scope of this project.

Attenuation due to dry air can be modeled as:

$$\gamma_{dry\ air}(h) = \begin{cases} \gamma_{da_{57}}(h) \cdot \gamma_{da_{end}}(h), & f \leq 57\ GHz \\ \gamma_{da_{63}}(h) \cdot \gamma_{da_{end}}(h), & 63\ GHz \leq f < 350\ GHz \end{cases} \quad (2.4.f)$$

Where $\gamma_{da_{57}}(h)$, $\gamma_{da_{63}}(h)$, and $\gamma_{da_{end}}(h)$ are given by:

$$\gamma_{da_{57}}(h) = \left[\frac{7.27 r_t(h)}{f^2 + 0.351 r_p(h)^2 r_t(h)^2} + \frac{7.5}{(f-57)^2 + 2.44 r_p(h)^2 r_t(h)^5}\right] \quad (2.4.g)$$

$$\gamma_{da_{63}}(h) = \left[2 \cdot 10^{-4} r_t(h)^{1.5}(1 - 1.2 \cdot 10^{-5} f^{1.5}) + \frac{4}{(f-63)^2 + 1.5 r_p(h)^2 r_t(h)^5} + \frac{0.28 r_t(h)^2}{(f-118.75)^2 + 2.84 r_p(h)^2 r_t(h)^2}\right] \quad (2.4.h)$$

$$\gamma_{da_{end}}(h) = f^2 r_p(h)^2 r_t(h)^2 \cdot 10^{-3} \quad (2.4.i)$$

Attenuation due to water vapor can be modeled as:

$$\gamma_{vapor}(h) = [\gamma_{vA}(h) + \gamma_{vB}(h)] \cdot \gamma_{v_{end}}(h) \quad (2.4.j)$$

Where $\gamma_{vA}(h)$, $\gamma_{vB}(h)$, and $\gamma_{v_{end}}(h)$ are given by:

$$\gamma_{vA}(h) = 3.27 \cdot 10^{-2} r_t(h) + 1.67 \cdot 10^{-3} \frac{\rho(h) r_t(h)^7}{r_p(h)} + 7.7 \cdot 10^{-4} f^{0.5} + \frac{3.79}{(f-22.235)^2 + 9.18 r_p(h)^2 r_t(h)} \quad (2.4.k)$$

$$\gamma_{vB}(h) = \frac{11.73 r_t(h)}{(f-183.31)^2 + 11.85 r_p(h)^2 r_t(h)} + \frac{4.01 r_t(h)}{(f-325.153)^2 + 10.44 r_p(h)^2 r_t(h)} \quad (2.4.l)$$

$$\gamma_{v_{end}}(h) = f^2 \rho(h) r_p(h) r_t(h) 10^{-4} \quad (2.4.m)$$

Where $r_p(h) = \frac{P(h)}{1013}$ and $r_t(h) = \frac{288}{T_p(h)}$. (Zhang, 1997)

NASA's Jet Propulsion Laboratory's Deep Space Network's surface weather model is used to model temperature as a function of height ($T_p(h)$), as is shown in Eq. (2.4.n). The function $T_{US}(h)$, referenced in Eq. (2.4.n), refers to the U.S. Standard Atmosphere model and is shown in Eq. (2.4.o).

$$T_p(h) = \begin{cases} T_{h_0} + \dfrac{h - h_0}{2}\left(T_{US}(h_0 + 2) - T_{h_0}\right) & h_0 \le h \le h_0 + 2 \\ T_{US}(h) & h_0 + 2 < h \le 20 \\ 217 & 20 < h \le 30 \end{cases} \tag{2.4.n}$$

$$T_{US}(h) = \begin{cases} 288.16 - 6.5h & h < 10.95\ km \\ 217 & 10.95\ km \le h < 20\ km \\ 197 + h & otherwise \end{cases} \tag{2.4.o}$$

(Shambayati, 2008)

NASA's model also models pressure as a function of height ($P(h)$). Shown in Eq. (2.4.p), P_{h_0} is the pressure measured at an altitude of h_0.

$$P(h) = P_{h_0} \cdot e^{\left(\frac{8.387(h_0 - h)}{(8.387 - 0.0887h_0)(8.387 - 0.0887h)}\right)} \tag{2.4.p}$$

(Shambayati, 2008)

Seen in Eqs. (2.4.q) through (2.4.s) from (Shambayati, 2008), $\gamma_{rain}(h)$ is modeled as a function of altitude ($h\ in\ km$) for a given frequency ($f\ in\ GHz$). Furthermore, the model incorporates a model for the rainfall rate ($r(h)\ in\ mm/hr$) as a function altitude.

$$\gamma_{rain}(h) = a_{rain}(f) r(h)^{b_{rain}(f)} \tag{2.4.q}$$

$$a_{rain}(f) = \begin{cases} 6.39 \cdot 10^{-5} f^{2.03} & f \le 2.9\ GHz \\ 4.21 \cdot 10^{-5} f^{2.42} & 2.9\ GHz < f \le 54\ GHz \\ 4.9 \cdot 10^{-2} f^{0.699} & 54\ GHz < f < 180 GHz \end{cases} \tag{2.4.r}$$

$$b_{rain}(f) = \begin{cases} 0.851 f^{0.158} & f \le 8.5\ GHz \\ 1.41 f^{-0.0779} & 8.5\ GHz < f \le 25\ GHz \\ 2.65 f^{-0.272} & 25\ GHz < f < 164\ GHz \end{cases} \tag{2.4.s}$$

(Shambayati, 2008)

Finally, as shown in Eq. (2.4.t) from (Shambayati, 2008), γ_{cloud} is modeled as a function of altitude ($h\ in\ km$) for a given frequency ($f\ in\ GHz$). Furthermore, it incorporates a model for the liquid water content profile of the atmosphere ($p_{lwc}(h)\ in\ g/m^3$) and the temperature ($T_p(h)\ in\ K$) as functions of altitude.

$$\gamma_{cloud}(h) = p_{lwc}(h) \cdot f^{1.95} \cdot e^{1.5735 - 0.0309 \cdot T_p(h)} \tag{2.4.t}$$

(Shambayati, 2008)

Given initial conditions for all variables in this section, a function for the total atmospheric attenuation as a function of height, $\gamma_{total}(h)$ as described in Eq. (2.4.e), can be found. Most of these conditions, while numerous, can be calculated or measured at the time of interest. This total attenuation is used to calculate the loss in signal power as a beam travels through the atmosphere. However, once the electromagnetic beam has propagated to its target, the beam must also penetrate the target's shielding.

2.4.4 Target Penetration

Faraday cages present an effective defense to an HPM weapon as they prevent electromagnetic waves from entering the inside of the cage. A perfect faraday cage is made by completely enclosing a volume inside of an ideal conductor. Implementing a perfect faraday cage on an ICBM is not possible due to the complex nature of the weapon. A report published in 1973, which specifically looked at the effects of electromagnetic radiation on an early ballistic missile, asserts that a maximum level of shielding exists:

> *In a large weapon system, total shielding for levels above* 40 *dB are very difficult to attain because of the numerous interfaces and different materials used in the shielding structure. (Cox, 1973)*

The various stages of an ICBM must interface with each other to operate properly. Due to these stages, there exist discontinuities in surface planes and materials which would act as

windows to damaging electromagnetic radiation. Thus, 40 dB is used as a baseline value for the electromagnetic shielding that an HPM system must overcome to be effective. Once the shielding of a target is penetrated, the energy carried in the wave must be coupled to a target.

2.4.5 Physics of Microwave-Target Coupling

Since microwaves are defined at a frequency range which is several orders of magnitude lower than lasers, they carry a significantly smaller amount of energy. As such, microwaves are unsuitable for the melting or vaporization of a target through the transfer of energy. Instead, microwaves are more suited to the goal of a soft kill, in this case the disruption of the guidance systems of an intercontinental ballistic missile.

The ability of a microwave system to achieve a soft kill is dependent on the particular vulnerabilities of the target. Any part of the missile that is entirely encased in a metallic surface is well-protected from microwave radiation, since microwaves are reflected by such surfaces. However, "due to their long wavelength, microwaves are strongly diffracted as they pass through small apertures and can irradiate areas which would seem to be well shielded by the target's external surface" (Nielsen, 1994). These small apertures present opportunities for the microwaves to enter the target and damage the target's circuits.

If any part of the target's systems contains microwave receivers, the target may have a high vulnerability to HPM systems. If the HPM system operates at the same frequency as the target's receivers, the HPM system could send radiation that reaches the target at too great an intensity for the target to handle. If the signals received have a sufficiently high intensity, currents will be induced which can heat and, ideally, burn out wires and other elements in the target's circuitry. The amount of power, and therefore energy, dissipated within a wire is related to the square of current. As such, a great enough induced current can deposit more energy and heat into the wire than the target's heat sinks and cooling systems can handle, causing the wire to melt. This type of damage requires intensities of only 10^{-4} to $10^{-2}\ W/m^2$ on target. (Nielsen, 1994)

If a microwave receiver does not exist within the target, an HPM system can deliver a kill through the deposition of raw power into the target's circuits. Sensitive electronic components can absorb enough energy from microwave radiation to burn out. Even without a microwave receiver, microwave radiation can still induce currents, since the radiation is a time-dependent electromagnetic field. Additionally, if a microwave system were able to ignite plasmas at the surface of the target, a higher amount of radiation could be coupled to the target. However, the intensity threshold for such a reaction to occur is in the range of 10^6 to 10^7 W/m^2. (Nielsen, 1994)

Additionally, a study performed by the United States Air Force states that circuit disruption requires intensity levels of 10^{-2} to 10^1 W/m^2 for commercial devices (Crawford, Jordan, Kendall, Powers, & Varni, 1996).

The three ranges identified in this section to effective couple electromagnetic radiation to a target are identified in Figure 2.4.e on a logarithmic scale.

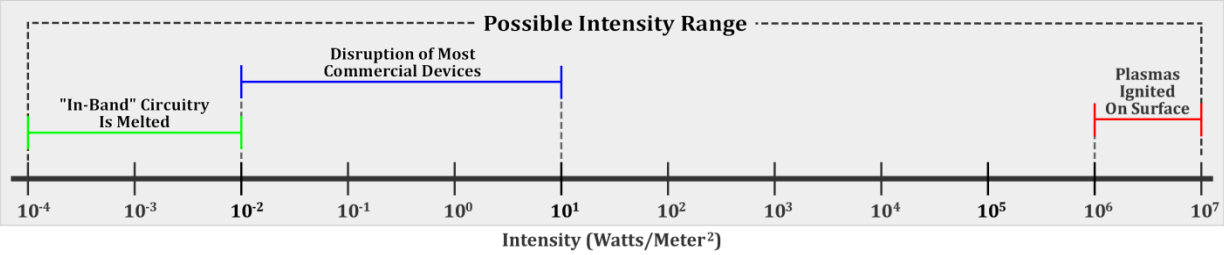

Figure 2.4.e: HPM Intensity Range on Logarithmic Scale

The three ranges of intensities found to effectively couple electromagnetic radiation to a target are shown on a logarithmic scale spanning eleven orders of magnitude.

Clearly a large range of intensities can be considered. Once an electromagnetic wave has delivered some level of intensity onto a target, the target can respond in a number of ways.

2.4.6 Target Response

Microwave beams have empirically demonstrated an ability to disrupt or destroy circuitry. Eureka Aerospace has created a system that remotely disables cars by using

microwave beams to disrupt or destroy the engine control unit circuitry. The system's power specifications were detailed in a recent report:

> *The device's peak power output is two gigawatts, although the average power emitted in a single shot is about 100 watts. Each radiated pulse lasts about 50 nanoseconds. All the test cars' engines were shut off using a single pulse at a distance of approximately 15 meters, making the total energy output 100 joules… (Sauser, 2007)*

A report to congress in 2008 also detailed the ability for HPM weapons to destroy electronics, "An HPM weapon has a shorter possible range than HEMP, but it can induce currents large enough to melt circuitry..." (Wilson, 2008). The report goes on to state that in addition to short-order effects, such as the physical destruction of circuitry long-order effects can also occur. For example, U.S. Comanche helicopter was responsible for a two-week disruption of global positioning systems after running a radar test involving HPM weapons in Albany, New York.

The specific response witnessed by a given target is a function of the target itself, the power levels involved, the frequency, and the underlying physics of such interactions.

2.4.7 Definition of Success for Soft Kill

Since the method of destruction for an HPM system is not a hard kill, such as the vaporization of a target, it is not obvious as to what qualifies a success. Unfortunately, there is no instant visual feedback to say whether or not the system was effective. However, because the missile's navigational systems have been neutralized, its trajectory is entirely subject to atmospheric effects, and is now highly dependent on wind and drag. If an intercept is achieved, the missile's final destination may be so uncertain that the enemy decides not to arm the payload. Small uncertainties in the initial part of a several thousand kilometer path can lead to very high uncertainties in a missile's end position. As the effects of atmosphere are unpredictable, however, it is difficult to quantify the amount by which a missile will miss its target.

2.5 Platform Realms of Deployment

Defense platforms can be deployed into a number of different realms such as land, sea, air, and space. Each realm has natural considerations which must be made when discussing the deployment of defensive platforms. Specifically, this project examines ground, which is a combination of land and sea, and space-based realms of deployment for HPM systems.

2.5.1 Ground-Based Platforms

All currently deployed missile defense systems employ ground-basing and are located either on land bases or upon naval vessels. The stationary nature of ground-based platforms is in many ways advantageous. The weight and size of such systems is often of minimal concern, while the ability to easily apply repairs and upgrades reduces the redundancies which must be built in. Furthermore, ground-based systems often have access to high quality power sources which are difficult to attain in other realms.

In addition to these advantages, however, ground-based systems do face a number of obstacles. Unlike satellite-based systems, ground-based systems must consider the effects of the atmosphere. High-powered microwaves, depending on the operational frequency, may be attenuated heavily as they pass through the atmosphere. This effect must be compensated for by increasing system parameters such as signal power, antenna diameter, or by selecting operating frequencies which fall into the natural attenuation windows, which are shown in Figure 2.4.d.

Another issue for ground-based systems concerns the politics of platform location. Being as it is not possible to place these systems inside the country of concern, they must be placed as close as possible, potentially residing on foreign, albeit friendly, territory. The range of such systems must therefore be capable of reaching from the proximity of the threat country's borders and into its center in order to be capable of guaranteeing coverage.

2.5.2 Space-Based Platforms

Space-based platforms address many of the drawbacks of ground-based systems. For one, the HPM system operates out of the atmosphere, removing effects of atmospheric attenuation. Secondly, political borders do not exist in space, allowing systems to directly pass over threat regions.

As shown in Eq. (2.4.d), the width of HPM's beam diverges over distance - a natural phenomenon which reduces the delivered intensity of the beam. As such, it is beneficial to place space-based HPM systems in lower orbits to limit signal power requirements. Pursuing this benefit, however, necessitates the use of low Earth orbits (LEOs), as opposed to medium Earth orbits (MEOs) or geosynchronous orbits (GEOs).

2.5.2.1 Earth Orbits

There are three main altitude bands of geocentric orbits that can be considered for missile defense platforms. They are LEOs (low Earth orbits), MEOs (medium Earth orbits), and GEOs (geosynchronous orbits) as Figure 2.5.a demonstrates below.

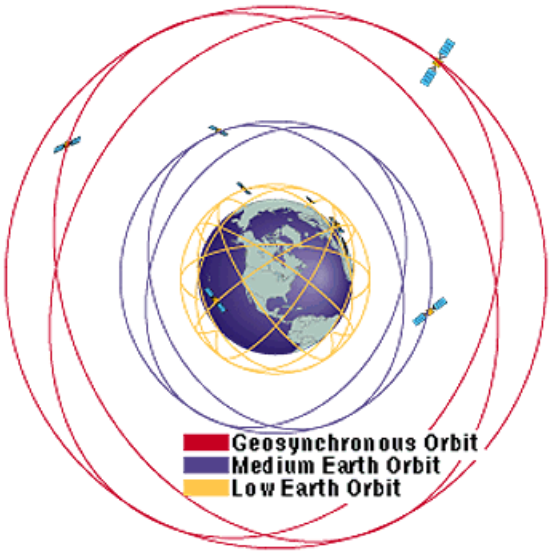

Figure 2.5.a: Various Types of Earth Orbits

Low Earth, medium Earth, and geosynchronous orbits, some of possible orbits that can be achieved, each correspond to a specific altitude band. Distances not to scale. (Federation of American Scientists, 1998)

LEOs (low Earth orbits) have the advantage of being relatively close to the target, reducing requirements on initial power for HPMs. Although these orbits are defined as being from 0-2,000 kilometers in altitude (Vallado, 2007), orbits below 300 kilometers have too much atmospheric drag to remain useful for more than a few years (Barton, et al., 2004). Because of their low altitudes, satellites in LEO have short orbital periods (roughly between 90 and 120 minutes) and consequently their coverage zones relative to the Earth move quickly as a function of time. This movement necessitates constellations of satellites, seen in Figure 2.5.b, to achieve continuous global coverage.

Figure 2.5.b: Low Earth Orbit Satellite Constellation

Low Earth orbits often make use of satellite constellations in order to achieve reliable coverage. Distances not to scale. (Kowoma, 2009)

As the total cost of a space-based system is related closely to its total mass, the addition of satellites to complete a constellation can be prohibitively expensive. Currently, placing payloads into LEO costs approximately $3,000-5,000 per kilogram (Space Exploration Technologies Corporation, 2010).

MEOs (medium Earth orbits) can range in altitude from 2,000 to below 35,786 kilometers with orbital periods ranging from two to just under 24 hours (Vallado, 2007). The coverage zone of a satellite in MEO moves as a function of time, though at a reduced pace as compared to LEOs. While favorable to applications such as communications, HPM

systems do not share in this regard. A MEO necessitates achieving ranges in excess of 2,000 kilometers, a requirement which is prohibitive.

Geosynchronous orbit (GEO) corresponds to an orbital altitude of 35,786 kilometers, giving the satellite an orbital period equal to the earth's rotational period (Vallado, 2007). This period means that the satellite looks down upon roughly the same area over time. However, because of the long distance from the target, the accuracy and power required for directed energy weapons is again prohibitive.

Each of the aforementioned orbit types, LEO, MEO, and GEO, correspond to ranges of orbital altitudes. Along with orbital altitude, inclination can be considered. Inclination is the angle between the plane of Earth's equator and the orbital plane of the satellite. If this angle is 90 degrees, the orbit is called a polar orbit. Polar orbits employ the only inclination which results in a path of coverage which crosses over every latitude in a single orbital period. Consequently, satellites in a polar orbit have the opportunity to cover every part of Earth as the Earth rotates underneath them. Thus, polar orbits are preferable when attempting to achieve continuous Earth coverage. A constellation of satellites in low polar orbit can be seen in Figure 2.5.c below.

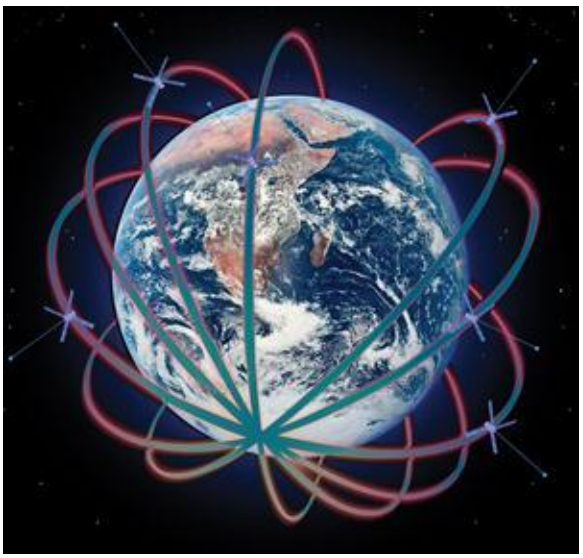

Figure 2.5.c: Constellation of Low Earth Polar Orbits

Satellites in polar orbits can be thought of as orbiting parallel to lines of longitude. Thus, if a constellation of satellites in polar orbit is employed, the distance between the various rings of such a constellation would be

greatest at the equator of the Earth. Satellites in polar orbit cross over every line of latitude in a single orbital period. Distances not to scale. (Clark, Langer, & Powell, 2010)

Satellites in polar orbits can be thought of as orbiting along lines of longitude. Thus, if a constellation of satellites in polar orbit is employed, the distance between the various rings of such a constellation would be greatest at the equator of the Earth.

3 Methods

In order to ensure a mission kill, an HPM system must deliver a minimum level of power per unit area, i.e. intensity, onto a target ($I_{req}\ in\ W/m^2$). This quantity places an upper bound on a high-powered microwave (HPM) system's range. Section 3.1 derives the maximum vacuum range (R_{vac}), where R_{vac} is the distance a microwave beam can travel in free space while delivering a level of intensity greater than or equal to I_{req}.

3.1 Maximum Vacuum Range

To find the maximum vacuum range (R_{vac}), it is first necessary to find the intensity delivered at an arbitrary distance. The intensity delivered ($I_d\ in\ W/m^2$) by a microwave beam, at a distance ($R\ in\ m$), is found by taking the system's source power ($P\ in\ W$) and dividing it by the area of the beam at that distance ($A_{beam}(R)$), as is shown in Eq. (3.1.a).

$$I_d = \left(\frac{P}{A_{beam}(R)}\right) \tag{3.1.a}$$

Assuming a circular antenna, Eq. (2.4.d), which employs the Rayleigh Criterion (see Section 2.4.2) to calculate the width of the beam ($\omega(R)\ in\ m$) at a distance (R) from the source, is used to define the area of the beam at that distance using the equation for the area of a circle with a radius $r(R) = \frac{\omega(R)}{2}$, as is shown in Eq. (3.1.b).

$$A_{beam}(R) = \pi \cdot r(R)^2 = \pi \cdot \left(\frac{\omega(R)}{2}\right)^2 \tag{3.1.b}$$

Substituting Eq. (2.4.d), for the width of the beam (ω), then gives the circular area of the beam in terms of the distance (R), the speed of light ($c\ in\ m/s$), the antenna diameter ($D\ in\ m$), and the operating frequency of the beam ($f\ in\ Hz$), as is seen in Eq. (3.1.c).

$$A_{beam}(R) = \frac{\pi}{4} \cdot \left(\frac{1.22 \cdot R \cdot c}{D \cdot f}\right)^2 \tag{3.1.c}$$

Finally, substituting the beam area ($A_{area}(R)$) into Eq. (3.1.a) gives the delivered intensity, as shown in (3.1.d).

$$I_d = \left(\frac{P}{\frac{\pi}{4} \cdot \left(\frac{1.22 \cdot R \cdot c}{D \cdot f} \right)^2} \right) = \frac{4 \cdot P}{\pi} \cdot \left(\frac{D \cdot f}{1.22 \cdot R \cdot c} \right)^2 \tag{3.1.d}$$

Next, the electromagnetic shielding of the target must be considered. The electromagnetic shielding ($\gamma_s \; in \; dB$) of a given target is measured in decibels of loss and is thus computed using a ratio of the system's source power (P) to the power which penetrates a missile's shielding ($P_{penetration} \; in \; W$), as shown in (3.1.e).

$$\gamma_s = 10 \cdot \log_{10} \left(\frac{P}{P_{penetration}} \right) \tag{3.1.e}$$

To find the intensity delivered onto a target ($I_{d_t} \; in \; W/m^2$) at R meters from the source after penetrating through γ_s decibels of shielding, the delivered intensity, defined above in Eq. (3.1.d) as I_d, is multiplied by the inverse of the logarithmic power ratio. This relationship is shown below in Eq. (3.1.f).

$$I_{d_t} = I_d \cdot \left(\frac{P_{penetration}}{P} \right) \tag{3.1.f}$$

Using the properties of logarithms, one can extract the inverse of the power ratio from the electromagnetic shielding level (γ_s), as shown in Eq. (3.1.g) through Eq. (3.1.j).

$$x = \log_{10}(b^x) \tag{3.1.g}$$

$$-\gamma_s = 10 \cdot \log_{10} \left(\left(\frac{P}{P_{penetration}} \right)^{-1} \right) \tag{3.1.h}$$

$$-\frac{\gamma_s}{10} = \log_{10} \left(\frac{P_{penetration}}{P} \right) \tag{3.1.i}$$

$$\frac{P_{penetration}}{P} = 10^{\left(\frac{-\gamma_s}{10}\right)} \tag{3.1.j}$$

Thus, an equation for the intensity delivered onto a target (I_{d_t}) is found by substituting the values for I_d and $\left(\frac{P_{penetration}}{P}\right)$ into Eq. (3.1.f).

$$I_{d_t} = I_d \cdot \left(\frac{P_{penetration}}{P}\right) = \left(\frac{4 \cdot P}{\pi} \cdot \left(\frac{D \cdot f}{1.22 \cdot R \cdot c}\right)^2\right) \cdot 10^{\left(\frac{-\gamma_s}{10}\right)} \tag{3.1.k}$$

$$I_{d_t} = \frac{4 \cdot P \cdot 10^{\left(\frac{-\gamma_s}{10}\right)}}{\pi} \cdot \left(\frac{D \cdot f}{1.22 \cdot R \cdot c}\right)^2 \tag{3.1.l}$$

The maximum vacuum range (R_{vac}) is defined at the point where the intensity delivered onto a target (I_{d_t}) is equal to minimum required intensity (I_{req}). The maximum vacuum range can therefore be found by solving Eq. (3.1.l) for R with I_{d_t} set equal to I_{req}, as shown in Eq. (3.1.m).

$$R_{vac} = \frac{2 \cdot D \cdot f}{1.22 \cdot c \cdot \sqrt{\pi}} \sqrt{\frac{P \cdot \left(10^{-\left(\frac{\gamma_s}{10}\right)}\right)}{I_{req}}} \tag{3.1.m}$$

Eq. (3.1.m) above shows that the maximum range (R_{vac}) is positively influenced by frequency ($f\ in\ Hz$), antenna diameter ($D\ in\ m$), and signal power ($P\ in\ W$), while being negatively influenced by the required intensity ($I_{req}\ in\ W/m^2$) and the electromagnetic shielding of the target ($\gamma_s\ in\ dB$).

3.2 Target Critical Altitude

An ICBM flying a downrange distance of 5,500 kilometers has a characteristic altitude (h_b) and time (t_b) for when it leaves boost phase. Additionally, there exists a time margin (t_m) in which an HPM system must engage an ICBM prior to the completion of boost phase in order to induce enough navigational error to qualify for a mission kill. The altitude corresponding to the end of boost time (t_b) minus the margin time (t_m) is called

the critical altitude (h_c). The critical altitude describes the greatest height that an ICBM travelling 5,500 kilometers can be hit during the boost phase while still providing a great enough margin to induce a mission killing error.

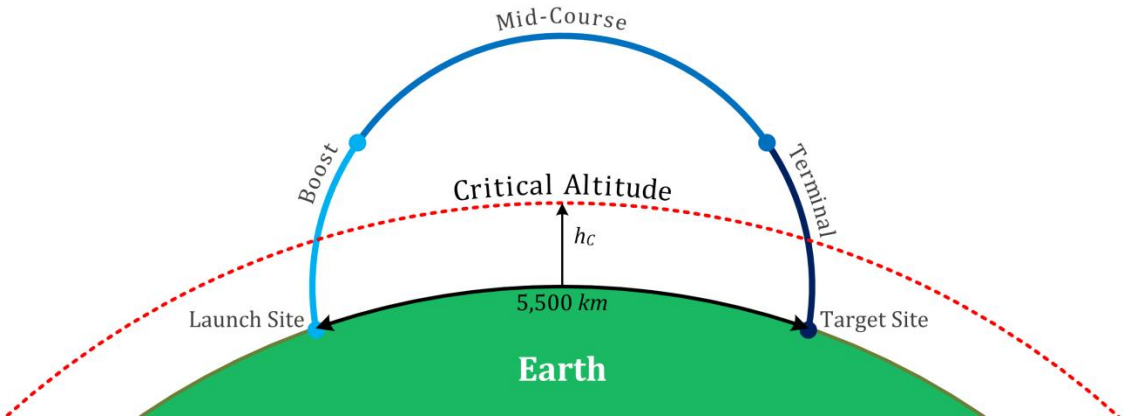

Figure 3.2.a: Critical Altitude Explained

For an ICBM flying a downrange distance of 5, 500 km, there exists a critical altitude. The critical altitude, seen here as a dotted red line, describes the greatest height the ICBM can be hit during the boost phase while still inducing a mission killing error. Distances are not to scale.

ICBMs flying distances greater than 5,500 kilometers have characteristic altitudes (h_{b*}) and times (t_{b*}) that are greater than h_b and t_b because these ICBMs must spend a greater amount of time in boost phase due to the increased energy requirements of travelling longer distances. Consequently, its critical altitude (h_{c*}) will be greater as well, since t_m remains constant. Therefore, all ICBMs of a given type are guaranteed to travel through h_c with at least the minimum margin time remaining regardless of downrange distance travelled. Consequently, an HPM system which is capable of targeting an ICBM flying a downrange distance of 5,500 km would be able to successfully intercept ICBMs travelling greater downrange distances as well.

3.3 Ground-Based System Analysis

A ground-based HPM is defined as any system which is either land or sea-based. Discussed in detail below, the proximity of a ground-based system to the surface of the Earth raises unique considerations. The fired microwave beam must propagate through the atmosphere, encountering attenuation not previously accounted for in the maximum

vacuum range. Thus, an atmospheric attenuation model must be used to calculate the attenuated range of the beam. Next, the curvature of the Earth must be considered when calculating the altitude of the beam above the surface. In this regard, the use of a Cartesian coordinate system and a spherical Earth model can greatly simplify the geometry of the system. Additionally, the concept of a system's downrange must be introduced to precisely describe the surface area covered by a single installment. And finally, the effective range of a system must be defined.

As a microwave beam propagates, the atmosphere attenuates the intensity it can apply to a target, thus decreasing its range. As shown in Section 2.4.3, atmospheric attenuation is modeled as a function of altitude above sea level ($h\ in\ km$) for a given frequency ($f\ in\ GHz$). Before this model is utilized, however, the geometry of a ground-based system must first be defined.

3.3.1 System Geometry

The Earth is modeled as a sphere with a radius (R_E) equal to the Earth's equatorial radius ($R_E = 6{,}378.1\ km$). A two-dimensional cross-section of this spherical Earth model is be placed in a Cartesian coordinate system with the topmost point of the Earth's surface residing at the origin (for ground-basing analysis only) and the center of the cross-section residing at the point $(0, -R_E)$. The position of a single ground-based system deployed at or above this topmost point is described solely by its altitude (h_0) above the surface, as illustrated in Figure 3.3.a below.

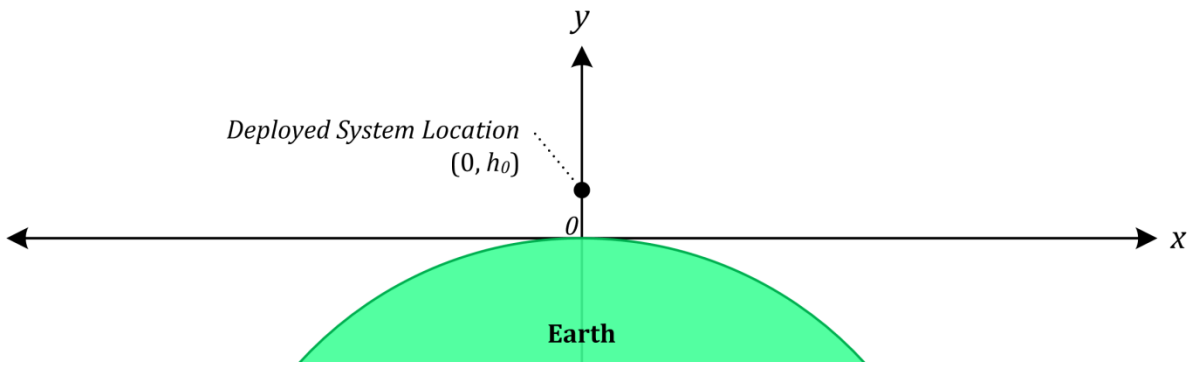

Figure 3.3.a: Ground-Based Deployed System Geometry

When modeled as a sphere, a cross-section of the Earth is placed in a Cartesian coordinate system with the topmost point of the Earth's surface residing at the origin. The position of a single ground-based system at or above this topmost point is described solely by its altitude (h_0) above the surface.

For a ground-based HPM, if deployed as seen in the geometry of Figure 3.3.a above, the microwave beam itself is described by a vector ($\boldsymbol{R_{beam}}$). This vector, extending from the deployed system location $(0, h_0)$, is defined at a firing angle ($\theta\ in\ radians$), which ranges between 0 and $\pi\ radians$ as measured from the local horizon. The endpoint of the beam vector, which is defined as (x_r, y_r), represents the farthest point at which the minimum required intensity (I_{req}) is delivered by the beam. Furthermore, a second vector ($\boldsymbol{h_{beam}}$) is drawn normal to the surface of the Earth such that its magnitude represents the minimum distance, i.e. altitude, between the surface of the Earth and the point (x_r, y_r). Finally, the distance along the surface of the Earth from the origin to the base of the vector $\boldsymbol{h_{beam}}$ is measured. This distance, henceforth referred to as the downrange distance (R_{dr}), represents the farthest point on the surface of the Earth which is covered by the beam described by the $\boldsymbol{R_{beam}}$ vector. The geometry of Figure 3.3.a is extended below by Figure 3.3.b to depict these concepts.

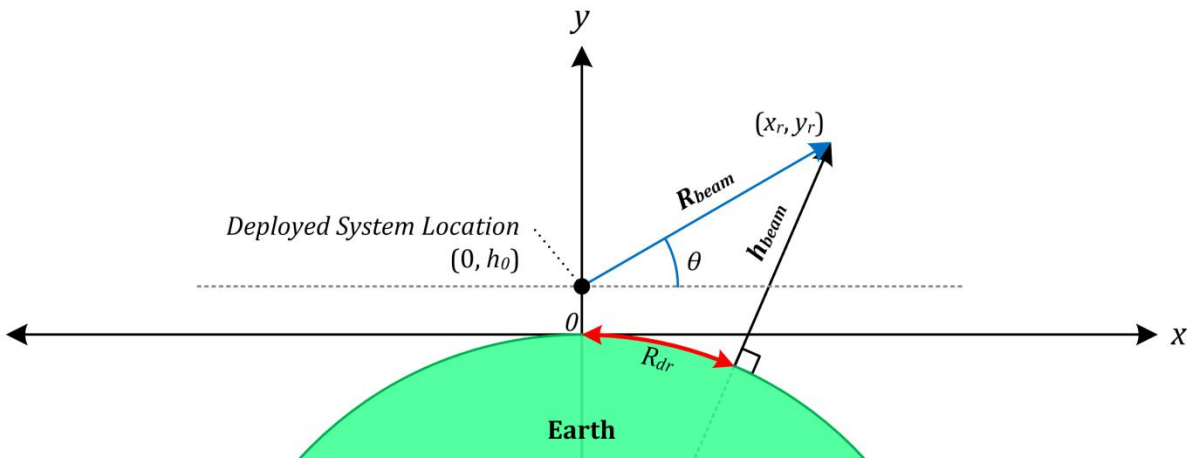

Figure 3.3.b: Ground-Based Beam Range Geometry

For a system deployed at $(0, h_0)$, a microwave beam fired at an angle (θ) is described by the R_{beam} vector. An altitude vector (h_{beam}) is drawn normal to the surface of the Earth such that its magnitude represents the altitude of (x_r, y_r). Finally, the downrange distance (R_{dr}) of the beam described by the R_{beam} vector is measured along the surface of the Earth from the origin to the base of the h_{beam} vector.

The endpoint coordinates (x_r, y_r) of the vector $\boldsymbol{R_{beam}}$, is defined as shown in Eqs. (3.3.a) and (3.3.b).

$$x_r = R_{beam}\cos(\theta) \tag{3.3.a}$$

$$y_r = R_{beam}\sin(\theta) + h_0 \tag{3.3.b}$$

For the geometry depicted in Figure 3.3.b, it is necessary to derive a means of calculating the downrange distance (R_{dr}), as well as the magnitude of $\boldsymbol{h_{beam}}$, for any arbitrary $\boldsymbol{R_{beam}}$ vector. This calculation is accomplished via linear algebra by introducing the vectors $\boldsymbol{R_E}$, $\boldsymbol{R_{h_0}}$, and $\boldsymbol{R_{sum}}$. The vector $\boldsymbol{R_E}$, which has a magnitude equal to the equatorial radius of the Earth (R_E), extends from the point $(0, -R_E)$ to the origin. The vector $\boldsymbol{R_{h_0}}$, which has a magnitude equal to the system deployment altitude (h_0), extends from the origin to the deployed system location. Finally, as seen in Eqs. (3.3.c) and (3.3.d), the vector $\boldsymbol{R_{sum}}$, which has a magnitude equal to the magnitude of $\boldsymbol{h_{beam}}$ plus the magnitude of $\boldsymbol{R_E}$, is the summation of the vectors $\boldsymbol{R_E}$ and $\boldsymbol{R_{h_0}}$ with $\boldsymbol{R_{beam}}$ and is placed at the deployed system location.

$$\|\boldsymbol{R_{sum}}\| = R_{sum} = R_E + h_{beam} \tag{3.3.c}$$

$$\boldsymbol{R_{sum}} = \boldsymbol{R_E} + \boldsymbol{R_{h_0}} + \boldsymbol{R_{beam}} \tag{3.3.d}$$

The geometry of Figure 3.3.b is extended below in Figure 3.3.c to depict these additional vectors.

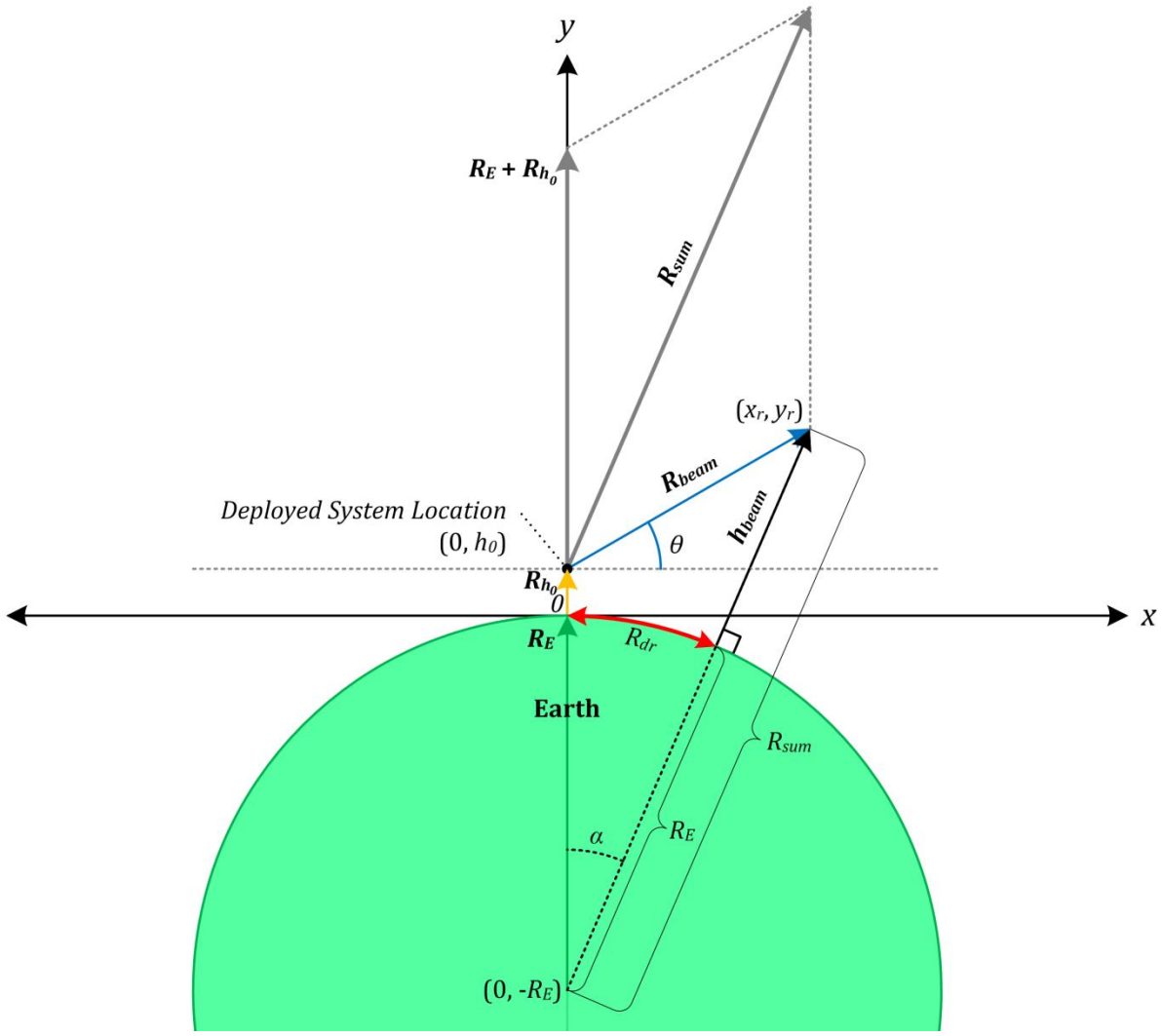

Figure 3.3.c: Complete Ground-Based Beam Range Geometry

The vectors R_E, R_{h_0}, and R_{sum} are used to calculate the values of the downrange distance (R_{dr}), as well as the magnitude of h_{beam}, for any arbitrary R_{beam} vector.

We will begin by deriving an equation for the downrange distance (R_{dr}), given an arbitrary $\boldsymbol{R_{beam}}$ vector. Note that, as shown in Figure 3.3.c, the downrange distance is the

arc of a circle defined by the angle α and the radius of the Earth (R_E). Thus it may be calculated as seen in Eq. (3.3.e).

$$R_{dr} = \alpha \cdot R_E \tag{3.3.e}$$

The angle θ between two vectors $\mathbf{v}$ and $\mathbf{w}$ is defined as seen in Eq. (3.3.f). Thus, the angle α may be found by applying this formula to the vectors $\mathbf{R_E}$ and $\mathbf{R_{sum}}$ and then applying the inverse cosine. This calculation is shown below in Eqs. (3.3.f) through (3.3.h).

$$\cos(\theta) = \frac{\mathbf{v} \cdot \mathbf{w}}{\|\mathbf{v}\|\|\mathbf{w}\|} \tag{3.3.f}$$

$$\cos(\alpha) = \frac{\mathbf{R_E} \cdot \mathbf{R_{sum}}}{R_E R_{sum}} = \frac{R_E(R_E + R_{beam}\sin(\theta))}{R_E\sqrt{{R_{beam}}^2 + {R_E}^2 + 2 \cdot R_{beam} \cdot R_E \sin(\theta)}} \tag{3.3.g}$$

$$\alpha = \cos^{-1}\left(\frac{(R_E + R_{beam}\sin(\theta))}{\sqrt{{R_{beam}}^2 + {R_E}^2 + 2 \cdot R_{beam} \cdot R_E \sin(\theta)}}\right) \tag{3.3.h}$$

Thus, the downrange distance may be found by substituting α, as seen in Eq. (3.3.h), back into Eq. (3.3.e).

$$R_{dr} = R_E \cdot \cos^{-1}\left(\frac{(R_E + R_{beam}\sin(\theta))}{\sqrt{{R_{beam}}^2 + {R_E}^2 + 2 \cdot R_{beam} \cdot R_E \sin(\theta)}}\right) \tag{3.3.i}$$

Next, we will look at an equation for the magnitude of $\boldsymbol{h_{beam}}$, given an arbitrary $\boldsymbol{R_{beam}}$ vector. As seen in Figure 3.3.c, the magnitude of $\boldsymbol{R_{sum}}$ is equal to the magnitude of $\boldsymbol{h_{beam}}$ plus the magnitude of $\boldsymbol{R_E}$. As shown in Eq. (3.3.j), $\|\boldsymbol{h_{beam}}\|$ is found by subtracting $\|\boldsymbol{R_E}\|$ from $\|\boldsymbol{R_{sum}}\|$.

$$\|\boldsymbol{h_{beam}}\| = \|\boldsymbol{R_{sum}}\| - \|\boldsymbol{R_E}\| = h_{beam} = R_{sum} - R_E \tag{3.3.j}$$

It is next helpful to express $\boldsymbol{R_{sum}}$ in terms of its components, as is done in Eq. (3.3.k). The magnitude of $\boldsymbol{R_{sum}}$ is found by summing the squares of its components and taking the square root.

$$\boldsymbol{R_{sum}} = R_{beam}\cos(\theta)\hat{\boldsymbol{\imath}} + (R_{beam}\sin(\theta) + R_E + h_0)\hat{\boldsymbol{\jmath}} \tag{3.3.k}$$

$$R_{sum} = \sqrt{{R_{beam}}^2\cos^2(\theta) + (R_{beam}\sin(\theta) + R_E + h_0)^2} \tag{3.3.l}$$

$$R_{sum} = \sqrt{{R_{beam}}^2(\sin^2(\theta) + \cos^2(\theta)) + (R_E + h_0)^2 + 2 \cdot R_{beam}(R_E + h_0)\sin(\theta)} \tag{3.3.m}$$

$$R_{sum} = \sqrt{{R_{beam}}^2 + (R_E + h_0)^2 + 2 \cdot R_{beam}(R_E + h_0)\sin(\theta)} \tag{3.3.n}$$

Substituting R_{sum} into Eq. (3.3.j), gives the magnitude of $\boldsymbol{h_{beam}}$ in terms of R_{beam} and the firing angle (θ). Finally, replacing R_{beam} with r_b allows one to create a function for h_{beam}. Seen in Eq. (3.3.p), $h_{beam}(\theta, r_b)$ is the altitude of a beam after traveling a distance (r_b) at a firing angle (θ).

$$R_{sum} - R_E = \sqrt{{R_{beam}}^2 + (R_E + h_0)^2 + 2 \cdot R_{beam}(R_E + h_0)\sin(\theta)} - R_E \tag{3.3.o}$$

$$h_{beam}(\theta, r_b) = \sqrt{{r_b}^2 + (R_E + h_0)^2 + 2 \cdot r_b(R_E + h_0)\sin(\theta)} - R_E \tag{3.3.p}$$

With this geometry defined, we can now calculate atmospheric attenuation.

3.3.2 Calculating Atmospheric Attenuation

As seen in Eq. (2.4.e), the total attenuation is defined as a function of altitude ($\gamma_{total}(h)\ in\ dB/km$). Thus, to calculate the attenuation of a microwave beam through the atmosphere, we can sum the total attenuation at each altitude the beam passes through. To find the atmospheric attenuation ($\gamma_d\ in\ dB$) encountered by a microwave beam traveling an arbitrary distance through the atmosphere, one can evaluate the integral of $\int \gamma_{total}\big(h_{beam}(\theta, r_b)\big)dr$ from 0 to d_{atm}, where d_{atm} represents the length of the beam contained within the atmosphere. In other words, d_{atm} measures the specific distance over

which the beam is being attenuated by the atmosphere and is thus unique for each firing angle. This unique attenuation is shown below in Eq. (3.3.q), where γ_d is defined as a function of both the firing angle θ and d_{atm}.

$$\gamma_d(\theta, d_{atm}) = \int_0^{d_{atm}} \gamma_{total}\big(h_{beam}(\theta, r_b)\big)dr \tag{3.3.q}$$

To address the calculation of d_{atm}, it is necessary to introduce two concepts: the maximum system range and the atmospheric cutoff altitude. The maximum system range (R_{sys}) is the farthest a beam fired from an HPM system can propagate while accounting for all deployment considerations, such as atmospheric attenuation. The atmospheric cutoff altitude is the altitude at which the effects of atmospheric attenuation become negligible.

The maximum system range is defined using the already defined maximum vacuum range. Atmospheric attenuation, like the electromagnetic shielding of a target, is measured in decibels of loss. Thus, if γ_a is to represent the decibels of shielding encountered by a beam, it may be combined with the shielding (γ_s) to form an equation for the maximum system range in Eq. (3.3.r).

$$R_{sys} = \frac{2 \cdot D \cdot f}{1.22 \cdot c \cdot \sqrt{\pi}} \sqrt{\frac{P \cdot \left(10^{-\left(\frac{\gamma_s + \gamma_a}{10}\right)}\right)}{I_{req}}} \tag{3.3.r}$$

The second concept, an atmospheric cutoff altitude, is necessary because our atmosphere model was not continuous for all altitudes. Examination of Figure 2.4.d, which shows atmospheric attenuation for different nominal altitudes, revealed that attenuation at an altitude of 18 kilometers is less than $10^{-2}\ dB/km$ within all atmospheric windows. Thus, 18 kilometers was chosen as the atmospheric cutoff altitude.

To find the distance along a straight line from the system deployment location to the atmospheric cutoff altitude of 18 kilometers ($r_{b_{18}}$), Eq. (3.3.p) is solved for the range (r_b), replacing $h_{beam}(\theta, r_b)$ with h, and evaluating the result at $h = 18$.

$$h = \sqrt{{r_b}^2 + (R_E + h_0)^2 + 2 \cdot r_b (R_E + h_0)\sin(\theta)} - R_E \tag{3.3.s}$$

$$(R_E + h)^2 = {r_b}^2 + (R_E + h_0)^2 + 2 \cdot r_b (R_E + h_0)\sin(\theta) \tag{3.3.t}$$

$${r_b}^2 + 2 \cdot r_b (R_E + h_0)\sin(\theta) + (R_E + h_0)^2 - (R_E + h)^2 = 0 \tag{3.3.u}$$

The form of Eq. (3.3.u) reveals a quadratic polynomial. Thus, a solution for the range (r_b) is found as follows:

$$r_b = \frac{-2(R_E + h_0)\sin(\theta) + \sqrt{(2(R_E + h_0)\sin(\theta))^2 - 4((R_E + h_0)^2 - (R_E + h)^2)}}{2} \tag{3.3.v}$$

$$r_b(\theta, h) = \sqrt{\left((R_E + h_0)\sin(\theta)\right)^2 - (R_E + h_0)^2 + (R_E + h)^2} - (R_E + h_0)\sin(\theta) \tag{3.3.w}$$

$$r_b(\theta, 18) = \sqrt{\left((R_E + h_0)\sin(\theta)\right)^2 - (R_E + h_0)^2 + (R_E + 18)^2} - (R_E + h_0)\sin(\theta) \tag{3.3.x}$$

$$r_{b_{18}}(\theta) = r_b(\theta, 18) \tag{3.3.y}$$

If the maximum system range (R_{sys}), evaluated for an atmospheric attenuation of $\gamma_d\left(\theta, r_{b_{18}}(\theta)\right)$, is defined as shown in Eq. (3.3.z) to be $R_{sys_{18}}(\theta)$, then using the result arrived at in Eq. (3.3.x), the value of d_{atm}, the distance over which the beam is attenuated by the atmosphere, can at last be defined as $r_{b_{18}}(\theta)$ if $R_{sys_{18}}(\theta)$ is greater than $r_{b_{18}}(\theta)$; otherwise, d_{atm} is equal to R_{sys} at the point where R_{sys}, evaluated for an atmospheric attenuation of $\gamma_d(\theta, r_{atm})$ is equal to r_{atm}, where r_{atm} is defined as some distance ranging between 0 and $r_{b_{18}}(\theta)$, as is shown in Eqs. (3.3.z) and (3.3.aa).

$$R_{sys_{18}}(\theta) = R_{sys}\big|_{\gamma a = \gamma_d(\theta, r_{b_{18}})} \tag{3.3.z}$$

$$d_{atm}(\theta) = \begin{cases} r_{b_{18}}(\theta), & R_{sys_{18}}(\theta) > r_{b_{18}}(\theta) \\ R_{sys}, & R_{sys}\big|_{\gamma a = \gamma_d(\theta, r_{atm})} = r_{atm}, \ \ where\ 0 \le r_{atm} < r_{b_{18}}(\theta) \end{cases} \tag{3.3.aa}$$

Given the definition of d_{atm} in Eq. (3.3.aa), r_{atm} must be defined as well. The value of r_{atm} is calculated numerically in MATLAB. Given that the maximum distance a beam will

travel through the atmosphere while being attenuated is $r_{b_{18}}(\theta)$, MATLAB sets the value of r_{atm} equal to an initialized step size (ε) and increases it by integral multiples of ε until its value reaches $r_{b_{18}}(\theta)$. Although the step size is parametric, a default step size of 0.5 kilometers was defined. For each value of r_{atm}, the average altitude (h_{ave}) was calculated by summing half of h_{beam} for ranges of r_{atm} and $r_{atm} - \varepsilon$. The calculation of h_{ave} is shown below in Eq. (3.3.bb).

$$h_{ave}(\theta, r_{atm}) = \frac{h_{beam}(\theta, r_{atm})}{2} + \frac{h_{beam}(\theta, r_{atm} - \varepsilon)}{2} \tag{3.3.bb}$$

For each average altitude ($h_{ave}(\theta, r_{atm})$) along the path of the beam, the total attenuation ($\gamma_{total}(h)$) is found, multiplied by the step size (ε), and stored as an element in an array. Each of these elements defines the attenuation for one step of the beam's path. This step attenuation is defined as $\gamma_{step}(\theta, r_{atm})$ in Eq. (3.3.cc) below. Additionally, while looping over each value of r_{atm}, the conditions of d_{atm}, defined in Eq. (3.3.aa), are checked. If d_{atm} is defined, the loop is exited and the step attenuations are summed over the range of $[\varepsilon, d_{atm}]$ to form $\gamma_{atm}(\theta)$.

$$\gamma_{step}(\theta, r_{atm}) = \gamma_{total}\big(h_{ave}(\theta, r_{atm})\big) \cdot \varepsilon \tag{3.3.cc}$$

$$\gamma_{atm}(\theta) = \sum_{r_{atm}=\varepsilon}^{d_{atm}} \gamma_{step}(\theta, r_{atm}) \tag{3.3.dd}$$

This summation can then be used to define the maximum system range in terms of some angle θ. Substituting $\gamma_{atm}(\theta)$ for γ_d is shown in Eq. (3.3.ee).

$$R_{sys}(\theta) = R_{sys}\big|_{\gamma_a = \gamma_{atm}(\theta)} = \frac{2 \cdot D \cdot f}{1.22 \cdot c \cdot \sqrt{\pi}} \sqrt{\frac{P \cdot \left(10^{-\left(\frac{\gamma_S + \gamma_{atm}(\theta)}{10}\right)}\right)}{I_{req}}} \tag{3.3.ee}$$

For a ground-based system, the maximum system range is a function of the firing angle θ. To determine the complete range of a system, one must sweep the firing angle

between 0 and π radians. This sweep is done in MATLAB by dividing the angle into a large number of divisions and calculating the angle at each division. Although the number of divisions was handled parametrically, a default of 5,000 divisions was defined.

3.3.3 Effective System Range

As described in Section 3.2, the critical altitude (h_c) is the height that an HPM must hit a target by to induce a mission kill. The maximum system range of a ground-based system (R_{sys}), however, is often capable of reaching beyond this altitude. Thus, it is necessary to define an effective system range (R_{eff}) which is defined as the farthest a beam fired from an HPM system can propagate while delivering the minimum required intensity, accounting for all deployment considerations, and remaining effective should it come into contact with a target. This range is mathematically described below by Eq. (3.3.ff).

$$R_{eff}(\theta) = \begin{cases} R_{sys}(\theta), & h_{beam}\left(\theta, R_{sys}(\theta)\right) < h_c \\ r_b(\theta, h_c), & else \end{cases} \tag{3.3.ff}$$

Shown here, R_{eff} is defined by the maximum system range as long as the altitude of the beam, given by $h_{beam}\left(\theta, R_{sys}(\theta)\right)$, is less than the critical altitude (h_c). When the maximum system range has an altitude in excess of the critical altitude, however, the effective range is then defined by the distance along a straight line from the system deployment location to the critical altitude ($r_b(\theta, h_c)$).

Thus far, three ranges for an HPM system have been described: R_{vac}, R_{sys}, and R_{eff}. To further clarify each of these ranges, their definitions have been organized below in Table 3.3.a.

HPM Range	Definition
Maximum Vacuum Range (R_{vac})	The farthest a microwave beam can propagate while delivering a level of intensity greater than or equal to the minimum required intensity (I_{req}).
Maximum System Range (R_{sys})	The farthest a microwave beam can propagate while delivering a level of intensity greater than or equal to the minimum required intensity (I_{req}) and accounting for all deployment considerations, such as atmospheric attenuation.
Effective System Range (R_{eff})	The farthest a microwave beam can propagate while delivering a level of intensity greater than or equal to the minimum required intensity (I_{req}), accounting for all deployment considerations, such as atmospheric attenuation, and remaining at an altitude below or equal to the critical altitude (h_c).

Table 3.3.a: HPM Range Definitions

Three ranges for an HPM system have been described. Their definitions reveal that the maximum system range (R_{sys}) is less than or equal to the maximum vacuum range (R_{vac}) and that the effective system range (R_{eff}) is less than or equal to the maximum system range (R_{sys}).

Further discussion of these ranges is aided be the geometry presented in Figure 3.3.d.

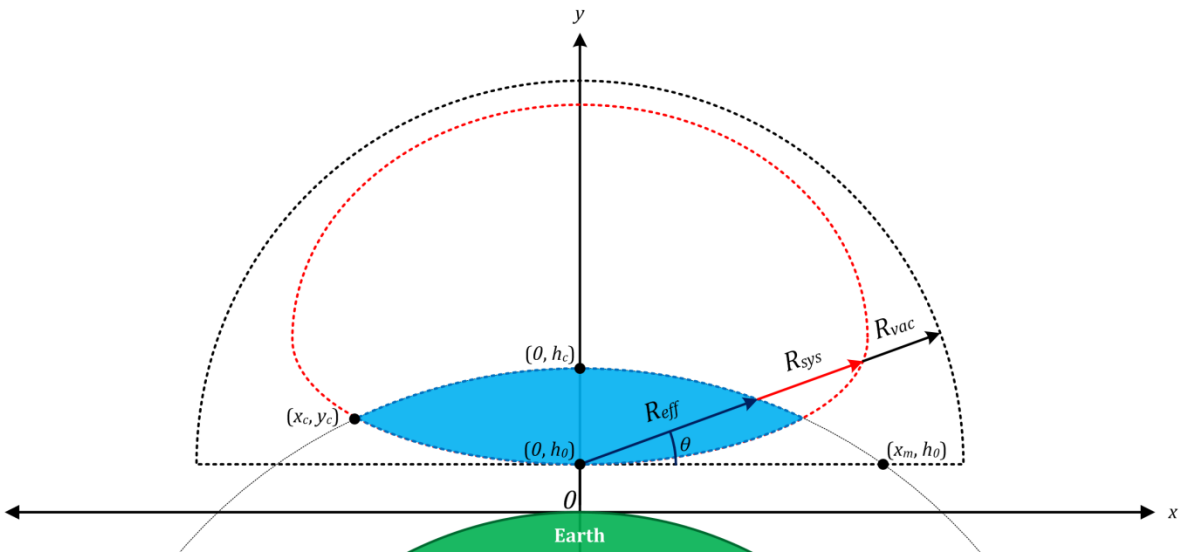

Figure 3.3.d: HPM Range Geometry

For an HPM system deployed at the location $(0, h_0)$, the distance a microwave beam fired at a firing angle θ will propagate for different conditions is defined at the maximum vacuum range (R_{vac}), which is shown as a dotted black line, the maximum system range (R_{sys}), which is shown as a dotted red line, and the effective system range (R_{eff}), which is shown as a dotted blue line and is shaded in. Also of note are the points (x_c, y_c) and (x_m, h_0). The former is known as the critical intersection and represents the point at which the downrange of the effective system range (for a given system) is greatest. The latter, meanwhile, defines the point at which the downrange of the effective system range (for a given critical altitude) reaches its maximum value.

For a system deployed at the location $(0, h_0)$ in a Cartesian coordinate system, which contains a cross-section of a spherical Earth model at the point $(0, -R_E)$, where R_E is the equatorial radius of the Earth, cross-sections of an HPM system's range is depicted as "bubbles" extending from the deployment location. Seen above in Figure 3.3.d, the three ranges which have been defined thus far are shown. The maximum vacuum range (R_{vac}), being a constant for a given set of system parameters, is shown as a dotted black line and takes the form of a half-circle. The maximum system range (R_{sys}), a function of the firing angle due to atmospheric attenuation, is shown as a dotted red line. As the firing angle is swept, R_{sys} reflects the quantity of low atmosphere the beam passes through. For angles near the horizon, the amount of low-level atmosphere traveled through is great, and thus R_{sys} is much less than R_{vac}. While for angles near vertical, the amount of low-level atmosphere traveled through is small and R_{sys} is close to R_{vac}. Finally, the effective system range (R_{eff}), which is shown as a dotted blue line, is shaded in. As can be seen, as the firing angle, as measured from the local horizon, is swept from 0 to $\pi\ radians$, the effective system range follows the maximum system range until the altitude reached would exceed the critical altitude. This point, labeled as (x_c, y_c), is defined as the critical intersection point and represents the farthest downrange that a particular system can achieve. Note that for different combinations of system parameters, the range bubbles will change, thus affecting the position of (x_c, y_c).

There does exist, however, another point of significance which does not change with system parameters, but rather with the critical altitude (h_c). The maximum downrange point (x_m, h_0) defines the point at which the downrange of a beam reaches the maximum possible value for a given critical altitude. Or alternatively, it represents the point where a beam fired at 0 $radians$ reaches an altitude above the surface equal to the critical altitude. Using the definition of the critical altitude, and the geometry of the system as previously described, it is possible to derive an equation for the maximum possible downrange that can be achieved for a given critical altitude.

The equation for a circle, shown in Eq. (3.3.gg), is modified to describe the path followed by the critical altitude in Figure 3.3.d by using a radius equal to the equatorial

radius of the Earth plus the critical altitude ($r = R_E + h_c$), an x offset of zero ($a = 0$), and a y offset of one Earth radius below the origin ($b = -R_E$). The equation of a circle which describes the path of the critical altitude is seen in Eq. (3.3.hh).

$$(x - a)^2 + (y - b)^2 = r^2 \tag{3.3.gg}$$

$$x^2 + (y + R_E)^2 = (R_E + h_c)^2 \tag{3.3.hh}$$

Rearranging Eq. (3.3.hh) for x gives:

$$x = \sqrt{(R_E + h_c)^2 - (y + R_E)^2} \tag{3.3.ii}$$

Given that the maximum downrange occurs at the point (x_m, h_0), the point x_m is found by calculating the point of intersection of the line $y = h_0$ and Eq. (3.3.ii). Substituting h_0 for y in Eq. (3.3.ii) produces:

$$x_m = \sqrt{(R_E + h_c)^2 - (h_0 + R_E)^2} \tag{3.3.jj}$$

With the maximum downrange point defined, a right-triangle can be formed with points at the center of the Earth $(0, -R_E)$, the system deployment location $(0, h_0)$, and the maximum downrange point (x_m, h_0). Using this triangle, the law of sines is used to find the angle (θ), which when multiplied with the Earth's radius (R_E), defines the maximum possible downrange ($R_{dr_{max}}$).

$$\frac{\sin\frac{\pi}{2}}{\sqrt{{x_m}^2 + (R_E + h_0)^2}} = \frac{\sin\theta}{x_m} \tag{3.3.kk}$$

$$\theta = \sin^{-1}\left(\frac{x_m}{\sqrt{{x_m}^2 + (R_E + h_0)^2}}\right) \tag{3.3.ll}$$

$$R_{dr_{max}}(h_0, x_m) = \theta \cdot R_E = \sin^{-1}\left(\frac{x_m}{\sqrt{{x_m}^2 + (R_E + h_0)^2}}\right) \cdot R_E \tag{3.3.mm}$$

$$R_{dr_{max}}(h_0, h_c) = \sin^{-1}\left(\frac{\sqrt{(R_E + h_c)^2 - (h_0 + R_E)^2}}{\sqrt{\left(\sqrt{(R_E + h_c)^2 - (h_0 + R_E)^2}\right)^2 + (R_E + h_0)^2}}\right) \cdot R_E \qquad (3.3.nn)$$

This maximum downrange is used to perform a quick assessment of whether an HPM system, for a given critical altitude, can cover a particular country. If the distance from a country's borders to its center exceeds $R_{dr_{max}}$, then an HPM system would be incapable (*regardless of its system parameters*) of providing coverage.

3.4 Space-Based System Analysis

As described in Section 3.2, for a given target, there exists a critical altitude (h_c) which is the greatest height an ICBM traveling 5,500 kilometers can be hit during boost phase to induce a mission kill. Consequently, an HPM system that guarantees worldwide coverage at h_c would be able to successfully intercept ICBMs travelling greater downrange distances as well. To calculate worldwide coverage, an HPM system must be able to reach h_c at all times and all places. Using a spherical Earth model, this worldwide coverage qualifier describes a sphere surface of required coverage ($Critical\ Surface$ [S_C]) with a radius equal to the radius of the Earth (R_E) plus h_c.

Analysis using the h_c coverage approach can only be performed for a given ICBM type, however. As discussed in section 2.1.1.2, liquid fueled missiles burn longer than solid fuel missiles to reach the same distance. Additionally, the design of the missile itself, such as its mass and aerodynamics also influence burn time. Therefore, calculating h_c for an ICBM can only be done for a specified ICBM profile. The user of MECSTAR is expected to supply the ICBM profile, or can choose to use the program's default profile, which characterizes a generic solid fueled ICBM. Alternatively, a user can opt to specify h_c without modeling a specific ICBM.

Given that a space-based system's orbital altitude can be assumed to be above the critical cutoff altitude of 18 kilometers (as defined in Section 3.3.2), an HPM satellite's maximum system range (R_{sys}) is equal to the maximum vacuum range (R_{vac}), as defined in

Eq. (3.1.m). Therefore, an HPM system's volume of coverage in free space is a sphere with a radius equal to the maximum system range (R_{sys}) of the system. When an HPM satellite is placed in orbit at a particular altitude (h_o), S_C must intersect an HPM's coverage volume, else no coverage can be assumed. $C(x)$ describes the two-dimensional cross section of S_C and is a circle with a radius equal to $h_c + R_E$ (cross section plane includes origin of S_C). The function $R(x)$ describes the two-dimensional cross section of an HPM coverage volume and is a circle with a radius equal to R_{sys} (cross section plane includes origin of coverage volume). Intersection is tested by describing $C(x)$ and $R(x)$ on a plane that touches the orbital path of the HPM satellite at all points. If $C(x)$ and $R(x)$ are ever equal to eachother, then an intersection exists. For example: if the range of the system is 10 km, the critical altitude is 20 km, and the system is in orbit at 100 km, the system would be unable to reach the critical altitude from that orbit, translating into no guaranteed coverage. In cases where S_C and the coverage volume intersect, the intersection appears as a shallow bowl (S_B) opening towards the Earth. The radius of the circle shown by projecting S_B onto a two-dimensional plane (a plane containing the lip of the "bowl"), is called the projected radius (R_p). The path from the center of S_B, following the surface of S_B, to the edge of S_B, is called the projected arc (L_p). From the center of the Earth, each point of S_B is exactly $h_c + R_E$ away because it exists exactly at the critical altitude above Earth. The angle swept from the center of S_B to the edge of S_B from the perspective of the center of the Earth is called the sigma sweep (σ). The described geometry is shown on a plane that touches the orbital path of the HPM satellite at all points in Figure 3.4.a. Further details on how the described values were calculated can be found in Appendix B: Background Space Methods Calculations.

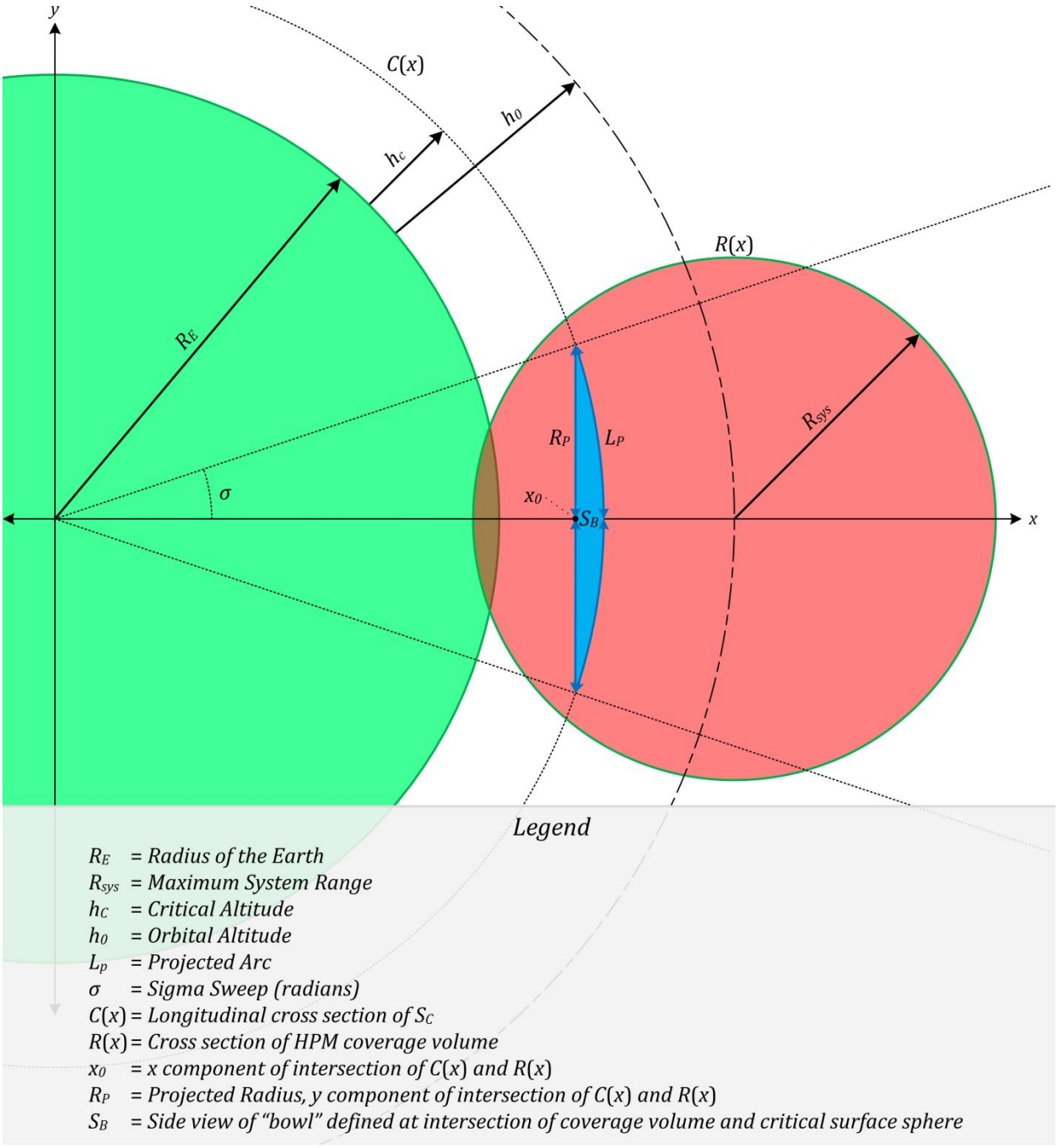

Figure 3.4.a: Two-Dimensional Satellite Coverage Outline

Earth and an HPM satellite's coverage range, both with origins resting on the x-axis of a Cartesian coordinate plane. All values are in kilometers unless otherwise noted. The orange area bounded by R_p and L_p is the side view of a S_B "bowl" opening towards Earth.

Complete coverage is realized by patterning S_B bowls onto the critical surface S_C while leaving no spacial gaps. In order to obtain world coverage, a polar orbit is assumed because it is the only orbit to cross all latitudes, as discussed in section 2.5.2.1. A constant

orbital altitude is used so that the geometry describing S_B does not vary during the orbital period. Continuous worldwide coverage necessitates a minimum number of orbital rings (N_{orbits}), and a minimum number of satellites per orbital ring ($N_{sat/ring}$). A solution is found when the least amount of S_B coverage overlap is calculated while leaving no coverage gaps. Being as the orbital rings will be at their greatest separation at the equator (polar orbits travel parallel to longitudes so they spread in the same manner), minimum coverage is calculated there.

Polar orbital rings exclusively exist on planes that are parallel to longitudes; a given orbital plane will perfectly bisect the Earth. Every point on a polar orbital ring must be within range of an HPM satellite to insure continuous coverage along the ring. However, as seen in Figure 3.4.b, if S_B coverage zones are placed edge to edge around the orbital ring, the there is no guaranteed minimum coverage width (W_G $arc\ length\ in\ km$) because the satellites in the ring move relative to the surface of the Earth as a function of time. Note that W_G is an arc length because it exists at the critical surface, S_C.

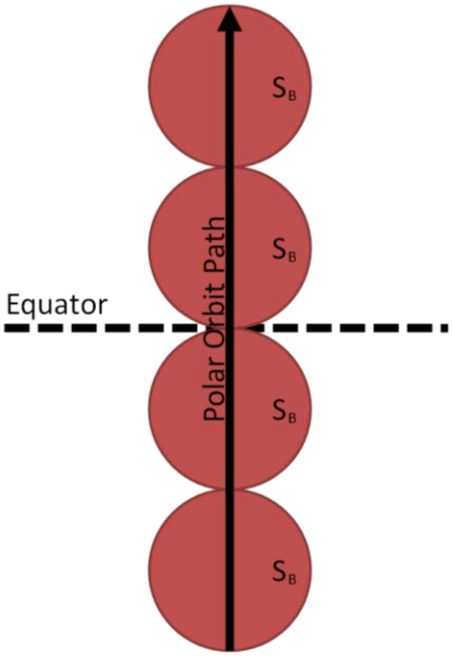

Figure 3.4.b: Errant Example of Full Orbital Path Coverage

Figure is zoomed in to the Equator locale at the critical altitude. As seen in the figure, the coverage cross sections (S_B) are lined along an arbitrary orbital path edge to edge. Though complete coverage exists along the orbital path, the path has no guaranteed minimum width at a given point as S_B sections move along the orbital path. Therefore, S_B sections must be moved closer together in order to have a non-zero minimum width.

The lack of W_G is a critical observation that must be acknowledged when calculating the total number of satellites in an orbital ring because it necessitates having to move S_B coverage zones closer together in order to guarantee a non-zero W_G on the orbital path. The method used to guarantee a non-zero W_G is to approximate the S_B coverage zone as a three-dimensional "hexagon" (S_H) at the critical altitude, and to align the "hexagons" edge to edge (see Figure 3.4.c). Being as S_H is a subset of the surface of S_B, S_H has the same "bowl" like feature.

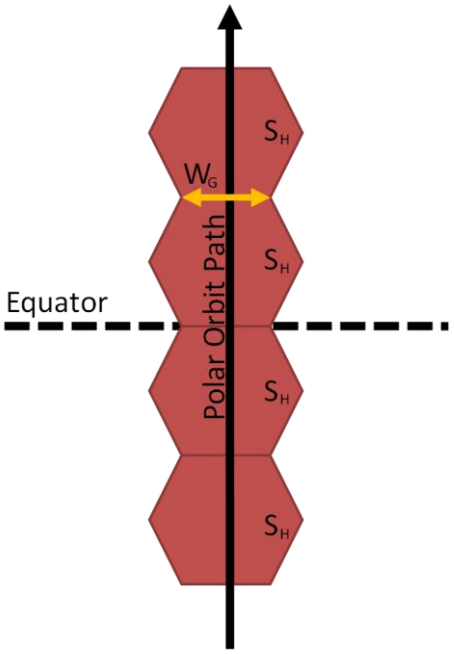

Figure 3.4.c: Valid Example of Full Orbital Path Coverage

Figure is zoomed in to the Equator locale at the critical altitude. As seen in the figure, the "hexagonal" coverage zones (S_H) are lined along an arbitrary orbital path edge to edge. Complete coverage exists along the polar orbit path, with a non-zero guaranteed minimum width (W_G).

An S_H is ideally constructed by using equilateral three-dimensional "triangles," as shown in Figure 3.4.d (see Appendix A: Equilateral Hexagon Proof). The "triangles" exist as a subset of the surface of S_H. Each side of a "triangle" is an arc length equal to the project arc, L_p. Exactly one vertex of each "triangle" exists at the center of the surface of S_H. The remaining vertices of the "triangles" exist at the corresponding vertices of S_H. The abbreviated projected arc (L_a) describes the path traveled from the center of an S_H to the middle of an arbitrary outside edge of S_H.

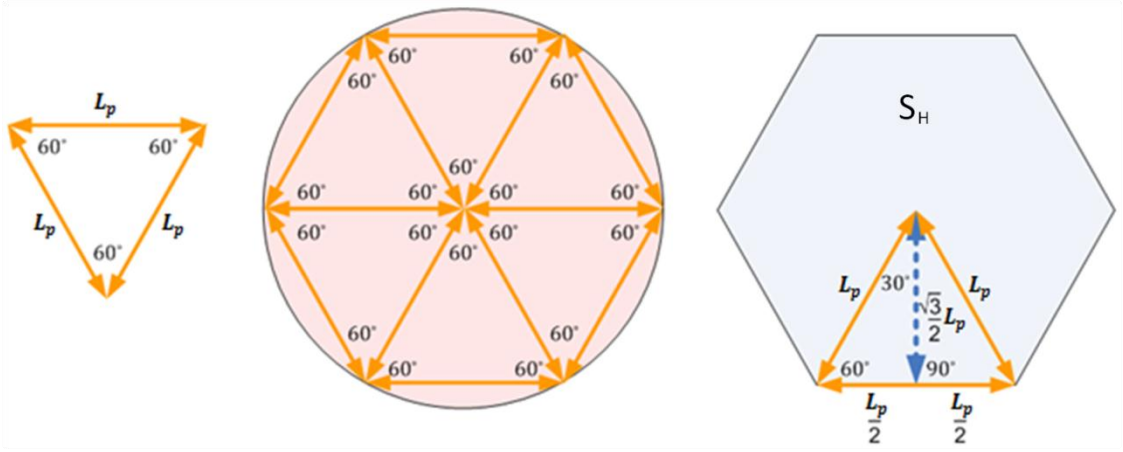

Figure 3.4.d: Constructing a Coverage "Hexagon"

Viewpoint from center of Earth is shown looking onto the intersection of an HPM's coverage volume with the critical surface (S_B, middle pink circle). The intersection is fitted by three-dimensional coverage "hexagon" (S_H, right blue "hexagon"), made of equilateral "triangles" (left figure) with "side" lengths equal to the projected arc L_p. The blue dashed line in the rightmost figure is equal to the abbreviated projected arc, L_a. The value of L_a is approximated by projecting an equilateral "triangle" onto a plane defined by the three vertices of same the "triangle," and applying Pythagorean Theorem.

Being as the hexagons must be arranged edge to edge to insure no gaps, the maximum adjacent satellite spacing (S_{max}) is twice L_a.

$$S_{max} = 2 \cdot L_a \tag{3.4.a}$$

As the orbital rings approach the poles, they begin to overlap, and they completely overlap at the poles themselves, so coverage does not have to be reanalyzed outside of the equator locale.

Being as S_H zones are made from equilateral "triangles" as shown in Figure 3.4.d, the coverage width arc of an orbital path over time cycles between L_p and $2 \cdot L_p$. As shown in Figure 3.4.e, overlapping coverage using orbital rings composed of S_H zones is minimized by alternating the "phase" between adjacent rings, but also has the effect of making the coverage width arc of adjacent pairs of orbital paths a constant value of three times L_p (see Eq. (3.4.c)).

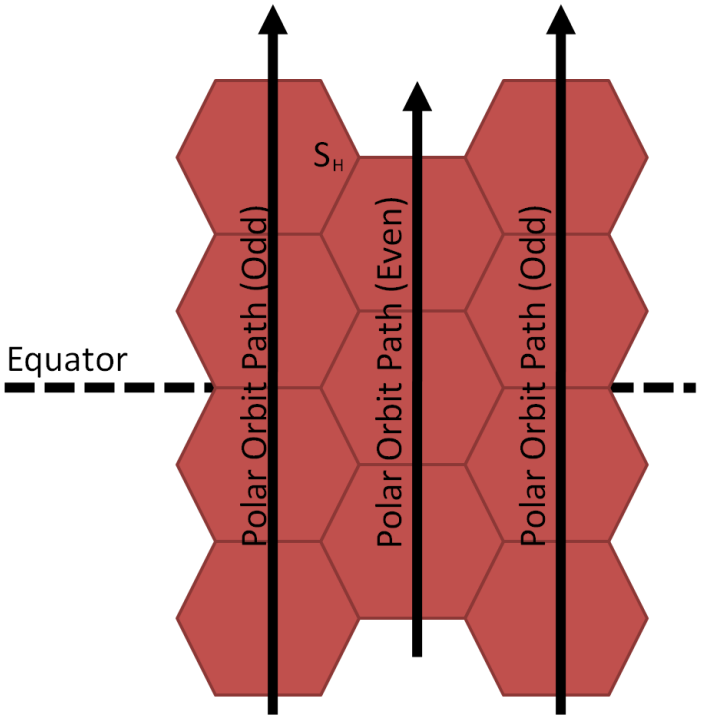

Figure 3.4.e: Alternating Orbital Paths

By constructing orbital rings out of iterations of S_H, overlapping coverage is minimized by alternating the "phase" of adjacent orbital rings. Being as satellites following an odd or even phase (phase names are arbitrary) still cover the same distance during their orbital periods, the phase offset between adjacent rings remains constant over time. The coverage width arc of a paired odd and even phase orbital path remains constant, though it will cyclically shift on the horizontal axis defined by the Equator.

The total number of satellites per ring ($N_{sat/ring}$) is equal to the circumference of a circle with a radius of $R_E + h_c$ (an arbitrary longitudinal cross-section of S_C), divided by the maximum satellite distance (S_{max}). The ceiling function necessitates an integer number of satellites.

$$N_{sat/ring} = \left\lceil \frac{2 \cdot \pi \cdot (R_E + h_c)}{S_{max}} \right\rceil \tag{3.4.b}$$

For a hexagonal arrangement of satellites, finding the optimal number of rings (N_{orbits}) is non-intuitive. Notably, full coverage only needs to be calculated for a single hemisphere (Earth divided along an arbitrary longitude, $0^0/180^0$ used in examples) because a single HPM satellite in a polar orbit symmetrically covers two hemispheres during its orbital period (see Figure 3.4.f).

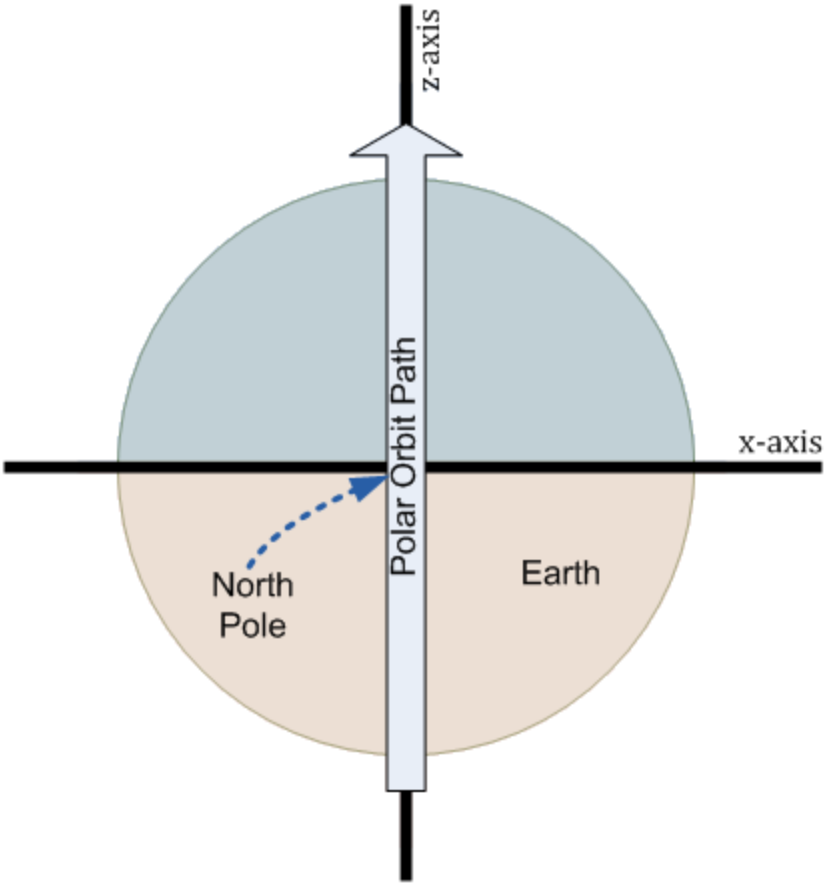

Figure 3.4.f: Polar Orbit Path over North Pole with Arbitrary Hemispheres

Top-Down view of Earth is shown with a polar orbit path. The red and blue zones show complementary but arbitrary hemispheres. Note that all polar orbit paths inherently cross the poles because they travel parallel to longitudes. Therefore, polar orbit paths are described as traveling exclusively on planes perpendicular to the x-z axis which pass through the origin (North Pole) shown in this figure. Due to the orbital path symmetry across the origin, once a full array of orbital paths has been arranged for full coverage for an arbitrary hemisphere, the complimentary hemisphere is covered as well.

Coverage analysis begins by grouping two adjacent satellite rings of which have a total width (W_{pair} in km) of three times L_p at the equator (see Eq. (3.4.c)).

$$W_{pair} = 3 \cdot L_p \tag{3.4.c}$$

The grouping is necessary because the width of a single satellite ring at the equator is not a constant value; the width alternates between L_p and $2 \cdot L_p$. However, the width of a pair of rings is constant. The relation of alternating widths to L_p is most easily observed in Figure 3.4.c through Figure 3.4.e.

Once adjacent satellite rings are paired, half the circumference of a circle with a radius of $R_E + h_c$ (a 0° latitudinal cross-section of S_C called C_{CS}, see Eq. (3.4.d)) is divided by W_{pair} and rounded up to the nearest integer to insure an integer number of satellite ring pairs (N_{pairs}, see Eq. (3.4.e)). Orbital ring patterning begins at an arbitrary longitude, and finishes at the arbitrary longitude plus 180^0 (see Figure 3.4.g, uses 0^0 as starting longitude reference).

$$C_{CS} = \pi \cdot (R_E + h_c) \tag{3.4.d}$$

$$N_{pairs} = \left\lceil \frac{C_{CS}}{W_{pair}} \right\rceil \tag{3.4.e}$$

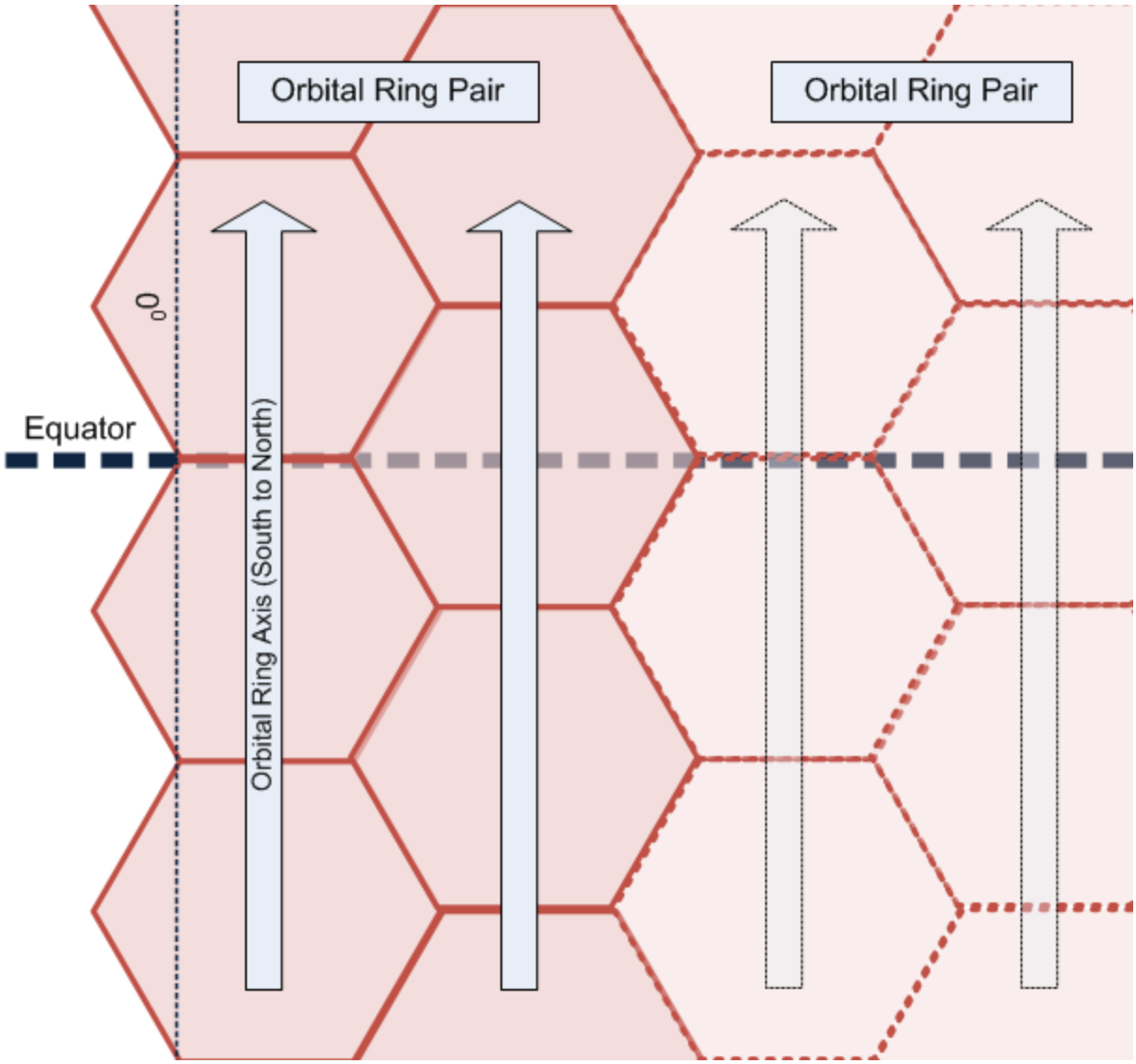

Figure 3.4.g: Satellite Coverage Initialization Reference

Zoomed in view of coverage rings in equator locale is shown. Vertical dashed line shows division between Earth hemispheres at 0^0 longitude. Horizontal dash line represents the Equator. Orbital ring pairs Orbital ring pairs are repeated until coverage is completed from 0^0-180^0 longitude. Due to the symmetry shown in Figure 3.4.f, if coverage is complete from 0^0-180^0 it is also complete from 180^0 to 360^0.

However, the pairing method may cause too many rings to be added when presented with the situation shown in Figure 3.4.h.

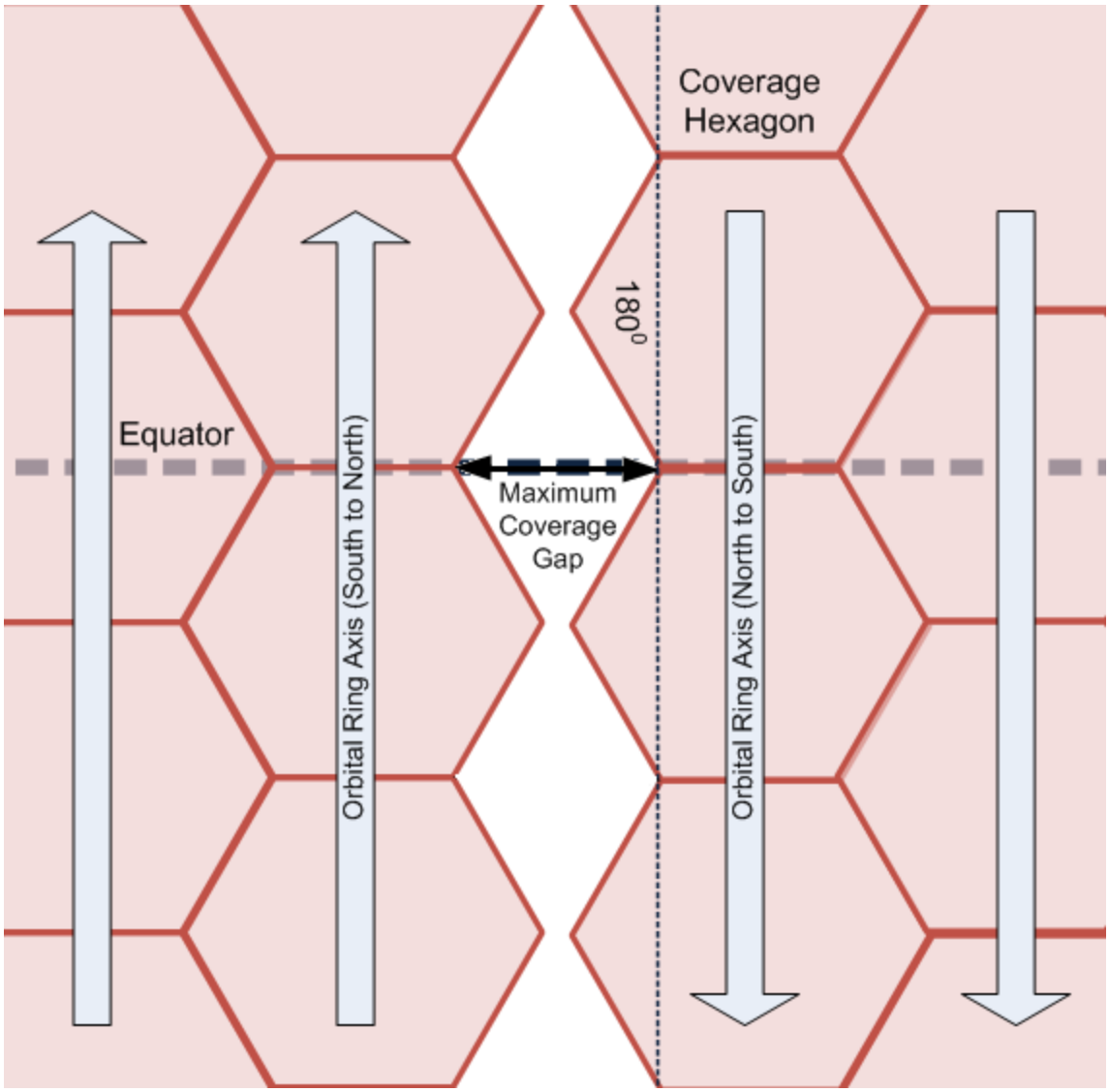

Figure 3.4.h: Satellite Orbit Coverage Gap Example

Zoomed in view of coverage rings in equator locale is shown. Vertical dashed line shows division between Earth hemispheres at 180⁰ longitude. Horizontal dash line represents the Equator. Note that the orbital paths travel in opposing directions due to the symmetry shown in Figure 3.4.f. Orbital rings from 180⁰ to 360⁰ are continuations of orbital rings from 0⁰ to less than 180⁰. All longitudes have continuous coverage except for the coverage gap shown. The coverage gap will be at its maximum value at the equator because polar orbit paths converge outside of this locale.

Because rings are being added in groups of two, the computation will add another group of two rings in order to close the maximum coverage gap shown in Figure 3.4.h, even though possibly only one ring is needed. The "only one ring needed" condition ($RingCon\ in\ boolean, see\ Eq.$ (3.4. f)) is found by removing one ring pair from the total

rings, then adding the least width of a single ring (L_p) and then checking to see if the total distance covered is still greater than C_{CS}.

$$RingCon = \begin{cases} True & if\ \left(N_{pairs} - 1\right) \cdot W_{pair} + L_p > C_{CS} \\ False & otherwise \end{cases} \tag{3.4.f}$$

As seen in Eq. (3.4.g), if $RingCon$ evaluates to false, then the total number of orbital rings (N_{orbits}) is simply twice the number of orbital ring pairs (N_{pairs}). However, if $RingCon$ evaluates to true, meaning one less ring is required for full coverage, then N_{orbits} is twice N_{pairs} minus one.

$$N_{orbits} = \begin{cases} 2 \cdot N_{pairs} - 1 & if\ RingCon = True \\ 2 \cdot N_{pairs} & otherwise \end{cases} \tag{3.4.g}$$

Because N_{pairs} is insured to be an integer due to the ceiling function and that Eq. (3.4.g) just performs subtraction and multiplication with whole numbers, N_{orbits} is insured to be an integer value as well.

The total number of satellites (N_{total}) is calculated by multiplying the number of satellites per ring ($N_{sat/ring}$) and the total number of orbital rings (N_{orbits}).

$$N_{total} = N_{sat/ring} \cdot N_{orbits} \tag{3.4.h}$$

Note that N_{total} does not have to be rounded because both N_{orbits} and $N_{sat/ring}$ are integer values.

3.5 MECSTAR – Program Structure

The MECSTAR coverage analysis tool was written in the MATLAB programming language. Classes were used to represent components of an effective coverage simulation by storing specific parameters in class properties and implementing calculations in methods. The design of this tool followed a top-down approach. First, the high-level structure was developed, followed by the lower level implementation.

3.5.1 High-Level Structure

MECSTAR's code base is broken into five functional blocks: profiles, models, simulations, configurations, and the graphical user interface. Each block is represented via as a package in the code base and contains classes responsible for handling a core piece of functionality. The structure of these packages with respect to a general project "root" package can be seen in Figure 3.5.a below in the form of a unified modeling language (UML) diagram.

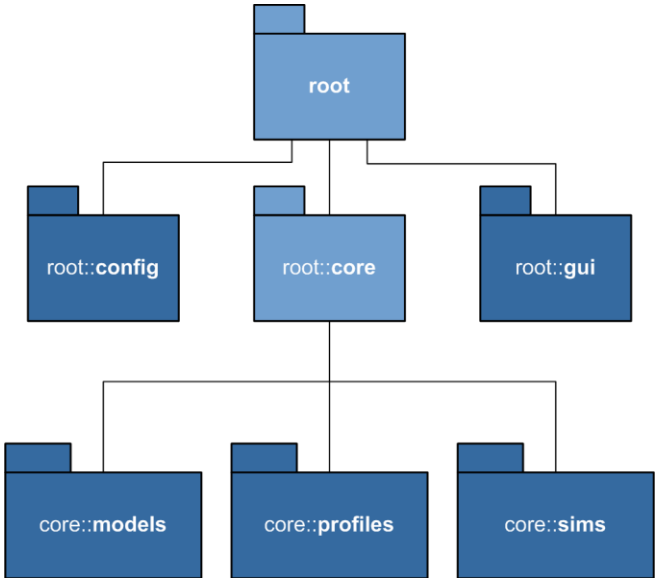

Figure 3.5.a: High-Level Package Structure Diagram of MECSTAR

Each of the five functional blocks is represented with a package in MECSTAR's code base. The configuration and graphical user interface blocks are contained in the packages "config" and "gui" within the project "root" package. The three remaining packages, "models," "profiles," and "simulations," are contained with an organizational package "core."

As depicted, only two of the packages, "config" and "gui" exist at the "root" level while an additional "core" package groups the "models," "profiles," and "sims" packages. These three packages are grouped because of their direct contributions to the core functionality of the MECSTAR tool. Meanwhile, the "config" and "gui" packages are left in the root package as they are more tangential to the core operation of the tool.

The "profiles" package contains classes and packages which describe each of the three input profiles: defense, sensor, and threat. The "models" package contains classes

which assist profile and simulation classes with calculations involving natural phenomenon. The “config” package contains classes which provide a means of saving and loading both profiles and simulations from previous program sessions. The “gui” package contains classes which provide a simple and intuitive way of running simulations, saving and loading configurations, and viewing results. Finally, the “simulations” package contains classes which coordinate profile and model classes for coverage simulations.

3.5.1.1 Package - root::core::profiles

The “profiles” package contains classes and packages which programmatically describe each of the three input profiles: defense, sensor, and threat. Within MECSTAR, a class which describes all of the parameters for a particular defense, sensor, or threat is referred to as a profile class. A UML diagram below in Figure 3.5.b is used to depict the “profiles” package’s classes and packages.

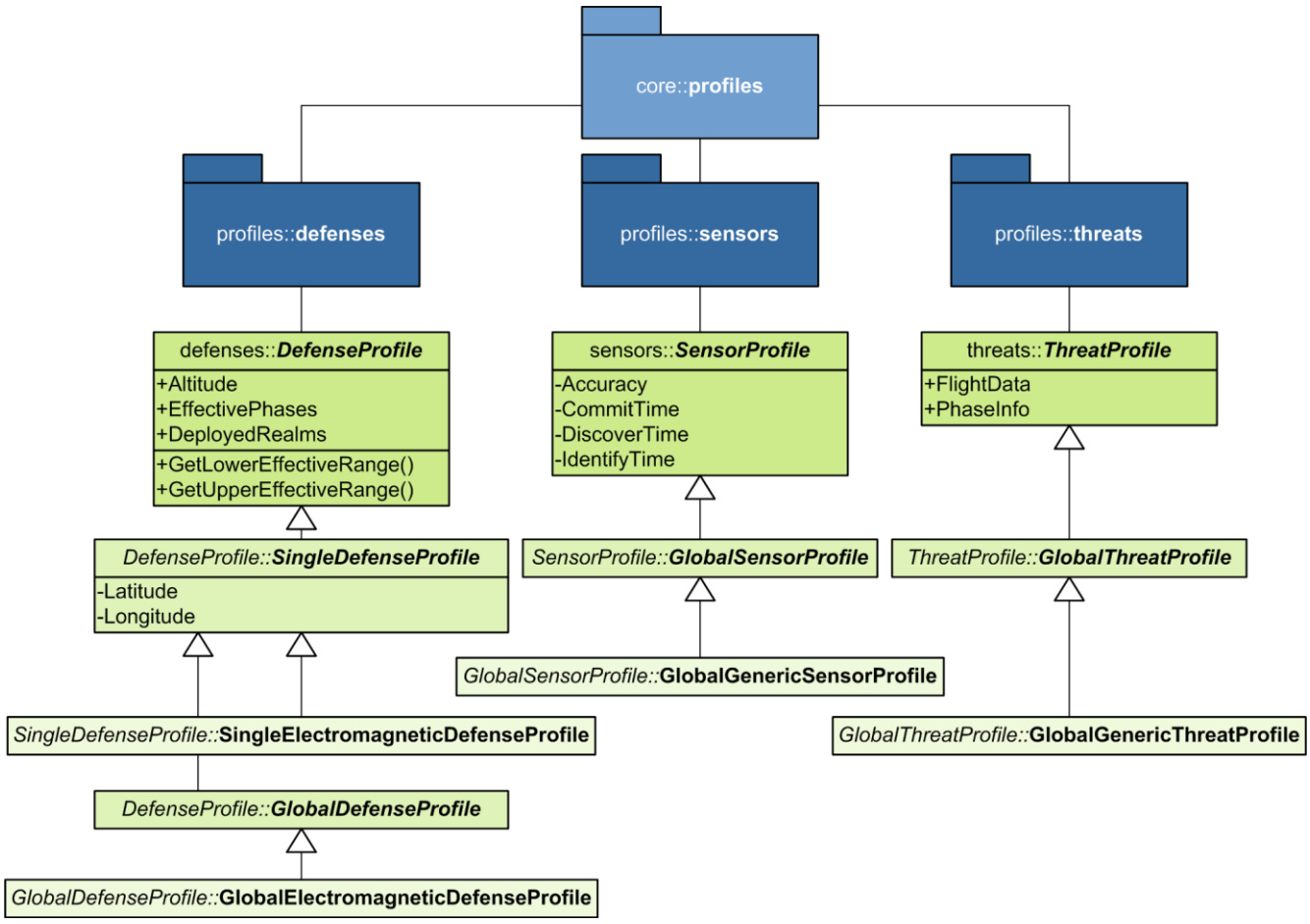

Figure 3.5.b: Class-Level Structure Diagram of Profiles Package

The "profiles" package contains a sub-package for each of the input profile types of defenses, sensors, and threats. Each of these sub-packages defines an abstract top-level profile class such as *DefenseProfile*. From this top-level class, a number of abstract, scope-specific classes such as *SingleDefenseProfile* are derived. Finally, from the scope-specific classes, concrete, type specific classes such as *SingleElectromagneticDefense-Profile* are derived.

The "profiles" package defines three additional sub-packages: "defenses," "sensors," and "threats." Each of these packages directly correlates to one of the three input profiles and defines an abstract, top-level profile class. For the input defense profile, sensor profile, and threat profile, the associated top-level profile classes are **DefenseProfile**, **SensorProfile**, and **ThreatProfile**. Each of these profile classes subclasses an additional abstract class named **ProfileBase**.

In MECSTAR, an input profile has a particular "scope" associated with it. A scope dictates what can be thought of as the level of commitment in a particular area or realm.

For example, a number of potential scopes are “Single”, “Theater”, and “Global”. A scope of “Single” indicates in the case of the defense and sensor platforms, that an element is deployed in a single fixed location, or, in the case of the threat profile, is traveling between two known points. Alternatively, in the case of defense and sensor platforms, a scope of “Global” would indicate that an element is deployed in such a way as to be effective over the entire Earth, or, in the case of the threat profile, is traveling between two unknown points. As indicated in Figure 3.5.b by the abstract subclasses, such as **SingleDefenseProfile**, of profile base classes, such as **DefenseProfile**, this project dealt with single and global defense profiles, global sensor profiles, and global threat profiles.

In addition to “scope”, each input profile has a particular “type” associated with it. A type dictates what can be thought of as the method of action. Each type of profile for a given scope is represented as a concrete class such as **SingleElectromagneticDefense-Profile** which subclasses its respective scope class, **SingleDefenseProfile**. Note that it is this final level of classes, specific to both scope, and type, which are, by design, instantiable. All other profile classes are, by design, abstract and cannot be constructed. This abstraction of classes ensures that no simulation can be run using an element profile class which does not specify the necessary scope and type information. Furthermore, the use of abstract base classes allows for the flexibility to define a specific type of element profile as only being valid for a single scope.

3.5.1.2 Package - root::core::models

The “models” package contains classes which assist profile and simulation classes with calculations involving natural phenomenon. A UML diagram below in Figure 3.5.c is used to depict the “models” package’s classes.

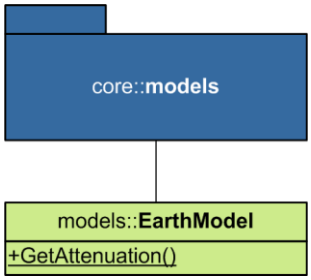

Figure 3.5.c: Class-Level Structure Diagram of Models Package

The "models" package contains a single class *EarthModel*. This class defines an atmospheric model for electromagnetic wave propagation.

The single class of the "models" package, **EarthModel**, defines an atmospheric model for electromagnetic wave propagation for altitudes which range from sea level to 18 kilometers. The Earth model was implemented as a static class so profile classes have uniform access to its methods when performing their own internal calculations.

3.5.1.3 Package - root::core::sims

The "sims" package contains classes which coordinate profile and model classes for coverage simulations. A UML diagram below in Figure 3.5.d is used to depict the "sims" package's classes.

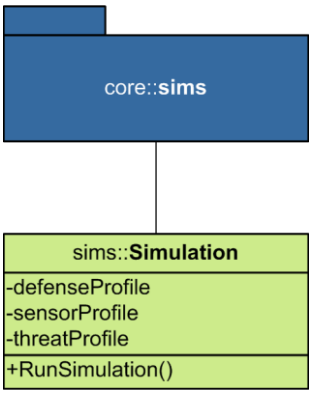

Figure 3.5.d: Class-Level Structure Diagram of Simulations Package

The "sims" package contains a single class, *Simulation*. This class defines the execution path for a coverage simulation and returns a results struct from its *RunSimulation()* method.

The single class of the "sims" package, **Simulation**, defines the execution path for a MECSTAR coverage simulation. This functionality is accomplished by calling upon functions that the concrete profile classes must implement due their abstract ancestry.

Similarly to profile classes, simulations can also be saved. Given that, internally, the **Simulation** class holds references to three profile classes, a simulation only needs the three profile classes to run; thus, it can be defined in terms of the referenced profile classes. If the referenced profile classes are saved as configurations, so too can the simulation itself be saved.

3.5.1.4 Package - root::config

The "config" package contains classes which provide a means of saving and loading both profiles and simulations as MATLAB data files from previous program sessions. The UML diagram below in Figure 3.5.e is used to depict the "config" package's classes and directories.

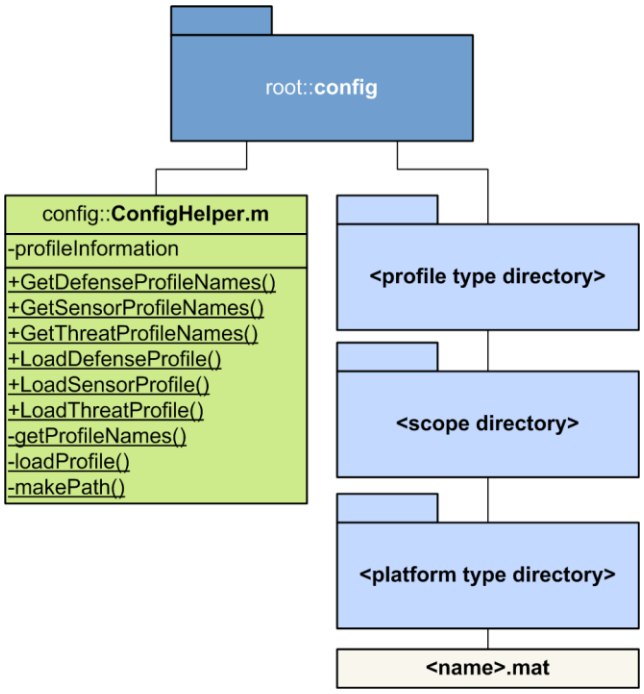

Figure 3.5.e: Class-Level Structure Diagram of Configuration Package

The "config" package contains a single class *ConfigHelper* and a structure of various subdirectories which store configuration files. The first level of subdirectories specifies the profile type, defenses, sensors, or threats. The second level of subdirectories specifies the scope, single or global. The third level of level of subdirectories specifies the platform type. In the third level of subdirectories, MAT-files store saved profile configurations.

The "config" package contains a single helper subclass **ConfigHelper** which provides an interface to saving and loading profile configurations. This helper class defines methods

for retrieving lists of available profile configurations as well as methods for saving new profiles. Profile configurations make use of MATLAB's built-in **save** and **load** functions which allow one to save and load workspace variables to special MATLAB formatted binary files (MAT-files) with an extension of **.mat**. To save a particular profile configuration, MECSTAR in fact saves an entire instance of a class. Thus, all of the class's parameters are preserved as well as its type. This method is preferable to other means of saving configurations, such as flat files which introduce unnecessary overhead.

In addition to the **ConfigHelper** class, the "config" package contains a directory structure for storing profile configuration files. In order to differentiate between profile types, scopes, and platform types, three levels of directories are used. In the third directory level, MAT-files are stored which contain the configuration instance variables. To further illustrate this directory structure, consider a saved electromagnetic defense profile named "HPM" with a global scope. Such a configuration MAT-file would be located by the following file path: **./root/config/defenses/global/electromagnetic/HPM.mat**.

3.5.1.5 Package - root::gui

The "gui" package contains classes which provide a simple and intuitive way of running simulations, saving and loading configurations, and viewing results. A UML diagram below in Figure 3.5.f is used to depict the "gui" package's classes and directories.

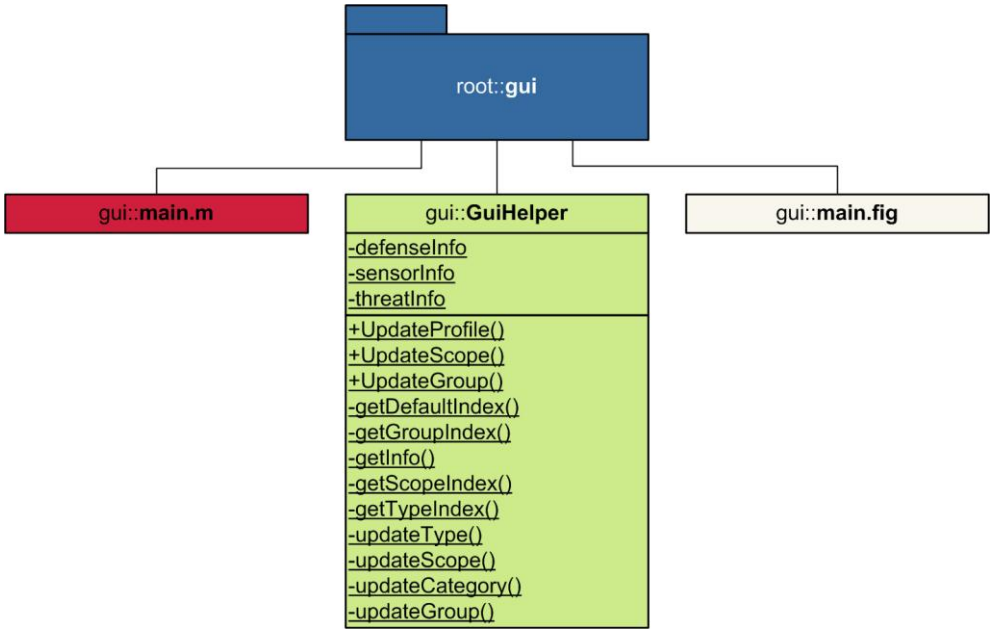

Figure 3.5.f: Class-Level Structure Diagram of Graphical User Interface Package

The "gui" package contains a single class, *GuiHelper*, an executable script, *main.m*, and a GUI figure, *main.fig*. The files, *main.m* and *main.fig*, are products of MATLAB's GUIDE program which was used to construct the layout of buttons, text, and user inputs. The *GuiHelper* class is used to facilitate advanced GUI actions such as automatically graying out user input controls.

The graphical user interface (GUI) was developed using MATLAB's GUI design environment (GUIDE) program. This interface design program was used to construct the layout of buttons, text, user inputs for each for the input elements, and program outputs. Figure 3.5.g shows the layout of the program with fields populated with default values.

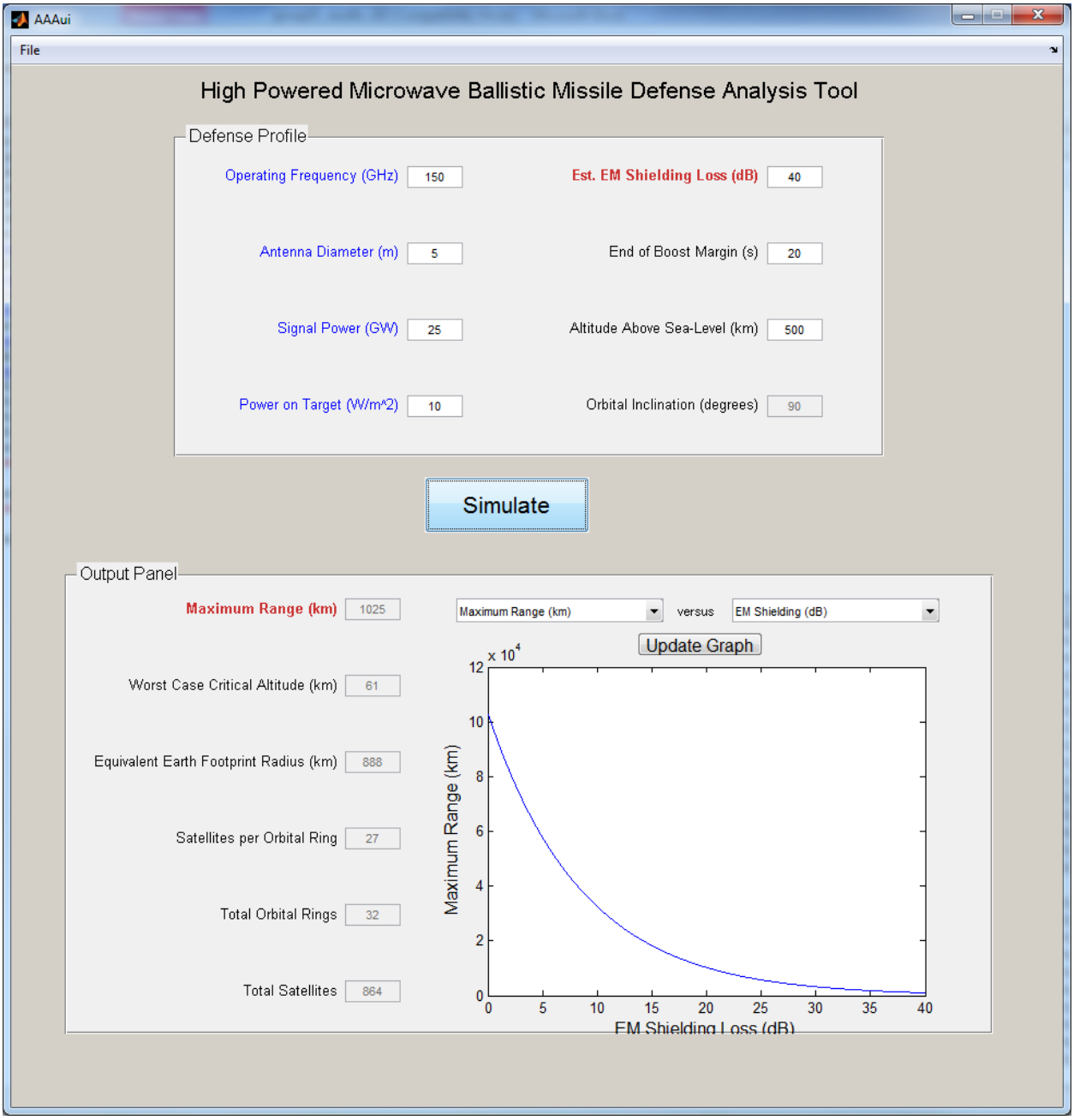

Figure 3.5.g: Graphical User Interface Screenshot

The GUI handles all input/output for MECSTAR. Inputs include operating frequency, antenna diameter, signal power, power on target, estimated shielding loss, boost margin, and orbital altitude. Outputs include maximum range, critical altitude, equivalent earth footprint, satellites per orbital ring, total orbital rings, total satellites, and dynamic relational graphs.

When using the GUIDE program, MATLAB figure, **main.fig**, and script, **main.m**, files are automatically created to define the component layout and callback functionality respectively. In addition to these files, it was necessary to create a GUI helper class,

GuiHelper, to facilitate several more advanced GUI actions such as automatically graying out user input controls based on possible parameter selections and form validation.

3.5.2 Class UML Diagram

The following unified modeling language (UML) diagram in Figure 3.5.h below indicates the complete internal structure of the previously mentioned classes and packages.

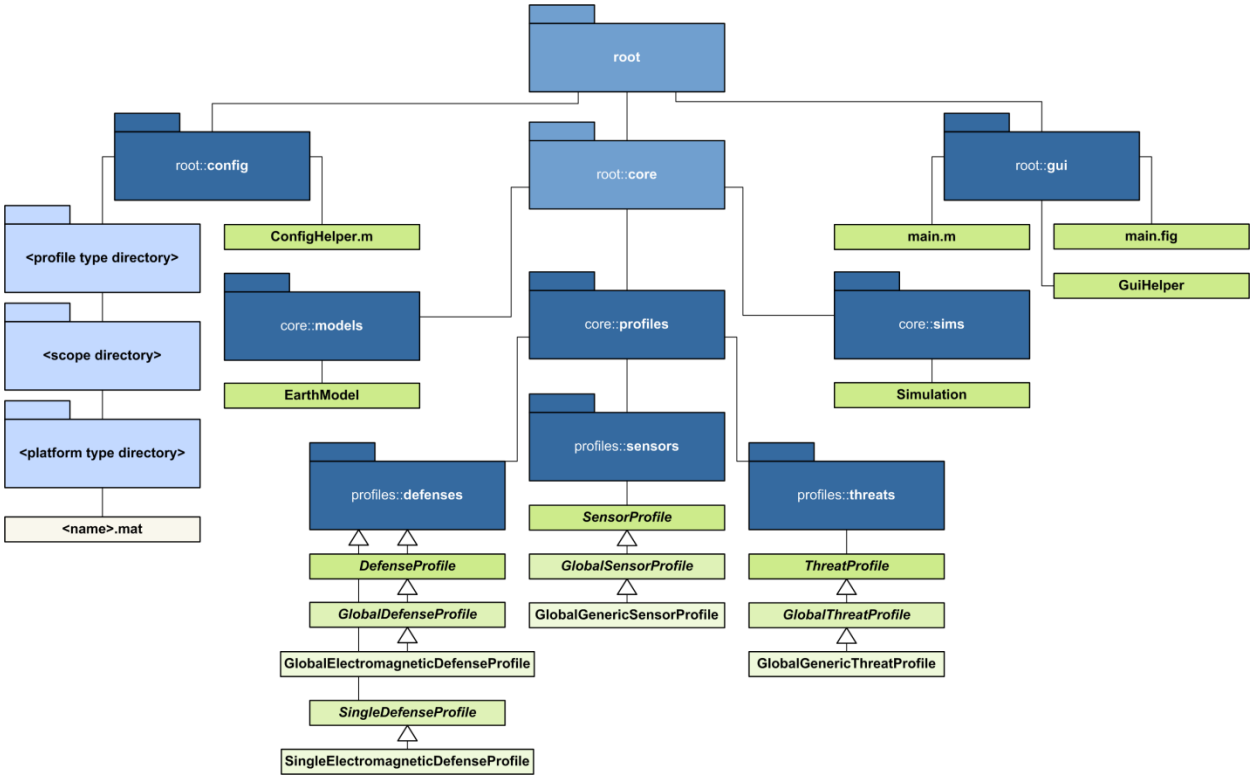

Figure 3.5.h: Class UML Diagram

Each of the five functional blocks is represented with a package in MECSTAR's code base. Each package defines additional classes and packages as necessary.

4 Results

In considering ground and space-based high-powered microwave (HPM) platforms for boost phase interception, the maximum vacuum range (R_{vac}) of the system is a critical factor in determining the deployment possibilities. Given in Eq. (3.1.m), the formula for R_{vac} relates parameters such as operating frequency, antenna diameter, and signal power. The effect of each parameter on the maximum vacuum range is generalized below in Table 4.0.a.

System Parameter	Relation to Maximum Vacuum Range (R_{vac})
Operating Frequency	*Positive (Linear)*
Antenna Diameter	*Positive (Linear)*
Signal Power	*Positive (Root)*
Intensity on Target	*Negative (Linear)*
Electromagnetic Shielding	*Negative (Exponential)*

Table 4.0.a: Generalized Range Relations

The maximum vacuum range (R_{vac}) is positively influenced by operating frequency, antenna diameter, and signal power. Additionally, it is negatively influenced by the required intensity on target, and the electromagnetic shielding of the target.

As shown, three of the five system parameters have a positive correlation to the maximum vacuum range (R_{vac}). An increase in a positively correlated parameter increases R_{vac}. The remaining two parameters have a negative correlation to R_{vac}. An increase in a negatively correlated parameter decreases R_{vac}.

The generalized range relations above are based purely on the natural divergence of the microwave beam and therefore do not necessarily hold for a ground-based systems where other effects, such as atmospheric attenuation (which affects the relation of operating frequency) must be considered.

As seen in Figure 2.4.e, the range of intensities which can effectively couple electromagnetic radiation is quite large, spanning eleven orders of magnitude. To cover this range, we introduced the concept of target Vulnerability Models (VMs). Given that the vulnerability of a target can be quantified by the intensity required to disrupt its guidance

electronics, each VM considered was primarily defined around a specific intensity level. Shown below in Figure 4.0.a, our analysis of HPM systems was performed using three VMs defined by intensities of 0.01 W/m^2, 10 W/m^2 , and 100,000 W/m^2.

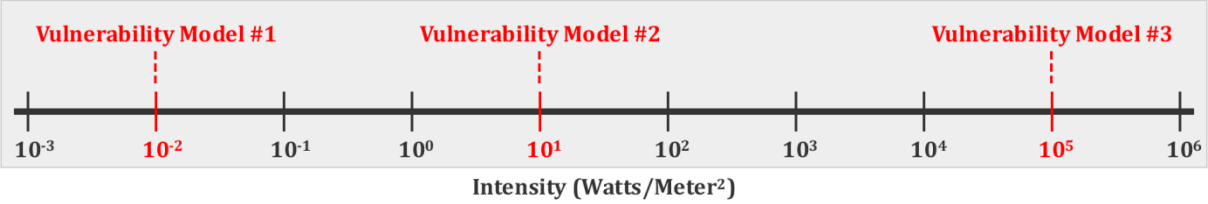

Figure 4.0.a: Vulnerability Model Intensity Levels on Logarithmic Scale

To cover the spectrum of intensities required to couple a microwave beam to a target's circuitry, three vulnerability models were used.

Specifically, VM 1-3 were chosen represent highly vulnerable, moderately vulnerable, and highly resistant targets respectively. Each VM, the results of which are detailed in the following sections, consisted of a core value set and a number of sweep values or limits. For each VM, being as there are too many dimensions to sweep on a single graph, the core values are each swept independently in order to show system effectiveness relations with respect to each considered parameter.

4.1 Ground Basing

For each of the three aforementioned VMs, results for ground-based HPM platforms were generated. As mentioned in Section 2.4.3, the atmospheric attenuation model used in this analysis required a number of parameters to be initialized.

For the results generated in the following sections, environmental data for the country of Iraq was used. Specifically, regional yearly averages were taken for pressure ($P_{h_0} = 1013\ mbar$), temperature ($T_{h_0} = 290\ K$), and water vapor density ($\rho_{h_0} = 8\ g/m^3$).

Two general types of plots were used to demonstrate the effect of different parameters on the maximum and effective ranges of the system.

4.1.1 *Plot Types*

Explained in detail below, two-dimensional "Earth" plots depict the maximum system and effective ranges as they extend from the surface of the earth. Three-dimensional "Downrange Surface" plots show the downrange from the platform as a function of various parameters. Each of the two types of plots is exemplified by Figure 4.1.a below.

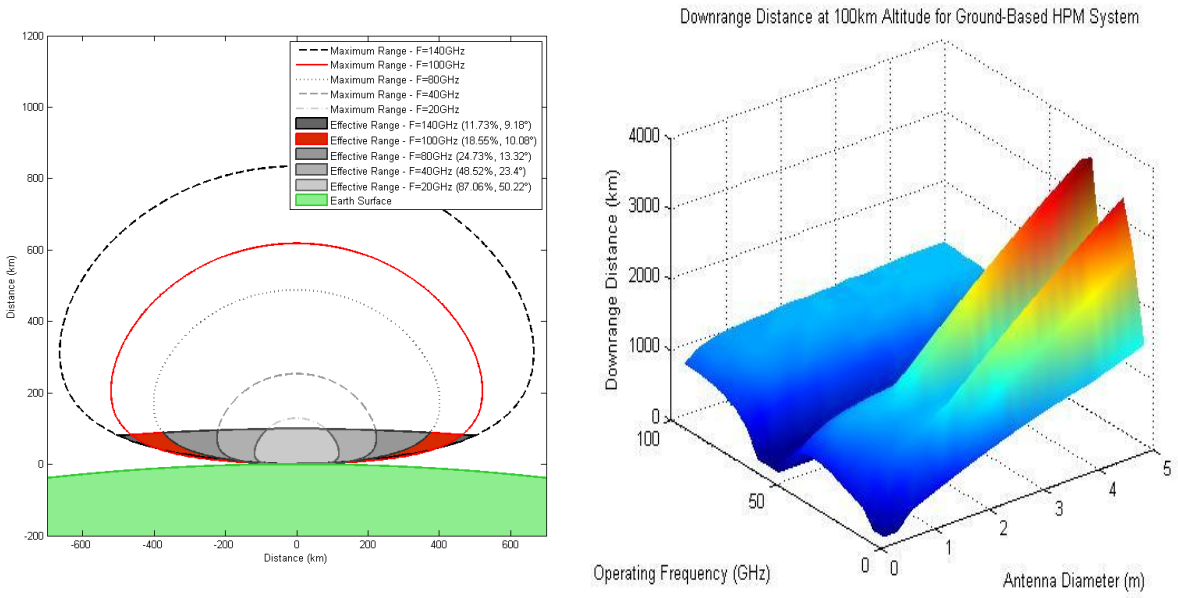

(a) **(b)**

Figure 4.1.a: Ground-Based Plot Types

Example (a) "Earth" and (b) "Downrange Surface" plots are shown for a ground-based HPM system.

4.1.1.1 *Earth Plots*

As described in Section 3.3.1, the Earth is modeled as a sphere with a radius equal to the Earth's equatorial radius ($R_E = 6{,}378.1\ km$). In an "Earth" plot, a two-dimensional cross-section of this spherical Earth model is placed in a Cartesian coordinate system with the topmost point of the Earth's surface residing at the origin and the center of the cross-section residing at the point $(0, -R_E)$. Then, from the point $(0, h_0)$, where h_0 is the deployment altitude of an HPM system, the maximum system range (R_{sys}) of a ground-based HPM system, as defined in Eq. (3.3.ee), is plotted as a single plot line for a firing angle

(θ) ranging between 0 and π radians. Finally, the effective system range (R_{eff}), as defined in Eq. (3.3.ff), is plotted and shaded in. An example "Earth" plot can be seen below in Figure 4.1.b. Note that because the Earth was modeled as a sphere, the results presented would seem to be valid regardless of an HPM's actual location. This observation is not the case, however, as the atmospheric model required initial conditions for temperature, pressure, and water vapor. As noted in the introduction to this section (4.1), these values were initialized to environmental data specific to the country of Iraq. Thus, the results are only valid for locations matching the general temperature, pressure, and humidity of Iraq.

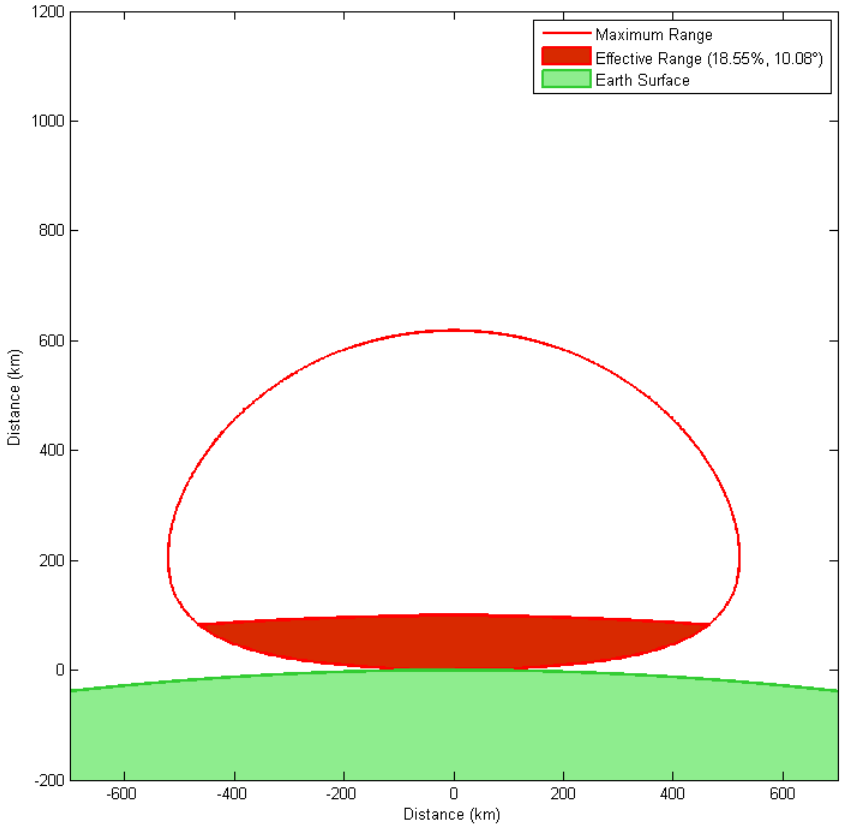

Figure 4.1.b: Example Ground-Based "Earth" Plot

Plot of a ground-based HPM's range as it sits on the Earth. The outer plot represents the systems maximum range while the shaded area represents the system's effective range.

Figure 4.1.b is indicative of an "Earth" plot for a set of core model values. "Earth" plots of core model values are identified by a solid red maximum system range (R_{sys}) plot

line and an effective system range (R_{eff}) filled in with dark red. Given that an "Earth" plot is really an image of the platform range viewed at platform "eye level," the axes do not represent specific parameters, but rather represent the distance in kilometers. All "Earth" plots have square axes so as to prevent a distortion of the image.

The legend of each "Earth" plot contains useful information as well. While the maximum system range, effective system range, and Earth surface are all clearly marked, the effective system range entry contains two additional pieces of information. The first element in parenthesis following the effective range entry is a percentage of the maximum range represented by the effective range. This percentage is found by taking the total area of the maximum system range and dividing it by the area circumscribed by the effective system range. For example, the "Earth" plot in Figure 4.1.b depicts a system whose effective range comprises 18.55% of the maximum range. The second parenthetical element meanwhile corresponds to the firing angle (10.08° in Figure 4.1.b) needed to achieve an effective range which has the farthest downrange. This point is also known as the critical intersection and is defined in Figure 3.3.d.

"Earth" plots are also generated for parameter sweeps. An example of such a plot can be seen below in Figure 4.1.c.

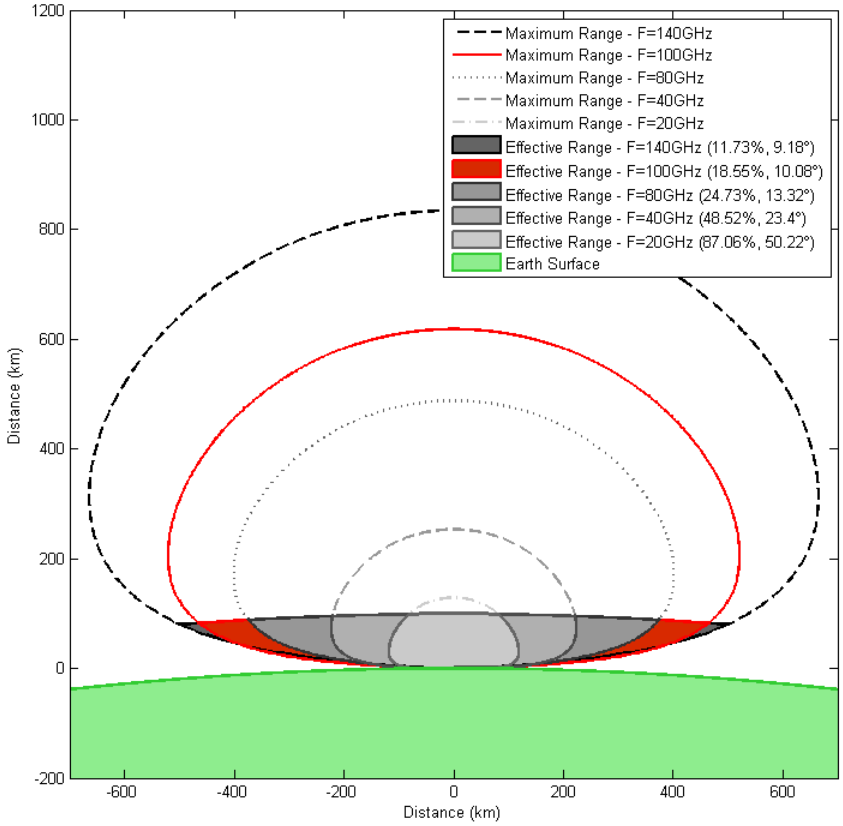

Figure 4.1.c: Example Ground-Based "Earth" Plot with Parameter Sweep

Plot of a ground-based HPM's ranges as it sits on the Earth for various operating frequencies. The outer plots represent the maximum ranges of the system for the specified operating frequencies while the shaded areas represent the system's effective range.

In "Earth" plots with parameter sweeps, the core case values are always plotted in red as a reference with the effective range shaded dark red. Additionally, for each set of model plots, the axes for "Earth" plots are held constant to permit comparisons between each of the plots for a given case. This effort to enable comparisons is exemplified by Figure 4.1.b and Figure 4.1.c which both use axis limits of $[-700\ km, 700\ km]$ for the $x\text{-}axis$ and $[-200\ km, 1200\ km]$ for the $y\text{-}axis$.

When plotting parameter sweeps, the legend specifies the value of the swept parameter for each of the figure's subplots. As identified by the legend of the plot in Figure

4.1.c, the system's range was plotted for operating frequencies of 20 GHz, 40 GHz, 80 GHz, 100 GHz, and 140 GHz.

4.1.1.2 Earth Plot Accuracy

The distance accuracy of "Earth" plots is described using two values: the range accuracy and angular accuracy.

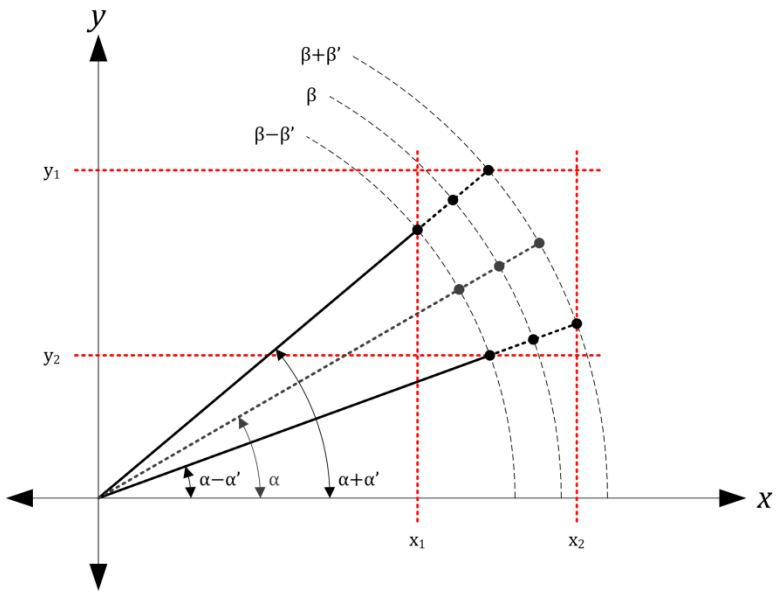

Figure 4.1.d: Distance Accuracy of "Earth" and "Altitude/Downrange" Plots Examined
If for a firing angle (α *in degrees*), within an angular accuracy (α' *in degrees*), a range point is calculated to have some range (β *in km*), within an accuracy (β' *in km*), then its actual location lies between the points x_1 and x_2 on the X axis and y_1 and y_2 on the Y axis.

As shown above in Figure 4.1.d, for a given range (β *in km*) and firing angle (α *in degrees*), a particular range point's actual position varies as a function of the range, firing angle, range accuracy (β' *in km*), and angular accuracy (α' *in degrees*). Figure 4.1.d defines the points x_1, x_2, y_1, and y_2 which bound the potential locations of a range point. These bounding points may be calculated using Eqs. (4.1.a) through (4.1.d).

$$x_1 = (\beta - \beta') \cdot \cos(\alpha + \alpha') \tag{4.1.a}$$

$$x_2 = (\beta + \beta') \cdot \cos(\alpha - \alpha') \tag{4.1.b}$$

$$y_1 = (\beta - \beta') \cdot \sin(\alpha + \alpha') \tag{4.1.c}$$

$$y_2 = (\beta + \beta') \cdot \sin(\alpha - \alpha') \tag{4.1.d}$$

While we do not specifically utilize this analysis to assess the accuracy of our findings, each "Earth" plot included in the following sections specifies, within the caption, the range and angular accuracies used. Thus, this analysis is included to provide the reader with the tools and information necessary to determine the accuracy of a system's range if they should be required to do so.

4.1.1.3 Downrange Plots

The second plot type, "Downrange," shows the maximum range at the critical altitude as a function of two other parameters considered, and how those parameters affect the range at that altitude. Since the range is most highly varying with frequency because of atmospheric dependencies, frequency is held on for one of the independent axes.

4.1.2 Ground-Based - Vulnerability Model 1

The first Vulnerability Model considered for a ground-based HPM system was a highly vulnerable target model. The core values of the ground-based Vulnerability Model 1 (GB-VM1) can be seen below in Table 4.1.a.

Parameter Name	Core Value	Units
Operating Frequency	100	$[GHz]$
Antenna Diameter	3	$[m]$
Source Power	50	$[GW]$
Intensity on Target	0.01	$[W/m^2]$
Electromagnetic Shielding	40	$[dB]$
Critical Altitude	100	$[km]$

Table 4.1.a: Ground-Based - Vulnerability Model 1 (Highly Vulnerable) - Core Values

Vulnerability Model 1 was used to represent a highly vulnerable target model with a required intensity of $0.01\ W/m^2$.

The sweep values for GB-VM1 can be seen below in Table 4.1.b. All parameter sweeps attempt to predictably span a range near the core value with the exception of frequency. Due to atmospheric attention, certain frequencies such as 60 GHz and 120 GHz are unusable. Such frequencies were avoided in parameter sweeps.

Parameter Name	Sweep Values	Units
Operating Frequency	$[20, 40, 80, 100, 140]$	$[GHz]$
Antenna Diameter	$[1, 2, 3, 4, 5]$	$[m]$
Source Power	$[10, 30, 50, 70, 90]$	$[GW]$
Intensity on Target	[N/A]	$[W/m^2]$
Electromagnetic Shielding	$[30, 35, 40, 45, 50]$	$[dB]$
Critical Altitude	$[100, 125, 150, 175, 200]$	$[km]$

Table 4.1.b: Ground-Based - Vulnerability Model 1 (Highly Vulnerable) - Sweep Values

Vulnerability Model 1 sweep values indicate the values used for each parameter sweep in "Earth" plots. For example, when sweeping operating frequency, 20 GHz, 40 GHz, 80 GHz, 100 GHz, and 140 GHz were used.

Using the core model values, "Earth" plots were generated. The "Earth" plot for the core GB-VM1 values can be seen below in Figure 4.1.e. The maximum horizontal range of GB-VM1 is ≈16,490 kilometers at a vertical location of ≈6,506 kilometers, while the maximum effective range is ≈1,091 kilometers at a vertical location of ≈8.537 kilometers. As the shaded effective range is indiscernible due to the scale of the plot, a higher-resolution "Earth" plot in Figure 4.1.k visually confirms these results.

Additional "Earth" plots for GB-VM1 which sweep the parameters of operating frequency, antenna diameter, source power, electromagnetic shielding, and critical altitude can be seen in Figure 4.1.f, Figure 4.1.g, Figure 4.1.h, Figure 4.1.i, and Figure 4.1.j respectively. Higher-resolution versions of the plots (labeled as "Enhanced") which display the otherwise hidden effective ranges are included as well in Figure 4.1.k, Figure 4.1.l, Figure 4.1.m, Figure 4.1.n, Figure 4.1.o, and Figure 4.1.p.

Ground-Based - Model 1 - "Earth" - Core Values

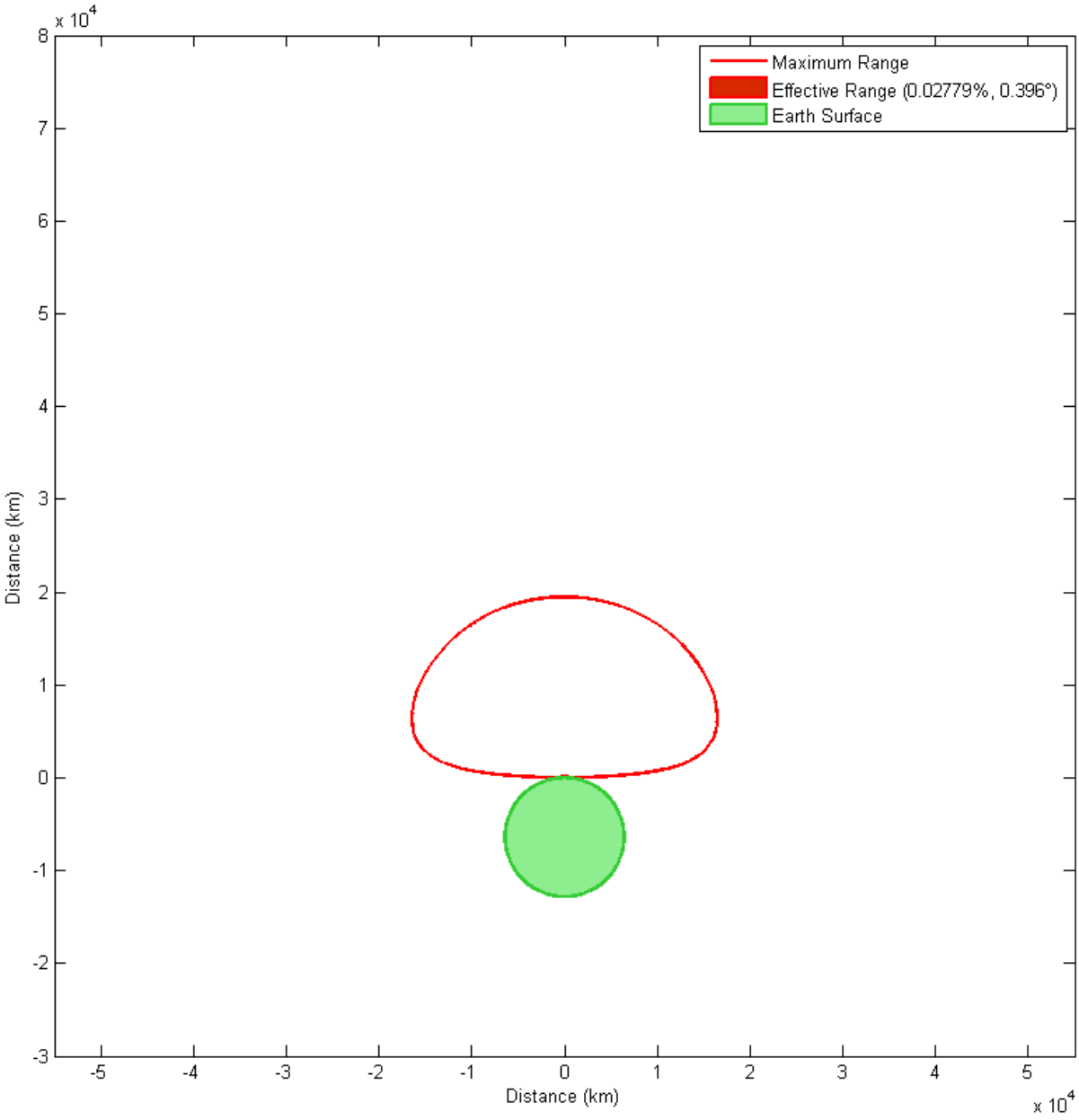

Figure 4.1.e: Ground-Based - Model 1 - "Earth" Plot - Core Values

For the core values: The maximum horizontal range is ≈16,490 km at an altitude of ≈6,506 km. The maximum vertical range is ≈19,550 km. The effective range comprises ≈0.0272% of the maximum range and the critical intersection is encountered at a firing angle of ≈0.396°. Angular accuracy: 0.036°. Range accuracy: 0.5 km. Note that due to the scale of this plot, the effective system range is not visible.

Ground-Based - Model 1 - "Earth" - Operating Frequency

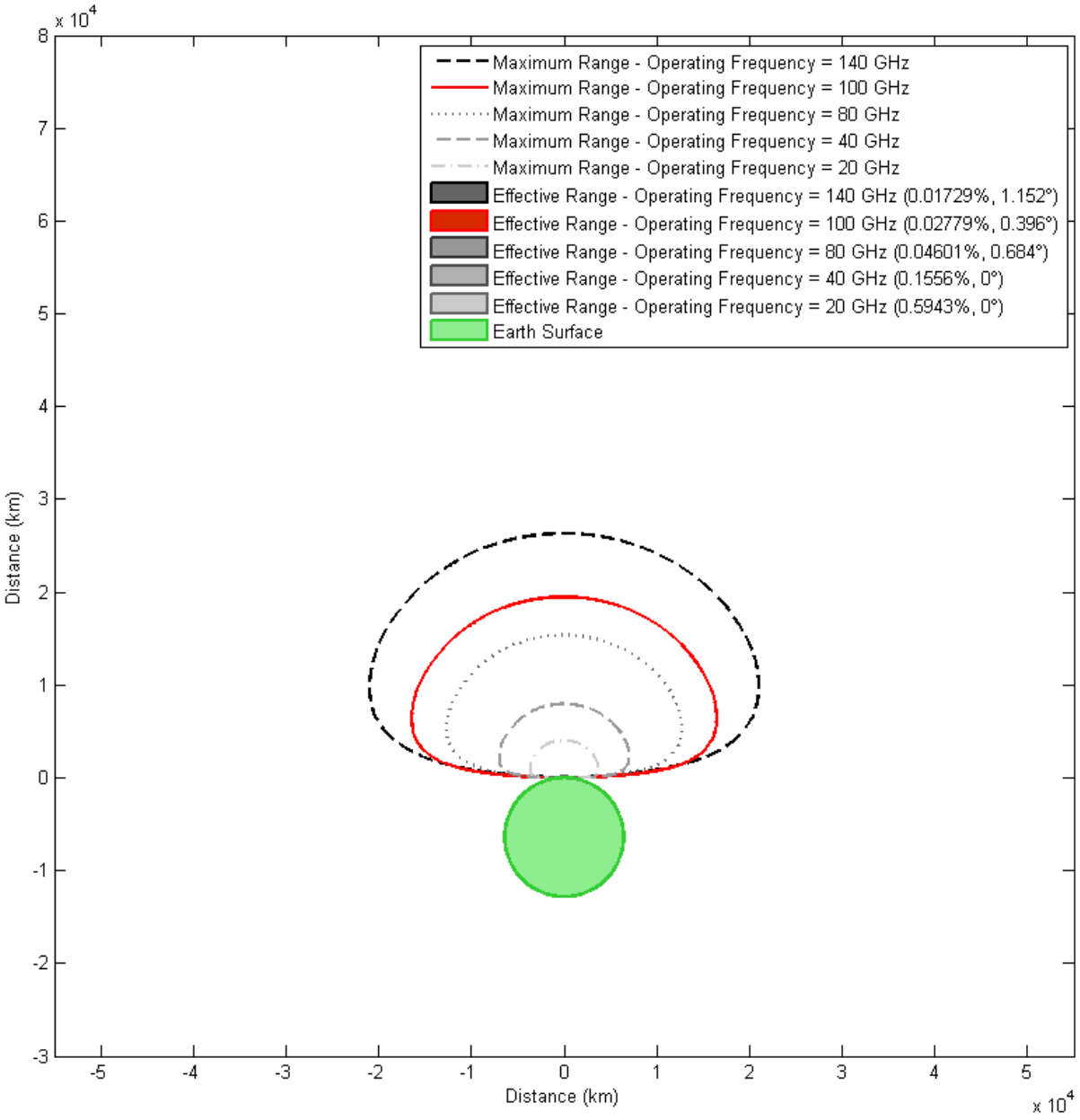

Figure 4.1.f: Ground-Based - Model 1 - "Earth" Plot - Sweeping Operating Frequency

For operating frequencies of 20 GHz, 40 GHz, 80 GHz, 100 GHz, and 140 GHz: Maximum horizontal ranges are ≈3,763 km, 7,084 km, 12,730 km, 16,490 km, and 21,040 km at altitudes of ≈952.1 km, 2,289 km, 5,432 km, 6,506 km, and 9,837 km. Maximum vertical ranges are ≈4,075 km, 8,012 km, 15,430 km, 19,550 km, and 26,390 km. Maximum effective horizontal ranges are ≈1,445 km, 1,406 km, 1,057 km, 1,091 km, and 1,055 km at altitudes of ≈1 km, 1 km, 13.62 km, 8.537 km, and 22.22 km. Maximum effective vertical ranges are all 100 km. The effective ranges comprise ≈0.5943%, 0.1556%, 0.046%, 0.0278%, and 0.0173% of the maximum range. The critical intersection is encountered at firing angles of ≈0°, 0°, 0.684°, 0.396°, and 1.152°. Angular accuracy: 0.036°. Range accuracy: 0.5 km. Note that due to the scale of this plot, the effective system range is not visible.

Ground-Based - Model 1 - "Earth" - Antenna Diameter

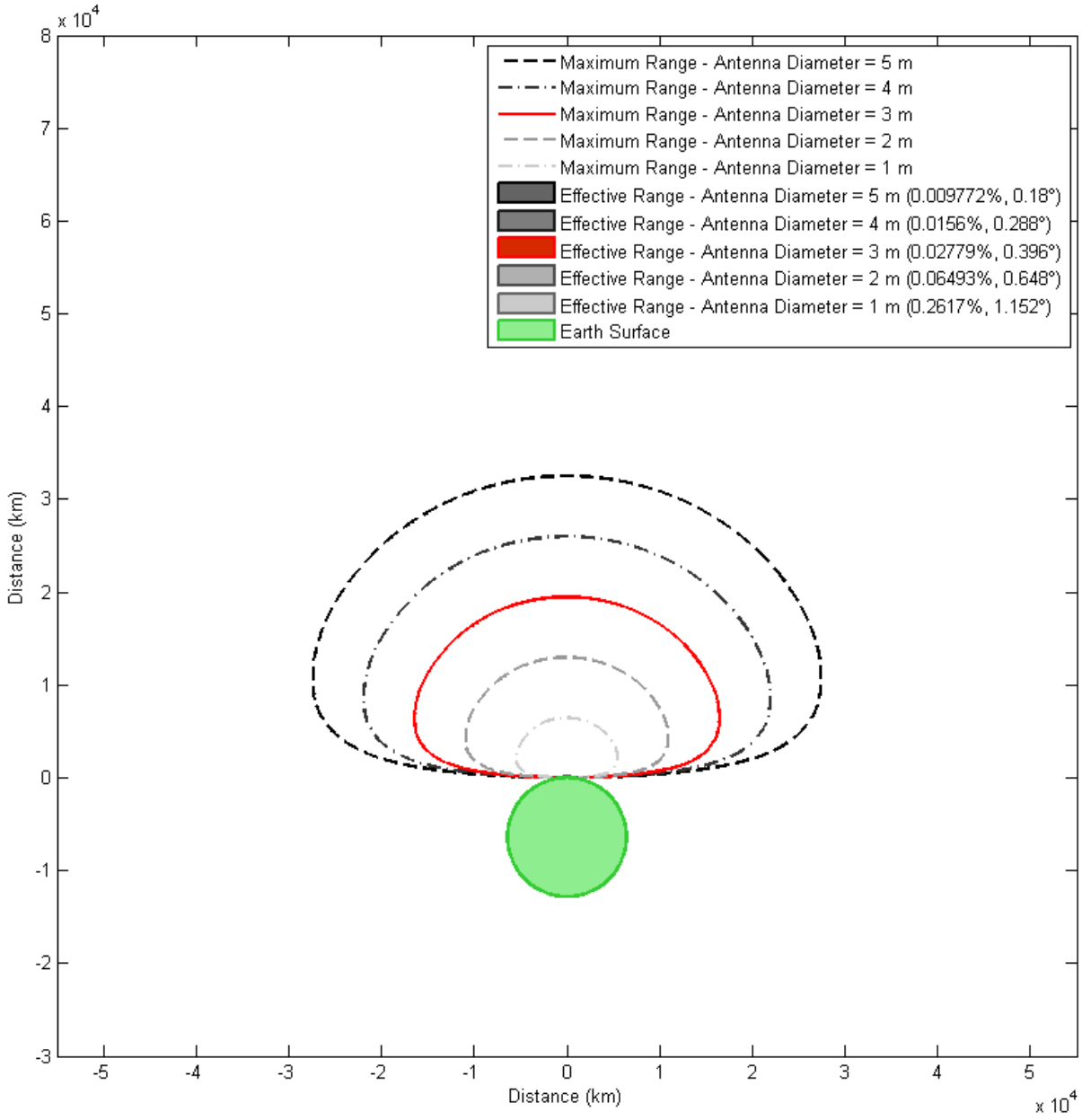

Figure 4.1.g: Ground-Based - Model 1 - "Earth" Plot - Sweeping Antenna Diameter

For antenna diameters of 1 m, 2 m, 3 m, 4 m, and 5 m: Maximum horizontal ranges are ≈5,497 km, 10,990 km, 16,490 km, 21,990 km, and 27,480 km at altitudes of ≈2,169 km, 4,338 km, 6,506 km, 8,674 km, and 10,840 km. Maximum vertical ranges are ≈6,519 km, 13,040 km, 19,550 km, 26,070 km, and 32,590 km. Maximum effective horizontal ranges are ≈1,016 km, 1,121 km, 1,091 km, 1,160 km, and 1,120 km at altitudes of ≈21.43 km, 13.67 km, 8.537 km, 6.829 km, and 4.52 km. Maximum effective vertical ranges are all 100 km. The effective ranges comprise ≈0.2617%, 0.0649%, 0.0278%, 0.0156% and 0.0098% of the maximum range. The critical intersection is encountered at firing angles of ≈1.152°, 0.648°, 0.396°, 0.288°, and 0.18°. Angular accuracy: 0.036°. Range accuracy: 0.5 km. Note that due to the scale of this plot, the effective system range is not visible.

Ground-Based - Model 1 - "Earth" - Source Power

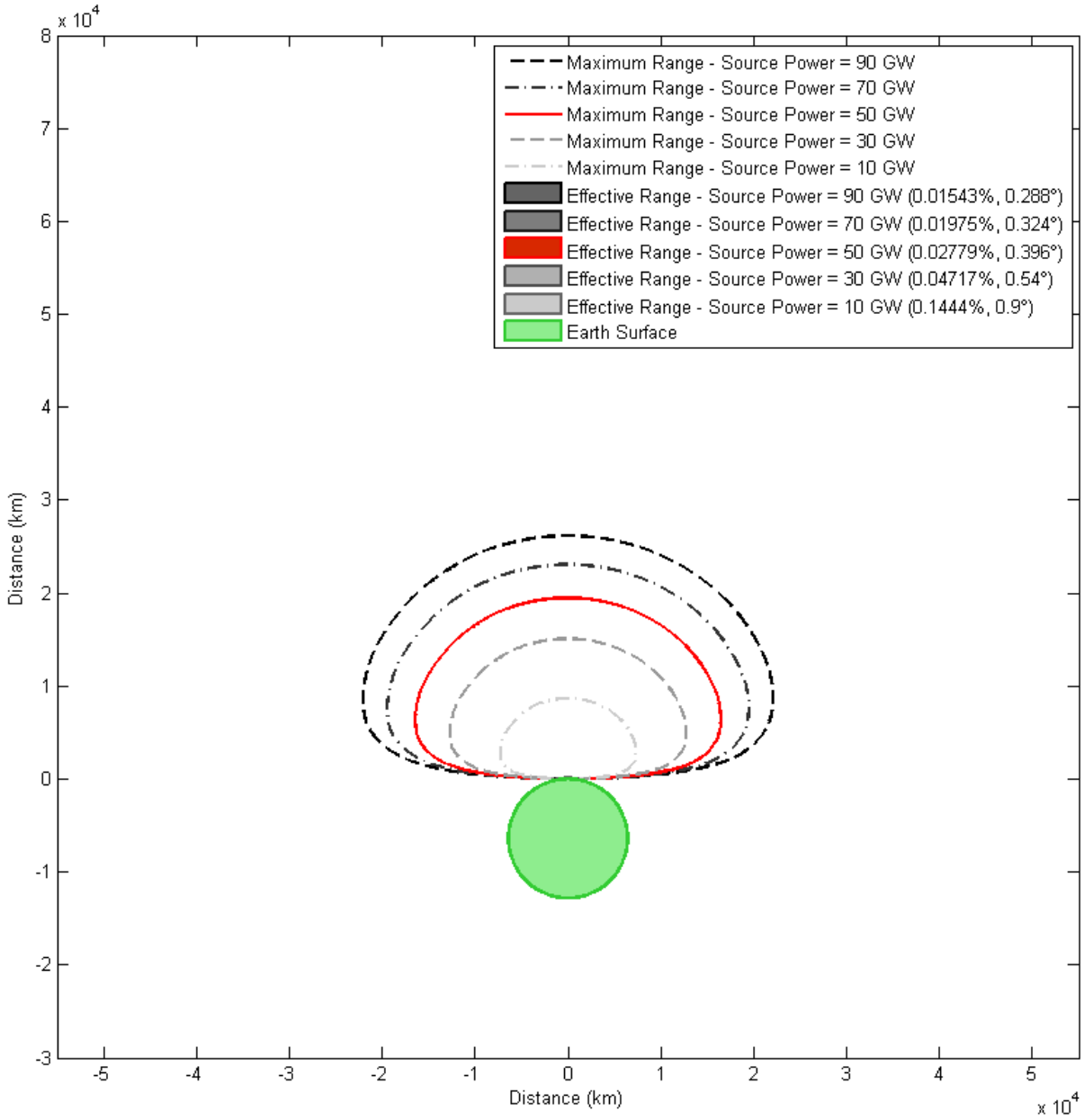

Figure 4.1.h: Ground-Based - Model 1 - "Earth" Plot - Sweeping Source Power

For power levels of 10 GW, 30 GW, 50 GW, 70 GW, and 90 GW: Maximum horizontal ranges are ≈7,374 km, 12,770 km, 16,490 km, 19,510 km, and 22,120 km at altitudes of ≈2,910 km, 5,040 km, 6,506 km, 7,698 km, and 8,728 km. Maximum vertical ranges are ≈8,745 km, 15,150 km, 19,550 km, 23,140 km, and 26,230 km. Maximum effective horizontal ranges are ≈1,049 km, 1,097 km, 1,091 km, 1,113 km, and 1,167 km at altitudes of ≈17.47 km, 11.34 km, 8.537 km, 7.295 km, and 6.865 km. Maximum effective vertical ranges are all 100 km. The effective ranges comprise ≈0.1444%, 0.0472%, 0.0278%, 0.0198%, and 0.0154% of the maximum range. The critical intersection is encountered at firing angles of ≈0.9°, 0.54°, 0.396°, 0.324°, and 0.288°. Angular accuracy: 0.036°. Range accuracy: 0.5 km. Note that due to the scale of this plot, the effective system range is not visible.

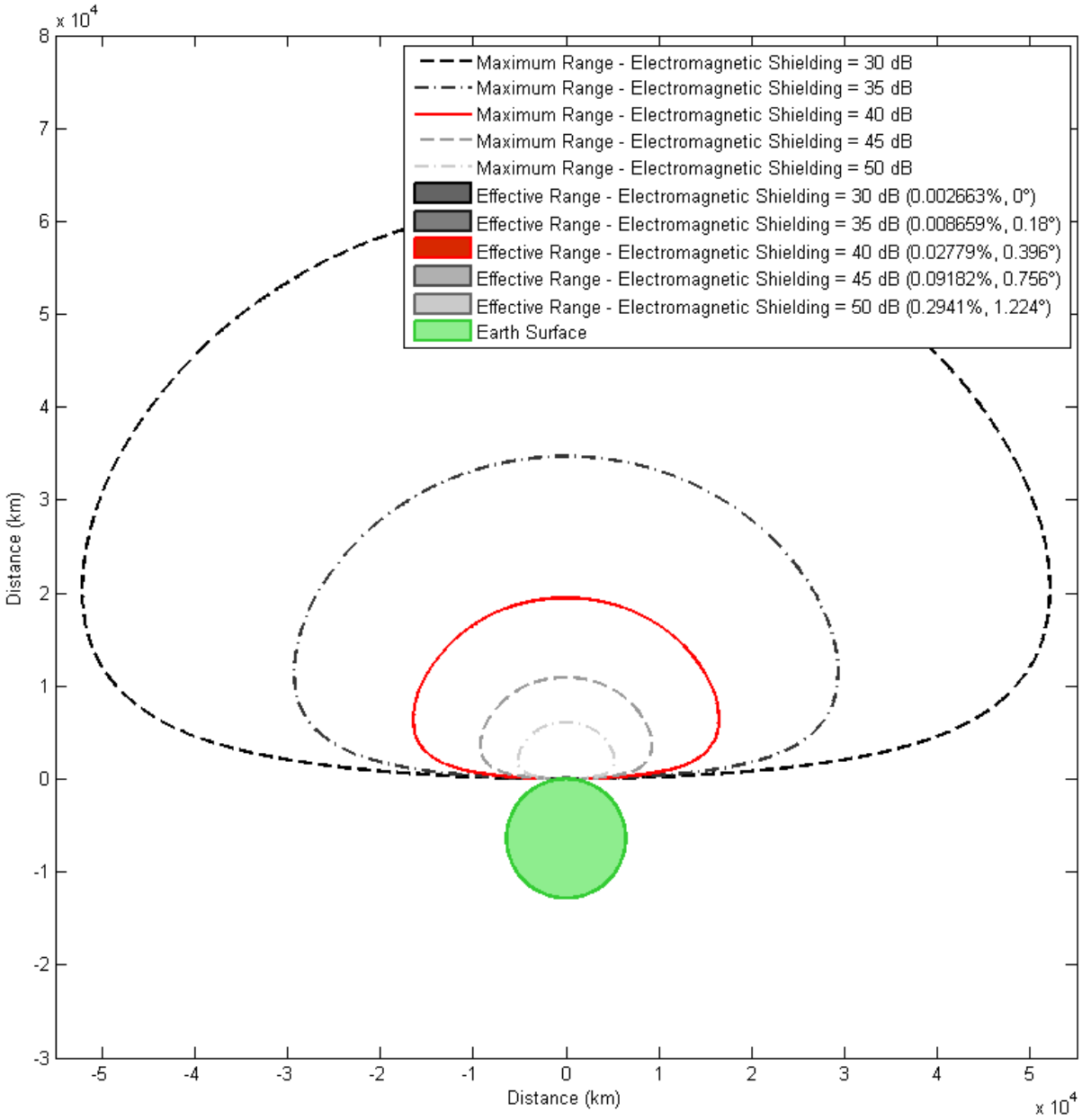

Figure 4.1.i: Ground-Based - Model 1 - "Earth" Plot - Sweeping Electromagnetic Shielding

For electromagnetic shielding levels of 50 dB, 45 dB, 40 dB, 35 dB, and 30 dB: Maximum horizontal ranges are ≈5,215 km, 9,273 km, 16,490 km, 29,320 km, and 52,150 km at altitudes of ≈2,058 km, 3,659 km, 6,506 km, 11,570 km, and 20,570 km. Maximum vertical ranges are ≈6,148 km, 11,000 km, 19,550 km, 34,770 km, and 61,830 km. Maximum effective horizontal ranges are ≈1,028 km, 1,101 km, 1,091 km, 1,195 km, and 1,269 km at altitudes of ≈22.97 km, 15.53 km, 8.537 km, 4.756 km, and 1 km. Maximum effective vertical ranges are all 100 km. The effective ranges comprise ≈0.2941%, 0.0918%, 0.0278%, 0.0087%, and 0.0027% of the maximum range. The critical intersection is encountered at firing angles of ≈1.224°, 0.756°, 0.396°, 0.18°, and 0°. Angular accuracy: 0.036°. Range accuracy: 0.5 km. Note that due to the scale of this plot, the effective system range is not visible.

Ground-Based - Model 1 - "Earth" - Critical Altitude

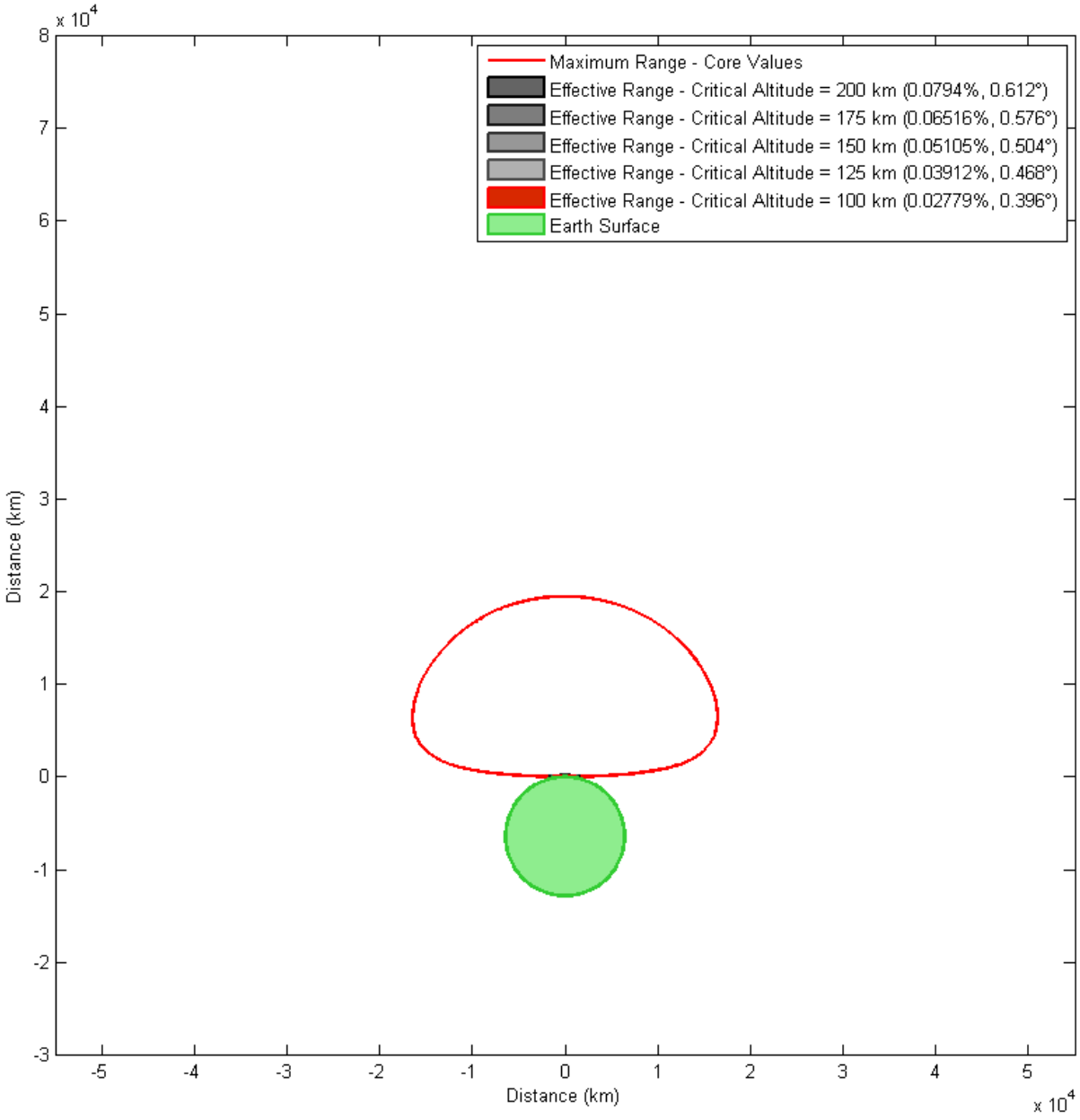

Figure 4.1.j: Ground-Based - Model 1 - "Earth" Plot - Sweeping Critical Altitude

For critical altitudes of 100 km, 125 km, 150 km, 175 km, and 200 km: Maximum effective horizontal ranges are ≈1,091 km, 1,249 km, 1,332 km, 1,503 km, and 1,591 km at altitudes of ≈8.537 km, 11.21 km, 12.72 km, 16.11 km, and 18 km. The effective ranges comprise ≈0.0278%, 0.0391%, 0.0511%, 0.0652%, and 0.0794% of the maximum range. The critical intersection is encountered at firing angles of ≈0.396°, 0.468°, 0.504°, 0.576°, and 0.612°. Angular accuracy: 0.036°. Range accuracy: 0.5 km. Note that due to the scale of this plot, the effective system range is not visible.

Ground-Based - Model 1 - "Earth" - Core Values (Enhanced)

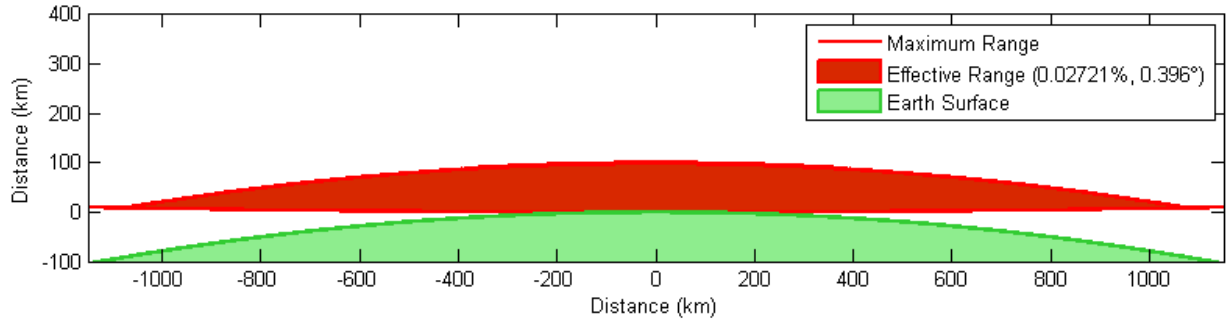

Figure 4.1.k: Ground-Based - Model 1 - "Earth" Plot - Core Values (Enhanced)

For the core values: The maximum effective horizontal range is ≈1,091 km at a vertical location of ≈8.537 km. The maximum effective vertical range is 100 km. The effective range comprises ≈0.0272% of the maximum range. The critical intersection is encountered at a firing angle of ≈0.396°. Angular accuracy: 0.036°. Range accuracy: 0.5 km.

Ground-Based - Model 1 - "Earth" - Operating Frequency (Enhanced)

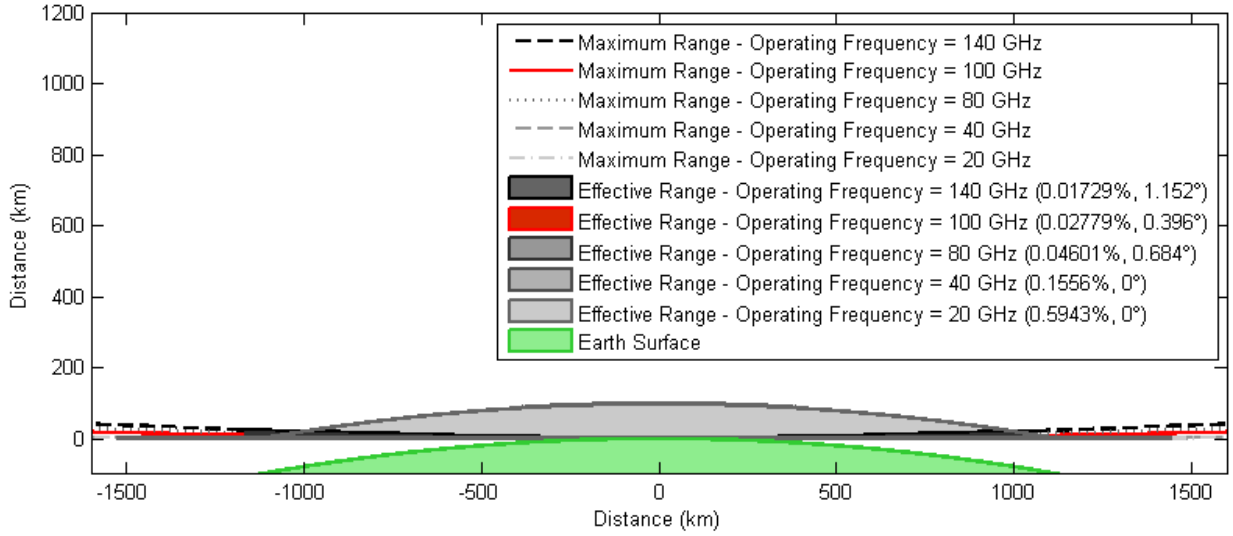

Figure 4.1.l: Ground-Based - Model 1 - "Earth" Plot - Sweeping Operating Frequency (Enhanced)

For operating frequencies of 20 GHz, 40 GHz, 80 GHz, 100 GHz, and 140 GHz: Maximum effective horizontal ranges are ≈1,445 km, 1,406 km, 1,057 km, 1,091 km, and 1,055 km at altitudes of ≈1 km, 1 km, 13.62 km, 8.537 km, and 22.22 km. Maximum effective vertical ranges are all 100 km. The effective ranges comprise ≈0.5943%, 0.1556%, 0.046%, 0.0278%, and 0.0173% of the maximum range. The critical intersection is encountered at firing angles of ≈0°, 0°, 0.684°, 0.396°, and 1.152°. Angular accuracy: 0.036°. Range accuracy: 0.5 km.

The plot in Figure 4.1.l depicts the "enhanced" plot for the effective coverage regions of GB-VM1 when sweeping operating frequency. Due to the extreme maximum ranges, the effective ranges are all quite similar and appear to be stacked on top of each other. This observation is the case for nearly all enhanced GB-VM1 plots. For this reason, the maximum effective horizontal ranges are explicitly detailed in the caption of each enhanced plot.

Ground-Based - Model 1 - "Earth" - Antenna Diameter (Enhanced)

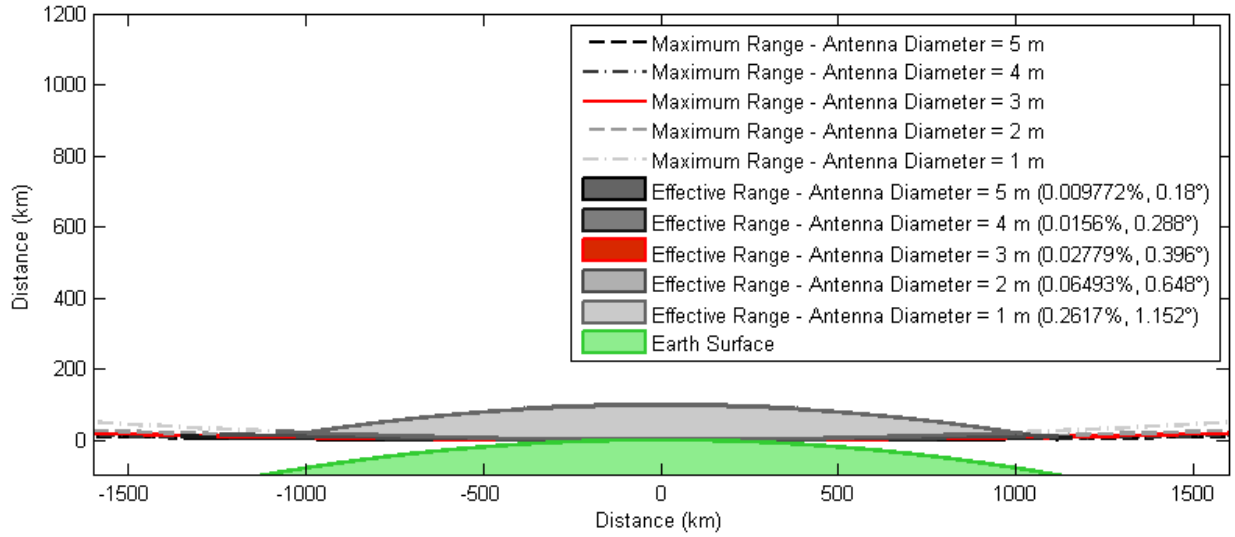

Figure 4.1.m: Ground-Based - Model 1 - "Earth" Plot - Sweeping Antenna Diameter (Enhanced)

For antenna diameters of 1 m, 2 m, 3 m, 4 m, and 5 m: Maximum effective horizontal ranges are ≈1,016 km, 1,121 km, 1,091 km, 1,160 km, and 1,120 km at vertical locations of ≈21.43 km, 13.67 km, 8.537 km, 6.829 km, and 4.52 km. Maximum effective vertical ranges are all 100 km. The effective ranges comprise ≈0.2617%, 0.0649%, 0.0278%, 0.0156% and 0.0098% of the maximum range. The critical intersection is encountered at firing angles of ≈1.152°, 0.648°, 0.396°, 0.288°, and 0.18°. Angular accuracy: 0.036°. Range accuracy: 0.5 km.

Ground-Based - Model 1 - "Earth" - Source Power (Enhanced)

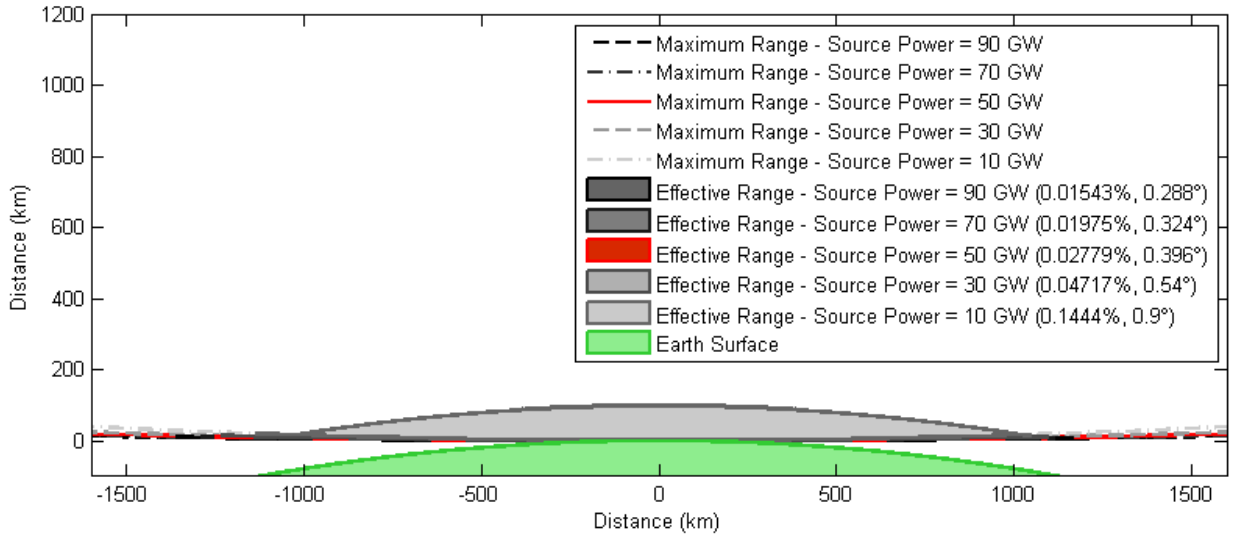

Figure 4.1.n: Ground-Based - Model 1 - "Earth" Plot - Sweeping Source Power (Enhanced)

For power levels of 10 GW, 30 GW, 50 GW, 70 GW, and 90 GW: Maximum effective horizontal ranges are ≈1,049 km, 1,097 km, 1,091 km, 1,113 km, and 1,167 km at vertical locations of ≈17.47 km, 11.34 km, 8.537 km, 7.295 km, and 6.865 km. Maximum effective vertical ranges are all 100 km. The effective ranges comprise ≈0.1444%, 0.0472%, 0.0278%, 0.0198%, and 0.0154% of the maximum range. The critical intersection is encountered at firing angles of ≈0.9°, 0.54°, 0.396°, 0.324°, and 0.288°. Angular accuracy: 0.036°. Range accuracy: 0.5 km.

Ground-Based - Model 1 - "Earth" - Electromagnetic Shielding (Enhanced)

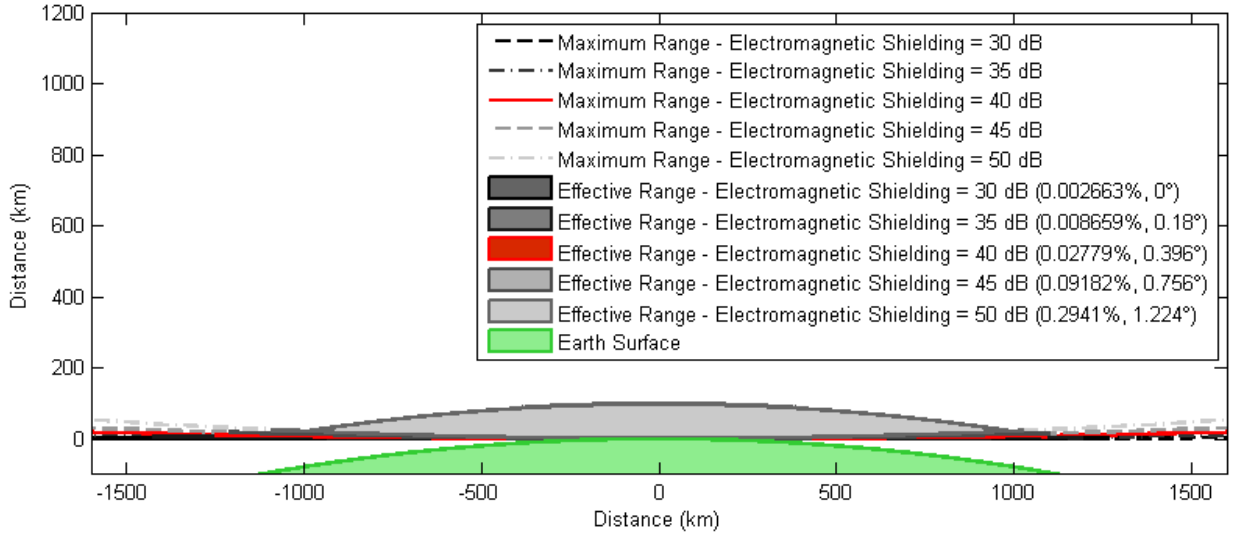

Figure 4.1.o: Ground-Based - Model 1 - "Earth" Plot - Sweeping Electromagnetic Shielding (Enhanced)

For electromagnetic shielding levels of 50 dB, 45 dB, 40 dB, 35 dB, and 30 dB: Maximum effective horizontal ranges are ≈1,028 km, 1,101 km, 1,091 km, 1,195 km, and 1,269 km at vertical locationss of ≈22.97 km, 15.53 km, 8.537 km, 4.756 km, and 1 km. Maximum effective vertical ranges are all 100 km. The effective ranges comprise ≈0.2941%, 0.0918%, 0.0278%, 0.0087%, and 0.0027% of the maximum range. The critical intersection is encountered at firing angles of ≈1.224°, 0.756°, 0.396°, 0.18°, and 0°. Angular accuracy: 0.036°. Range accuracy: 0.5 km.

Ground-Based - Model 1 - "Earth" - Critical Altitude (Enhanced)

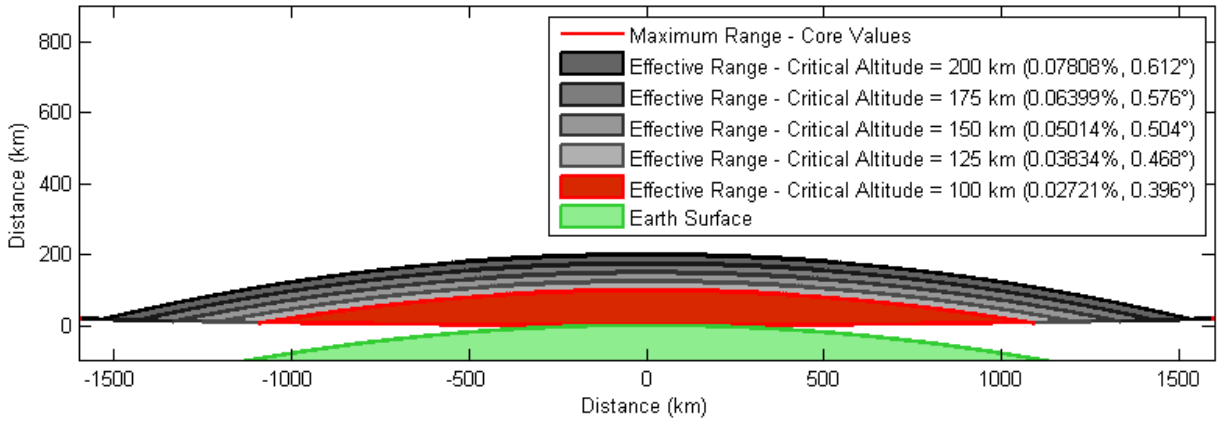

Figure 4.1.p: Ground-Based - Model 1 - "Earth" Plot - Sweeping Critical Altitude (Enhanced)
Effective ranges, for very large maximum ranges, take on the values of an Earth-centered circle with radius $R_E + h_c$, where R_E is the radius of the Earth and h_c is the critical altitude. For critical altitudes of 100 km, 125 km, 150 km, 175 km, and 200 km: Maximum effective horizontal ranges are ≈1,091 km, 1,249 km, 1,332 km, 1,503 km, and 1,591 km at vertical locations of ≈8.537 km, 11.21 km, 12.72 km, 16.11 km, and 18 km. The effective ranges comprise ≈0.0278%, 0.0391%, 0.0511%, 0.0652%, and 0.0794% of the maximum range. The critical intersection is encountered at firing angles of ≈0.396°, 0.468°, 0.504°, 0.576°, and 0.612°. Angular accuracy: 0.036°. Range accuracy: 0.5 km.

In Figure 4.1.l above, the critical intersection angle is 0° for both 20 GHz and 40 GHz. This observation is significant as it represents a unique case where the range of the system is continually in excess of the effective range and thus is maximally effective at all angles. This observation is confirmed by plot's data. The maximum effective downrange for both 20 GHz and 40 GHz is shown to be greater than the maximum effective downrange of the other subplots (1,117 kilometers versus 993.9 kilometers, 1,005 kilometers, and 980.8 kilometers). The downrange of 1,117 kilometers is, in fact, the maximum downrange distance for critical and deployment altitudes of one-hundred and one kilometers respectively. This result can be confirmed using the equation for the maximum downrange distance, as defined in Eq. (3.3.nn), which gives a maximum possible downrange of $R_{dr_{max}}(h_0 = 1, h_c = 100) = 1{,}116.49\ km$.

"Downrange Surface" plots were generated for Vulnerability Model 1. As stated in Section 4.1.1.3, all surface plots are done as a function of operating frequency and one other parameter. "Downrange Surface" plots are shown below in Figure 4.1.q, Figure 4.1.r, and

Figure 4.1.s for the additional parameter of antenna diameter, source power, and electromagnetic shielding.

Ground-Based - Model 1 - "Downrange" - Frequency/Antenna Diameter

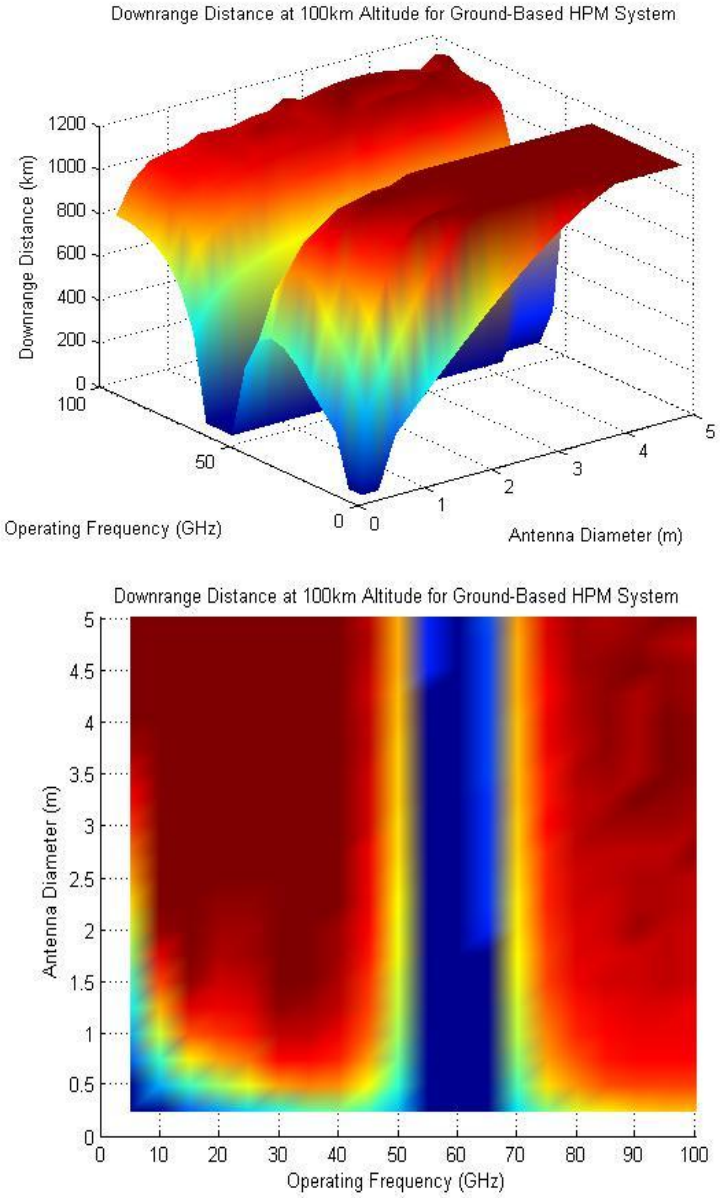

Figure 4.1.q: Ground-Based - Model 1 - "Downrange" Plot - Frequency/Antenna Diameter

Surface plot of an HPM System's Downrange Distance at an Interception Altitude of 100 km as a Function of Operating Frequency and Antenna Diameter is shown. At lower frequencies, the atmosphere is nearly transparent to microwave radiation. Therefore, when the diameter is increased beyond a certain point, the maximum downrange distance levels off at 1128 km, representing the maximum distance achievable by a horizontally fired beam under an altitude of 100 km for a system stationed at an altitude of one kilometer. This value is limited by the curvature of the earth, and as such further improvements of an HPM system do not affect this value. Outside of this frequency range, however, atmospheric restrictions constrain the maximum range more heavily and allow less variation with antenna diameter. Coincidentally, this balances out to nearly the same downrange value as the physical limit presented by the curvature of the earth.

Ground-Based - Model 1 - "Downrange" - Frequency/Source Power

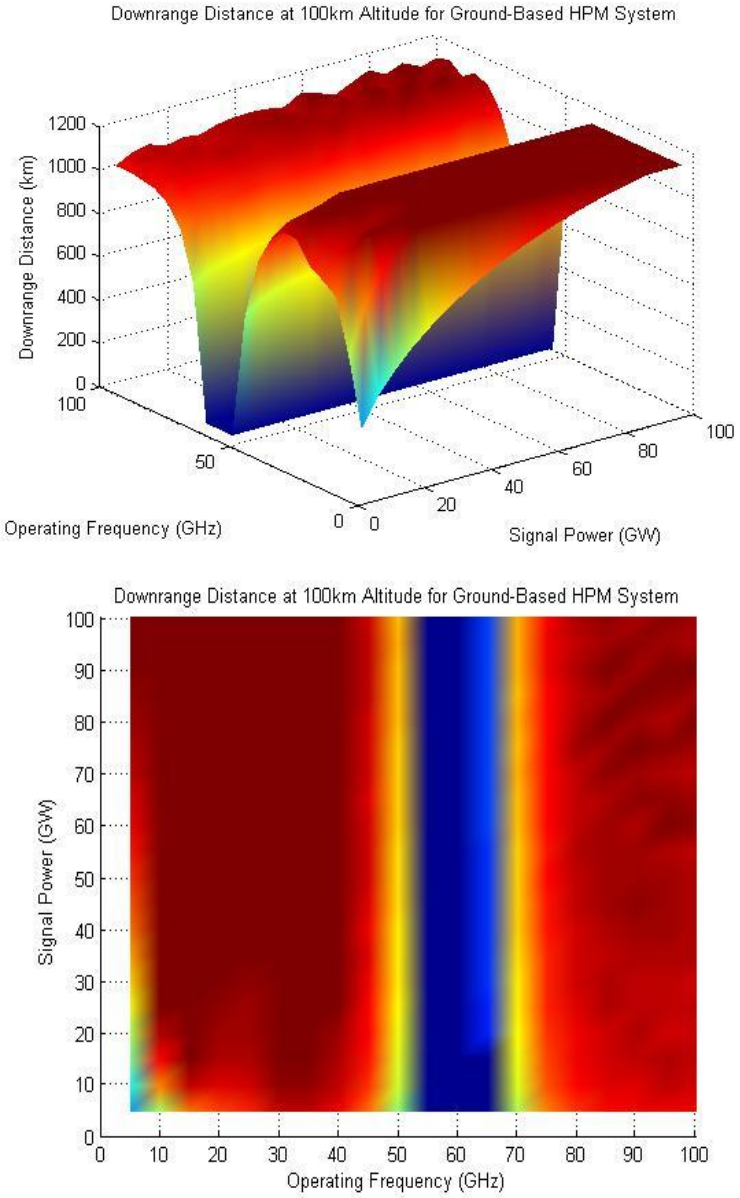

Figure 4.1.r: Ground-Based - Model 1 - "Downrange" Plot - Frequency/Source Power

Surface plot of an HPM System's Downrange Distance at an Interception Altitude of 100 km as a Function of Operating Frequency and Signal Power is shown. The relationship shown here is very similar to that shown in the previous figure. At frequencies near to the resonant frequencies of oxygen, the atmosphere is nearly opaque to electromagnetic radiation. The downrange distances near this "60 GHz complex" are zero, as the beams are attenuated too heavily to reach the critical altitude.

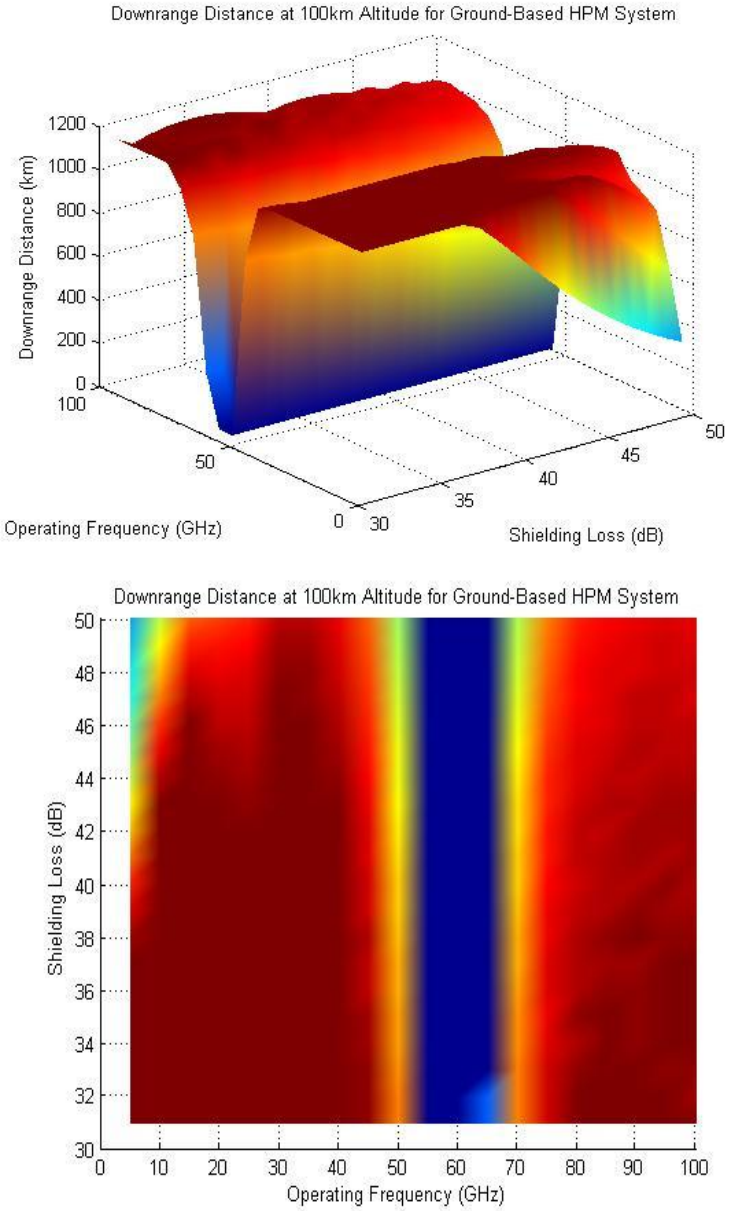

Figure 4.1.s: Ground-Based - Model 1 - "Downrange" Plot - Frequency/Electromagnetic Shielding

Surface plot of an HPM System's Downrange Distance at an Interception Altitude of 100 km as a Function of Operating Frequency and Attenuation Due to Shielding is shown. At low frequencies, the maximum downrange distance is achieved for low levels of shielding attenuation. However, at higher levels, this range quickly drops off to much lower values.

4.1.3 Ground-Based - Vulnerability Model 2

The second Vulnerability Model considered for a ground-based HPM system was a moderately vulnerable target model. The core values of the ground-based Vulnerability Model 2 (GB-VM2) can be seen below in Table 4.1.c. GB-VM2 is nearly identical to GB-VM1 with the exception of the required intensity on target, which increases to 10 W/m^2 from 10^{-2} W/m^2.

Parameter Name	Core Value	Units
Operating Frequency	100	$[GHz]$
Antenna Diameter	3	$[m]$
Source Power	50	$[GW]$
Intensity on Target	10	$[W/m^2]$
Electromagnetic Shielding	40	$[dB]$
Critical Altitude	100	$[km]$

Table 4.1.c: Ground-Based - Vulnerability Model 2 (Moderately Vulnerable) - Core Values
Vulnerability Model 2 was used to represent a highly moderately target model with a required intensity of 0.01 W/m^2. In comparison to Vulnerability Model 1, all other parameters with the exception of intensity on target were held constant.

The sweep limits for GB-VM2 can be seen below in Table 4.1.d. Again, all parameter sweeps attempt to predictably span a range near the core values with the exception of frequency.

Parameter Name	Sweep Values	Units
Operating Frequency	$[20, 40, 80, 100, 140]$	$[GHz]$
Antenna Diameter	$[1, 2, 3, 4, 5]$	$[m]$
Source Power	$[10, 30, 50, 70, 90]$	$[GW]$
Intensity on Target	[N/A]	$[W/m^2]$
Electromagnetic Shielding	$[30, 35, 40, 45, 50]$	$[dB]$
Critical Altitude	$[100, 125, 150, 175, 200]$	$[km]$

Table 4.1.d: Ground-Based - Vulnerability Model 2 (Moderately Vulnerable) - Sweep Values
The Vulnerability Model 2 sweep values indicate the values used for each parameter sweep in "Earth" plots. For example, when sweeping operating frequency, 20 GHz, 40 GHz, 80 GHz, 100 GHz, and 140 GHz were used.

Using the case values, “Earth” plots were generated. The “Earth” plot for the core GB-VM2 values can be seen below in Figure 4.1.t. The maximum range of GB-VM2 extends to ≈521.5 kilometers horizontally at an altitude of ≈206.7 kilometers, while the maximum effective range reaches ≈466.1 kilometers at an altitude of ≈83.25 kilometers.

Additional “Earth” plots for GB-VM2 which sweep the parameters of operating frequency, antenna diameter, source power, electromagnetic shielding, and critical altitude can be seen in Figure 4.1.u, Figure 4.1.v, Figure 4.1.w, Figure 4.1.x, and Figure 4.1.y respectively.

Ground-Based - Model 2 - "Earth" - Core Values

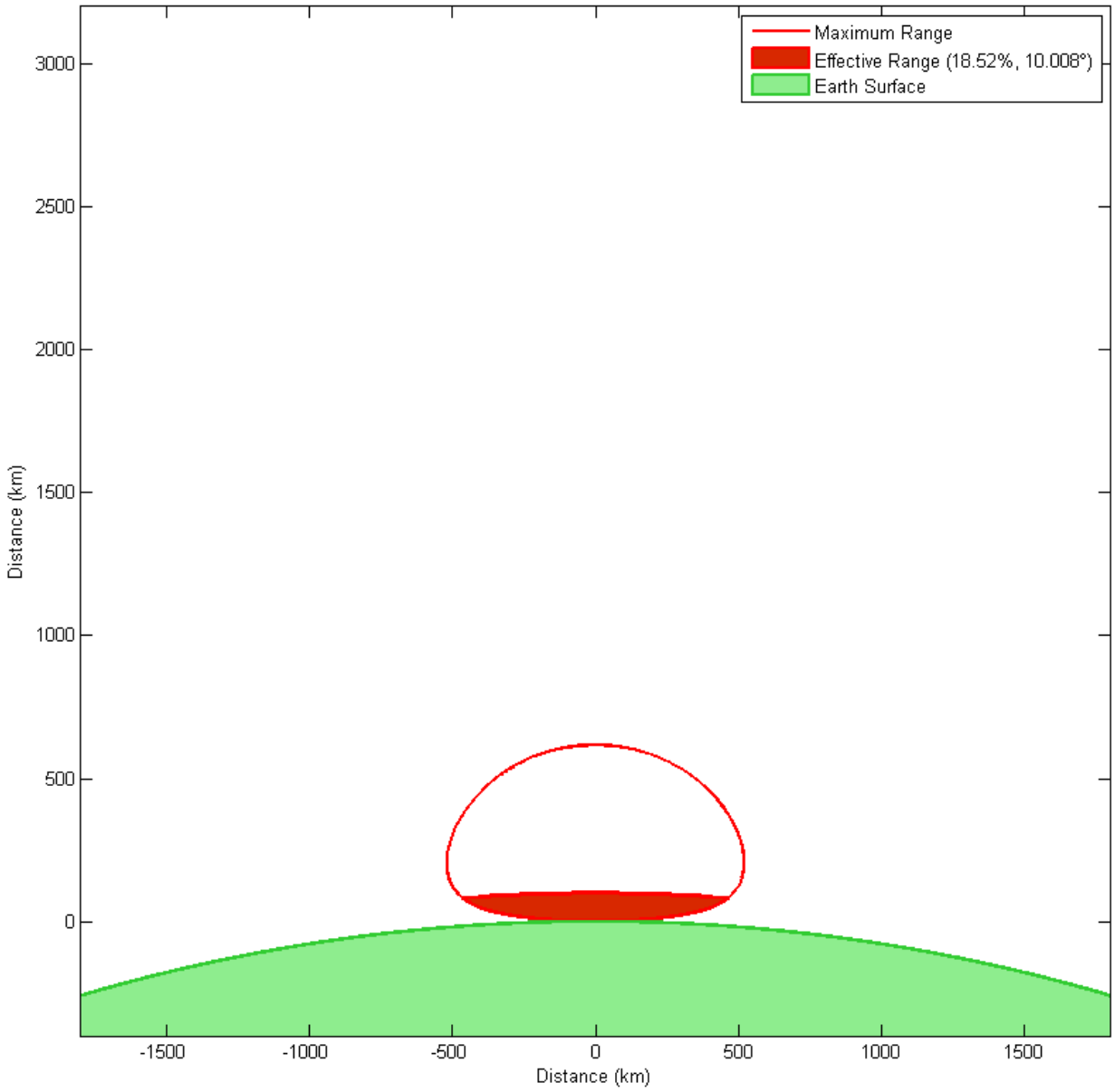

Figure 4.1.t: Ground-Based HPM - Model 2 - "Earth" Plot - Core Values

For core values: The maximum horizontal range is ≈521.5 km at a vertical location of ≈206.7 km. The maximum vertical range is ≈619.3 km. The maximum effective horizontal range is ≈466.1 km at an altitude of ≈83.25 km. The maximum effective vertical range is 100 km. The effective range comprises ≈18.52% of the maximum range. The critical intersection is encountered at a firing angle of ≈10.008°. Angular accuracy: 0.036°. Range accuracy: 0.5 km.

Ground-Based - Model 2 - "Earth" - Operating Frequency

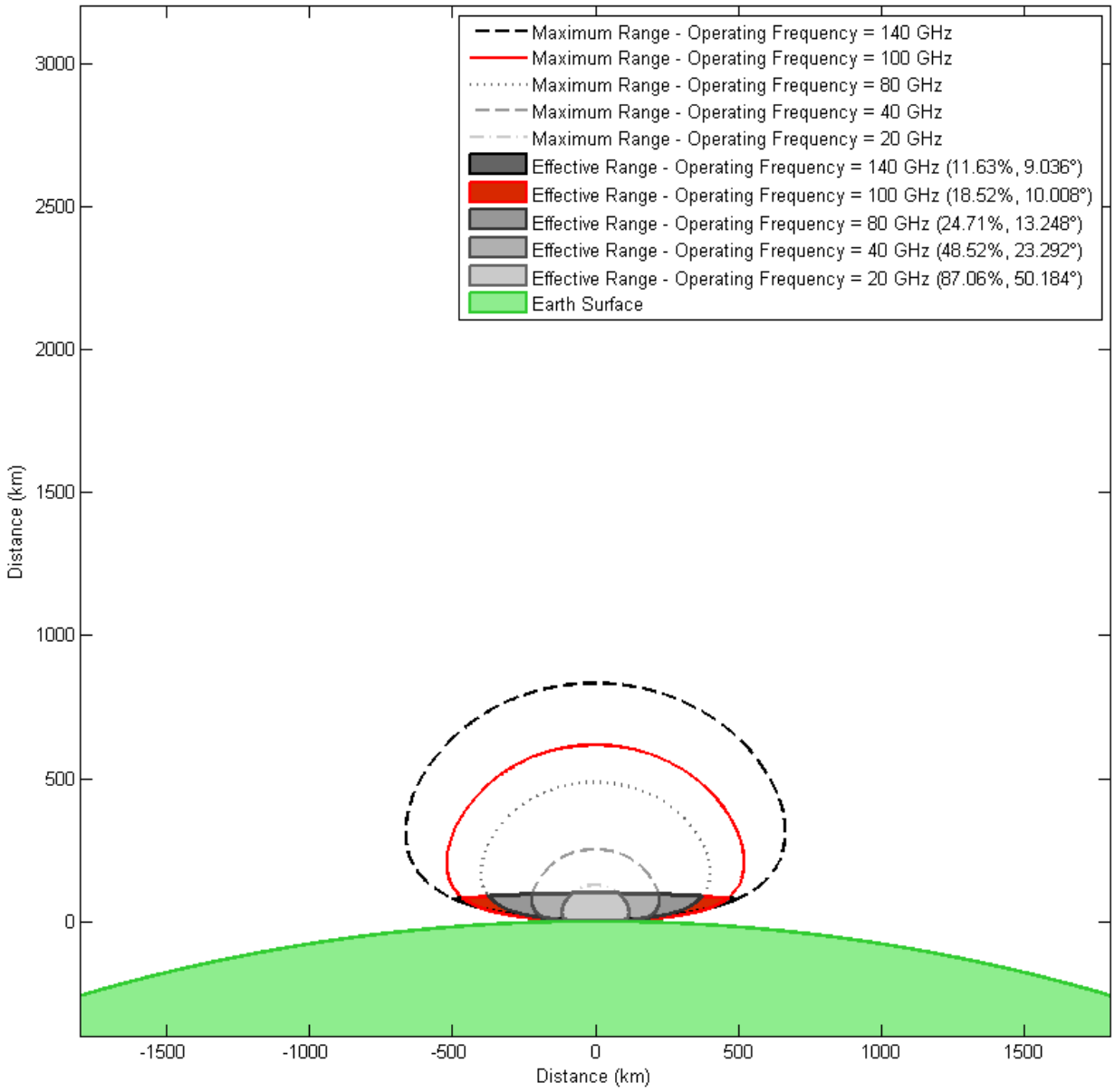

Figure 4.1.u: Ground-Based HPM - Model 2 - "Earth" Plot - Sweeping Operating Frequency

For operating frequencies of 20 GHz, 40 GHz, 80 GHz, 100 GHz, and 140 GHz: Maximum horizontal ranges are ≈119 km, 224 km, 402.4 km, 521.5 km, and 665.3 km at vertical locations of ≈31.08 km, 73.63 km, 172.8 km, 206.7 km, and 312 km. Maximum vertical ranges are ≈129.8 km, 254.3 km, 488.9 km, 619.3 km, and 835.5 km. Maximum effective horizontal ranges are ≈119 km, 224 km, 375.4 km, 466.1 km, and 501.3 km at vertical locations of ≈31.08 km, 73.63 km, 89.39 km, 83.25 km, and 80.72 km. Maximum effective vertical ranges are all 100 km. The effective ranges comprise ≈87.06%, 48.52%, 24.71%, 18.52%, and 11.63% of the maximum range. The critical intersection is encountered at firing angles of ≈50.184°, 23.292°, 13.248°, 10.008°, and 9.036°. Angular accuracy: 0.036°. Range accuracy: 0.5 km.

Ground-Based - Model 2 - "Earth" - Antenna Diameter

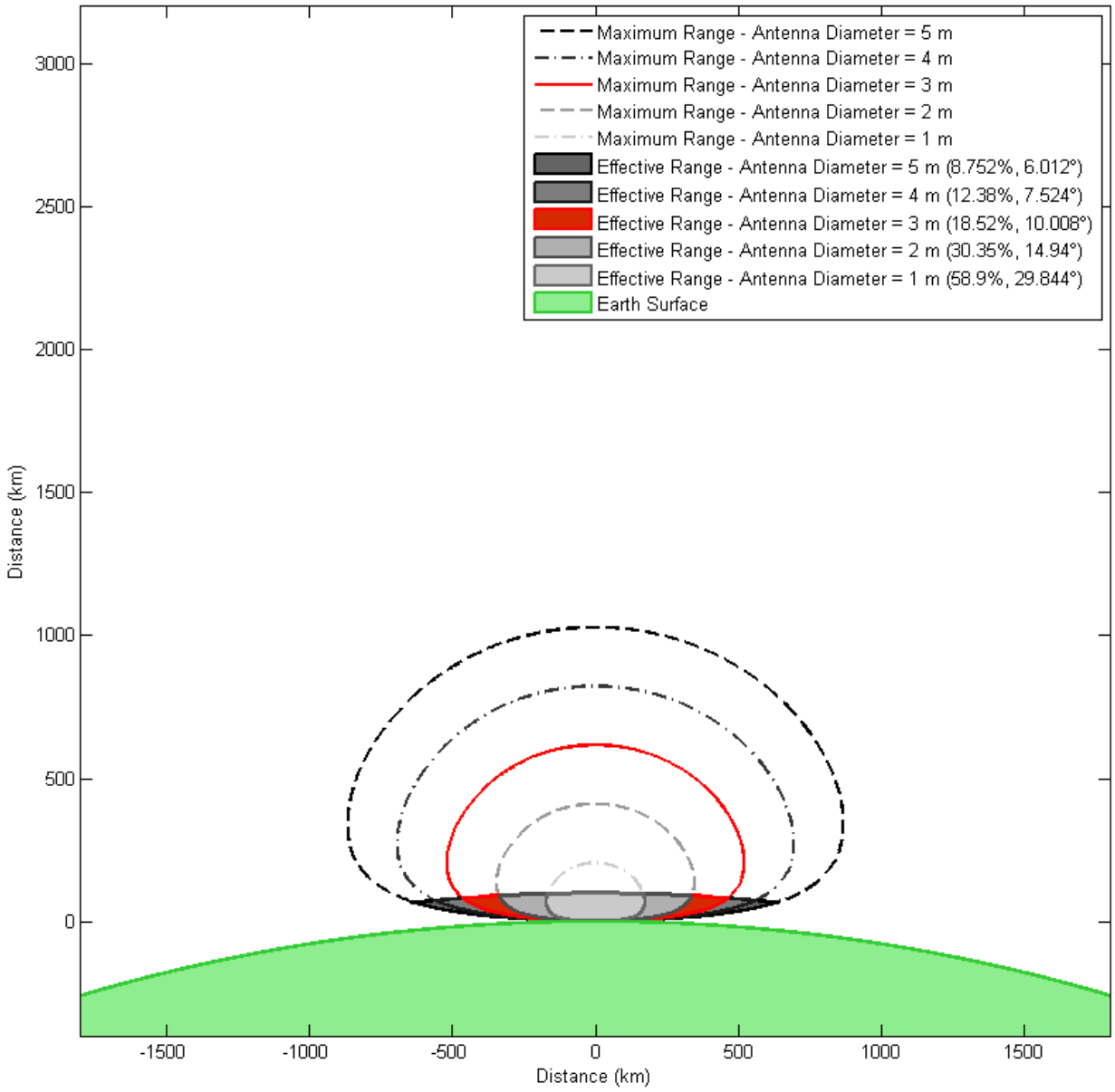

Figure 4.1.v: Ground-Based HPM - Model 2 - "Earth" Plot - Sweeping Antenna Diameter

For antenna diameters of 1 m, 2 m, 3 m, 4 m, and 5 m: Maximum horizontal ranges are ≈173.8 km, 347.6 km, 521.5 km, 695.3 km, and 869.1 km at vertical locations of ≈69.57 km, 138.1 km, 206.7 km, 275.3 km, and 343.8 km. Maximum vertical ranges are ≈207.1 km, 413.2 km, 619.3 km, 825.4 km, and 1,032 km. Maximum effective horizontal ranges are ≈173.8 km, 338.3 km, 466.1 km, 564.8 km, and 640.3 km at vertical locations of ≈69.57 km, 91.28 km, 83.25 km, 75.6 km, and 68.44 km. Maximum effective vertical ranges are all 100 km. The effective ranges comprise ≈58.9%, 30.35%, 18.52%, 12.38%, and 8.752% of the maximum range. The critical intersection is encountered at firing angles of ≈29.844°, 14.94°, 10.008°, 7.524°, and 6.012°. Angular accuracy: 0.036°. Range accuracy: 0.5 km.

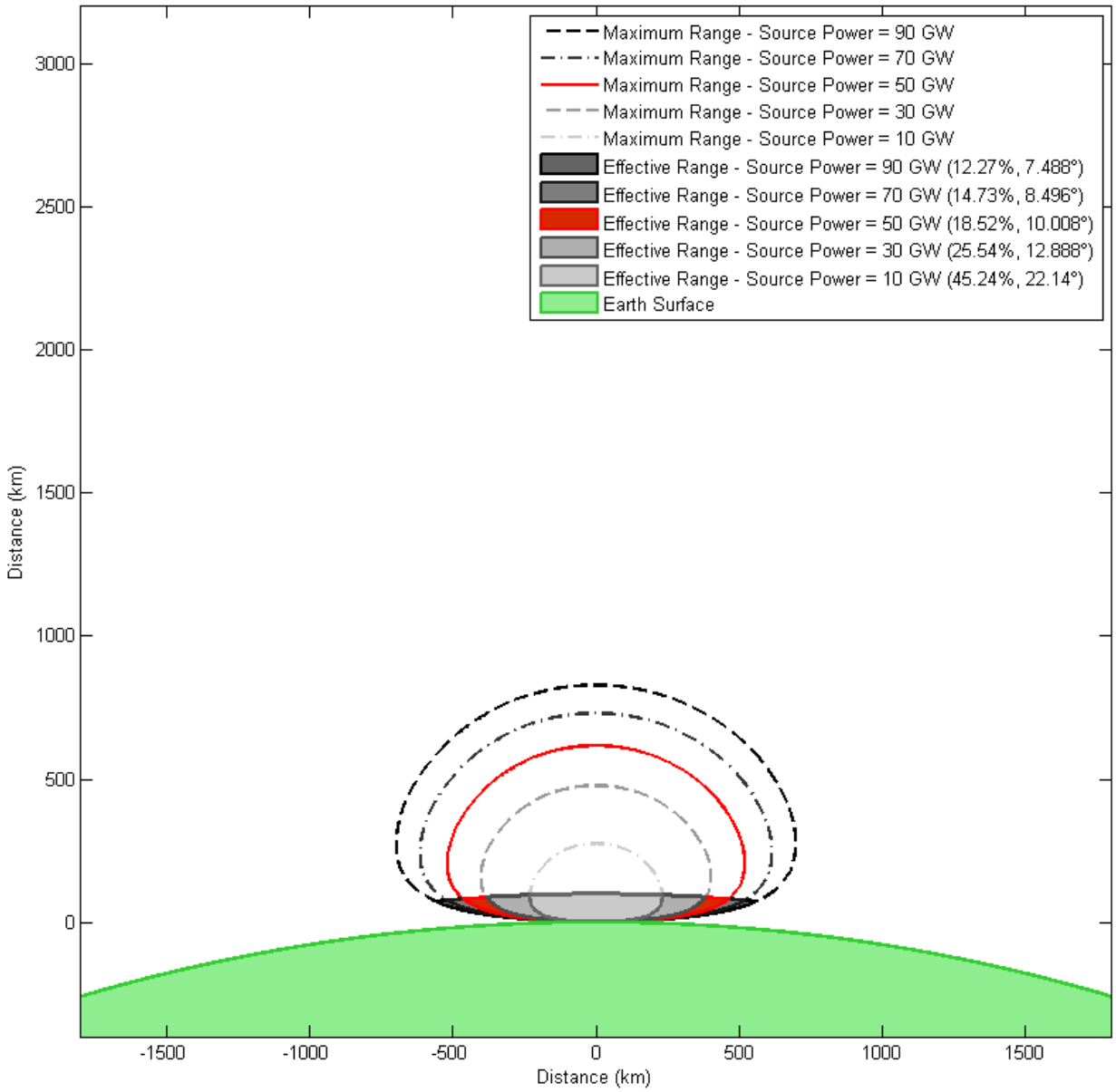

Figure 4.1.w: Ground-Based HPM - Model 2 - "Earth" Plot - Sweeping Source Power

For source power levels of 10 GW, 30 GW, 50 GW, 70 GW, and 90 GW: Maximum horizontal ranges are ≈233.2 km, 403.9 km, 521.5 km, 617 km, and 699.6 km at vertical locations of ≈92.99 km, 160.3 km, 206.7 km, 244.4 km, and 277 km. Maximum vertical ranges are ≈277.5 km, 479.9 km, 619.3 km, 732.6 km, and 830.5 km. Maximum effective horizontal ranges are ≈233.2 km, 383.4 km, 466.1 km, 524 km, and 567.3 km at vertical locations of ≈92.99 km, 88.74 km, 83.25 km, 79.28 km, and 75.56 km. Maximum effective vertical ranges are all 100 km. The effective ranges comprise ≈45.24%, 25.54%, 18.52%, 14.73%, and 12.27% of the maximum range. The critical intersection is encountered at firing angles of ≈22.14°, 12.888°, 10.008°, 8.496°, and 7.488°. Angular accuracy: 0.036°. Range accuracy: 0.5 km.

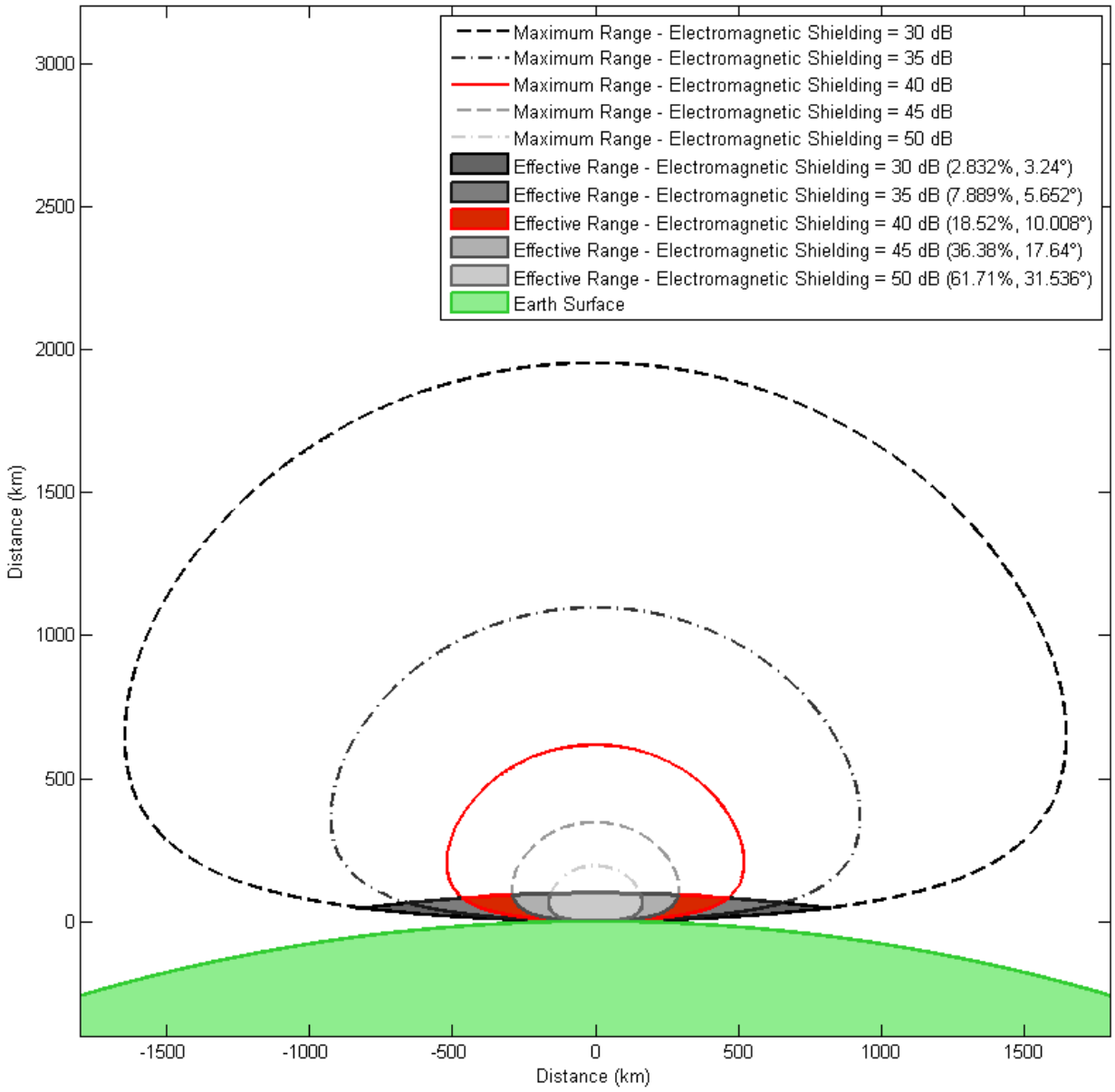

Figure 4.1.x: Ground-Based HPM - Model 2 - "Earth" Plot - Sweeping Electromagnetic Shielding

For electromagnetic shielding levels of 50 dB, 45 dB, 40 dB, 35 dB, and 30 dB: Maximum horizontal ranges are ≈164.9 km, 293.2 km, 521.5 km, 927.3 km, and 1,649 km at vertical locations of ≈66.05 km, 116.7 km, 206.7 km, 366.8 km, and 651.5 km. Maximum vertical ranges are ≈196.5 km, 348.7 km, 619.3 km, 1,101 km, and 1,956 km. Maximum effective horizontal ranges are ≈164.9 km, 290.8 km, 466.1 km, 662.6 km, and 825.3 km at vertical locations of ≈66.05 km, 93.47 km, 83.25 km, 66.58 km, and 47.72 km. Maximum effective vertical ranges are all 100 km. The effective ranges comprise ≈61.71%, 36.38%, 18.52%, 7.889%, and 2.832% of the maximum range. The critical intersection is encountered at firing angles of ≈31.536°, 17.64°, 10.008°, 5.652°, and 3.24°. Angular accuracy: 0.036°. Range accuracy: 0.5 km.

Ground-Based - Model 2 - "Earth" - Critical Altitude

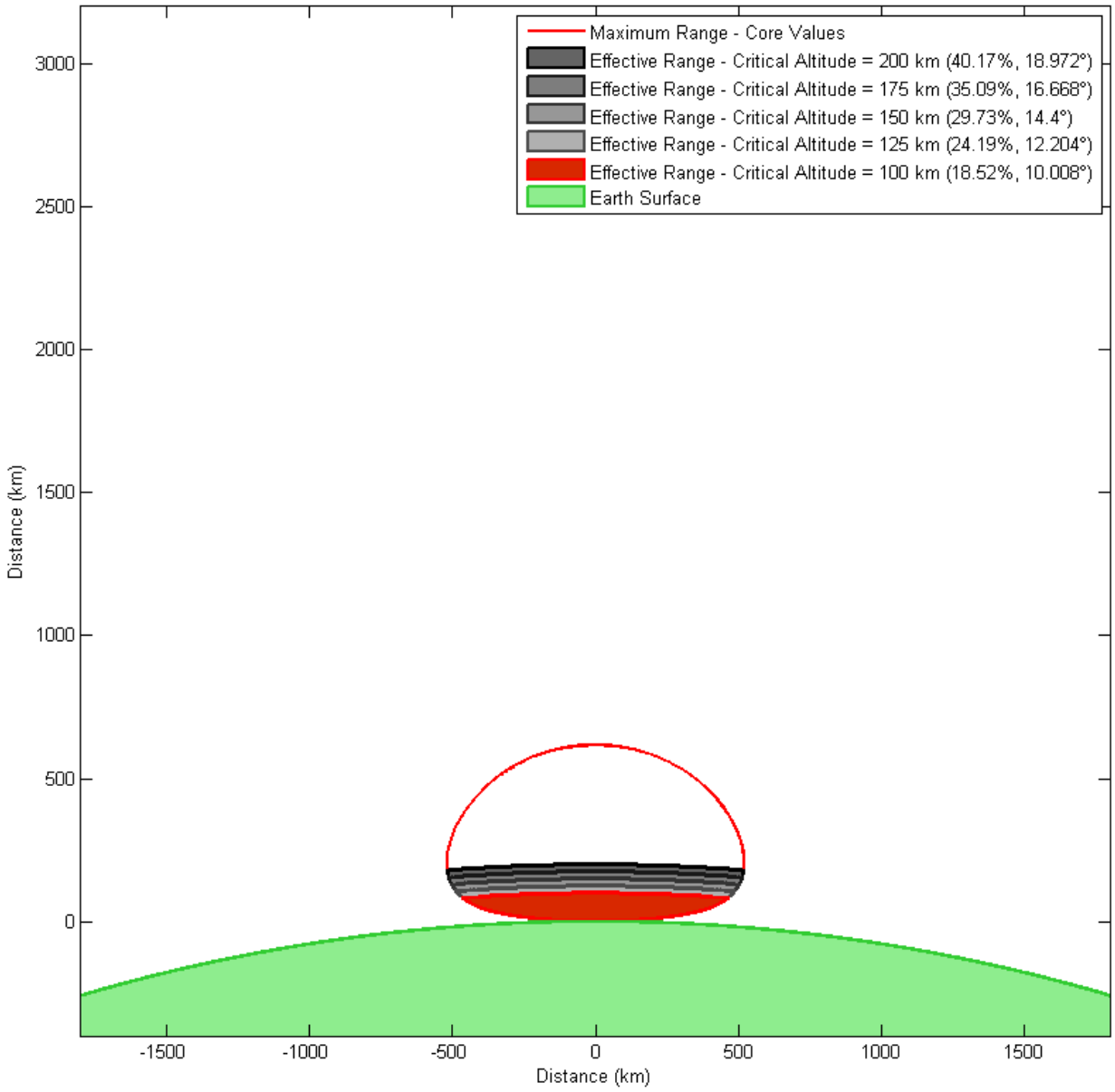

Figure 4.1.y: Ground-Based HPM - Model 2 - "Earth" Plot - Sweeping Critical Altitude

For critical altitudes of 100 km, 125 km, 150 km, 175 km, and 200 km: Maximum effective horizontal ranges are ≈466.1 km, 489.6 km, 504.7 km, 514.4 km, and 519.7 km at vertical locations of ≈83.25 km, 106.9 km, 130.6 km, 155 km, and 179.7 km. The effective ranges comprise ≈18.52%, 24.19%, 29.73%, 35.09%, and 40.17% of the maximum range. The critical intersection is encountered at firing angles of ≈10.008°, 12.204°, 14.4°, 16.668°, and 18.972°. Angular accuracy: 0.036°. Range accuracy: 0.5 km.

"Downrange" plots were generated for GB-VM2. Again downrange distance and operating frequency were plotted against antenna diameter, source power, and electromagnetic shielding in Figure 4.1.z, Figure 4.1.aa, and Figure 4.1.bb respectively.

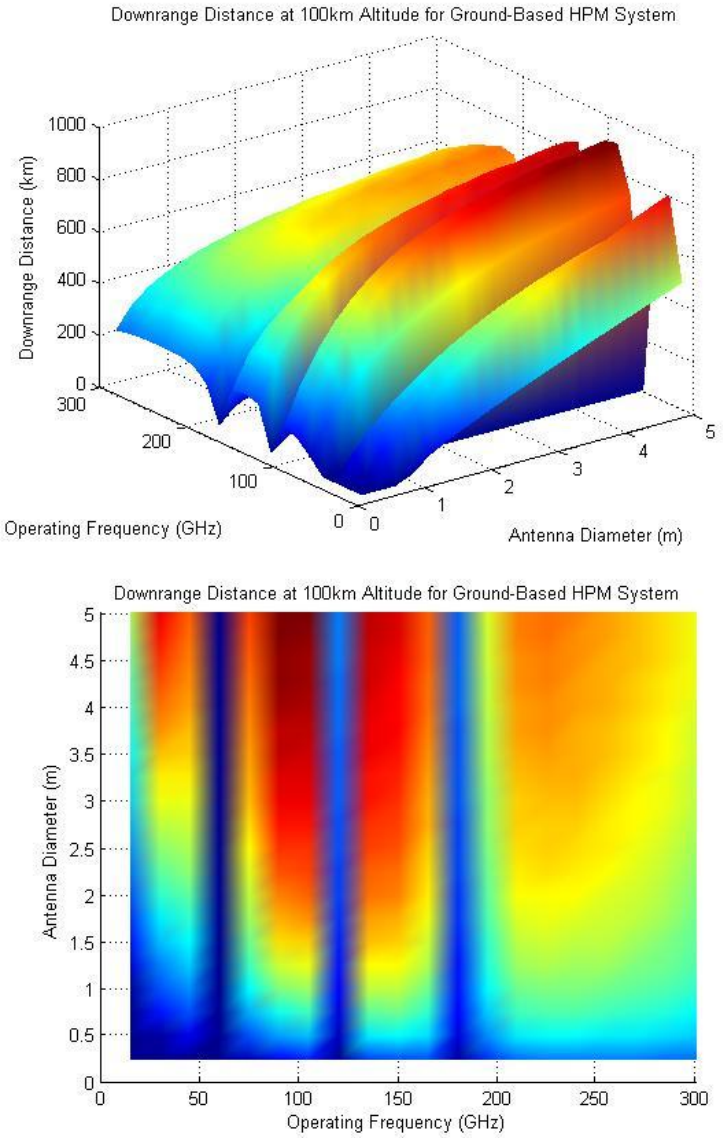

Figure 4.1.z: Ground-Based - Model 2 - "Downrange" Plot - Frequency/Antenna Diameter

Surface plot of an HPM System's Downrange Distance at an Interception Altitude of 100km as a Function of Operating Frequency and Attenuation Due to Shielding is shown. At very low frequencies, the atmosphere is nearly transparent to microwaves and as such the linear relationship of range to antenna diameter predicted by Eq. (3.1.m) can be seen. However, because of the non-linear effects of atmospheric attenuation, this relationship becomes less obvious at higher frequencies.

Ground-Based - Model 2 - "Downrange" - Frequency/Source Power

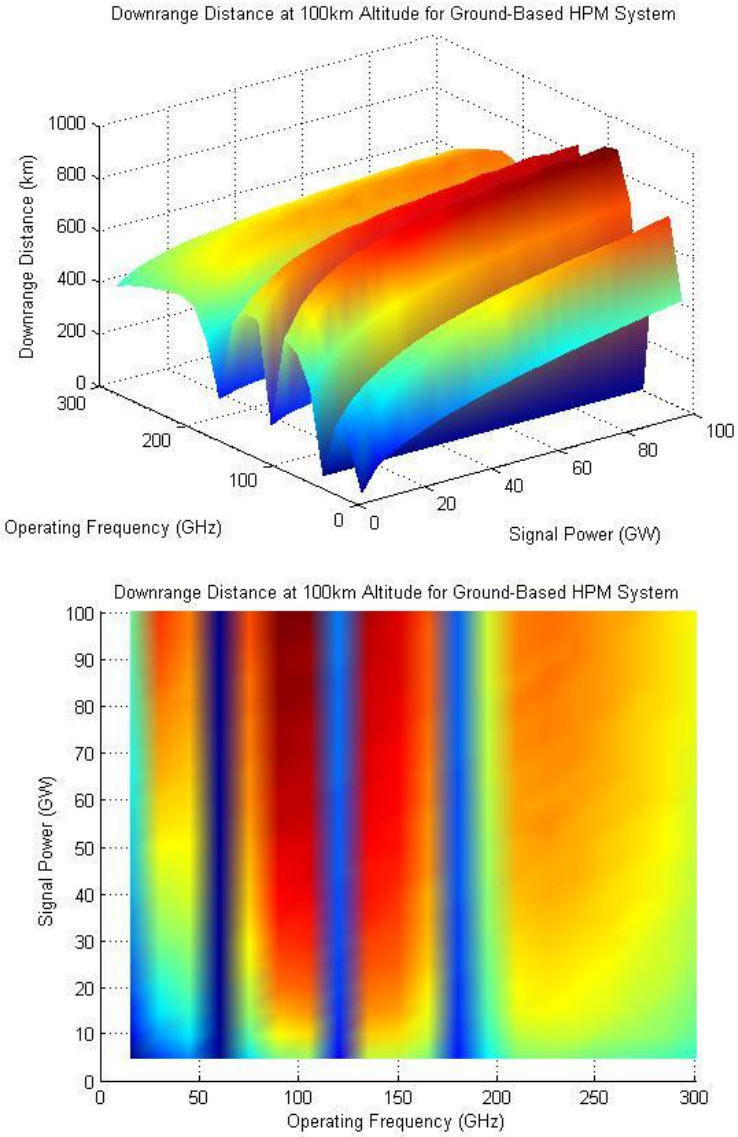

Figure 4.1.aa: Ground-Based - Model 2 - "Downrange" Plot - Frequency/Source Power

Surface plot of an HPM System's Downrange Distance at an Interception Altitude of 100km as a Function of Operating Frequency and Power is shown. Downrange distance increases as a function of signal power. However, at high frequencies, the atmospheric attenuation constrains the maximum range much more heavily, so this relationship becomes much less obvious.

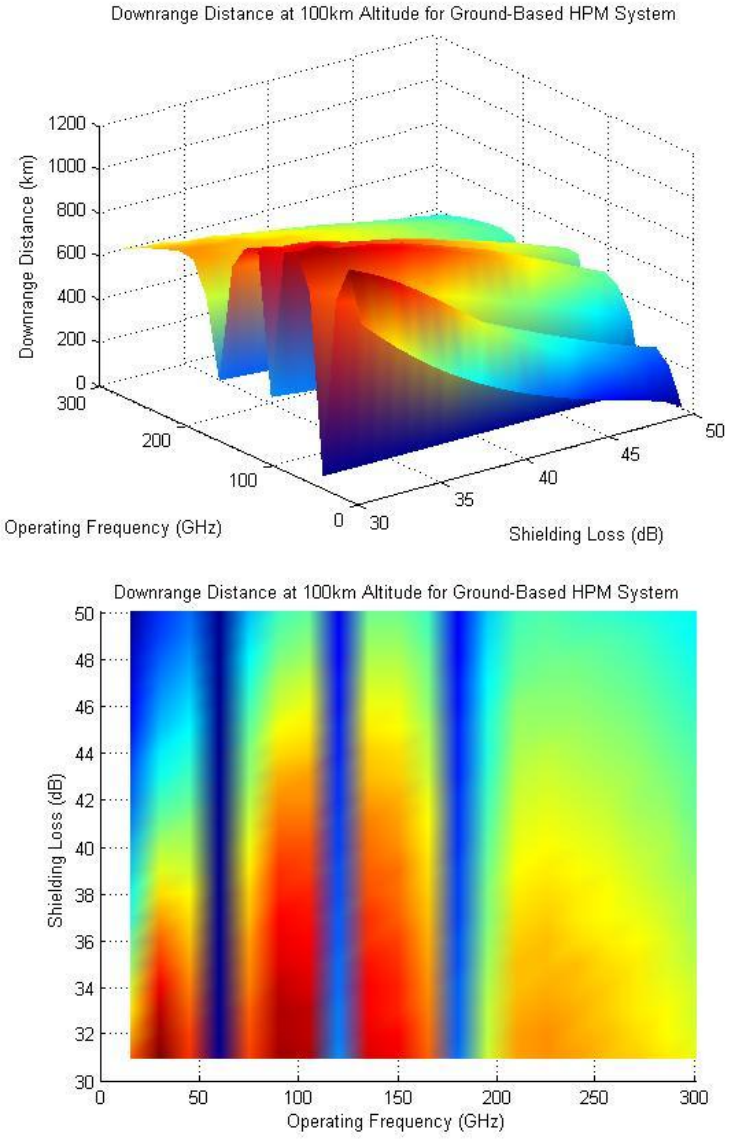

Figure 4.1.bb: Ground-Based - Model 2 - "Downrange" Plot - Frequency/Electromagnetic Shielding Surface Plot of an HPM System's Downrange Distance at an Interception Altitude of 100km as a Function of Operating Frequency and Attenuation Due to Shielding As the amount of shielding attenuation by the target is increased, the maximum downrange distance of an HPM system drops off very quickly. There also exist several frequency ranges which are completely attenuated by the atmosphere, causing the downrange distance to drop to zero.

4.1.4 Ground-Based - Vulnerability Model 3

The third and final Vulnerability Model considered for a ground-based HPM system was a highly resistant target model. The core values of the ground-based Vulnerability Model 3 (GB-VM3) can be seen below in Table 4.1.e. GB-VM3 varies from both GB-VM1 and GB-VM2 in required intensity, which was increased to 100,000 W/m^2 from 10^{-2} W/m^2 (GB-VM1) and 10 W/m^2 (GB-VM2), antenna diameter, which was increased to five meters from three meters, source power, which was increased to one-hundred gigawatts from fifty gigawatts, and electromagnetic shielding, which was decreased to thirty decibels from forty decibels.

Parameter Name	Core Value	Units
Operating Frequency	100	$[GHz]$
Antenna Diameter	5	$[m]$
Source Power	100	$[GW]$
Intensity on Target	100,000	$[W/m^2]$
Electromagnetic Shielding	30	$[dB]$
Critical Altitude	100	$[km]$

Table 4.1.e: Ground-Based - Vulnerability Model 3 (Highly Resistant) - Core Values

Vulnerability Model 3 was used to represents an invulnerable target model with a required intensity of 100,000 W/m^2. In comparison to Vulnerability Models 1 and 2, antenna diameter was increased to 5 m, source power was increased to 100 GW, and electromagnetic shielding was decreased to 30 dB. All other parameters were held constant.

The sweep limits for GB-VM3 can be seen below in Table 4.1.f. Again, all parameter sweeps attempt to predictably span a range near the core values with the exception of frequency.

Parameter Name	Sweep Values	Units
Operating Frequency	[20, 40, 80, 100, 140]	[GHz]
Antenna Diameter	[1, 2, 3, 4, 5]	[m]
Source Power	[10, 25, 50, 75, 100]	[GW]
Intensity on Target	[N/A]	[W/m^2]
Electromagnetic Shielding	[30, 35, 40, 45, 50]	[dB]
Critical Altitude	[100, 125, 150, 175, 200]	[km]

Table 4.1.f: Ground-Based - Vulnerability Model 3 (Highly Resistant) - Sweep Values

The Vulnerability Model 3 sweep limits indicate the values used for each parameter sweep in "Earth" plots. For example, when sweeping operating frequency, 20 GHz, 40 GHz, 80 GHz, 100 GHz, and 140 GHz were used.

Using the core values, "Earth" plots were generated. The "Earth" plot for the core GB-VM3 values can be seen below in Figure 4.1.cc. The maximum horizontal range of GB-VM3 is ≈38.88 kilometers at an altitude of ≈16.11 kilometers. As the range fails to reach the critical altitude of 100 kilometers, the entire range is effective and, thus, shaded. Additionally, the critical firing angle is excluded from the plots as there is no minimum angle for which the range intersects with the critical altitude.

Ground-Based - Model 3 - "Earth" - Core Values

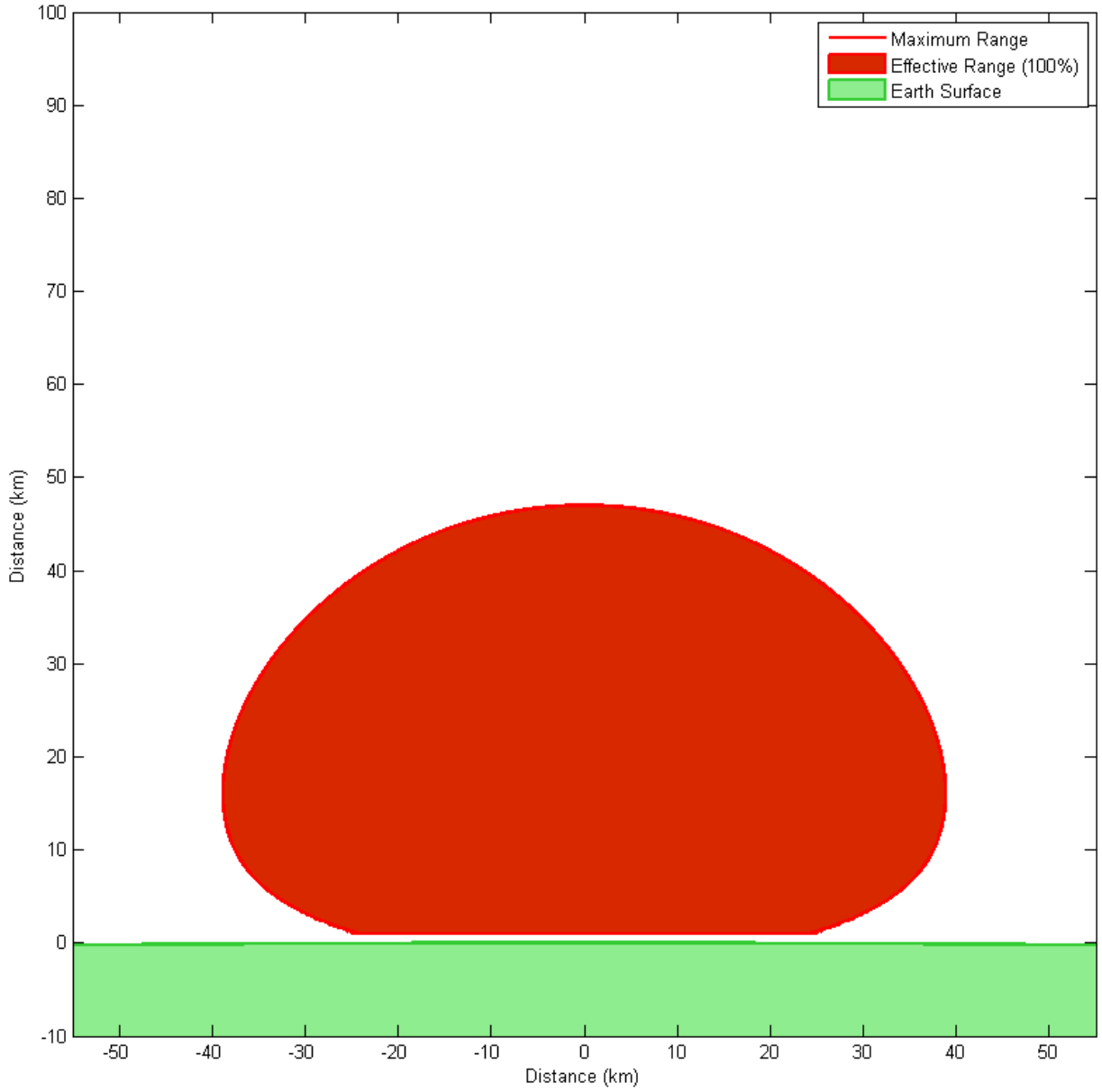

Figure 4.1.cc: Ground-Based - Model 3 - "Earth" Plot - Core Values

For core values: The maximum effective horizontal range is ≈38.88 km at a vertical location of ≈16.11 km. The maximum effective vertical range is 47.09 km. The effective range comprises ≈100% of the maximum range. Angular accuracy: 0.036°. Range accuracy: 0.5 km.

Ground-Based - Model 3 - "Earth" - Operating Frequency

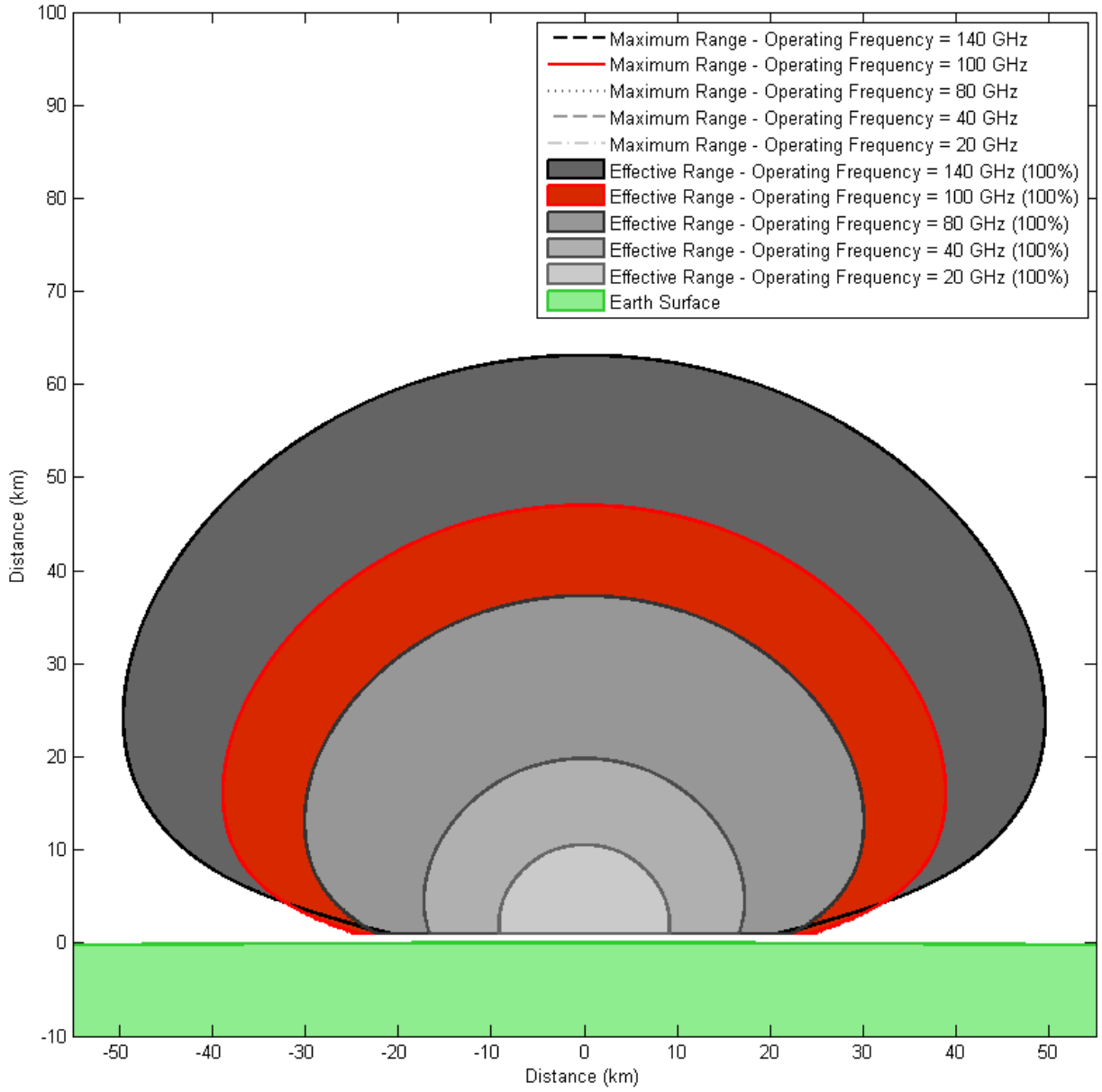

Figure 4.1.dd: Ground-Based - Model 3 - "Earth" Plot - Sweeping Operating Frequency

For operating frequencies of 20 GHz, 40 GHz, 80 GHz, 100 GHz, and 140 GHz: Maximum effective horizontal ranges are ≈9.214 km, 17.28 km, 30.1 km, 38.88 km, and 49.59 km at vertical locations of ≈1.982 km, 4.635 km, 13.14 km, 16.11 km, and 24.18 km. Maximum effective vertical ranges are ≈10.61 km, 19.88 km, 37.37 km, 47.09 km, and 63.2 km. The effective ranges all comprise ≈100% of the maximum range. Angular accuracy: 0.036°. Range accuracy: 0.5 km.

Ground-Based - Model 3 - "Earth" - Antenna Diameter

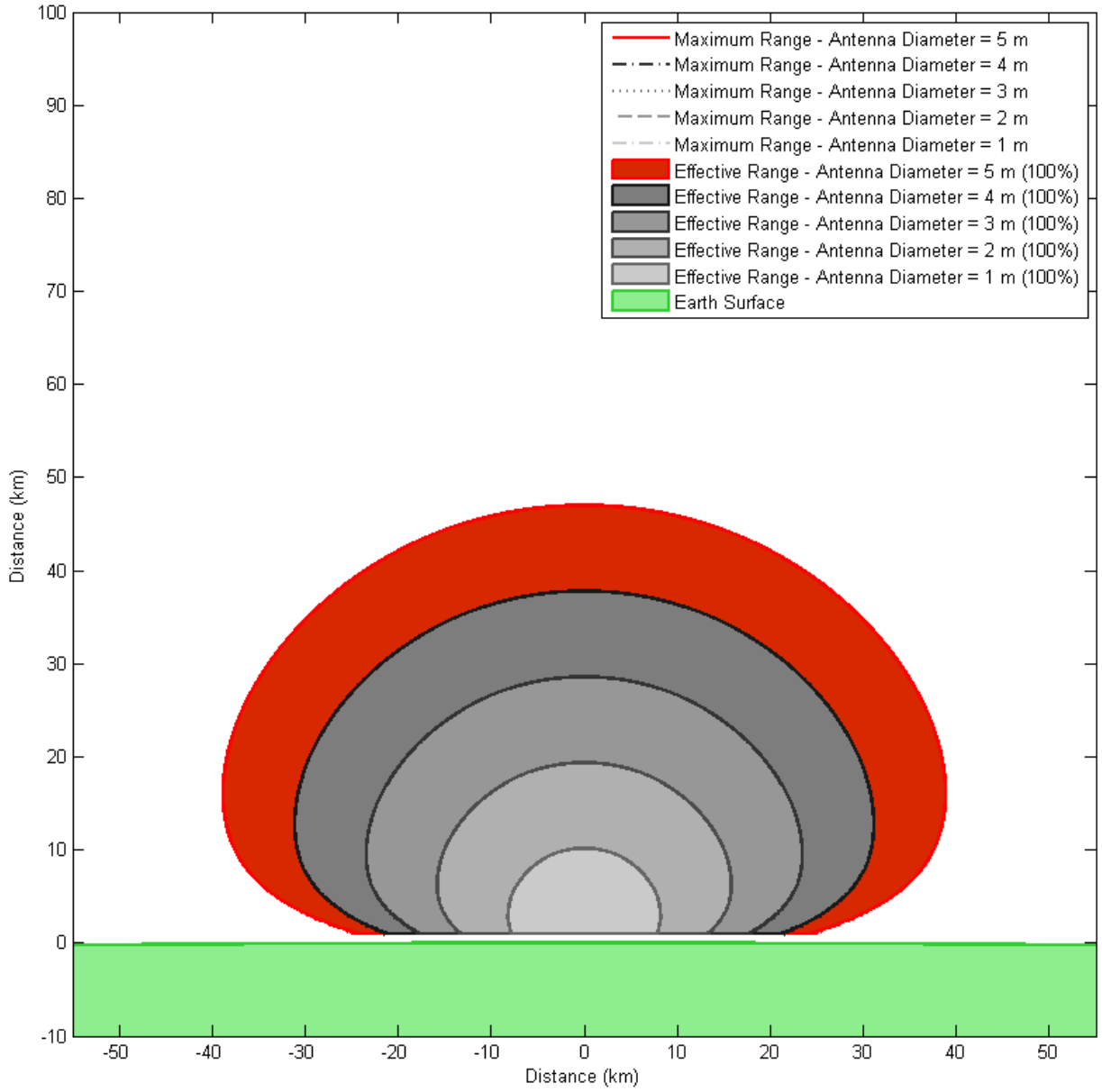

Figure 4.1.ee: Ground-Based - Model 3 - "Earth" Plot - Sweeping Antenna Diameter

For antenna diameters of 1 m, 2 m, 3 m, 4 m, and 5 m: Maximum effective horizontal ranges are ≈8.249 km, 15.84 km, 23.49 km, 31.16 km, and 38.88 km at vertical locations of ≈3.03 km, 19.43 km, 28.65 km, 37.87 km, and 47.09 km. Maximum effective vertical ranges are ≈ km, km, km, km, and km. The effective ranges all comprise ≈100% of the maximum range. Angular accuracy: 0.036°. Range accuracy: 0.5 km.

Ground-Based - Model 3 - "Earth" - Source Power

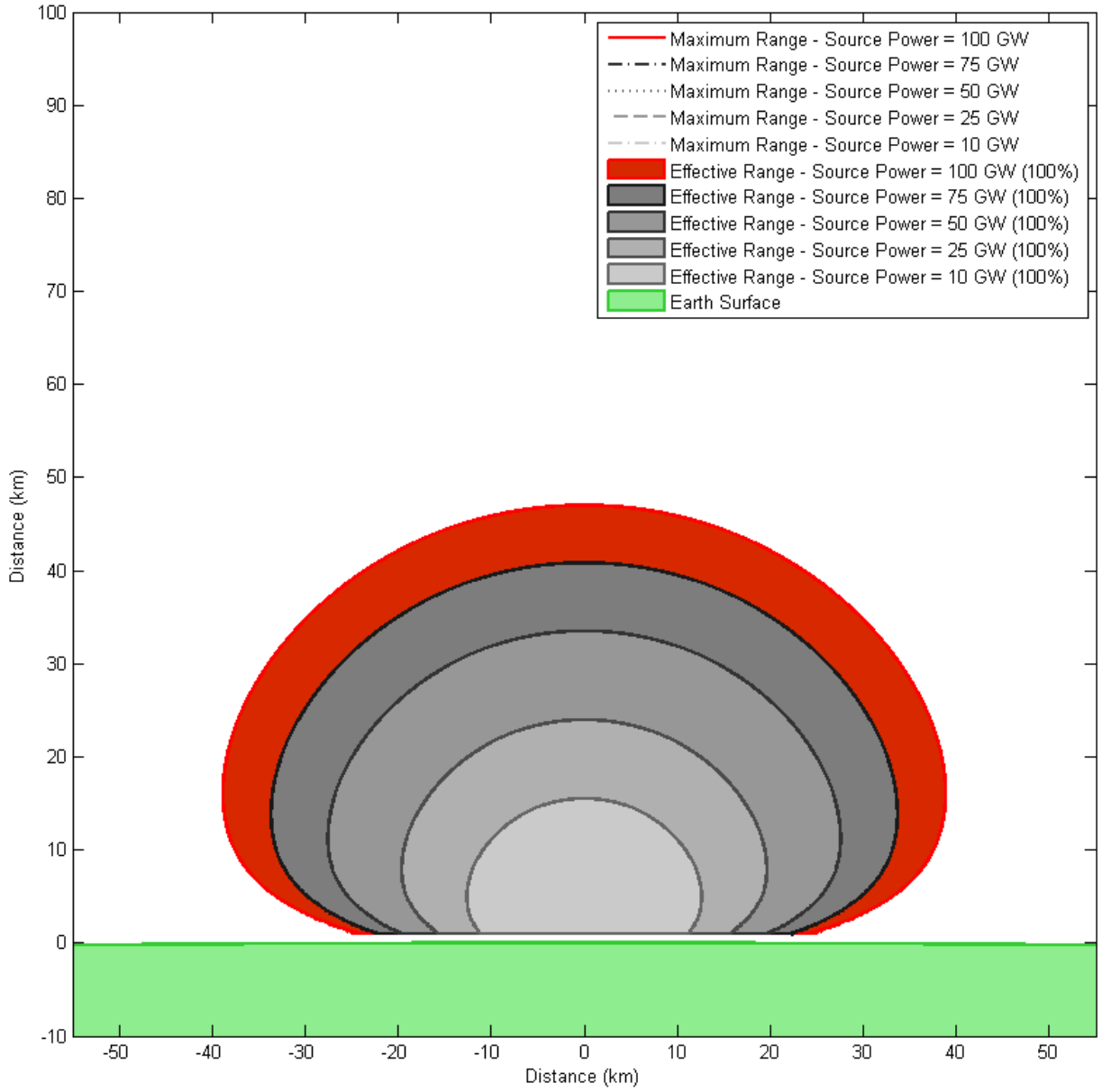

Figure 4.1.ff: Ground-Based - Model 3 - "Earth" Plot - Sweeping Source Power

For source power levels of 10 GW, 30 GW, 50 GW, 70 GW, and 90 GW: Maximum effective horizontal ranges are ≈12.65 km, 19.67 km, 27.59 km, 33.7 km, and 38.88 km at vertical locations of ≈5.032 km, 7.997 km, 11.33 km, 13.64 km, and 16.11 km. Maximum effective vertical ranges are ≈15.58 km, 24.04 km, 33.59 km, 40.91 km, and 47.09 km. The effective ranges all comprise ≈100% of the maximum range. Angular accuracy: 0.036°. Range accuracy: 0.5 km.

Ground-Based - Model 3 - "Earth" - Electromagnetic Shielding

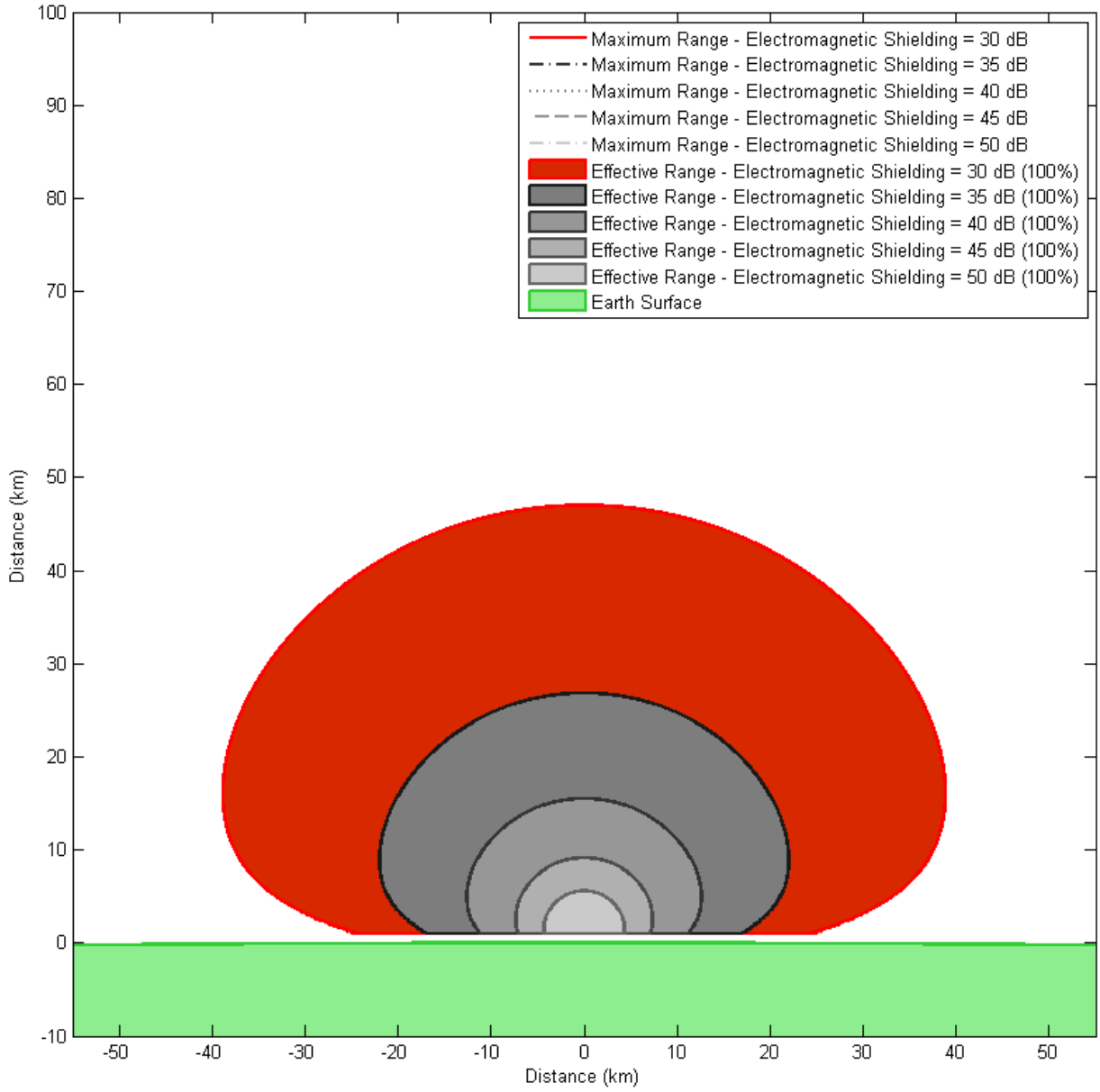

Figure 4.1.gg: Ground-Based - Model 3 - "Earth" Plot - Sweeping Electromagnetic Shielding

For electromagnetic shielding levels of 50 dB, 45 dB, 40 dB, 35 dB, and 30 dB: Maximum effective horizontal ranges are ≈4.382 km, 7.397 km, 12.65 km, 22.05 km, and 38.88 km at vertical locations of ≈1.506 km, 2.238 km, 5.032 km, 8.986 km, and 16.11 km. Maximum effective vertical ranges are ≈5.633 km, 9.238 km, 15.58 km, 26.92 km, and 47.09 km. The effective ranges all comprise ≈100% of the maximum range. Angular accuracy: 0.036°. Range accuracy: 0.5 km.

An “Earth” plot sweeping critical altitude was not created for GB-VM3 as the core values do not reach the minimum critical altitude of 100 kilometers.

“Downrange Surface” plots were not made for GB-VM3 since very few combinations of parameters resulted in system ranges achieving the minimum required altitude of 100 km. The modifications to the critical altitude required to accommodate the low maximum ranges are either too varying or too great to depict presentable data; many configurations have maximum ranges of thirty kilometers or less and require a decision concerning a course of action to be made almost as soon as the threat can be detected.

4.1.5 Coverage Maps

Once a set of parameters is chosen based on the previous viewgraphs, a coverage map is made, as described in Section 3.3. These maps show the circular footprints of possible HPM systems placed at chosen latitudes and longitudes. The footprints are made assuming intercept altitudes of 100 kilometers, and are sized based on the assumption that atmosphere is constant in the area considered. This assumption will not be true, but numbers chosen are regional averages, and thus appropriate approximations.

Ground-Based - Coverage Map - Iran

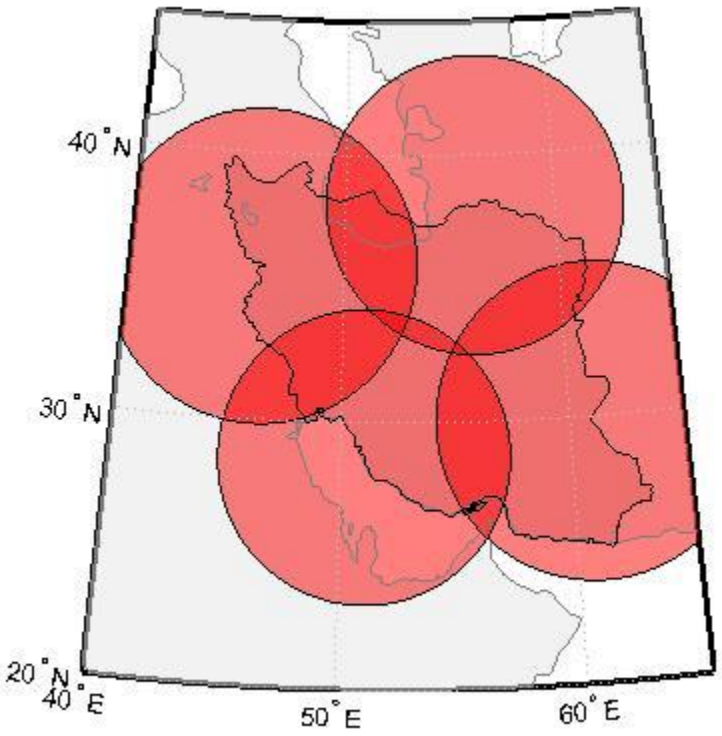

Figure 4.1.hh: Example Coverage Map of Four HPM Systems over Iran

Though each system plotted has the same parameters, the size of each footprint varies because of the initial altitudes of the systems. Notice that the bottom footprint, which is placed at sea level, is much smaller than either the right or left footprints which are located well above sea level. This plot was made using the core values for Vulnerability Model 2.

Ground-Based - Coverage Map - North Korea

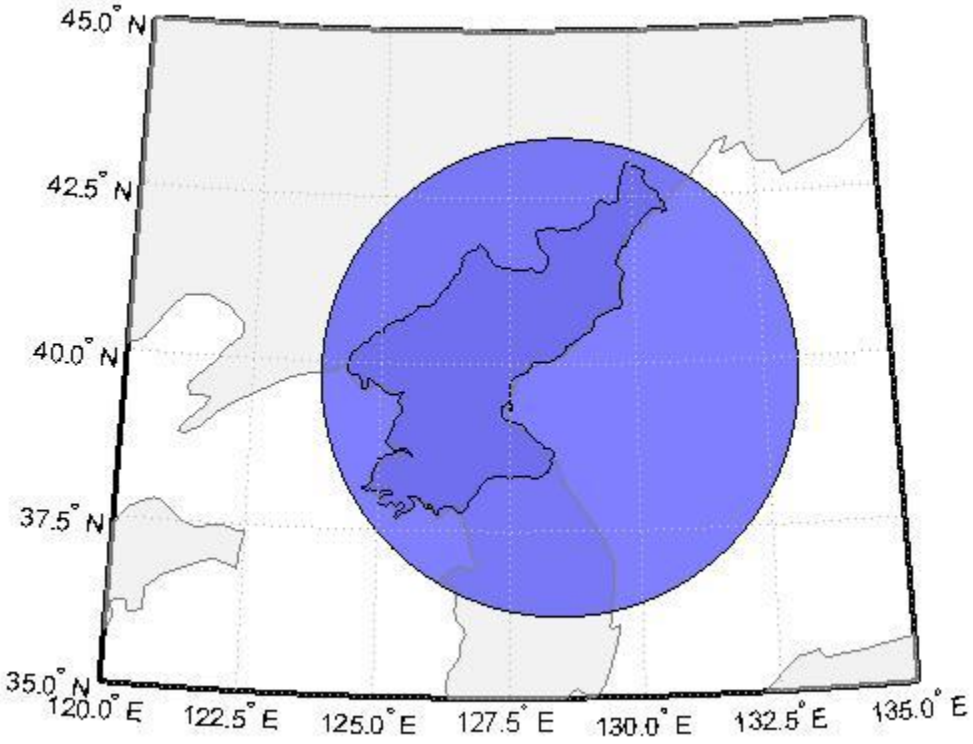

Figure 4.1.ii: Example Coverage Map of One HPM System over North Korea

This map shows that, using the core values for Vulnerability Model 2, only one system is needed for coverage of North Korea. Because of the geographic shape of this region, a circular footprint fits nicely around the country to provide full coverage.

Ground-Based - Coverage Map - North Korea (Alternate)

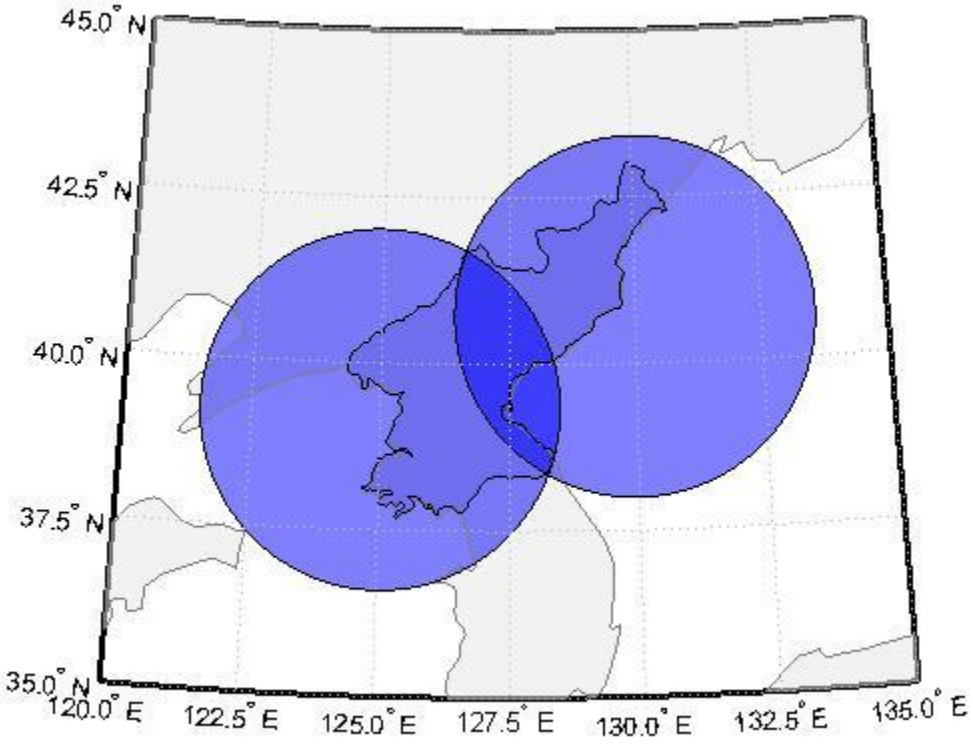

Figure 4.1.jj: Example Coverage Map of Two HPM Systems over North Korea

This coverage map is created using two HPM systems from Vulnerability Model 2, with the signal power reduced to nine gigawatts. Even with a lower than nominal power parameter, only a pair of systems is needed to provide full coverage over this country in this example case.

4.2 Space Basing

As seen in Eqs. (3.4.b) through (3.4.h), the total number of satellites is a direct function of an HPM system's range, orbital altitude, and an ICBM's critical altitude. This relation is shown visually in Figure 4.2.a. Table 4.0.a shows generalized range relations, which are exemplified for three separate Vulnerability Models in Sections 4.2.1 through 4.2.3. All plots were created using MATLAB and have 100,000 sample points.

Space-Based - "Correlation" - Total Satellites/Maximum Range

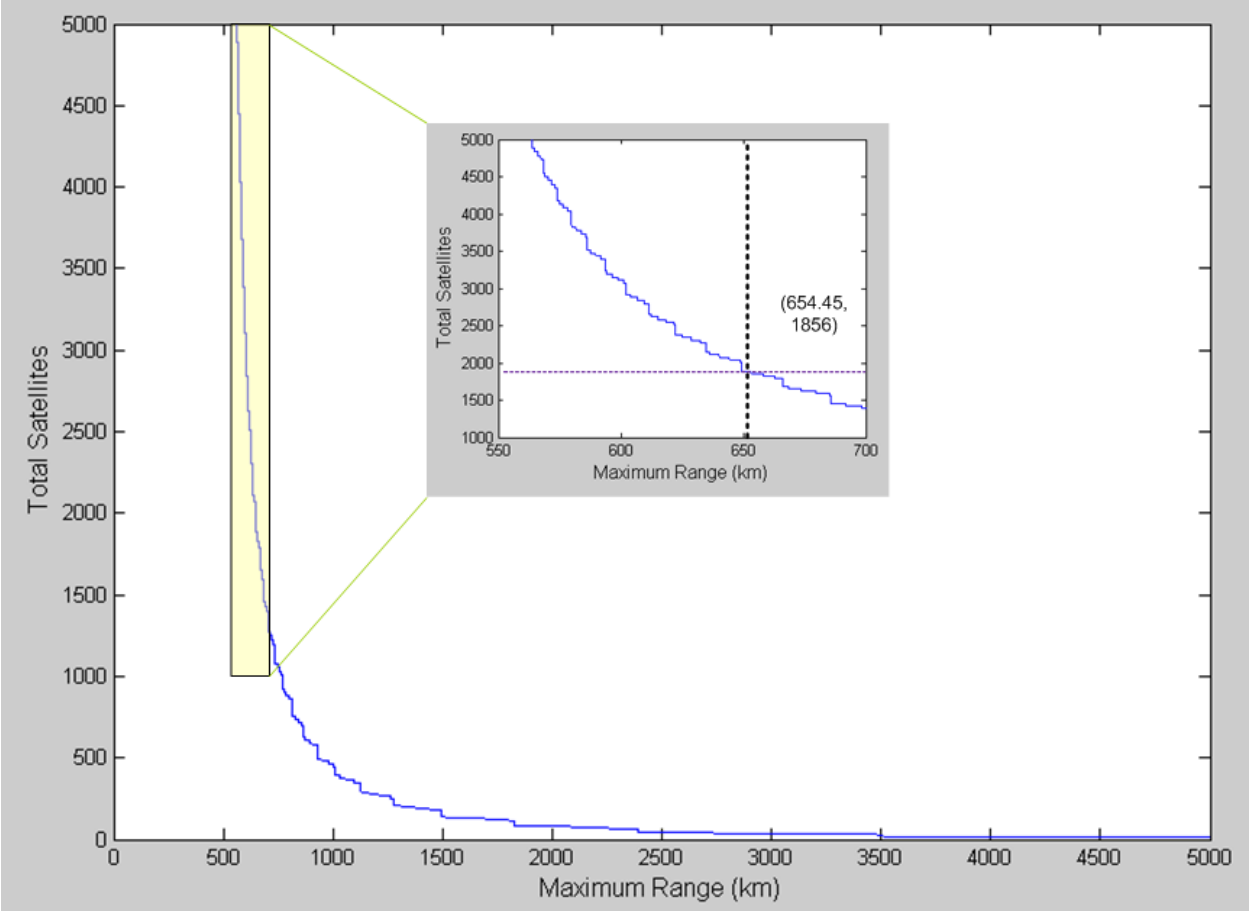

Figure 4.2.a: Space-Based - "Correlation" Plot - Total Satellites/Maximum Range

Critical altitude of 100 kilometers. Orbital altitude of 600 kilometers. Total satellites decreases in an exponential fashion against maximum range. The relation is not continuous due to an integer number of satellites required per orbital ring and an integer number of orbital rings, creating a "step" like appearance as shown in the zoomed in portions of the figure. Coordinate point represents the total satellites required for vulnerability model 2, the only vulnerability model that can be displayed on this scale.

4.2.1 Space-Based - Vulnerability Model 1

The core values of the space-based Vulnerability Model 1 (SB-VM1) can be seen below in Table 4.2.a. SB-VM1 is primarily defined by lower bound of the intensity requirement to cause electrical damage as defined in "Effects of Directed Energy Weapons" (Nielsen, 1994). Using this lower intensity bound means that the target ICBM is highly vulnerable to electromagnetic attack. Shielding loss is defined by taking the upper bound of reasonable shielding ability for an ICBM (Cox, 1973).

Parameter Name	Core Value	Units
Operating Frequency	100	$[GHz]$
Antenna Diameter	3	$[m]$
Source Power	50	$[GW]$
Intensity on Target	0.01	$[W/m^2]$
Electromagnetic Shielding	40	$[dB]$
Critical Altitude	100	$[km]$
Orbital Altitude	600	$[km]$

Table 4.2.a: Space-Based - Vulnerability Model 1 (Highly Vulnerable) - Core Values
Vulnerability Model 1 was used to represent a highly vulnerable target model with a required intensity of $0.01\ W/m^2$.

The sweep limits for SB-VM1 can be seen below in Table 4.2.b.

Parameter Name	Sweep Limits	Units
Operating Frequency	$[0, 300]$	$[GHz]$
Antenna Diameter	$[0, 5]$	$[m]$
Source Power	$[0, 100]$	$[GW]$
Electromagnetic Shielding	$[0, 50]$	$[dB]$

Table 4.2.b: Space-Based - Vulnerability Model 1 (Highly Vulnerable) - Sweep Limits
Vulnerability Model 1 sweep limits indicate the values used as bounds for each parameter sweep in "Correlation" plots. For example, when sweeping maximum range versus operating frequency, frequencies between 0 GHz and 300 GHz are shown on the independent axis.

The results for SB-VM1 can be seen below in Table 4.2.c.

Result Name	Value
Maximum Range	20,696 km
Satellites/Orbital Ring	2 $satellites$
Total Orbital Rings	1 $ring$
Total Satellites	2 $satellites$

Table 4.2.c: Space-Based - Vulnerability Model 1 (Highly Vulnerable) - Summary Results

Vulnerability Model 1 results in a single system range of 20, 696 *km*. This range necessitates 2 satellites in 1 orbital ring resulting in 2 satellites to achieve global coverage.

Space-Based - Model 1 - "Correlation" - Operating Frequency

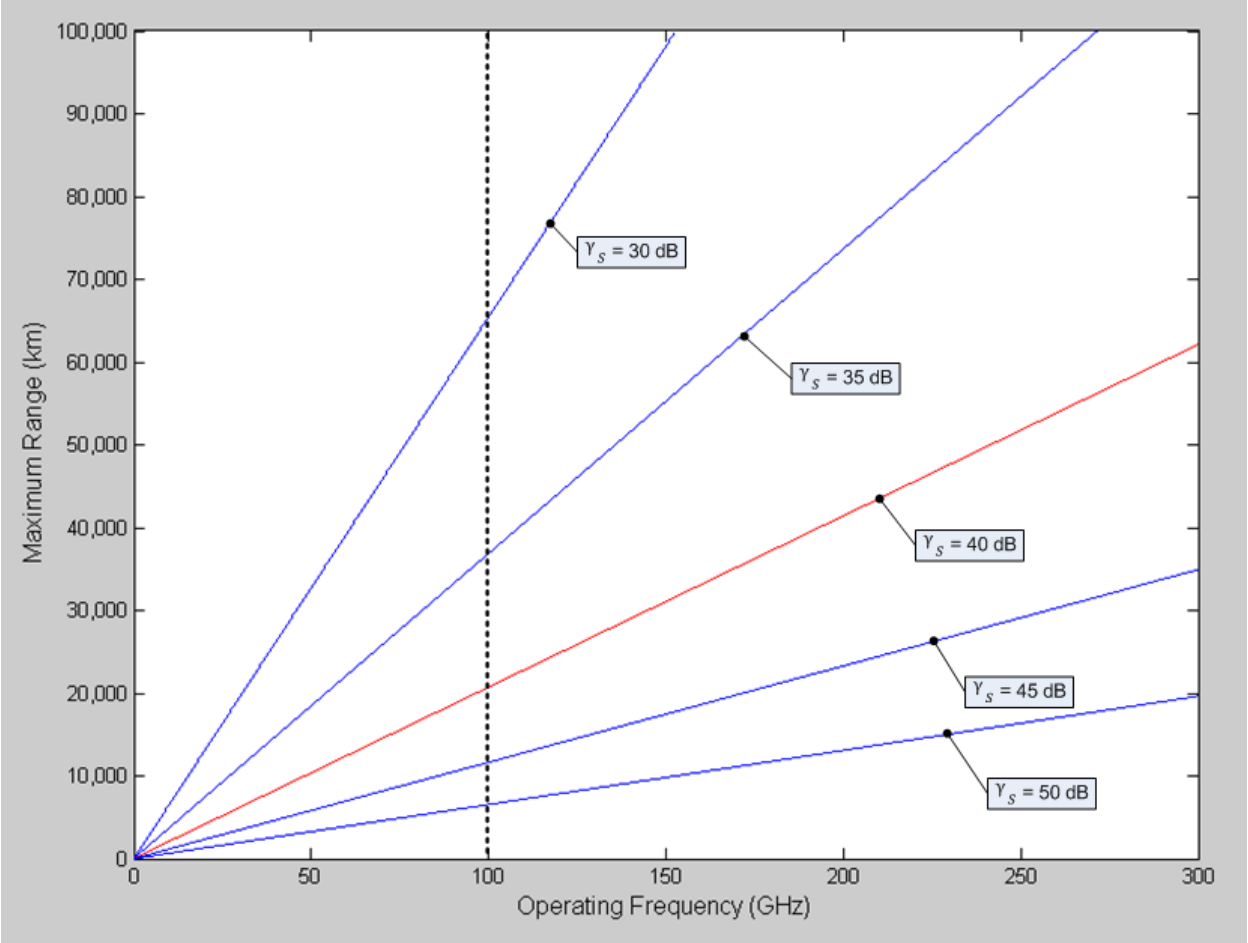

Figure 4.2.b: Space-Based - Model 1 - "Correlation" Plot - Maximum Range/Operating Frequency

Dashed vertical line describes Vulnerability Model 1 operating frequency core value. Red line describes Vulnerability Model 1 shielding loss core value. Maximum range increases linearly with operating frequency.

Space-Based - Model 1 - "Correlation" - Antenna Diameter

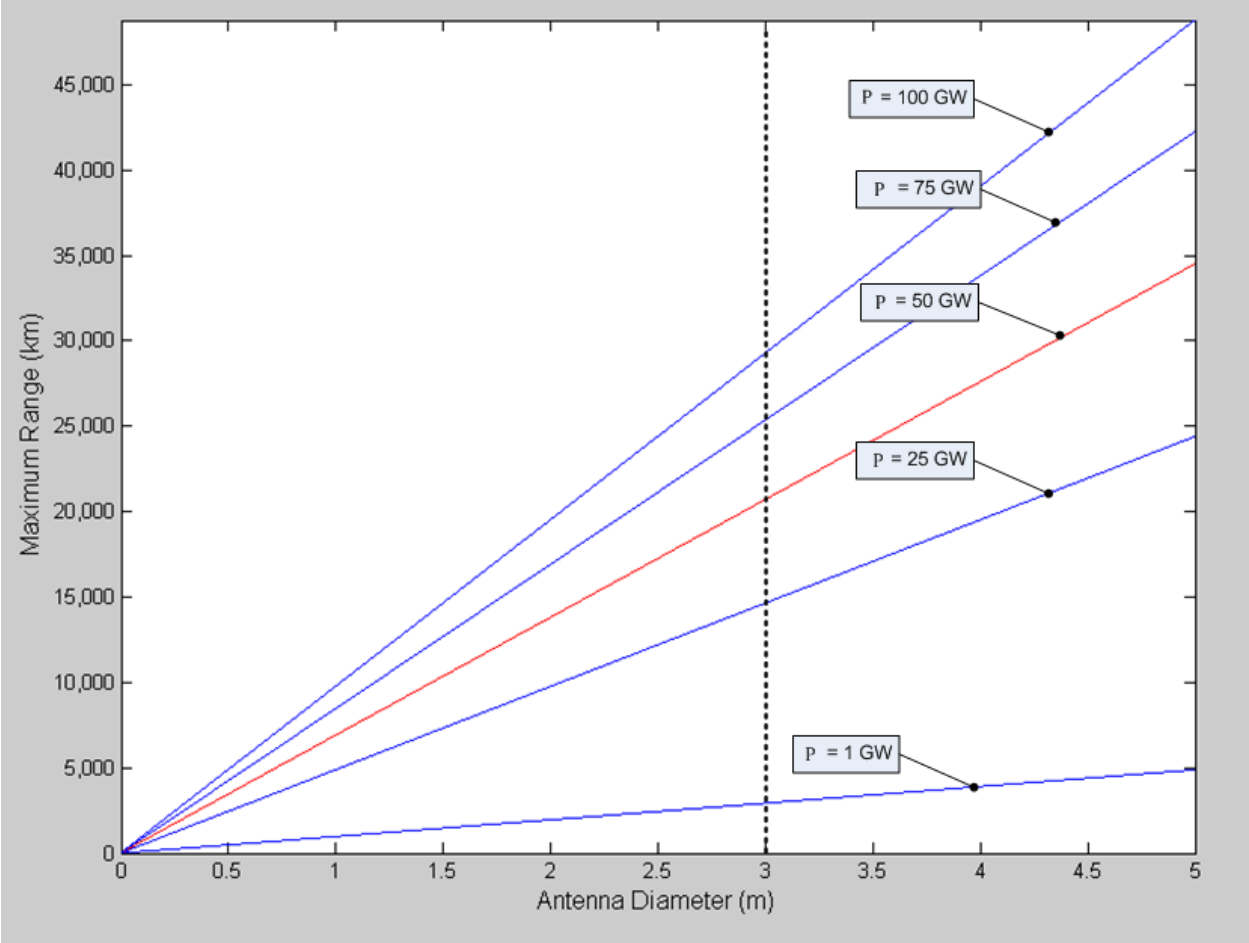

Figure 4.2.c: Space-Based - Model 1 - "Correlation" Plot - Maximum Range/Antenna Diameter

Dashed vertical line describes Vulnerability Model 1 antenna diameter core value. Red line describes Vulnerability Model 1 signal power core value. Maximum range increases linearly with antenna diameter.

Space-Based - Model 1 - "Correlation" - Source Power

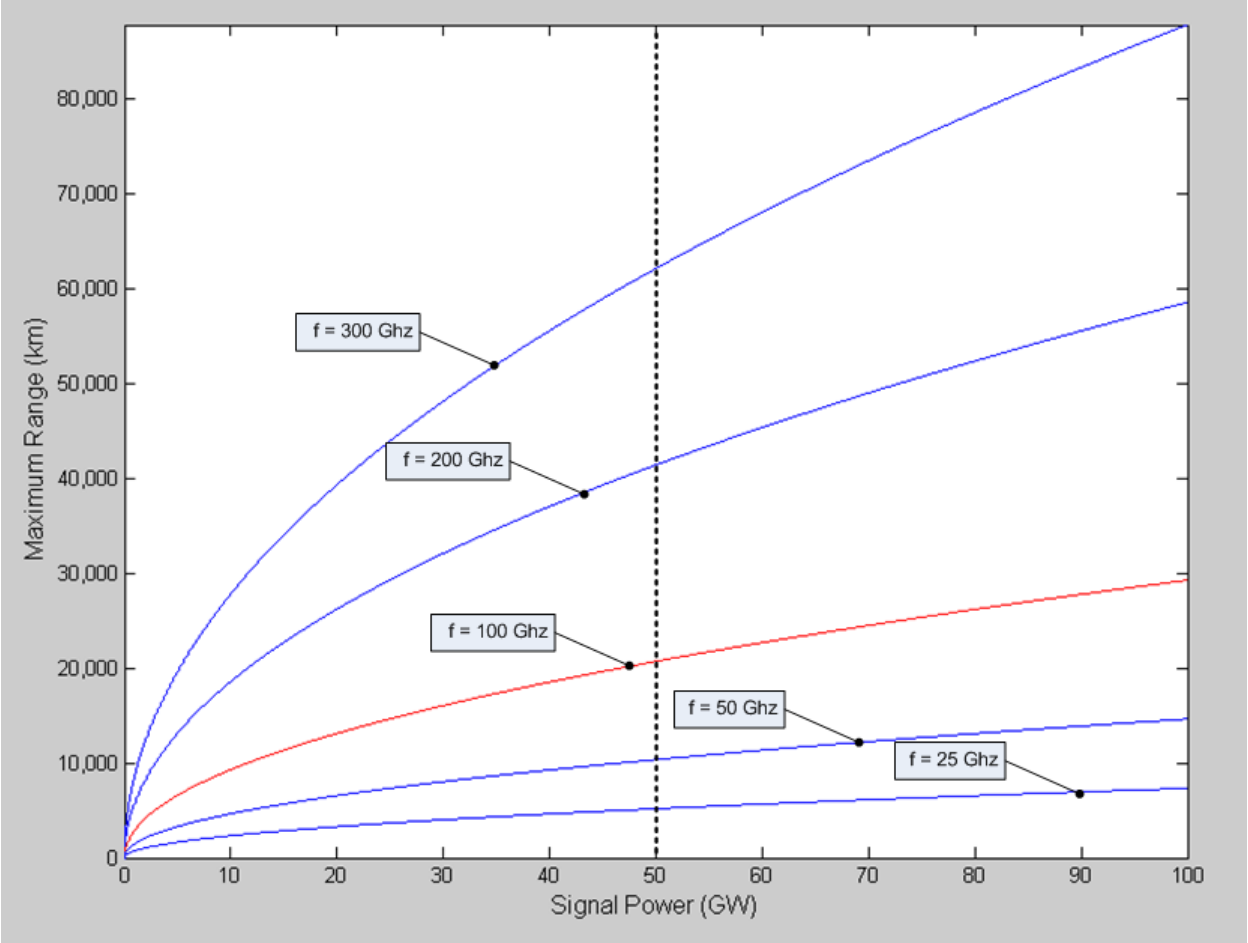

Figure 4.2.d: Space-Based - Model 1 - "Correlation" Plot - Maximum Range/Source Power

Dashed vertical line describes Vulnerability Model 1 signal power core value. Red line describes Vulnerability Model 1 operating frequency core value. Maximum range increases with the root of signal power.

Space-Based - Model 1 - "Correlation" - Electromagnetic Shielding

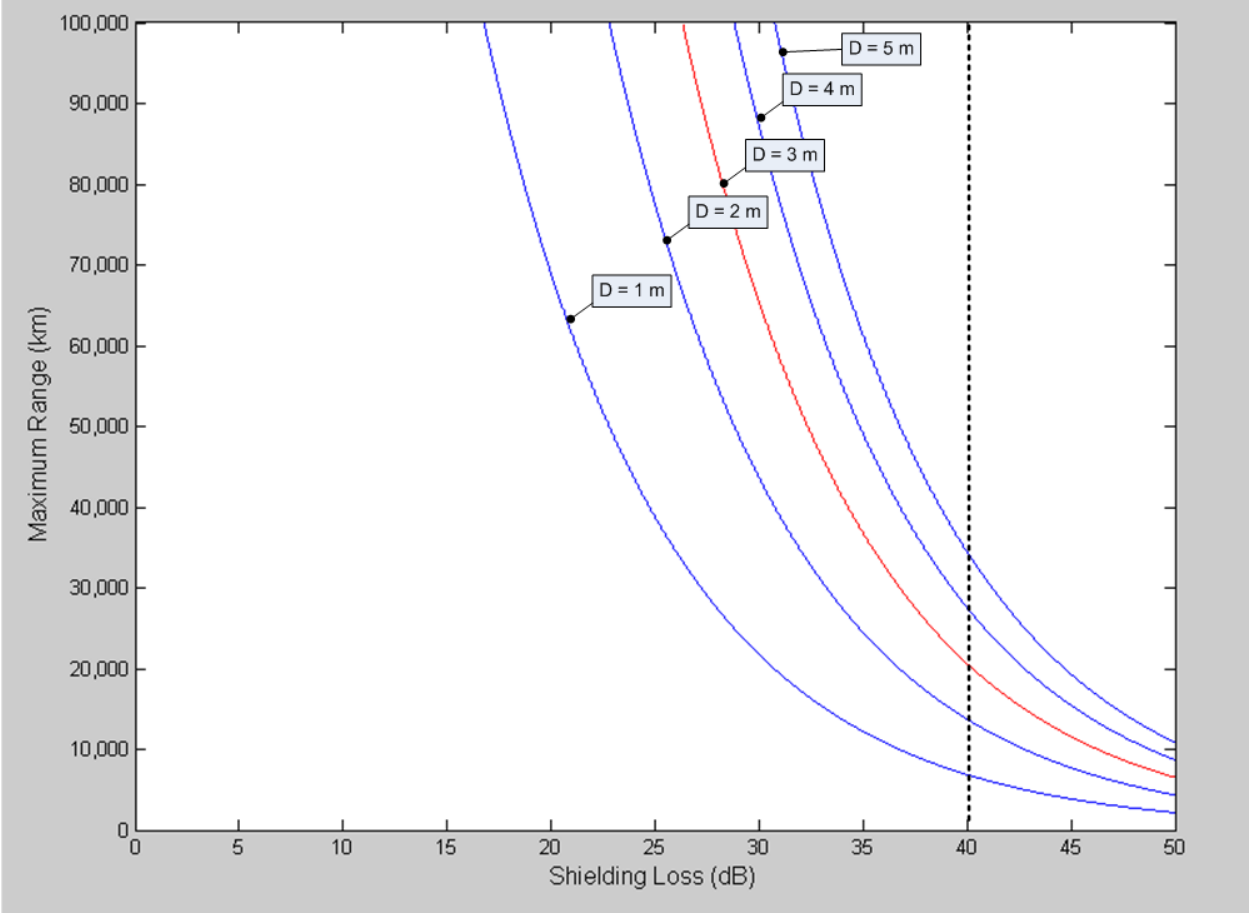

Figure 4.2.e: Space-Based - Model 1 - "Correlation" Plot - Maximum Range/Electromagnetic Shielding
Dashed vertical line describes Vulnerability Model 1 shielding loss core value. Red line describes Vulnerability Model 2 antenna diameter core value. Maximum range decreases exponentially with shielding loss.

4.2.2 Space-Based - Vulnerability Model 2

The core values of the space-based Vulnerability Model 2 (SB-VM2) can be seen below in Table 4.2.d. This model is primarily defined by using the generalized intensity requirements to cause electrical damage as defined in a United States Air Force report (Crawford, Jordan, Kendall, Powers, & Varni, 1996). Using this intensity requirement, an ICBM is 1,000 times less vulnerable to electromagnetic attack as compared to SB-VM1 and for the purposes of analysis is referred to as being moderately vulnerable. Shielding loss is defined by taking the upper bound of reasonable shielding ability for an ICBM (Cox, 1973).

Parameter Name	Core Value	Units
Operating Frequency	100	$[GHz]$
Antenna Diameter	3	$[m]$
Source Power	50	$[GW]$
Intensity on Target	10	$[W/m^2]$
Electromagnetic Shielding	40	$[dB]$
Critical Altitude	100	$[km]$
Orbital Altitude	600	$[km]$

Table 4.2.d: Space-Based - Vulnerability Model 2 (Moderately Vulnerable) - Core Values
Vulnerability Model 2 was used to represent a moderately vulnerable target model with a required intensity of 10 W/m^2.

The sweep limits for SB-VM2 can be seen below in Table 4.2.e.

Parameter Name	Sweep Limits	Units
Operating Frequency	$[0, 300]$	$[GHz]$
Antenna Diameter	$[0, 5]$	$[m]$
Source Power	$[0, 100]$	$[GW]$
Electromagnetic Shielding	$[0, 50]$	$[dB]$

Table 4.2.e: Space-Based - Vulnerability Model 2 (Moderately Vulnerable) - Sweep Limits
Vulnerability Model 2 sweep limits indicate the values used as bounds for each parameter sweep in "Correlation" plots. For example, when sweeping maximum range versus operating frequency, frequencies between 0 GHz and 300 GHz are shown on the independent axis.

The results for SB-VM2 can be seen below in Table 4.2.f.

Result Name	Value
Maximum Range	654.5 km
Satellites/Orbital Ring	58 $satellites$
Total Orbital Rings	32 $rings$
Total Satellites	1,856 $satellites$

Table 4.2.f: Space-Based - Vulnerability Model 2 (Moderately Vulnerable) - Summary Results

Vulnerability Model 2 results in a single system range of 654.5 *km*. This range necessitates 58 satellites in each of 68 orbital rings, resulting in 3,944 satellites to achieve global coverage.

Space-Based - Model 2 - "Correlation" - Operating Frequency

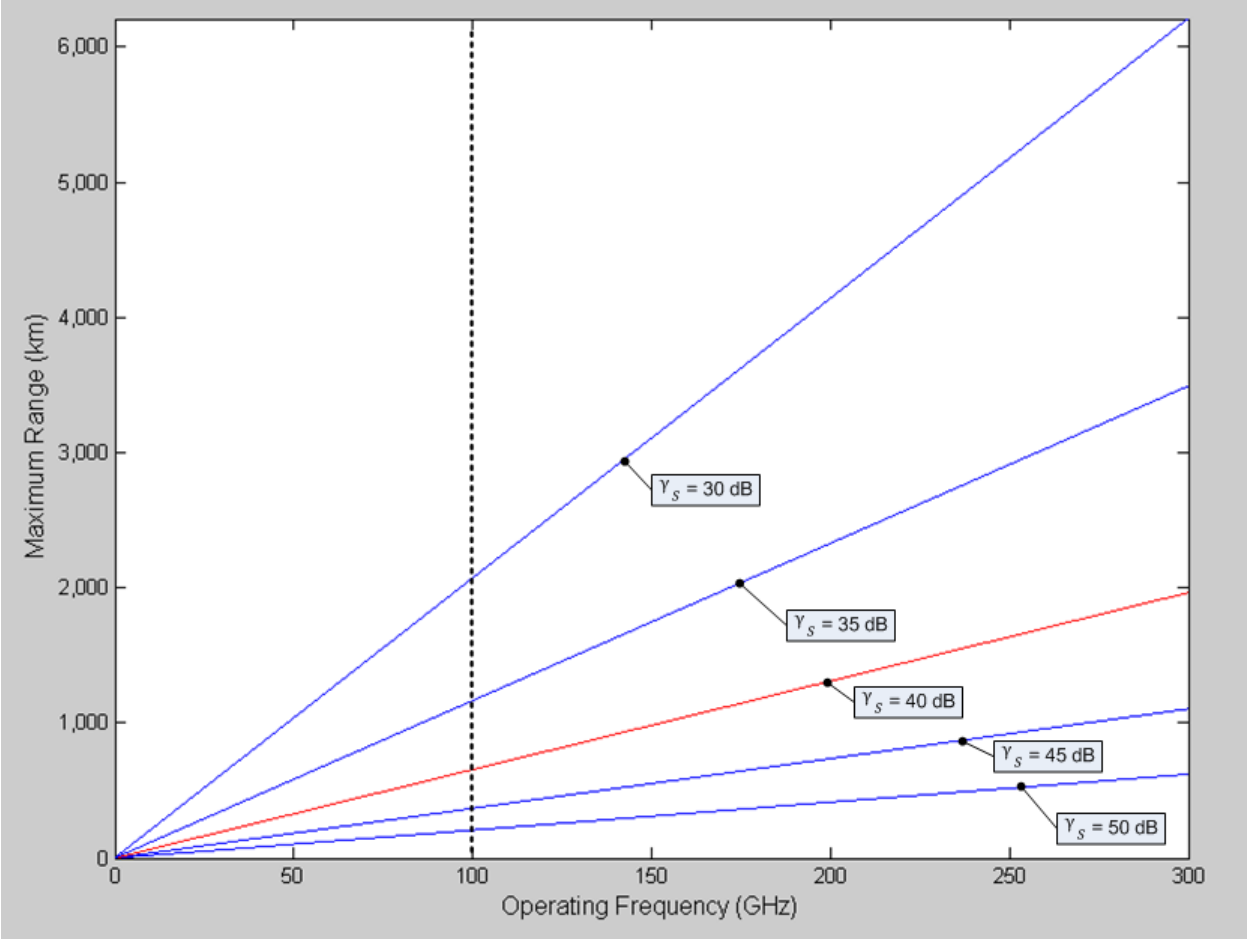

Figure 4.2.f: Space-Based - Model 2 - "Correlation" Plot - Maximum Range/Operating Frequency

Dashed vertical line describes Vulnerability Model 2 operating frequency core value. Red line describes Vulnerability Model 2 shielding loss core value. Maximum range increases linearly with operating frequency.

Space-Based - Model 2 - "Correlation" - Antenna Diameter

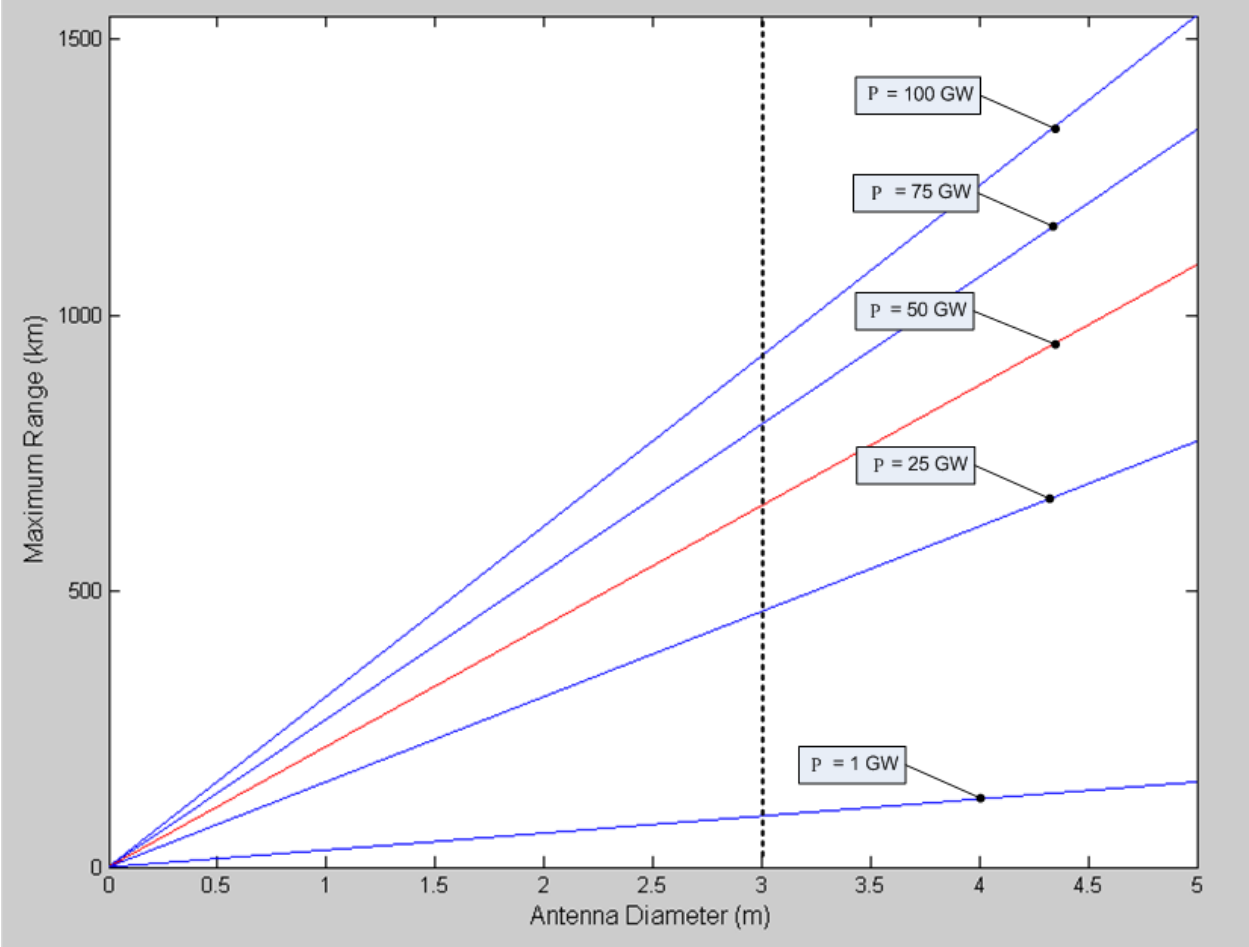

Figure 4.2.g: Space-Based - Model 2 - "Correlation" Plot - Maximum Range/Antenna Diameter

Dashed vertical line describes Vulnerability Model 2 antenna diameter core value. Red line describes Vulnerability Model 2 signal power core value. Maximum range increases linearly with antenna diameter.

Space-Based - Model 2 - "Correlation" - Source Power

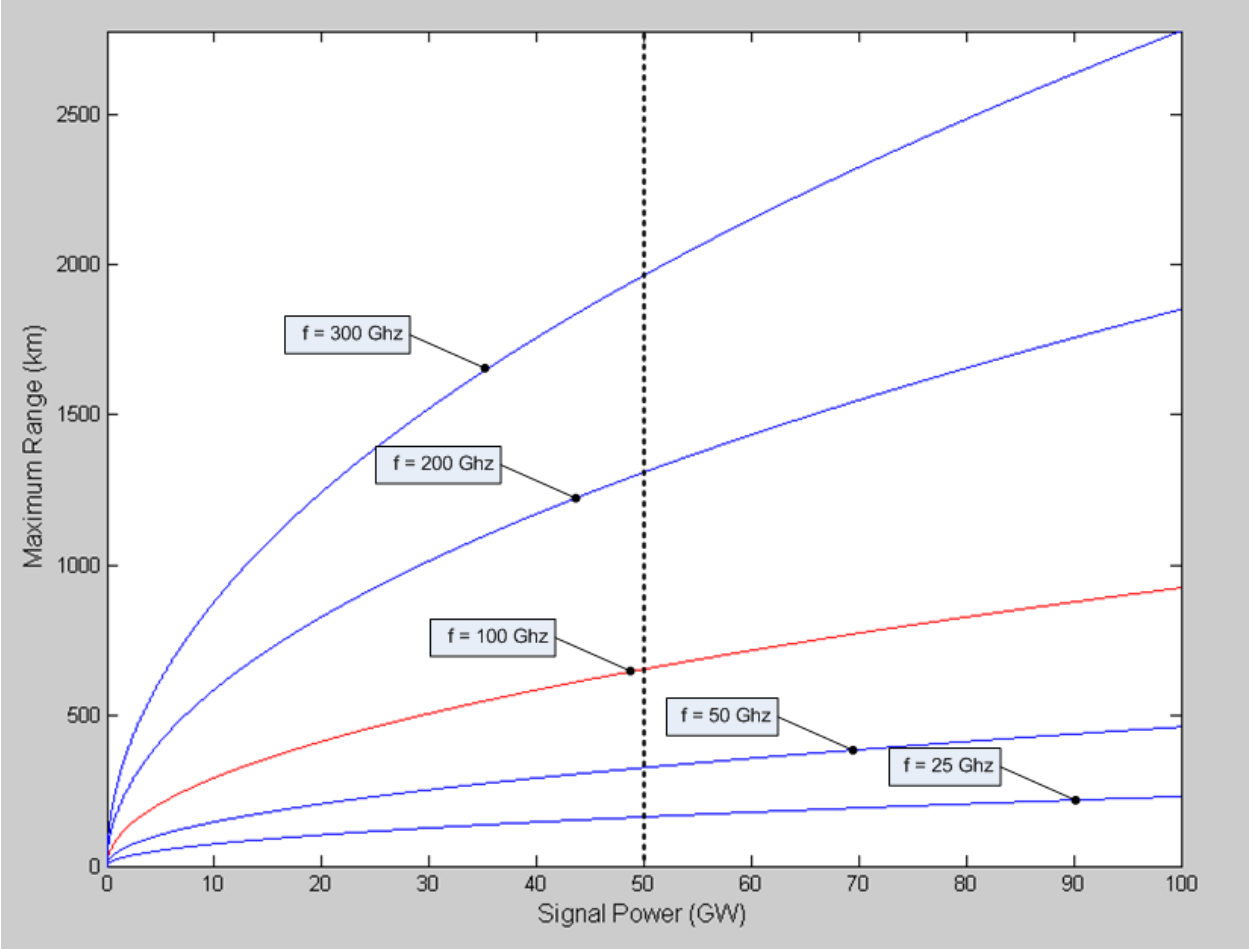

Figure 4.2.h: Space-Based - Model 2 - "Correlation" Plot - Maximum Range/Source Power

Dashed vertical line describes Vulnerability Model 2 signal power core value. Red line describes Vulnerability Model 2 operating frequency core value. Maximum range increases with the root of signal power.

Space-Based - Model 2 - "Correlation" - Electromagnetic Shielding

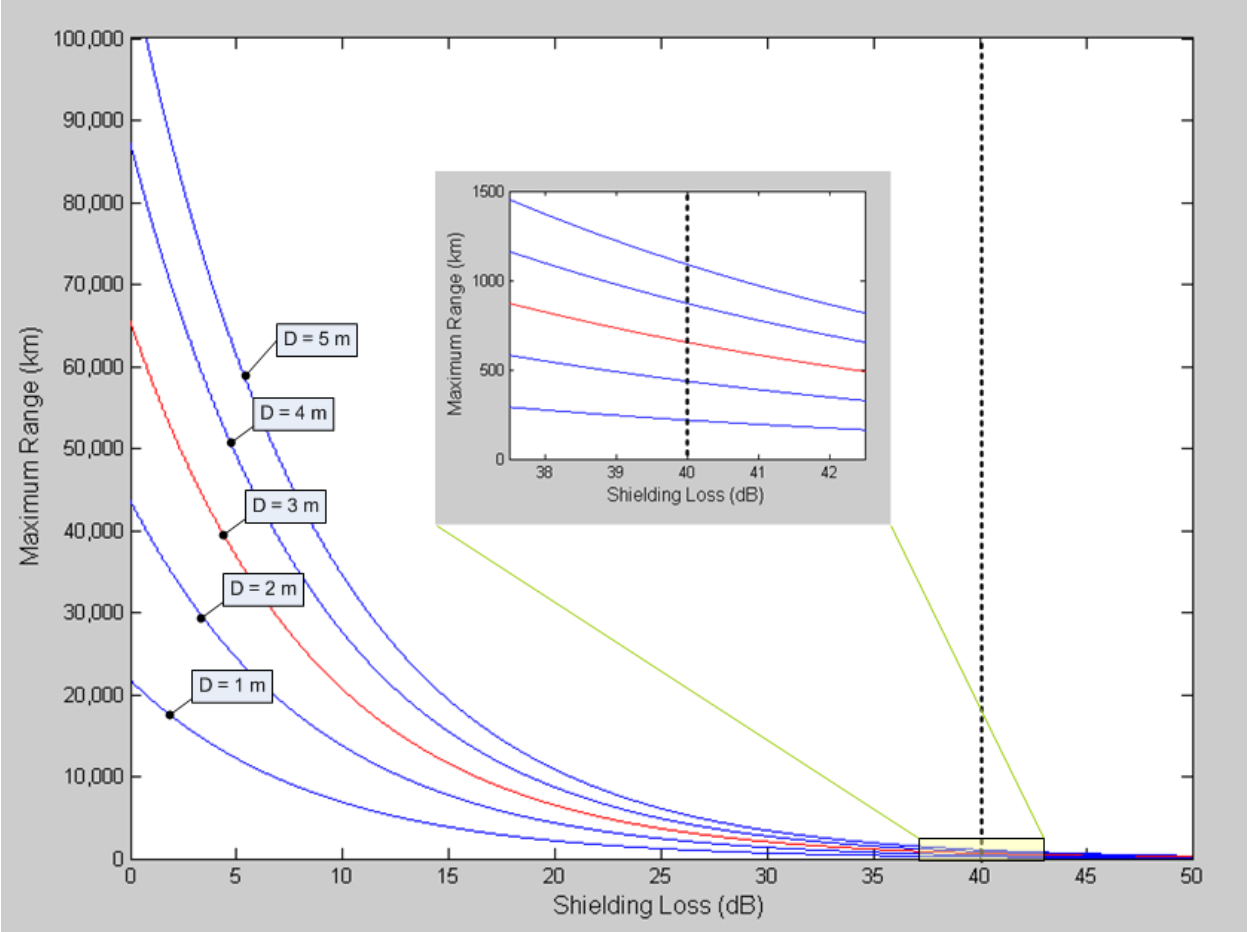

Figure 4.2.i: Space-Based - Model 2 - "Correlation" Plot - Maximum Range/Electromagnetic Shielding

Dashed vertical line describes Vulnerability Model 2 shielding loss core value. Red line describes Vulnerability Model 2 antenna diameter core value. Maximum range decreases exponentially with shielding loss.

4.2.3 Space-Based - Vulnerability Model 3

The core values of the space-based Vulnerability Model 3 (SB-VM3) can be seen below in Table 4.2.g. This model is primarily defined by using the intensity required to cause damage against targets not specifically vulnerable to microwave radiation as defined in "Effects of Directed Energy Weapons" (Nielsen, 1994). SB-VM3 uses ideal parameters for an HPM system as described by operating at the highest frequency while remaining in microwave spectrum, a large antenna diameter, and a shielding loss 10 dB less than the upper bound of reasonable shielding ability for an ICBM (Cox, 1973). While using idealized system parameters, the high intensity required for a mission kill still makes target ICBMs extremely resistant to electromagnetic attack.

Parameter Name	Core Value	Units
Operating Frequency	300	$[GHz]$
Antenna Diameter	5	$[m]$
Source Power	100	$[GW]$
Intensity on Target	100,000	$[W/m^2]$
Electromagnetic Shielding	30	$[dB]$
Critical Altitude	100	$[km]$
Orbital Altitude	600	$[km]$

Table 4.2.g: Space-Based - Vulnerability Model 3 (Highly Resistant) - Core Values
Vulnerability Model 3 was used to represent a highly resistant target model with a required intensity of $100,000\ W/m^2$.

The sweep limits for SB-VM3 can be seen below in Table 4.2.h.

Parameter Name	Sweep Limits	Units
Operating Frequency	$[0, 300]$	$[GHz]$
Antenna Diameter	$[0, 5]$	$[m]$
Source Power	$[0, 100]$	$[GW]$
Electromagnetic Shielding	$[0, 50]$	$[dB]$

Table 4.2.h: Space-Based - Vulnerability Model 3 (Highly Resistant) - Sweep Limits
Vulnerability Model 3 sweep limits indicate the values used as bounds for each parameter sweep in "Correlation" plots. For example, when sweeping maximum range versus operating frequency, frequencies between 0 GHz and 300 GHz are shown on the independent axis.

The results for SB-VM3 can be seen below in Table 4.2.i.

Result Name	Value
Maximum Range	146.3 *km*
Satellites/Orbital Ring	*Impossible*
Total Orbital Rings	*Impossible*
Total Satellites	*Impossible*

Table 4.2.i: Space-Based - Vulnerability Model 3 (Highly Resistant) - Summary Results

Vulnerability Model 3 results in a single system range of 146. 3 *km*. This range fails to reach the critical altitude from the model's orbital altitude, thus no coverage be insured in this scenario.

Space-Based - Model 3 - "Correlation" - Operating Frequency

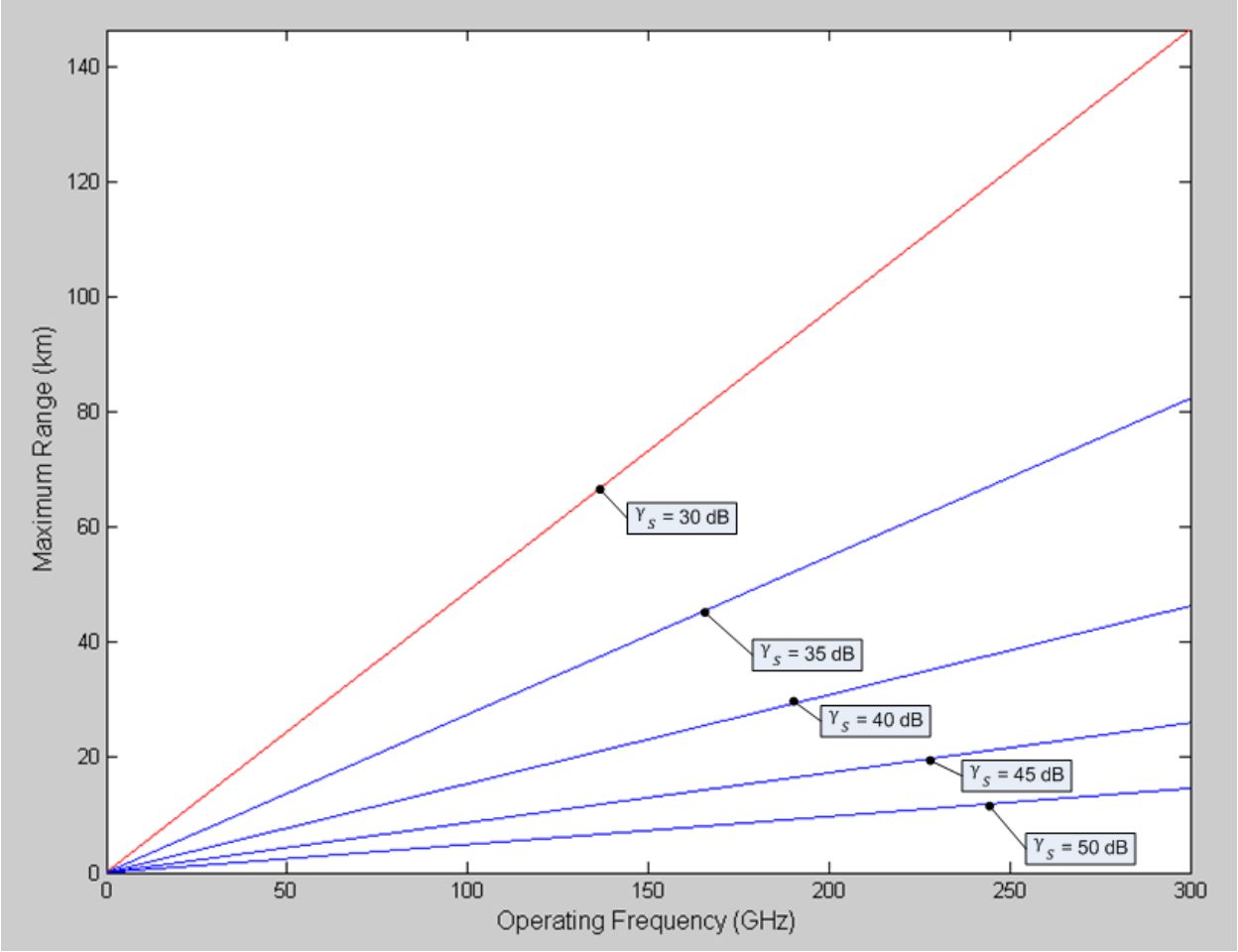

Figure 4.2.j: Space-Based - Model 2 - "Correlation" Plot - Maximum Range/Operating Frequency

Dashed vertical line would describe Vulnerability Model 3 operating frequency core value; however, the core value exists at the end of the microwave spectrum (300 GHz) so it is not visible. Red line describes Vulnerability Model 3 shielding loss core value. Maximum range increases linearly with operating frequency.

Space-Based - Model 3 - "Correlation" - Antenna Diameter

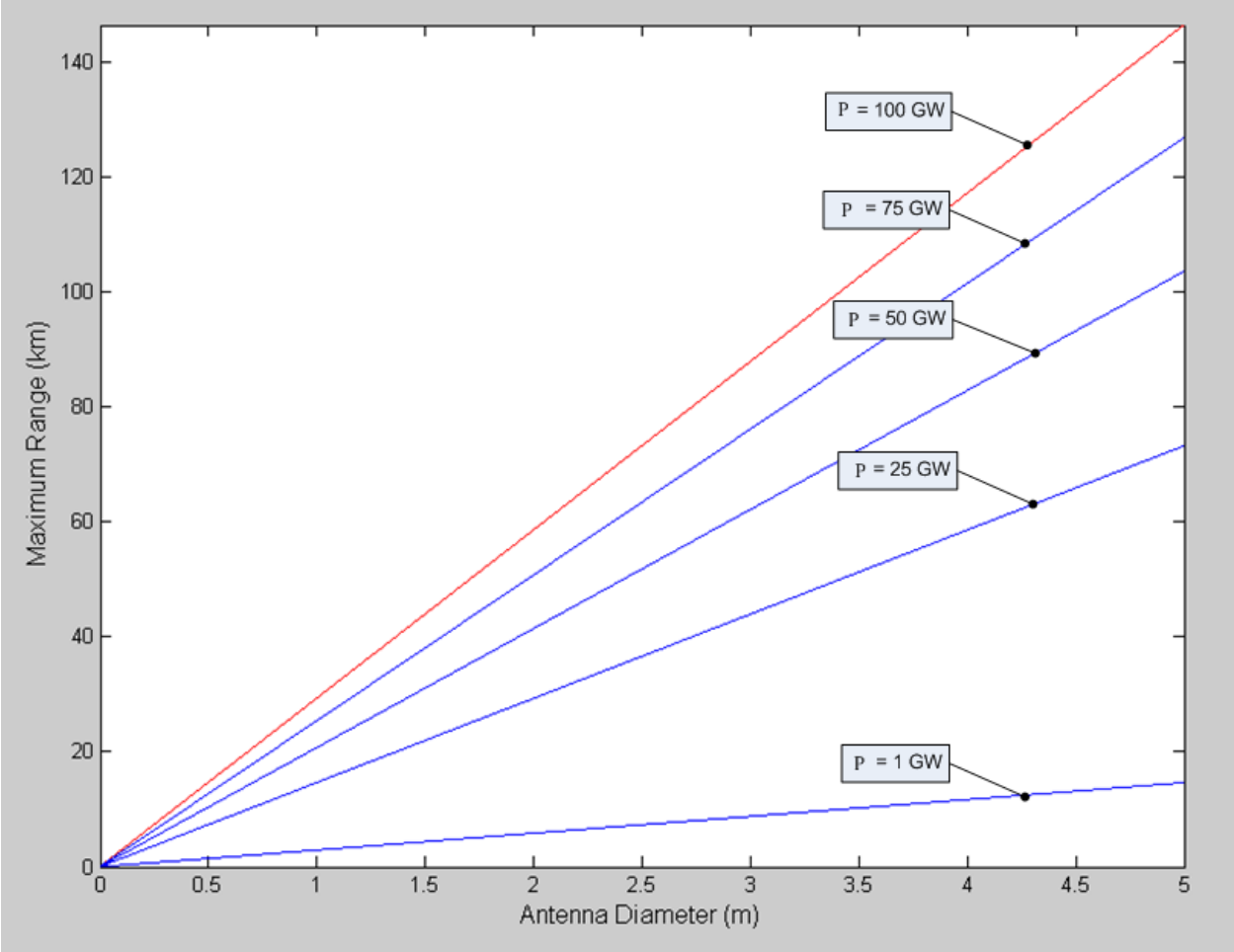

Figure 4.2.k: Space-Based - Model 3 - "Correlation" Plot - Maximum Range/Antenna Diameter

Dashed vertical line would describe Vulnerability Model 3 antenna diameter core value; however, the core value exists at the end of the maximum range (5 meters) so it is not visible. Red line describes Vulnerability Model 3 signal power core value. Maximum range increases linearly with antenna diameter.

Space-Based - Model 3 - "Correlation" - Source Power

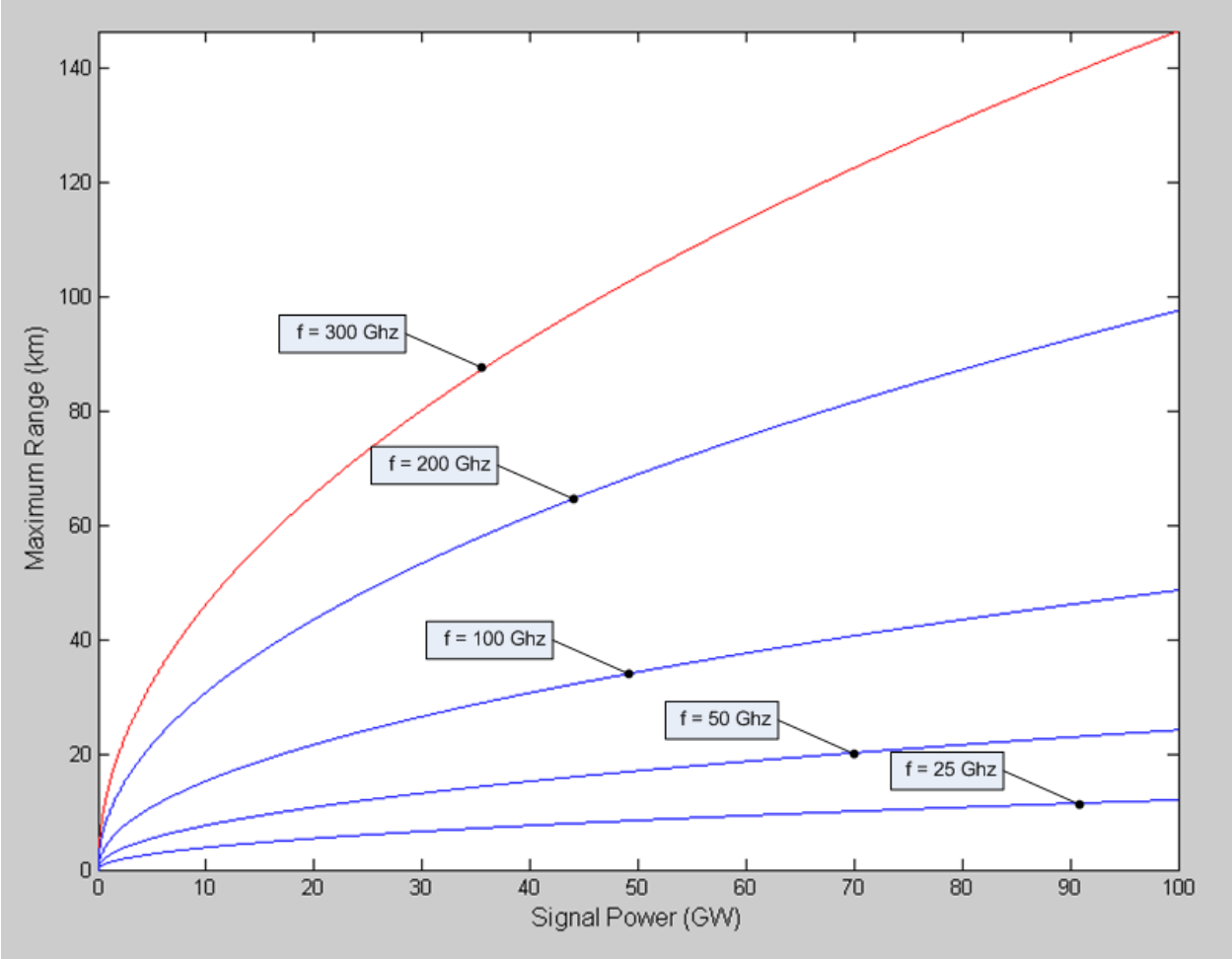

Figure 4.2.l: Space-Based - Model 3 - "Correlation" Plot - Maximum Range/Source Power

Dashed vertical line would describe Vulnerability Model 3 signal power core value; however, the core value exists at the end of the maximum range (100 gigawatts) so it is not visible. Red line describes Vulnerability Model 3 operating frequency core value. Maximum range increases with the root of signal power.

Space-Based - Model 3 - "Correlation" - Electromagnetic Shielding

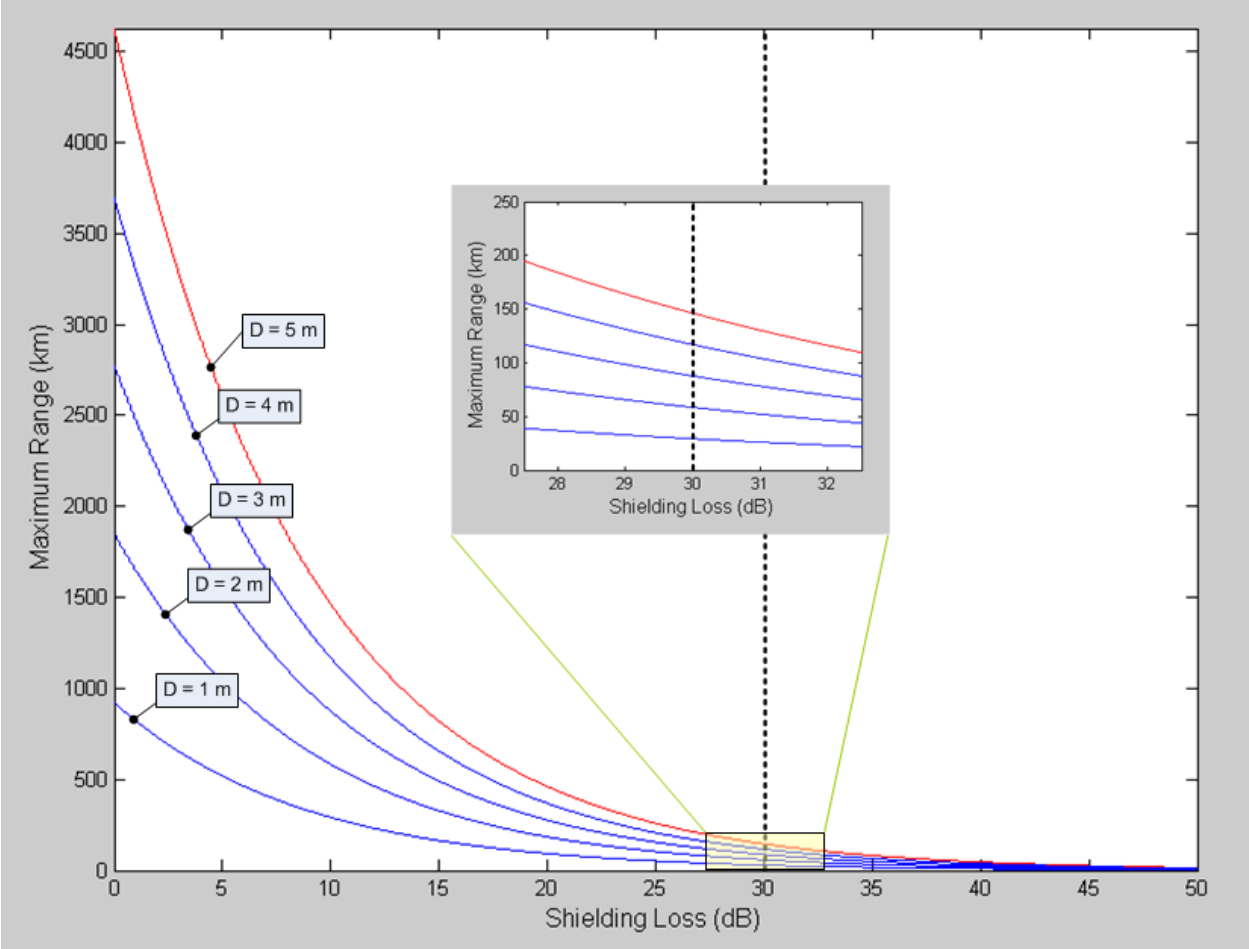

Figure 4.2.m: Space-Based - Model 3 - "Correlation" Plot - Maximum Range/Electromagnetic Shielding Dashed vertical line describes Vulnerability Model 3 shielding loss core value. Red line describes Vulnerability Model 3 antenna diameter core value. Maximum range decreases exponentially with shielding loss.

5 Discussion

5.1 Parameter Relations

The relationships described in this section focus only on a system's maximum vacuum range (R_{vac}) and not its effective downrange distance since the latter is only applicable for ground-based systems.

5.1.1 Antenna Diameter

For the purposes of analysis, a circular antenna is assumed. Different antenna geometries may produce different results by changing the area cross section of the beam; however, the general relations would remain the same. An increase in the diameter of the antenna corresponds to a linear increase in the maximum range of a system.

5.1.2 Signal Power

The signal power of the HPM systems considered in this analysis varies from 1-100 gigawatts. Although power levels in the terawatt range are reportedly achievable in the near future (Fulghum, 2007), this report is concerned only with currently available technology and does not investigate such systems of such power. An HPM system's maximum range increases with the positive square root of the power. As such, a fourfold increase in the signal power would double the system's range.

5.1.3 Operating Frequency

The frequency of the beam fired by an HPM system has the least obvious relationship with the maximum range. In a vacuum, such as with satellite-based systems, the maximum range increases linearly with increasing frequency, similar to the relationship with antenna diameter. However, because of atmospheric attenuation's frequency dependence, ground-based systems do not have an obvious relationship between maximum range and operating frequency. In general, the atmosphere's effects on a system increase in strength with increasing frequency. However, this relationship is non-

linear, and the attenuation level spikes at the resonant frequency of oxygen, which is around 60 GHz. Thus, despite a general increase in a system's range with increases in operating frequency, the rate is less than linear, and for frequencies near 60 GHz the range is significantly decreased.

5.1.4 Electromagnetic Shielding

A target's electromagnetic shielding produces a difficult challenge for an HPM system to overcome. Although 40 dB is considered an upper limit for ICBMs (Cox, 1973), this report takes a conservative approach and varies this value from 30-50 dB, extending ten decibels beyond the reported upper limit. The range of an HPM system varies with the negative exponential of the target's electromagnetic shielding. As such, a ten decibel increase corresponds to nearly an order of magnitude decrease in a system's range.

5.1.5 Required Intensity on Target

The maximum range of an HPM system varies with the ratio of the signal power to the required intensity. As such, an increase in the required intensity can be canceled out with an equivalent increase in the system's signal power, leaving the maximum range unchanged. However, the range of intensities extends nine orders of magnitude, varying from one milliwatt per square meter up to one megawatt per square meter. This spread of values is so great that moving from one end of the spectrum to the other results in system ranges varying from tens to tens of thousands of kilometers.

5.1.6 Atmospheric Considerations

For the purposes of this analysis, atmospheric conditions were calculated from regional yearly averages. As an exception, relative humidity was taken as a yearly high for the region considered, providing more conservative range estimates. Additionally, rainfall and cloud coverage were not considered in analysis. Each of these two factors can significantly reduce the range of a ground-based HPM system.

Additionally, the angle of fire has a significant impact on the total attenuation experienced along the HPM beam's path to target.

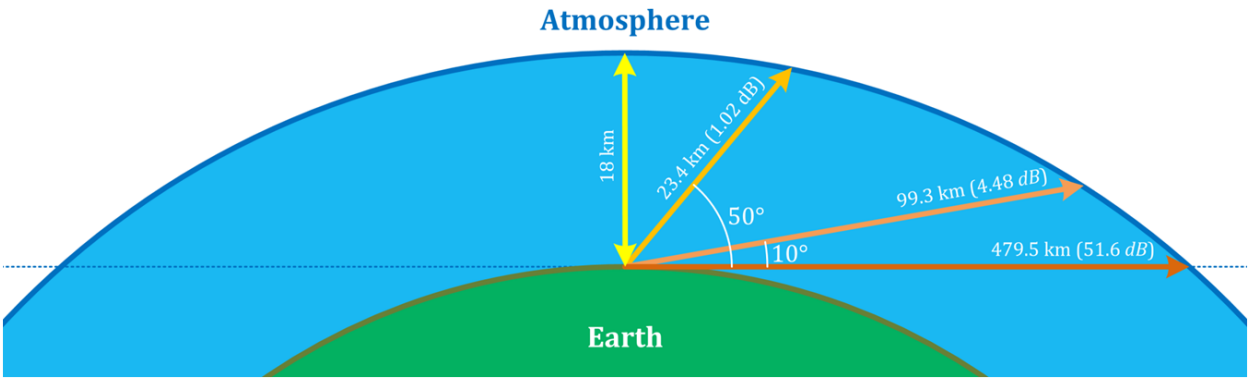

Figure 5.1.a: Distance traveled within atmosphere as a Function of Angle

At different angles of fire, a beam travels different distances within the atmosphere, and is attenuated by different amounts. A beam fired at 50° is only within the atmosphere for 23.4 kilometers and is attenuated by about 1.02 dB, whereas a horizontally fired beam travels a distance of 479.5 kilometers within the atmosphere and is attenuated by the much greater amount of 51.6 dB.

5.2 Ground-Based Systems

For both Vulnerability Models 1 and 2, High-Powered Microwave systems form a promising method for missile defense. Vulnerability Model 1 shows that for highly vulnerable targets (which correspond to a required intensity of 0.01 W/m^2), an HPM system is highly effective and is range limited by the curvature of the Earth. For this model, any number of parameters considered which positively affect the effective range of a system, with the exception of operating frequency, can be decreased by an order of magnitude or more while still maintaining the ability to cover entire countries with just one system. Although operating frequency is shown to positively affect the maximum vacuum range of a system, as defined in Eq. (3.1.m), its effects on ground-based systems, which must fire through the atmosphere, are more difficult to qualify. If operational frequencies near 60 GHz and other peaks of high attenuation shown in Figure 2.4.c are approached, the maximum system range of a ground-based system, as defined in Eq. (3.3.ee), is attenuated heavily. As the peaks of high atmospheric attenuation are related to frequency non-linearly, it is not possible to generalize the effect of frequency for the maximum system range of ground-based system. This effect is confirmed by the surface

figures shown in Section 4.1.2; it is clear to see that beyond 100 GHz there is no significant gain in system range, so considerations beyond this frequency offer little benefit.

Vulnerability Model 2 shows that for the intensity threshold defining most commercial electronic devices ($10\ W/m^2$) (Crawford, Jordan, Kendall, Powers, & Varni, 1996), an HPM system achieves ranges large enough to provide ground-based coverage of most smaller countries such as Iran and North Korea, providing locations close in proximity to the country of concern are available to the United States military. These values are all within system parameter limits based on background research of unclassified sources. From Figure 4.1.hh through Figure 4.1.jj, it is clear to see that, for the core values considered, only a few well-designed HPM systems are needed to provide protection against smaller countries. However, such systems are unable to reach the interior of countries like Russia or China.

Vulnerability Model 3 represents a highly resistant threat model and corresponds to an intensity of 100,000 W/m^2. Effective down ranges are well below those necessary for coverage over most countries. Using model three, high-powered microwave systems would require a significant technological advancement for practical ranges to be realized.

It is important to note a few key characteristics of the three-dimensional surface plots in Sections 4.1.2 and 4.1.3. The plots show an intersection of the downrange distance with an altitude of 100 km. Therefore, different maximum ranges correspond to different beam look angles. For instance, a beam with a very small range that barely reaches an altitude of 100 km would have to fire almost vertically, while a beam of infinite range can fire horizontally. Because of these different firing angles, each maximum range also corresponds to different levels of attenuation, since this value is dependent on the amount of distance traveled within the first 18 km of atmosphere. As such, an improvement in the system's parameters does not improve the maximum effective downrange distance as much as it increases the un-attenuated maximum range.

Since shorter ranges must fire more vertically, beams corresponding to these ranges travel less distance in the lower region of the atmosphere and are attenuated by lesser

amounts than longer-ranged systems. As such, for some frequencies, increases in system parameters are almost entirely offset by the increased level of attenuation. This effect explains some of the more level sections of these plots, and presents a problem when trying to find a general rule of thumb to follow.

5.3 Space-Based Systems

Table 4.0.a outlines a hard truth in High-Powered Microwave (HPM) design for space basing. There exist two compounding negative exponential effects (intensity required on target and attenuation due to target shielding or the atmosphere) on an HPM system's range, while the factors that positively influence range (operating frequency, antenna diameter, and power) have influences that are linear at best.

5.3.1 Vulnerability Models

Vulnerability Model 1 (Section 4.2.1) showed that large ranges are achieved with modest system parameters. Only two satellites are needed in Vulnerability Model 1 to guarantee continuous full Earth coverage. However, the exceptionally large range of the HPM system and the extremely low intensity requirement of model one highlighted that model one did not represent reasonable assumptions for system parameters.

Vulnerability Model 2 (Section 4.2.2) showed that while an HPM system operates assuming the target intensity requirements as described by the United States Air Force report (Crawford, Jordan, Kendall, Powers, & Varni, 1996), and while maintaining modest system parameters, that a functional system is possible. However, Vulnerability Model 2 would require close to 2,000 satellites in orbit in order to guarantee continuous full Earth coverage. A system requiring thousands of satellites is not considered a reasonable solution.

Vulnerability Model 3 (Section 4.2.3) showed that a functional system would require significant advances in technology to operate successfully. The intensity required on target severely limits the HPM system’s range, to the point at which no coverage can be

guaranteed because it fails the bounding test, shown in Eq. (B.e), which checks if the range of an HPM system is capable of reaching the critical altitude from its orbital altitude.

5.4 Collateral Damage Considerations

Since satellite-based HPM systems will be firing electromagnetic radiation towards the ground from distance of several hundred kilometers, the diverged beam will continue past the target, through the atmosphere, and possibly reach the ground. This divergence could cause a collateral damage to electronic equipment. The satellites could be disabled or disrupted, and electronics on the ground as well as aircraft in flight could be affected. To limit the collateral damage caused electronics within the atmosphere, space-based HPM systems can be operated at the 60 *GHz* complex (see section 2.4.3), as most of the radiation will be attenuated too heavily by the atmosphere to cause any damage.

Ground-based systems too have the potential to cause collateral damage. Emitting a high level of radiation beyond their target and into space, satellites in orbit may be irradiated and disabled. Furthermore, waves refracted by the atmosphere could cause damage to ground-based instruments as well.

5.5 Limitations

Analysis of HPM systems was done using two key assumptions. The first key assumption was that the propagation time from the HPM weapon to its target is instantaneous. For most practical considerations this assumption is appropriate as the wave propagates at the speed of light. However, this assumption may not be appropriate if an HPM system were firing over tens of thousands of miles to a target as the target may have to be led by several tenths of a second. Being as ICBMs travel at rates of several kilometers per second, this speed can translate into missing a target by a large spatial (but not temporal) margin. Target acquisition and tracking is not examined in MECSTAR HPM coverage analysis.

The second key assumption was that the time required for an HPM system to mission kill a target ("stare time") is instantaneous. Again, for most practical

considerations this assumption is appropriate as current HPM devices require nanoseconds to successfully disable electronic equipment. Further investigation is needed in determining the actual stare time required for an HPM system that targets ICBMs, as well as the time needed after firing for the system to "rest" before it can fire again.

The ability of two or more beams to focus on a single target simultaneously also merits investigation. If this method were to prove effective, it would then be possible to have a higher quantity of less advanced HPM systems, easing the constraints on technological capabilities.

Ground basing and space basing results each have their own constraints. Ground basing analysis was done in a regional context, as opposed to a global context in the case of space basing. Modeling the number of ground stations required for full Earth coverage is impossible due to political borders. The irregularity of political borders also prevented the creation of an automated coverage calculator. This irregularity means that though ranging is calculated dynamically by MECSTAR, ground station locations must be specified manually and checked against the coverage of other ground stations to insure coverage against a given region.

Space basing is done in a continuous global coverage context only. The method used for calculating satellite based coverage (see Section 3.4) is inappropriate for calculating regional coverage. The method works because the temporal component due to non-stationary orbits is removed by assuming a continuous coverage blanket. A regional-only coverage requirement would remove the simplifications used to calculate global coverage because it would re-introduce the time dimension to the analysis. Satellite position and coverage zone as a function of time would have to be calculated because continuous coverage would no longer be an assumption.

6 Conclusions

The main uncertainty within this research is the level of intensity required to disrupt the navigational system of an ICBM. Since this value is one of the most influential in defining the range of an HPM system due to its negative relation, the feasibility of HPM systems range from trivial to requiring significant technological advancements, as the intensity requirement ranges in value from low to high.

Feasibility for space basing depends on a system designer's criteria for a reasonable number of orbital platforms. However, due to the strong inverse relation between an HPM system's range and the number of required platforms, general criteria can be laid out. In order to get the number of required platforms to less than 50, an HPM system must have a range of several thousand kilometers. Currently, the technology for such a system, while using non-trivial ICBM vulnerability models, is lacking.

For both vulnerability models one and two, ground based HPM systems shows promising results. Less than 5 ground based stations are needed to provide negate an ICBM threat from small nations such as Iran or North Korea.

Addressing the third vulnerability model in both the space and ground based scenarios, is well beyond the technological and logistical ability for any nation. As such, further investigation is required in determining the actual intensity level required for a mission kill.

In summary, though current vulnerability models show promise in the case of ground basing, further research is necessary to in order to quantify an ICBM's actual in-flight response to various levels of applied microwave radiation.

7 References

Space Exploration Technologies Corporation. (2010, September). Retrieved from http://www.spacex.com.

Alexander, D., & Wolf, J. (2010, February 12). U.S. successfully tests airborne laser on missile. *Reuters*.

AlxTel, Inc. (n.d.). *Enterprise*. Retrieved September 7, 2010, from AlxTel: http://www.alxtel.com/html/enterprise.aspx

American Physical Society. (1987, July). The Science and Technology of Directed Energy Weapons. *Reviews of Modern Physics, 59*(3, Part 2).

Barton, D. K., Falcone, R., Kleppner, D., Lamb, F. K., Lau, M. K., Lynch, H. L., et al. (2004). *Report of the American Physical Society Study Group on Boost-Phase Intercept Systems for National Missile Defense: Scientific and Technical Issues.* American Physical Society.

Beaulieu, D., & Horgan, C. J. (2010). *SBI Parameter Effects and Coverage Analysis.* Lexington, MA: Massachusetts Institute of Technology Lincoln Laboratory.

Bloembergen, N., & Patel, C. (1987). Report to The American Physical Society of the study group on science and technology of directed energy weapons. *Reviews of Modern Physics, 76*(3, Part II), S1-S202.

Calow, R., & Zaloga, S. J. (2003). *V-2 ballistic missile 1942-52.* Osprey Publishing.

Clark, J., Langer, J., & Powell, T. (2010). What GPS Might Have Been - and What It Could Become. *Crosslink, 11*(1), pp. 70-77.

Cox, J. J. (1973). Circumvention for Electromagnetic Pulse. *IEEE Internation Electromagnetic Compatibility Symposium Record.*

Crawford, M. D., Jordan, M. C., Kendall, M. D., Powers, G. M., & Varni, L. C. (1996). *Space Operations: Through The Looking Glass.*

Defense Science Board. (2007, December). *Task Force on Directed Energy Weapons.* Washington, D.C.: Office of the Under Secretary of Defense.

Deutsches Bundesarchiv. (n.d.). Retrieved September 20, 2010, from http://www.bild.bundesarchiv.de/archives/barchpic/search/_1284997973/?search[view]=detail&search[focus]=1

Egea, A. N. (1990). ICBM Trajectories: Some Issues for the Superpowers' Neighbors. *Journal of Peace Research Volume 27, Number 4*, 373-384.

Federation of American Scientists. (1998, October 25). *Intercontinental Ballistic Missiles*. Retrieved September 12, 2010, from Federation of American Scientists: http://www.fas.org/nuke/intro/missile/icbm.htm

Federation of American Scientists. (1998, August 26). *Long-Haul Transmission Systems*. Retrieved October 15, 2010, from FAS: http://www.fas.org/spp/military/docops/army/lhaul/Lhfinweb.htm

Federation of American Scientists. (1998, December 26). *Safeguard*. Retrieved September 29, 2010, from Special Weapons Monitor: http://www.fas.org/spp/starwars/program/safeguard.htm

Federation of American Scientists. (2000, June 4). *Ballistic Missile Basics*. Retrieved September 12, 2010, from Federation of American Scientists: http://www.fas.org/nuke/intro/missile/basics.htm

Fulghum, D. A. (2007). Light Boosts Destructive Power of Microwave Weapons, Sensors. *Aviation Week*.

Hoffman, M. (2010, March 1). *Schwartz: Get those AF boots off the ground*. Retrieved September 22, 2010, from Air Force Times: http://www.airforcetimes.com/news/2010/02/airforce_budget_022610w/

Kopp, C. (2000). *Microwave and Millimetric Wave Propagation.* Kopp, Carlo.

Kowoma. (2009, April 19). *The GPS System*. Retrieved October 15, 2010, from kowoma.de: http://www.kowoma.de/en/gps/orbits.htm

Lesurf, J. C. (n.d.). *Radio & Coherent Techniques*. Retrieved October 16, 2010, from The Scots Guide to Electronics: http://www.st-andrews.ac.uk/~www_pa/Scots_Guide/RadCom/part8/page3.html

Nave, R. (n.d.). *The Rayleigh Criterion*. Retrieved from Hyperphysics: http://hyperphysics.phy-astr.gsu.edu/hbase/phyopt/raylei.html

Nielsen, P. E. (1994). *Effects of Directed Energy Weapons.* Fort Lesley J. McNair, Washington, DC: National Defense University, Center for Technology and National Security Policy.

Northrop Grumman Aerospace Systems. (2009). *Northrop Grumman Contribution to Support Missile Defense Workforce in Alaska.* Northrop Grumman.

Office of Technology Assessment. (1993). *Technologies Underlying Weapons of Mass Destruction.* U.S. Congress. Washington, D.C.: U.S. Government Printing Office.

O'Rourke, R. (2010). *Navy Aegis Ballistic Missile Defense (BMD) Program: Background and Issues for Congress.* Congressional Research Service.

Papp, D. D. (1987-88, Winter). From Project Thumper to SDI: The Role of Ballistic Missile Defense in US Security Policy. *Airpower Journal*.

Parrington, L. J. (1997, Winter). Mutually Assured Destruction Revisited: Strategic Doctrine in Question. *Airpower Journal, XI*(4), 4-19.

Pevler, A. (1997). Security Implications of High-Power Microwave Technology. *IEE International Symposium on Technology and Society*, (pp. 107-111). Glasgow, UK.

Pozar, D. M. (1993). *Microwave Engineering.* Addison-Wesley Publishing Company.

Reiss, E. (1992). *The Strategic Defense Initiative.* New York: Cambridge University Press.

Samson, V., & Black, S. (2007). *Flight Tests For Ground-Based Midcourse Defense (GMD) System.* Center for Defense Information.

Sauser, B. (2007, 11 13). *Stopping Cars with Radiation*. Retrieved 9 21, 2010, from Technology Review: http://www.technologyreview.com/computing/19699/page1/

Selinger, M. (2010, April 19). *Airborne Laser Test Bed: Science fiction no more*. Retrieved September 21, 2010, from Boeing Feature Story: http://www.boeing.com/Features/2010/04/bds_feat_ALTB_Shootdown_031210.html

Shambayati, S. (2008). Atmosphere Attenuation and Noise Temperature at Microwave Frequencies. In M. S. Reid, *Low-Noise Systems in the Deep Space Network* (pp. 255-281). Jet Propulsion Laboratory, California Institute of Technology.

SMDC. (n.d.). *Photo Gallery*. Retrieved September 21, 2010, from SMDC/ARSTRAT: http://www.smdc.army.mil/SMDCPhoto_Gallery/MissileDef/MissileDef.html

Strategic Studies Institute. (2004). *Getting MAD: Nuclear Mutual Assured Destruction, Its Origins and Practice.* (H. D. Sokolski, Ed.)

U.S. Department of Commerce. (2003, October). *United States Frequency Allocations.* Retrieved October 4, 2010, from National Telecommunications and Information Administration: http://www.ntia.doc.gov/osmhome/allochrt.pdf

U.S. Department of Defense. (n.d.). *History Resources*. Retrieved 9 21, 2010, from Missile Defense Agency: http://www.mda.mil/news/history_resources.html

Vallado, D. A. (2007). *Fundamentals of Astrodynamics and Applications.* Microcosm Press.

Warmkessel, D. B. (1999, June 7). *Threat Definition and Verification*. Retrieved October 12, 2010, from Vulcan Comets and the Impending Catastrophe: http://www.barry.warmkessel.com/1999PPaper.html

Werrell, K. P. (2000). *Hitting a Bullet with a Bullet: A History of Ballistic Missile Defense.* Air University, College of Aerospace Doctrine, Research and Education. Airpower Research Institute.

Williams, D. R. (2009, May 20). *Earth Fact Sheet*. Retrieved October 16, 2010, from Nasa Planetary Fact Sheets: http://nssdc.gsfc.nasa.gov/planetary/factsheet/earthfact.html

Wilson, C. (2008). *CRS Report to Congress - High Altitude Electromagnetic Pulse (HEMP) and High Power Microwave (HPM) Devices: Threat Assessments.*

Zhang, M. (1997). *A modification to previous ITU-R simplified model for gaseous attenuation.* Xinxiang, Henan, China: China Research Institute of Radiowave Propagation.

Appendix A: Equilateral Hexagon Proof

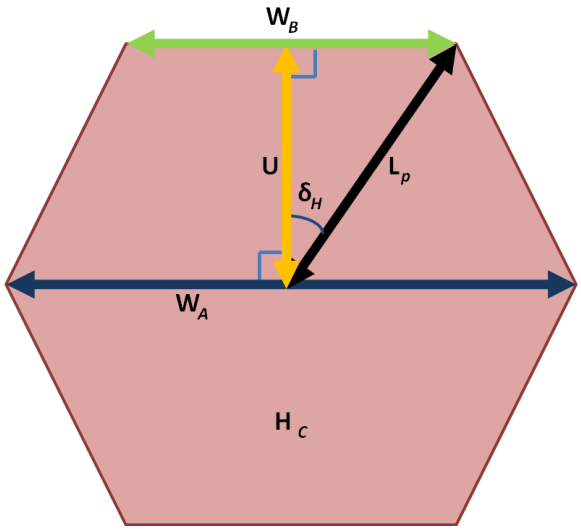

Figure A.a: "Hexagonal" Fit of Coverage Intersection

The constant 'C' is the circumference of an arbitrary cross section of the critical surface sphere, S_C, that passes through the origin.

$$C = 2 \cdot \pi \cdot (R_E + h_c) \tag{A.a}$$

The value 'U' is a special case of the abbreviated projected arc, L_a; the case in which L_a is defined as an arc length starting from the center of H_C and terminates at the midpoint of an edge which contains the orbital path (as opposed to an arbitrary edge). This value is approximated by temporarily treating H_C as a plane and also by treating the projected arc, L_p, as a line length instead of an arc length. This approximation is valid for as long as the curvature of S_C is small as compared to the localized area H_C occupies.

$$U = L_p \cdot \cos(\delta_H) \tag{A.b}$$

The value 'W_A' is the arc length between the two vertices on H_C of which are the furthest apart.

$$W_A = 2 \cdot L_p \tag{A.c}$$

The value 'W_A' is an arc length between the vertices that describe an edge that contains the orbital path. This value is approximated in the same manner as 'U.'

$$W_B = 2 \cdot L_p \cdot \sin(\delta_H) \tag{A.d}$$

The values of $N_{sat/ring}$, N_{orbits}, and N_{total} are allowed to be fractions in this special proof so that relation of δ_H to the total number of satellites is continuous and differentiable.

$$N_{sat/ring} = \frac{\mathrm{C}}{U} \tag{A.e}$$

$$N_{orbits} = \frac{\mathrm{C}}{W_A + W_B} \tag{A.f}$$

$$N_{total} = N_{sat/ring} \cdot N_{orbits} \tag{A.g}$$

$$N_{total} = \frac{\mathrm{C}}{U} \cdot \frac{\mathrm{C}}{W_A + W_B} \tag{A.h}$$

Substituting in values to relate N_{total} to δ_H is shown below.

$$N_{total}(\delta_H) = \frac{\mathrm{C}}{L_p \cdot \cos(\delta_H)} \cdot \frac{\mathrm{C}}{2 \cdot L_p + 2 \cdot L_p \cdot \sin(\delta_H)} \tag{A.i}$$

$$N_{total}(\delta_H) = \frac{\mathrm{C}^2}{2 \cdot {L_p}^2 \cdot \cos(\delta_H) \cdot (1 + \sin(\delta_H))} \tag{A.j}$$

$$N_{total}(\delta_H) = \frac{\mathrm{C}^2}{2 \cdot {L_p}^2} \cdot \frac{1}{\cos(\delta_H) \cdot (1 + \sin(\delta_H))} \tag{A.k}$$

To find the value of δ_H that relates to the lowest N_{total}, N_{total} is differentiated with respect to δ_H and then solved for when the differentiated function equals 0.

$$\frac{d(N_{total}(\delta_H))}{d\delta_H} = \frac{\mathrm{C}^2}{2 \cdot E^2} \cdot \frac{\tan^2(\delta_H) + \tan(\delta_H)\sec(\delta_H) - 1}{(\sin(\delta_H) + 1)^2} \tag{A.l}$$

$$\frac{d(N_{total}(30°))}{d\delta_H} = 0 = Local\ Minima \qquad \text{(A.m)}$$

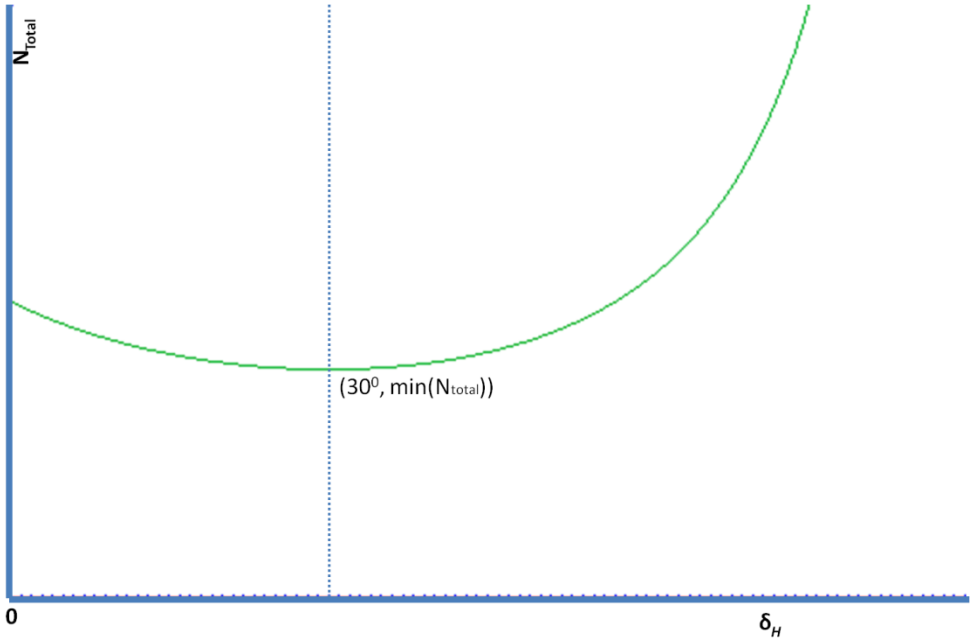

Figure A.b: Total Satellites versus Hexagonal Angle

Local minima at δ_H=30⁰. Value of N_{total} is arbitrary.

Figure A.a is redrawn below with $\delta_H = 30°$ and the consequential angles by again approximating the H_C locale as a plane.

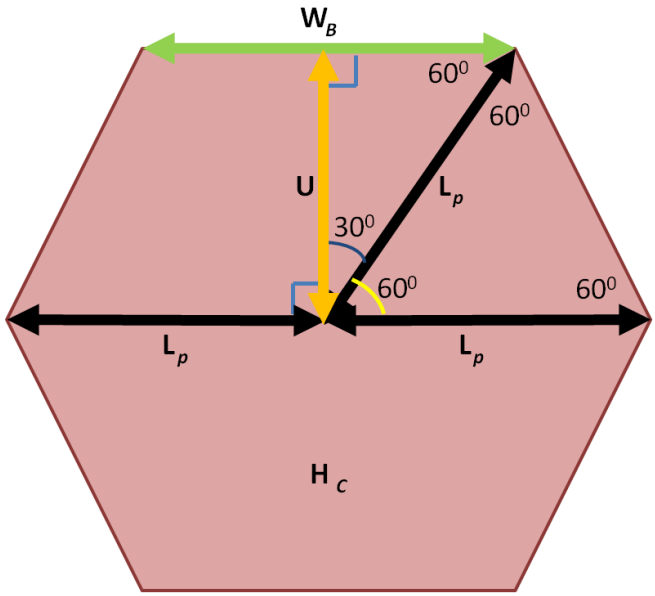

Figure A.c: Equilateral "Hexagon"

Appendix B: Background Space Methods Calculations

$$C(x) = \sqrt{(R_e + h_c)^2 - x^2} \tag{B.a}$$

$$R(x) = \sqrt{(R_{max})^2 - \left(x - (R_e + h_o)\right)^2} \tag{B.b}$$

The x-value of the intersection of the equations $C(x)$ and $R(x)$ is x_0 $(in\ km)$. Eq. (B.c) sets $C(x)$ and $R(x)$ equal to each other to solve for x_0. As shown in Eq. (B.d), the projected radius (R_p in km) is a function of x_0, and consequently of critical altitude $(h_c\ in\ km)$, radius of Earth $(R_e\ in\ km)$, orbiting altitude $(h_o\ in\ km)$, and maximum effective range $(R_{max}\ in\ km)$.

$$x_0 = \frac{(R_E + h_c)^2 - (R_{max})^2 + (R_E + h_o)^2}{2 \cdot (R_E + h_o)} \tag{B.c}$$

$$R_p = R(x_0) \tag{B.d}$$

A consequence of x_0 being the intersection of $C(x)$ and $R(x)$ is that there must be a bounds check to see if the intersection exists at all. Eq. (B.e) describes the bounding check taken to insure intersection.

$$Intersection = \begin{cases} True & if\ h_o - R_{max} < R_E + h_c \\ False & otherwise \end{cases} \tag{B.e}$$

Intersection is true if the orbital altitude, minus the maximum range, is less than the radius of Earth plus the critical altitude, as these are the adjacent radial extrema of the circles $C(x)$ and $R(x)$.

If an intersection exists, x_0 and R_p are used to calculate the projected arc $(L_p\ in\ km)$. Because x_0, R_p, and the origin of Earth form a right triangle as shown in Figure 3.4.a, the angle σ is found by using the arctangent function, as shown in Eq. (B.f). Once σ is solved, L_p is found using the equation to calculate arc length, as shown in Eq. (B.g).

$$\sigma = \text{atan2}\left(\frac{x_0}{R_p}\right) \tag{B.f}$$

$$L_p = \sigma \cdot (R_E + h_c) \tag{B.g}$$

The abbreviated projected arc, L_a, is roughly a scalar multiple of L_p, and is approximated using Pythagorean's theorem in the geometry described in Figure 3.4.d and below in Eq. (B.h).

$$L_a = \frac{\sqrt{3}}{2} L_p \tag{B.h}$$

With L_a known, Eq. (3.4.a) is applied to calculate the maximum satellite spacing.